The Impact of Efflux Transporters in the Human Lung Epithelium on the Pulmonary Bioavailability of Antibiotics after Systemic Administration

Dissertation

zur Erlangung des Grades

des Doktors der Naturwissenschaften

der Naturwissenschaftlich-Technischen Fakultät

der Universität des Saarlandes

von

Sina Simon

Saarbrücken

2025

Tag des Kolloquiums:	08.04.2026
Dekan:	Prof. Dr.-Ing. Dirk Bähre
Berichterstatter:	Prof. Dr. Claus-Michael Lehr Prof. Dr. Marc Schneider
Vorsitz:	Prof. Dr. Thorsten Lehr
Akad. Mitglied:	Dr. Dominik Selzer

“*Nothing in life is to be feared, it is only to be understood.*”

Marie Curie

Short summary

Antibiotics are typically administered to the systemic circulation to treat bacterial infections in the lung. To reach their target compartment within the epithelial lining fluid (ELF), drugs have to permeate across the lung epithelium. Therefore, it has been hypothesised that pulmonary bioavailability could be positively affected by efflux transporters located at the lung epithelium. Their expression has been characterised, whereas their contribution on pulmonary drug disposition is little understood.

The aim of this thesis is to provide a better understanding on the role of efflux transporters at the human lung epithelium and to investigate their impact on the pulmonary transport of antibiotics into the ELF. The thesis matured into the following chapters using a combined *in vitro* & *in silico* approach.

1. Characterising the expression and functional activity of MDR1, MRP1 and BCRP in cell lines and primary cells derived from human upper and lower airways epithelium
2. Investigating the rate and extent of antibiotics transport across the lung epithelium, focussing on efflux, permeability and fraction unbound in ELF & plasma
3. Employing physiologically based pharmacokinetic (PBPK) modelling to simulate the ELF concentration-time profiles of two antibiotics in human and rat

The results indicated a rather negligible role of ABC transporters on driving the pulmonary drug disposition of antibiotics in humans, which is in contrast to their role in other tissues of the human body.

Kurze Zusammenfassung

Antibiotika werden mehrheitlich über die systemische Zirkulation verabreicht, um bakterielle Infektionen in der Lunge zu behandeln. Dabei müssen sie das Lungenepithel permeieren, um ihre Wirkungsstätte in der Epithelschleimhautflüssigkeit (ELF) zu erreichen. Es wird davon ausgegangen, dass die dortige Bioverfügbarkeit von Antibiotika potenziell von Effluxtransportern im Lungenepithel beeinflusst wird. Deren Expression ist bereits umfassend charakterisiert, jedoch ist ihr Einfluss auf die pulmonale Pharmakokinetik nur unzulänglich erforscht.

Diese Dissertation zielt darauf ab ein besseres Verständnis zur Rolle der Effluxtransporter im menschlichen Lungenepithel zu ermöglichen und untersucht ihren Einfluss auf die Wirkstoffverteilung von Antibiotika in die ELF. Dafür wurde ein dreigliedriger *in vitro* & *in silico* Ansatz angewandt:

1. Charakterisierung der Expression und Aktivität von MDR1, MRP1 und BCRP in Zelllinien und Primärzellen des menschlichen Lungenepithels
2. Untersuchung der Antibiotikaverteilung durch das Lungenepithel mit Fokus auf Efflux, Permeabilität und ungebundenem Wirkstoffanteil in der ELF und dem Plasma
3. Anwendung von physiologisch-basierter pharmakokinetischer Modellierung zur Simulation der ELF-Exposition von zwei Antibiotika in Mensch und Ratte

Die Ergebnisse zeigten eine eher vernachlässigbare Rolle der Effluxtransporter auf die Wirkstoffverteilung von Antibiotika in die ELF auf. Dies steht im Gegensatz zu ihrer Rolle in anderen Epithelgeweben des Menschen.

List of Abbreviations

ABC	Adenosine triphosphate-binding cassette
AlogP	Octanol/water partition coefficient
ADME	Absorption, distribution, metabolism, excretion
ALI	Air-liquid interface
Ap PStc	Apical permeability surface area product
ATP	Adenosine triphosphate
$AUC_{0\text{-}th}$	Area under the plasma concentration-time curve for the respective simulation time
Ba PStc	Basolateral permeability surface area product
BAL	Bronchoalveolar lavage
BCRP	Breast cancer resistance protein
BMS	Bronchoscopic microsampling
BSA	Bovine serum albumin
5,6-CF	5,6-Carboxyfluorescein
C_0	Compound concentration at time 0 h
CI	Confidence interval
CL_b	Biliary clearance
CL_{diff}	Passive hepatic diffusion clearance
CL_h	Hepatic clearance
CL_r	Renal clearance
COPD	Chronic obstructive pulmonary disease
C_{max}	Maximal plasma concentration
C_t	Cycle threshold
DDI	Drug-drug interaction
DPBS	Dulbecco's phosphate buffered saline
ELF	Epithelial lining fluid
EMA	European Medicines Agency
ER	Efflux ratio
ER_i	Efflux ratio in presence of inhibitor
EVOM	Epithelial volt-ohm-meter
FBS	Foetal bovine serum
FDA	US Food and drug administration
$f_{u,plasma}$	Fraction unbound in plasma
$f_{u,ELF}$	Fraction unbound in epithelial lining fluid
$f_{u,sELF}$	Fraction unbound in simulated epithelial lining fluid

H33342	Hoechst 33342
hAEpC	Human alveolar type I-like epithelial cells
HRP	Horseradish peroxide
IPL	Isolated perfused lung
ITC	International Transporter Consortium
$K_{ELF/P,u}$	ELF to unbound plasma partition coefficient
K_m	Michaelis-Menten constant
K_p	Tissue to plasma partition coefficient
LCC	Liquid-covered culture
LC-MS/MS	Liquid chromatography coupled to tandem mass spectrometry
LLC-PK1 WT	Lilly Laboratories porcine kidney-1 wild type epithelial cells
L-MDR1	LLC-PK1 cells transfected with human MDR1
L-Mdr1a	LLC-PK1 cells transfected with mouse Mdr1a
logD	Octanol/water distribution coefficient
LY	Lucifer Yellow
M-199	Medium-199
MDCK-II	Madin-Darby canine kidney epithelial cells
M-BCRP	MDCK-II cells transfected with human BCRP
M-Bcrp1	MDCK-II cells transfected with mouse Bcrp1
MDR1	Multidrug resistance protein 1
MCL	Mucociliary clearance
ML	Machine learning
MRP1	Multidrug resistance associated protein 1
MW	Molecular weight
N.A.	Not applicable
N.D.	Not detected
NIR	Near-infrared
NHBE	Normal human bronchial epithelial cells
OAT	Organic anion transporter
OATP	Organic anion transporting polypeptide
OCT	Organic cation transporter
OCTN	Novel organic cation transporter
P_{app}	Apparent permeability
P_{app} AB	Apparent permeability from apical to basolateral side
P_{app} BA	Apparent permeability from basolateral to apical side
PBPK	Physiologically based pharmacokinetic modelling
PC	Phosphatidylcholine

PE	Phosphatidylethanolamine
P_{eff}	Effective intestinal permeability
PEPT	Peptide transporter
PET	Positron emission tomography
PG	Phosphatidylglycerol
P-gp	P-glycoprotein
PhiP	2-Amino-1methyl-6-phenyllimidazol[4,5-b]pyridine
PI	Phosphatidylinositol
PK	Pharmacokinetics
pKa	Acid dissociation constant
PS	Phosphatidylserine
PSA	Parameter sensitivity analysis
PStc	Permeability surface area product
Q	Blood flow
qPCR	Quantitative polymerase chain reaction
QSAR	Quantitative structure activity relationship
R^2	Coefficient of determination
Rh123	Rhodamine 123
SD	Standard deviation
sELF	Simulated epithelial lining fluid
SLC	Solute carrier
SLCO	Solute carrier organic anion
$t_{1/2}$	Half-life
TDI	Time-dependent inhibition
TEER	Transepithelial electrical resistance
w/o	Without
UR	Uptake ratio
V_{max}	Maximal velocity
V_{ss}	Volume of distribution

Table of Contents

1. Introduction

Parts of this chapter have been published as a review article:

Simon, S., Cantrill, C. and Lehr, C-M. (2025), The Role of ABC Transporters in the Human Lung Epithelium – Insights from and Limitations of Current *in vitro* Cell Models, *In vitro models*, DOI: 10.1007/s44164-025-00091-w

Contributions to the review paper from which parts of the following chapter have been adapted:

Sina Simon supported drafting the manuscript, performed the literature research, wrote the manuscript and created all the figures. Moreover, she was mainly involved in editing the revised manuscript.

Dr. Carina Cantrill and Prof. Dr. Claus-Michael Lehr supported drafting the review paper and critically evaluated the final manuscript.

1.1 General Introduction

Diseases affecting the lung are on the rise. Infections, which tackle the lower respiratory tract such as pneumonia have contributed to the deaths of around 2.1 million people worldwide in 2021 [1]. Besides, more than 550 million patients suffered from a chronic respiratory disease in 2017, and this number has increased during the last three decades by 40 % [2]. Therefore, the lung has grown more prevalence as a therapeutic target in recent decades to treat both acute and chronic pulmonary diseases, using a number of different chemical drug classes [3].

To treat pneumonia, antibiotics are administered to patients to combat the infection if caused by bacteria. The sites of action for the antibiotics are located either within the epithelial lining fluid (ELF, which covers the whole surface of the human airways) for extracellularly replicating bacteria, such as Streptococcus pneumoniae or within the alveolar macrophages for intracellularly replicating bacteria like Legionella pneumophila [4, 5]. Administered drugs can reach the lung lumen by two different routes: from the blood side (via the systemic circulation) or via inhalation. Over the last decades, there have been many efforts to deliver drugs effectively into the lung via inhalation. This route of application holds benefits including fast onset of action within the lung, likely less systemic side effects and a higher local pulmonary concentration may be reached [6-8]. However, the vast majority of antibiotics are administered to patients via the systemic circulation, either oral across the gastrointestinal tract or parentally [9, 10]. This trend is also observed for recently approved antibiotics [11]. Only for one specific indication, a chronic pulmonary Pseudomonas aeruginosa infection in cystic fibrosis patients, inhalable formulations of antibiotics are routinely used. For this purpose, inhalable powers and/or solutions of aztreonam, colistin, levofloxacin and tobramycin have been approved by health authorities [12-14]. Given that the preferred route of administration of antibiotics is still via the systemic circulation, it is of huge importance to mechanistically understand the factors that impact their pulmonary exposure, focussing on the distribution from the blood circulation across the pulmonary epithelium into the ELF [15].

Clinical studies have reported that certain antibiotic classes show a significantly higher concentration within the ELF compared to their free plasma concentration (>> 1). This has been mainly observed for macrolide and fluoroquinolone antibiotics [4, 15]. *In vitro* studies have reported that members of these antibiotic drug classes appear to be substrates of active efflux transporters, which are transmembrane proteins being capable to transport their substrates against a concentration gradient out of the cells, thus potentially contributing to increased ELF concentrations over time [16, 17]. The presence of these adenosine triphosphate-binding cassette (ABC) efflux transporters and their clinical impact on the pharmacokinetic processes of their substrates is well characterised in humans for organs like the intestine, liver or kidney. In these tissues, ABC transporters can limit the absorption or

enhance the elimination of their substrates with numerous clinical drug-drug interactions (DDI) being reported [18]. However, the role of these ABC efflux transporters within the human lung epithelium is still poorly understood [19].

Over the last decades, there have been many attempts to establish representative and sophisticated *in vitro* models of the human lung epithelium, consisting of cell lines, primary cells or complex co-culture systems. They have been extensively characterised in terms of active ABC transporters expression and functional activity [20]. However, there is still little known about the predictivity of these *in vitro* models in the context of ABC transporters' impact on pulmonary drug disposition [19].

Therefore, the aim of this thesis was to gain a better mechanistic understanding on the role of ABC transporters at the human lung epithelium and their contribution to the pulmonary bioavailability of antibiotics after administration vis the systemic circulation. First, the expression and functional efflux of ABC transporters was investigated within cells derived from the upper and lower human airway epithelium. Further, the interaction of antibiotics with expressed ABC transporters as well as their permeability across the pulmonary epithelium was assessed *in vitro*. In a last step, *in silico* modelling was applied to predict ELF concentration-time profiles of two antibiotics by incorporating measured *in vitro* properties.

The Chapter 1 provides the supportive background information regarding the lung physiology, available *in vitro*, *in vivo* and *in silico* models to study pulmonary drug disposition and an introduction to ABC transporters, their expression in the human lung epithelium and their interaction with antibiotics *in vitro*. In Chapter 2, the aim and objectives of this thesis are outlined. The Chapter 3 summarises the conducted *in vitro* and *in silico* studies aiming to elucidate the role of ABC transporters in human lung epithelium and their potential impact on pulmonary drug disposition of antibiotics and are followed by Chapter 4 that provides an overall summary and outlook.

1.2 Anatomical & Physiological Structure of the Human Lung

The human lung is located within the chest cavity and consists of a right and left lung, with an estimated total weight of around 840 g in men and 639 g in women [21, 22]. This organ is responsible for facilitating the blood oxygenation by the gas exchange of carbon dioxide with oxygen, where the carbon dioxide diffuses from the pulmonary endothelium via the alveolar epithelium into the inhaled air and vice versa for the oxygen [23].

The human respiratory tract is subdivided into the conducting (upper) and the respiratory (lower) airways. The inhaled air first passes the upper airways, consisting of the nasal cavity,

pharynx, larynx, trachea, bronchi and terminal bronchiole, before it passes to the lower airways constituted of the respiratory bronchioles and the alveoli [24]. The function of the conducting airways is to filter, warm and moisturise the air, whereas the gas exchange occurs across the alveolar surface within the alveolar sacs of the respiratory airways [25]. Figure 1 shows a graphical representation of the human upper and lower airways.

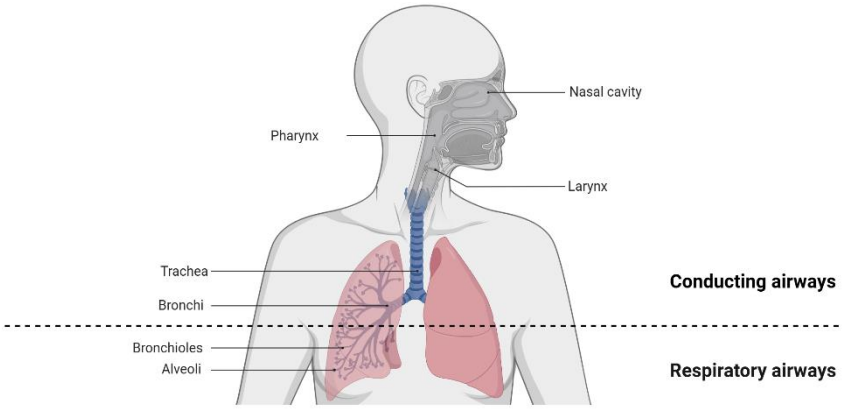

Figure 1. Overview of the human respiratory tract structure. It is subdivided into the upper and lower airways, as described by Han and Hirahara [24]. After inhalation, the air passes from the conducting airways via the respiratory airways to the alveoli, where the gas exchange takes place. The Figure was created with BioRender.com.

The airway branch starts at the level of the trachea with a single tube followed by a 23-fold bifurcation to the level of the alveolar sacs, described as the Weibel model [26]. Following the bifurcation, the airways diameter reduces from around 1.8 cm in the trachea to 0.04 cm in the alveolar sacs [25]. At the same time, the bifurcation causes a tremendous increase in surface area from around 1 to 2 m^2 in the upper airways to more than 140 m^2 within the lower airways. This offers a large surface within the alveoli for diffusion processes [27].

The cellular composition, morphology and function of the pulmonary epithelial cells that line the airway tract changes along the upper and lower airways with being adapted to the needs of respective regions [28]. The epithelial layer thickness reduces from 58 µm in the bronchi to 10 µm in the terminal bronchiole and further to 0.1 – 0.2 µm within the alveolar region [29]. This extremely thin epithelial layer of the alveoli, together with the large surface area and the high blood perfusion (complete cardiac output is received) offers ideal conditions for a fast absorption of drugs [6].

A pseudostratified columnar epithelium is characteristic of the tracheo-bronchial region and is composed of a variety of different cells such as beating ciliated cells, goblet cells producing and secreting mucus, neuroendocrine cells and basal cells acting as stem cells. Further the presence of club cells that produce anti-inflammatory proteins, was described [25, 28, 30, 31]. The bronchiolar region has a similar epithelium composition as the tracheo-bronchial region, although being classified as simple columnar epithelium, which changes to a simple cuboidal

epithelium within the respiratory bronchioles. The number of goblet cells is reduced whereas the number of club cells is increased compared to the bronchial epithelium [30, 32, 33]. The alveolar region is covered by the alveolar pneumocytes type I and II, where the type I cells have a squamous appearance and the type II cells a rather cuboidal one. Around 95 % of the surface area is covered by alveolar pneumocytes type I that are contributing to the gas exchange [34]. The alveolar pneumocytes type II constate 60 % of the cells within the alveolar region and are involved in producing, secreting and recycling the surfactant, which is important in regulating the surface tension within the alveoli [35, 36]. Alveolar macrophages, which are patrolling the lower airways, are innate immune cells engulfing particles and playing an important role in lung homeostasis [37]. Figure 2 provides a schematic overview of the cellular composition of the upper and lower airways.

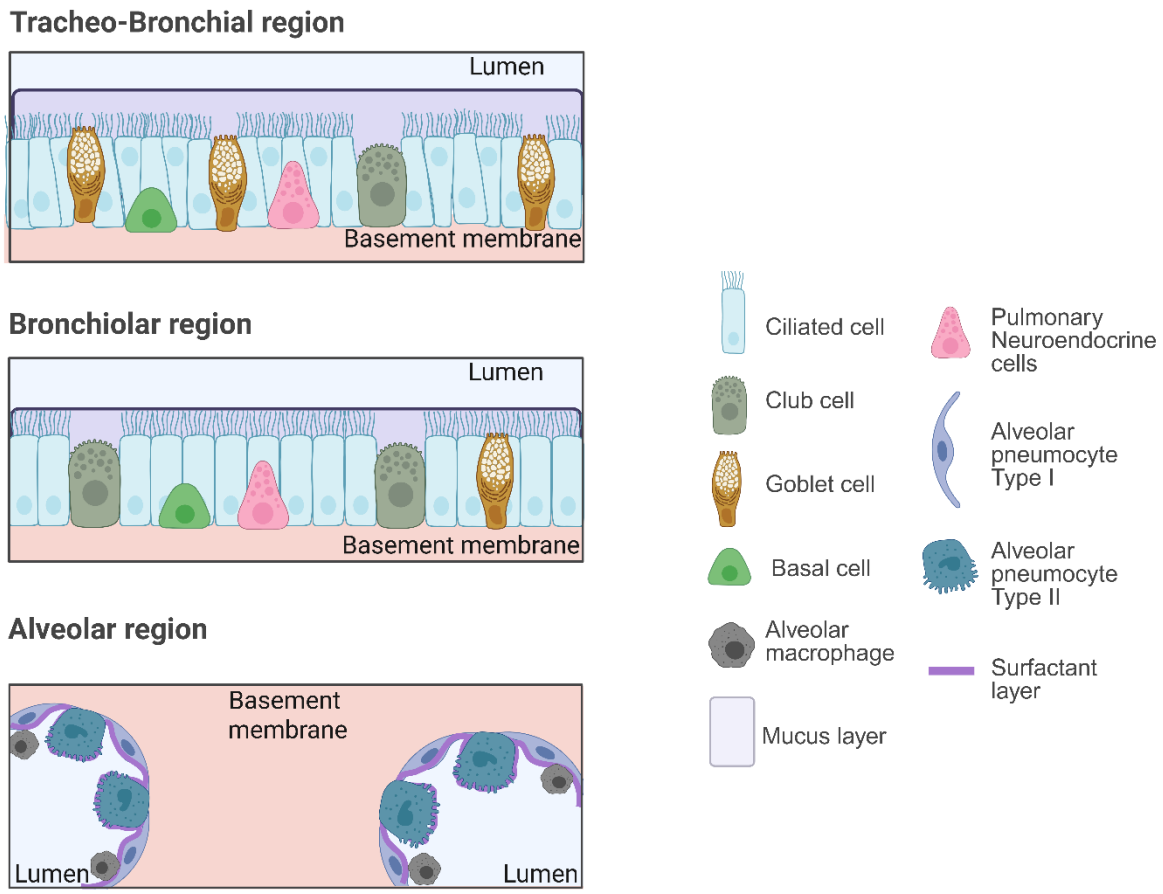

Figure 2. The cellular composition of the human airway epithelium in the tracheo-bronchial, bronchiolar and alveolar region. The airways are covered by the airway surface liquid, consisting of a bi-phasic layer [6] – due to illustrative purposes only the upper layer (mucus or surfactant) is shown. The Figure was adapted and simplified from [28] and was created with BioRender.

1.3 Lung Defence Mechanisms

The whole lung surface is covered by an fluid layer called ELF [38]. The thickness of this fluid layer decreases from 8 µM in conducting airways to 0.07 µM in respiratory airways [6]. It humidifies the airways and prevents a dehydration of the airway cells, whereas in the lower airways, it reduces the surface tension and prevents the alveoli from collapsing. The fluid layer is also considered as line of defence against inhaled particles, e.g. due to the presence of antioxidants [6, 8, 39]. The composition of the ELF differs between the upper and the lower airways [6]. Within the conducting airways, the ELF consists of an aqueous (periciliary) layer, covering the cells with a mucus layer on top. This mucus layer has a gel-like appearance and consists of a complex mixture of water, glycoproteins (mucins), lipids, salts and cell debris. Goblet cells and submucosal glands secrete different mucins [40-43]. For inhaled particles, the mucus layer is the first barrier to overcome in the upper airways [41]. It is further postulated that lipophilic drugs can show non-specific binding to mucus components, which might thus potentially reduce their permeability [44]. Further physicochemical properties such as solubility, size and charge were described to affect the permeation of a particle across the mucus layer [41]. A further specialised defence mechanism of the upper airways is the so-called mucociliary clearance or mucociliary escalator. In this process, secreted mucus is transported by continuous beating of the cilia from the ciliated epithelial cells towards the oesophagus. There, the mucus is either swallowed or coughed up. This removal mechanism is an effective protection against particles [29, 40].

In the alveolar region, the surface is covered by the so-called alveolar subphase fluid, which consists of a watery phase with a surfactant layer above [45]. The surfactant is produced by the alveolar pneumocytes type II within their lamellar bodies. It consists of a mixture of surface-active lipids and proteins with phospholipids making up 80 % of all constituents. Around 10 % are proteins including the four surfactant associated proteins SP-A, SP-B, SP-C and SP-D [46, 47]. The SP-B and SP-C have been described to be essential for reducing the alveolar surface tension, whereas SP-A and SP-D appear to contribute to host defence mechanisms [48].

The macrophages located in the alveoli are innate immune cells [37]. When they encounter pathogens, they trigger immune responses. They are capable of engulfing inhaled particles, transporting their cargo to the lymph nodes, and thus can contribute to the particles' clearance [49]. It has been shown that drug molecules, predominantly when being cationic and amphiphilic can accumulate in the lysosomes of alveolar macrophages due to their physicochemical properties and cause phospholipidosis (extensive accumulation of phospholipids) [50]. For macrolide antibiotics, intracellular accumulation in alveolar macrophages is required for effectively targeting and killing intracellular replicating bacteria

like Legionella [51, 52]. An *in vitro* study using isolated human primary alveolar macrophages demonstrated that the macrolide antibiotic clarithromycin showed extensive intracellular accumulation [53].

1.4 *In Vitro* Models Mimicking the Human Lung Epithelium

The use of *in vitro* systems is well established within the drug development to investigate pharmacokinetic processes, including absorption, distribution, metabolism and excretion (ADME) of new chemical entities. This allows, especially in early discovery, to test compounds in a high throughput manner [54]. Moreover, the use of *in vitro* models contributes to the so-called 3R principles to replace, refine and reduce animal experiments [55]. In terms of assessing drug's permeability across an epithelial barrier, Caco-2 cells are the most widely used in drug discovery. Caco-2 cells, derived from a human colon adenocarcinoma, were described to capture para-/transcellular diffusion and active transporter mediated processes, where reported permeability values showed a good correlation with human intestinal absorption data [54, 56, 57]. Further cell lines, that are well established in drug development to measure the *in vitro* permeability of drugs are the canine kidney epithelial cell line MDCK-II and the porcine kidney epithelial cell line LLC-PK1 [58, 59]. Considering permeability processes of drugs across the human lung epithelium, the tracheo-bronchial Calu-3 cell line is mainly used [60, 61]. It needs to be noted that Calu-3 cells are of tumour-origin and differentiate into a phenotype that is representative of the upper airways [41]. Therefore, they might not necessarily capture drug permeability processes within the alveoli, which are considered to be the predominant space for pulmonary drug absorption due to the larger surface area compared to the bronchial region [6]. To date, there is no study available that directly compared the permeability of a compound set across the bronchial versus the alveolar epithelium *in vitro* [20].

A variety of human cell models is available to study pulmonary drug disposition *in vitro*, including cell lines, primary cells and co-cultures. However, not all of these cells are considered suitable to study the transport of small molecules across the pulmonary epithelium [20, 62]. Primary cells, isolated from all regions of the lung, are available and have been used to study drug permeation and transport processes across the pulmonary epithelium [20, 63]. These cells have been described to differentiate into a native-like pulmonary epithelium once cultured on semi-permeable inserts. Primary tracheo-bronchial epithelial have been showing cilia beating and mucus production, whereas isolated alveolar pneumocytes type II trans-differentiated into type I-like alveolar cells with an increase in calveolin-1 and a decrease in surfactant-protein C, closely mimicking the *in vivo* phenotype [64, 65]. However, their use is often restricted to a few passages only (i.e. for primary bronchial cells) as the cells undergo

senescence, whereas primary alveolar type II cells do no proliferate *in vitro*. Due to the complex isolation processes or high costs of commercially available primary cells, this limits the high throughput. Furthermore, the variability across different donors needs to be accounted for, which can limit experimental reproducibility [25, 41, 66].

Pulmonary epithelial cell lines have been established either by viral immortalisation of primary cells or by isolation from tumours [66]. Cell lines bear the advantage of having an almost unlimited lifespan and rely on known culture techniques. Moreover, compared to primary cells, no donor-to-donor variability has to be considered and there is no need for a continuous supply of fresh tissue and sometimes complex isolation processes. Nevertheless, due to their immortalisation or cancerous origin, it remains unclear to what degree a cell line is mimicking the physiological phenotype [41, 67].

For assessing the permeability or the susceptibility of drugs to efflux transporters, cells are typically cultured on semi-permeable membrane inserts [59]. When studying permeability processes in cells derived from tissues like the intestinal epithelium, the medium (liquid) is usually kept on both sides of the insert membrane, which is called submerged condition or liquid-covered condition (LCC) [68, 69]. In order to more closely mimic the *in vivo* situation, human airway epithelial cells can be exposed to the so-called air-liquid interface (ALI). After seeding onto to the porous membrane inserts, the cells are grown under liquid coverage for a couple of days until they reach confluence. Then, the medium is removed from the apical compartment (‘airlifting’), whereas the medium on the basolateral side is kept [28, 67, 70]. This is illustrated in Figure 3.

In order to be a suitable model to study drug transport and permeability processes *in vitro*, the cells need to form a tight, confluent and polarised layer. The tightness of this barrier is achieved by the formation of tight junctions, which restrict paracellular transport [71, 72]. To verify the integrity of the cell layer *in vitro*, transepithelial electrical resistance (TEER) can be measured using a volt-ohm meter as a non-invasive technique [73]. The TEER is often measured directly before and after an experiment [74]. Values for TEER above 250 $\Omega*cm^2$ are typically accepted as threshold for a tight barrier formation [75]. Since TEER measurement is sensitive to different factors such as temperature, a further option to assess monolayer integrity is the determination of the apparent permeability of paracellular markers such as mannitol, dextran or Lucifer Yellow (LY) across the cell layer. Low apparent permeability coefficients confirm the formation of a tight cell layer [73, 76, 77]. A threshold of 25 nm/s has been proposed for LY [78].

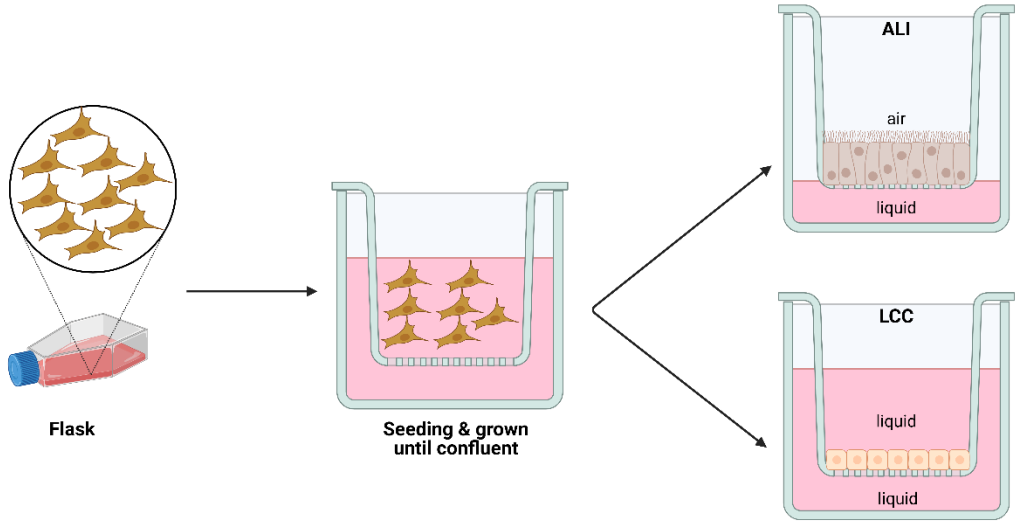

Figure 3. Comparison of the Air-liquid interface (ALI) and the Liquid-covered condition (LCC) of culturing lung epithelial cells. Once the cells reach confluence within the flask, they are passaged and seeded onto semi-permeable membrane inserts with keeping the medium on both sides of the membrane. Once the cells reach confluence within the membrane, they can be air-lifted by removing the medium on the apical side and lowering the total amount of medium on the basolateral side (i.e. ALI culture). If the medium is kept on both sides of the membrane during the whole culturing process, this is referred to as LCC. The cells in this illustration mimic the human tracheo-bronchial epithelial cell line Calu-3, that has been described to differentiate into a pseudostratified epithelium with microvilli when cultured at ALI. In contrast, a cuboidal epithelium was observed when cultured at LCC [79]. The Figure was created with BioRender.com.

The following section will provide more in-depth information around the lung epithelium-derived cell lines and primary cells, which were in scope of this thesis project. They are depicted in Figure 4. However, there are several different cell line and primary cell models described in literature, that were characterised to investigate pulmonary transport processes. Review articles by Richter & colleagues and Selo & colleagues provide a broad and detailed overview on further models, including co-culture systems [20, 80].

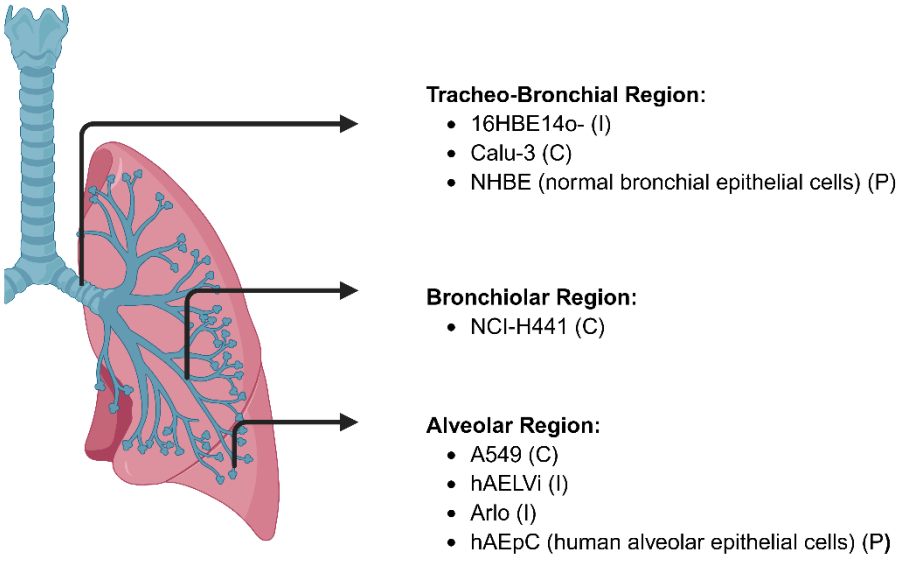

Figure 4. Summary of human epithelium-derived cell lines and primary cells, that were in scope of this thesis project. The Figure provides an overview of the cell origin and whether they are tumour-derived cell lines (C), immortalised cell lines (I) or primary cells (P). The Figure was created with BioRender.com.

1.4.1 Tracheo-Bronchial Region

The 16HBE14o- cell line has been derived by viral immortalisation of human primary bronchial cells using a SV40 large T antigen transformation [81]. At ALI, measured TEER values were relatively low with values ranging from 130 to 250 Ω*cm^2, whereas at LCC, TEER values in the range up to 800 Ω*cm^2 have been reported [82, 83]. Cross sections of the cell layers have revealed that the cell layer consisted of a partially monolayer and multilayer (up to five) at LCC, whereas at ALI an over ten-cells thick layer was formed. It has been proposed that a certain amount of liquid on the apical side of the insert may be needed in order to mimic the 'mucus' and thus enable 'normal' cell development [82]. The 16HBE14o- cells have been shown to express functional active efflux and uptake transporters [84, 85].

Calu-3 cells have been originally derived from a lung subepithelial gland adenocarcinoma patient and are of bronchial submucosal gland origin [41]. The Calu-3 cells develop into an *in vivo*-like pseudostratified epithelium and show some secretory activity when cultured at ALI, where the cell layer is predominantly a monolayer but in parts, multicellular. Under submerged conditions, the cell layer is classified as a simple cuboidal-like epithelium and thus less relevant compared to the *in vivo* bronchial phenotype [79]. Reported TEER values were ~ 300 Ω*cm^2 for ALI and > 1000 Ω*cm^2 for LCC cultures [86]. Different culture conditions such as the culture interface (ALI vs. LCC) or culture time appeared to affect the morphology, barrier formation and the expression of drug transporters [79]. Calu-3 cells were shown to express numerous functional uptake and efflux transporters [87, 88].

Primary normal human bronchial epithelial cells (NHBE) are isolated from non-diseased bronchial tissue [89]. When culturing these cells on semi-permeable filter inserts at ALI, they differentiate into a physiological relevant phenotype including mucus production and cilia beating. The differentiated epithelial cell layer is composed of different epithelial cell types including ciliated cells, goblet cells and basal cells, which closely represent the *in vivo* airway composition of the bronchial region [90]. TEER values at ALI have been reported to range from ~ 750 to 950 Ω*cm^2 ,whereas at LCC TEER values above 1500 Ω*cm^2 have been measured [89, 91]. However, cytometric analysis has revealed that NHBEs form multilayers at ALI, which is not representative of the *in vivo* lung physiology [92]. Besides, it has been shown that the use of different media has an impact on TEER and cell morphology during differentiation at ALI [65].

1.4.2 Bronchiolar Region

NCI-H441 cells were firstly retrieved by isolation of the pericardial fluid from a patient with pulmonary adenocarcinoma [93]. The cells showed properties of bronchiolar club cells as well as type II alveolar pneumocytes. TEER values of around 300 Ω*cm^2 at ALI and of around 1000 Ω*cm^2 under submerged conditions (i.e. LCC) have been reported [94]. To achieve these values, the addition of dexamethasone is needed, without the glucocorticoid, TEER values < 100 Ω*cm^2 have been measured [95, 96]. Dexamethasone is described to up-regulate claudin 8, a tight junctional protein, and thus likely contributes to higher TEER values if supplemented to the culture medium [97]. Further, NCI-H441 cells appear to show active influx as well as efflux transporters [94].

1.4.3 Alveolar Region

A549 is an adenocarcinoma-derived cell line from the alveolar region, having morphological hallmarks as seen for type II alveolar pneumocytes like lamellar bodies [41, 98]. These cells are not capable of forming a tight barrier, since they lack functional tight junctions. TEER values < 100 Ω*cm^2 at ALI and LCC have been reported [96, 99]. For this reason, the cell line is not well suited to investigate drug permeation studies and attention must be paid, when permeability coefficients were reported in A549 cells [20]. The A549 cells have been shown to express functional active efflux and influx transporters [100, 101]. Moreover, they have been extensively used to study nanoparticle interactions, respiratory toxicity or pulmonary drug metabolism [102-104].

An immortalised human alveolar epithelial cell line, ‘hAELVi’, has been established by isolating human alveolar type II epithelial cells and following immortalisation by lentivirus transfection. This cell line resembles a morphological alveolar type I-like phenotype [105]. When cultured at ALI or LCC, TEER values of 1000 to 2000 Ω*cm² have been reported [105-107]. Due to the heterogenous nature of the hAELVi cells, differences in barrier properties have been reported across laboratories [107]. The hAELVi cells have been found to express functional active efflux transporters [108].

More recently, a monoclonal cell line ‘Arlo’ has been derived from the polyclonal hAELVi cells via single-cell printing. Arlo has been described to display even a more pronounced barrier function with a TEER of 3000 Ω*cm² at ALI and around 2000 Ω*cm² at LCC. RNA bulk sequencing has revealed the expression of both efflux and uptake drug transporters [107].

Type II alveolar pneumocytes can be isolated from the distal lung of human donors and trans-differentiate in culture into predominantly type I-like alveolar pneumocytes (hAEpC) [109]. TEER values of ~ 1600 Ω*cm^2 and 1400 Ω*cm^2 have been reported at ALI and LCC,

respectively [107]. However, the isolation and purification process of these primary cells is quite complex and limits high-throughput [110]. In terms of drug transporter expression, hAEpC have been shown to express functional efflux and uptake transporters [111, 112].

1.5 *In Vivo & Ex Vivo* Models to Study Pulmonary Drug Disposition

In vivo studies play a crucial role in drug development, especially in the preclinical phase, to investigate the safety and efficacy of new chemical entities before testing in humans. Furthermore, *in vivo* studies are conducted to investigate organ toxicity and pharmacokinetic processes including DDIs [113-115].

The first *in vivo* studies to investigate pulmonary absorption of compounds after an intratracheal administration have been reported in 1970s and 1980s by Schanker and colleagues, focussing on the rat [116, 117]. Rodent models (i.e. mice or rats) are most commonly used. Reasons for this include lower costs compared to larger animals, the easier handing as well as the fact that less consumables and chemical substances are needed. Potential limitations include species differences in the airway composition (compared to humans) and the fragility of rodents' lungs making surgical procedures technically challenging [20]. For assessing pulmonary drug disposition processes *in vivo*, drugs are typically administered via inhalation to the respiratory tract under anaesthesia [118]. An appropriate vein or artery is then catheterised, which allows the collection of multiple blood samples at various time points within the same animal to determine drug concentration over time profiles. Based on this, pulmonary absorption kinetics can be calculated [119, 120].

To investigate drug transporter-mediated processes *in vivo*, transgenic transporter-knockout rats and mice were established, allowing the evaluation of the contribution of a single transporter to absorption, distribution and elimination processes [115]. At the end of the last century, Alfred Schinkel and colleagues were the first who successfully bred transporter-knockout mice that showed the same viability as wild type animals [121]. As a caveat of these models, the knockout of one transporter protein can result in expression changes of other proteins compared to wild type animals [122].

Over the last years, the use of transporter knockout animals in combination with a non-invasive, quantitative and three dimensional nuclear imagining approach has grown in popularity to investigate the contribution of drug transporters on pharmacokinetic processes within different tissues, including the lung [123, 124]. This technique is based on positron emission tomography (PET), where a radiolabelled drug is administered and its distribution across the tissues and organs is evaluated. The radiotracers are often labelled by fluorine-18 [^{18}F] or carbon-11 [^{11}C], which emit positrons while decaying. Limitations of this

approach are the short half-life of [^{11}C] with 20.4 min and the circumstance that only total radioactivity can be measured, i.e. it is not possible to distinguish between parent drugs and their metabolites [123, 125, 126].

Previous studies, that have aimed to investigate pulmonary absorption processes and the contribution of drug transporters at the level of the rodent lung epithelium, often used the isolated perfused lung (IPL), an *ex vivo* model [127, 128]. In brief, animals, mostly rats, are euthanised, the lungs are separated from the systemic circulation and an artificial perfusion through the pulmonary blood vessels is established. The lung is isolated and kept in an artificial thorax-like system, where further artificial ventilation and perfusion are applied. The compounds of interest are then administered into the airways via the tracheal opening and samples are taken from the perfusate to assess pulmonary absorption parameters. This technique holds some limitations such as a lifetime of only 2 to 3 h for proper lung functionality, risk of oedema formation and the need for sophisticated training of surgeons. Moreover, parts of the tracheo-bronchial region can be accidently removed due to the isolation and preparation procedure [119].

Literature examples, where the functional activity of pulmonary drug transporters was assessed by *in vivo* by PET imaging or IPL are described in section 1.9. In alignment with the 3R principle to reduce, refine and replace animal experiments, many efforts are currently made to develop and optimise *in vitro* and *in silico* models, to make them more ‘human-relevant’ and minimise the use of animals within research and drug development [129].

1.6 Physiologically based Pharmacokinetic Modelling (PBPK) – its Definition and its Use in Predicting Pulmonary Drug Disposition

The use of modelling and simulation approaches within the drug discovery and development has grown in utility over the past decades [130]. Mathematical pharmacokinetic (PK) models can be used to assess the concentration over time profile of a drug in the plasma or the tissue of interest. These so-called classical PK models consist of a central plasma compartment that is connected via rate constants to a peripheral compartment. Physiologically based pharmacokinetic (PBPK) models are similar to PK models, however they take physiological properties into account, which parameterise the model [131]. A PBPK model consists of several compartments, which typically include the intestine, liver, kidney, brain, heart, lung, adipose, muscle, bone, skin and spleen tissue. All are connected via a blood circulation [132]. This is depicted in Figure 5. Due to the connection of all tissues within a PBPK model, with processes being defined by mathematical equations, it can be used as mechanistic and quantitative framework for simulating and investigating the absorption, distribution, metabolism and

elimination of chemical entities. These processes can be simulated for human as well as for various preclinical species [131].

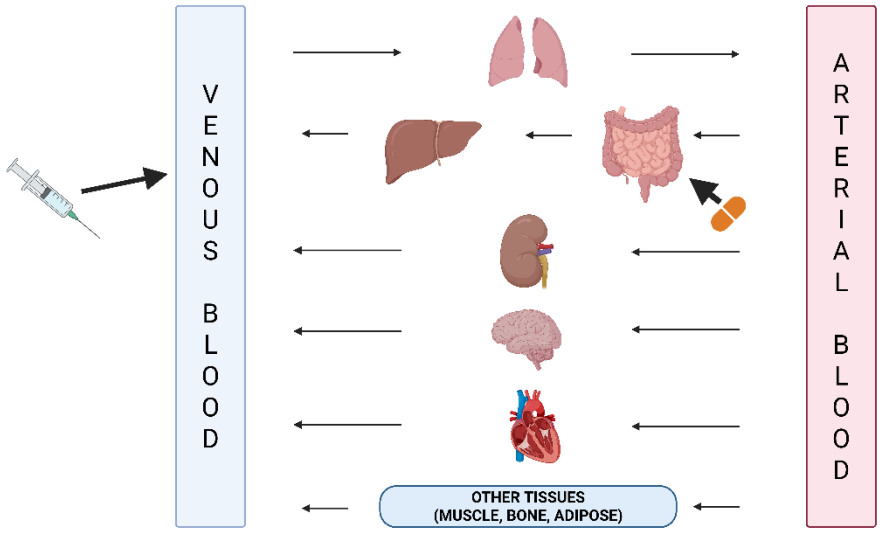

Figure 5. Simplified schematical representation of a physiologically based pharmacokinetic (PBPK) model. The compartments are depicted as organs, which are all connected to each other via a blood circulation. The oral (via the intestine) and parental drug administration (via an intravenous injection) is shown. The image was adapted and simplified from [133]. The Figure was created with BioRender.com.

To set up a PBPK model, information from different 'building blocks' is needed to enable the simulation of ADME processes. These include drug physicochemical properties (e.g. molecular weight or lipophilicity) and drug-related biological parameters (such cellular permeability or degree of binding to plasma proteins), which are either experimentally derived or predicted. Furthermore, anatomical/physiological properties of the organism (like blood flow rate and organ surface area) and information on the drug dosing regimen and formulation are required [134]. Within drug development, PBPK modelling is used for various applications: simulation of preclinical and clinical PK profiles including the extrapolation across species, prediction of DDIs and special population PK simulations (in paediatrics, elderly, disease) [135]. Due to the availability of commercial software to run PBPK simulations with a graphical interface such as GastroPlus™ or Simcyp™, the complexity in setting up a PBPK model from scratch has decreased [131]. This is also reflected in the rising number of PBPK models being part of application review files of new drugs, that were approved by the US Food and Drug Administration (FDA) between 2019 and 2023. Out of the 243 novel approved drugs within this time period, 74 application files contained PBPK data, with more than 50 % being attributed to enzyme-mediated DDIs and 18 % to transporter-mediated DDIs [136].

The use of PBPK models to investigate the fate of an inhaled drug within the lung or the prediction of ELF concentrations after a systemic drug administration were described in literature. As an example, a detailed human PBPK model was set up for inhaled nemiralisib, where the lung was divided into an extra-thoracic, thoracic, bronchiolar and alveolar

compartment, which allowed the simulation of drug absorption in the different lung compartments. The model has also been used to predict the systemic concentration after inhalation by taking pulmonary absorption and oral swallowing into account and was showing a good fit to the observed data [137]. Moreover, PBPK modelling has been used to predict the concentration of anti-tuberculosis drugs within the lung tissue of healthy and tuberculosis-infected individuals by extrapolating from preclinical species [138]. Further PBPK models were established to simulate antibiotics concentration within the ELF and alveolar macrophages, after a drug administration via the systemic circulation. It has been reported that parameters such as the pH of the ELF, the presence of active transporters or enhanced lysosomal trapping within the lung tissue have a tremendous impact on simulated ELF concentrations [139-141]. Overall, *in silico* models such as PBPK modelling appear to be a valuable tool to predict local pharmacokinetic processes [142].

1.7 ADME Processes affecting the Drug Transport across the Lung Epithelium

1.7.1 Permeability

Drugs, that are administered via the systemic circulation, need to permeate across the air-blood barrier to reach their site of action within the ELF or the alveolar macrophages. Thus, they have to permeate across two cellular membranes: the alveolar endothelium and the alveolar epithelium [15]. Both membranes are separated by the interstitial space, which is fluid-filled and contains cells such as fibroblasts and extracellular matrix networks including collagen fibres [143]. The alveolar endothelium has been described to consist of two cell types: aerocytes, that contain pores and are specialised for the gas exchange, and general capillary cells, that act as progenitor cells [144]. Due to the vasculature fenestration, it has been stated that molecules up to 1000 Da are permitted to passively diffuse between the cells of the pulmonary endothelium [15]. Therefore, the alveolar epithelium is considered to be the permeability barrier for drugs in the lung [29].

There are several pathways for drugs to permeate across biological cell membranes: via passive permeability (paracellular or transcellular) or by active transport processes (efflux or uptake) [145]. An overview of these processes is depicted in Figure 6.

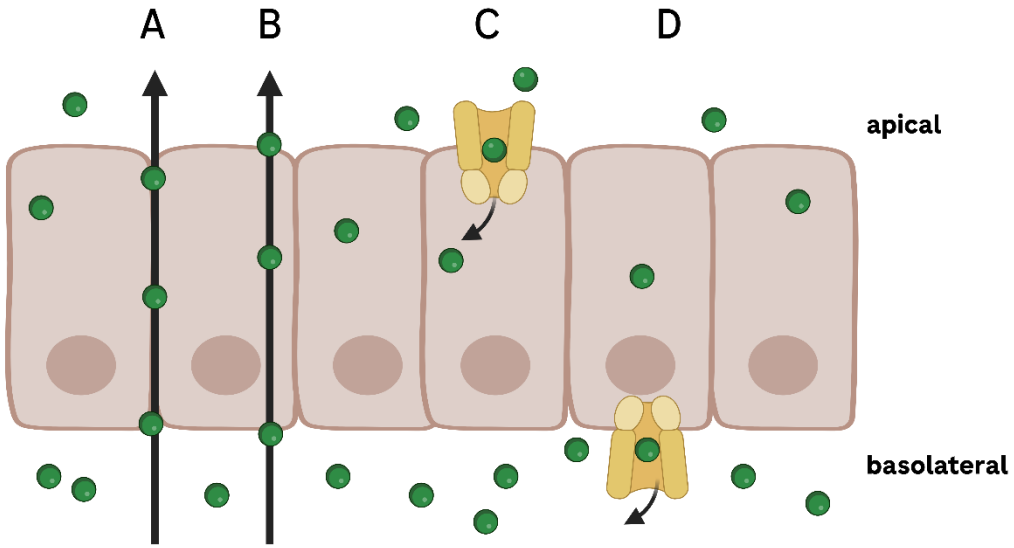

Figure 6. Overview of the different permeation pathways across a biological membrane, assuming a concentration gradient from basolateral to apical side. The following processes are depicted: (A) passive paracellular diffusion across the intercellular pores, (B) passive diffusion across the transcellular route, (C) active transporter-mediated uptake and (D) active transporter-mediated efflux. Efflux and uptake transporters can be found on both sides of the cell membrane of the lung epithelium [146]. For illustrative purposes, they were added to one membrane side only. The Figure was adapted from [20] and created with BioRender.com.

Passive diffusion has been described to be the major route of drugs crossing biological membranes. The passive diffusion processes follow a concentration gradient, with hydrophilic molecules permeating predominantly via the paracellular route and lipophilic via the transcellular route [145, 147]. The paracellular transport describes the diffusion of molecules between the individual cells via the intercellular pores, where the junctional complexes are located that consist of tight junctions, adherent junctions, gap junctions and desmosomes [148, 149]. Charged, hydrophilic and low-molecular weight molecules, including ions typically permeate via this route. The paracellular transport can be restricted due to the presence of the tight junction proteins, which span the pores and include proteins like claudin or occludin [150, 151]. The transcellular transport describes the permeation of compounds across the epithelial cell membrane via the phospholipid layer. The rate of transcellular permeability appears to be governed by the compound's molecular weight and lipophilicity. This route is predominantly taken by lipophilic and uncharged molecules. [145, 152]. The molecules' charge is typically determined at pH 7.4, which is considered as the physiological pH in plasma. Depending on the acid-base dissociation constant (pKa) of the molecule and the pH of the environment, a minor change in pH can directly affect the molecule's passive permeability [71, 153].

Active transporter proteins, being expressed in the cell membrane can facilitate the efflux or uptake of drug molecules across the transcellular route [146]. These are energy-dependent processes, where both primary and secondary active transport exists.

Primary active transporters use the energy of adenosine triphosphate (ATP) hydrolysis to transport molecules against a concentration gradient [154]. Secondary active transporters use ion gradients and electrochemical potential differences to facilitate the transport of their substrates [155]. Further information on the drug transporter proteins within the pulmonary epithelium is detailed in section 1.9.

1.7.2 Binding to Plasma Proteins and ELF Components

Another factor to be considered, when investigating distribution processes across the lung epithelium is the degree of drug binding to plasma proteins or components of the ELF [15, 156]. The free drug hypothesis states that only the unbound fraction can cross biological barriers and thus is an important determinant, when investigating pharmacokinetic processes [157]. For drugs administered via the systemic circulation, the extent of drug binding to plasma proteins and lipids defines the amount of drug, that is free to permeate into the tissues [158]. Albumin, α_1-acid glycoprotein and lipoproteins are considered the most relevant plasma proteins in terms of drug binding [159]. The routine measurement of protein binding is well integrated into the drug screening cascade [160].

It has previously been assumed that the unbound drug fraction within the ELF is 100 % free due to a negligible amount of proteins [161]. However, recent studies reported that drugs can show strong binding to lipids and proteins that are present within the ELF or the lung tissue [156, 162, 163]. A study by Keemink and colleagues measured the unbound fraction of 85 antibiotics within a simulated ELF (sELF), that consisted of the nine major components of the human ELF. They reported that especially basic antibiotics showed an increased binding to components of the sELF (average unbound fraction of 17 %) likely due to lipid binding. Further, a poor correlation was observed when comparing the unbound fraction of antibiotics in sELF versus plasma [156]. This finding is of particular importance for antibiotics, as these molecules often carry a positive charge, which appears to be an important pharmacophore when targeting gram-negative bacteria [164]. A further *in vitro* study has reported that the novel antibiotic lascufloxacin showed an extensive binding to phosphatidylserine, a phospholipid found in the surfactant [163].

1.8 Active Efflux Transporters

1.8.1 Membrane Transporters

Membrane transporters are proteins, which are embedded into the lipid bilayer of the cell membrane and can facilitate the efflux or uptake of their substrates out/into the cells. Both xenobiotic and endogenous molecules can be transported [18]. Efflux transporters protect the cells by extruding potentially toxic compounds, whereas influx transporters are involved in the uptake of vital nutrients. Therefore, these proteins play an important role in tissue homeostasis [165, 166].

Their mediated transport processes can be either passive or active, where passive transporters (i.e. ion channel and carrier proteins) do not require energy and transport their substrates along a concentration gradient (facilitated diffusion) [167]. In contrast, active transporter proteins can facilitate their substrates' translocation against a concentration gradient, which requires energy [168].

Three superfamilies of active membrane transporters are being considered relevant to significantly affect the absorption, distribution and elimination of xenobiotics in both human and several animal species. These include ABC, solute carrier (SLC) and solute carrier organic anion (SLCO) transporters, whereas the ABC transporters mainly act as efflux transporters and the SLC/SLCO proteins contribute to cellular uptake of their substrates [18, 169]. Members of these transporter families are expressed in the epithelia and endothelia of various organs including the intestine, liver, kidney and the blood brain barrier [170].

The ABC transporters are primary active transporters that are capable to extrude a broad and diverse range of structurally unrelated molecules across the cellular membrane against a concentration gradient [166]. Prominent members of this protein family include the multidrug resistance protein 1 (MDR1, also known as P-glycoprotein (P-gp)), multidrug resistance associated proteins (MRPs) and breast cancer resistance protein (BCRP) [169]. The broad substrate specificity of both MDR1 and BCRP has been reflected in the fact that 68 % and 43 % of all approved drugs by the FDA between 2017 to 2021 were classified as *in vitro* substrates of MDR1 and BCRP, respectively [171].

The SLC family is classified as secondary active transporters. Organic and inorganic, as well as charged and uncharged substrates are transported by this family. It comprises organic cation transporters (OCT), organic anion transporters (OAT), novel organic cation transporters (OCTN) and peptide transporters (PEPT) [155, 169]. The SLCO family has been reclassified in 2004 and includes the organic anion transporting polypeptides (OATP) superfamily and is transporting predominantly amphiphilic organic anions [172].

Numerous DDIs with regards to these drug transporters have been reported in literature, where the pharmacokinetic profile of a victim drug can be significantly changed due to the inhibition or induction of a transporter protein [173]. Therefore, it is a substantial part during drug development to assess, whether new chemical entities are substrates and/or inhibitors of drug transporters [18].

1.8.2 ABC Efflux Transporter

There are 48 ABC transporter proteins found in human, which are separated into 7 main subclasses according to their sequence homology. The naming of these classes is according to their gene code from ABCA to ABCG. ABC transporters, that contribute to active efflux of xenobiotics out of the cells are mainly found in the ABCB, ABCC and ABCG family. Examples for these are MDR1 (ABCB1), MRP1 (ABCC1) and BCRP (ABCG2) [166].

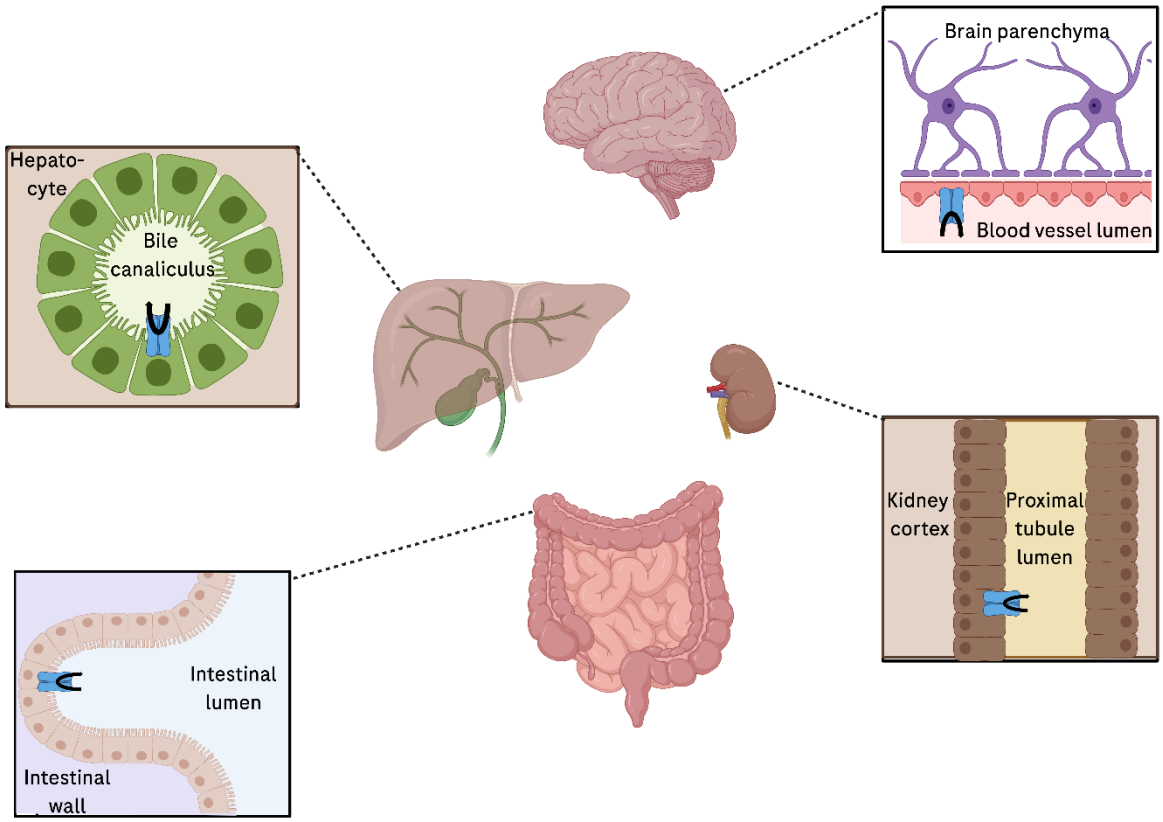

Figure 7. Overview of ABC efflux transporters' spatial expression in various organs of the human body. The efflux transporters are depicted as blue icons with the direction of mediated efflux illustrated by a black error (symbolising P-glycoprotein that is shown as an example ABC transporter). The illustration was adapted from [174] and modified according to [18]. The Figure was created with BioRender.com.

The ABC transporters play a pivotal role in shaping the pharmacokinetic processes of their substrates [18]. In terms of human clinical data, both MDR1 and BCRP are considered relevant due to their vast tissue expression and number of reported DDIs [18]. They are expressed in the intestine contributing to limiting drug absorption, at the blood brain barrier, where the limit the distribution of xenobiotics into the brain tissue and in the liver and kidney, where they can enhance the hepatobiliary and renal clearance [175]. This is illustrated in Figure 7. Moreover, ABC transporters were reported to be expressed in tumours, contributing to chemoresistance [176]. Their expression was also reported in the human lung epithelium, whereas the translation and relevance of these *in vitro* findings to clinical data is still lacking [177]. Further details on pulmonary ABC transporters' expression are described in section 1.9.

1.8.3 Assessing ABC Transporters' Efflux *in vitro*

Bidirectional transport studies can be conducted to investigate, whether an expressed ABC transporter protein is functionally active *in vitro*. The cells of interest are seeded onto semi-permeable inserts and are cultured until they form a polarised monolayer, with drug transporters expressed at the apical or basolateral side of the membrane [178]. Depending on the cell type, this can take a couple of days or weeks, like for the Caco-2 cells, where a culture period of 21 days on the inserts is recommended [179]. Moreover, an important prerequisite for these kind of studies is that the cells form a tight cell layer with the formation of tight junctions, restricting paracellular transport and thus separating apical and basolateral compartment from each other [20]. This is often assessed by measuring TEER or by co-incubation of a paracellular marker during the experiment such as dextran [180].

The functional activity of an ABC transporter is then assessed by measuring the permeability of a transporter substrate across the cell layer in a bidirectional manner. This is defined as apparent permeability (P_{app}), which quantifies the amount of drug that crosses the cell membrane in a defined time period. Both the absorptive permeability from apical to basolateral side (P_{app} AB) and the secretory permeability from basolateral to apical side (P_{app} BA) are measured [87, 181]. This is depicted in Figure 8. If there is an asymmetry in transport, i.e. the secretory permeability is two-fold higher than the absorptive, this indicates the presence of active efflux on the apical side. This is reflected in the so-called efflux ratio (ER) that is calculated by dividing P_{app} BA by P_{app} AB. According to the guidance rules from regulatory authorities (FDA and European Medicines Agency (EMA)), a compound is classified as substrate of active efflux on the apical side if the ER exceeds the threshold of two ($ER \geq 2$). Further, the ER needs to decrease at least by 50 %, when measuring the bidirectional P_{app} in the presence of a transporter-specific inhibitor. If these criteria are not met, the molecule is classified as non or poor transporter substrate. The cells in scope of these guidance rules

included ABC transporter-overexpressing cells, as well as epithelial cells that form a polarised monolayer, when grown on semi-permeable inserts like Caco-2 [18].

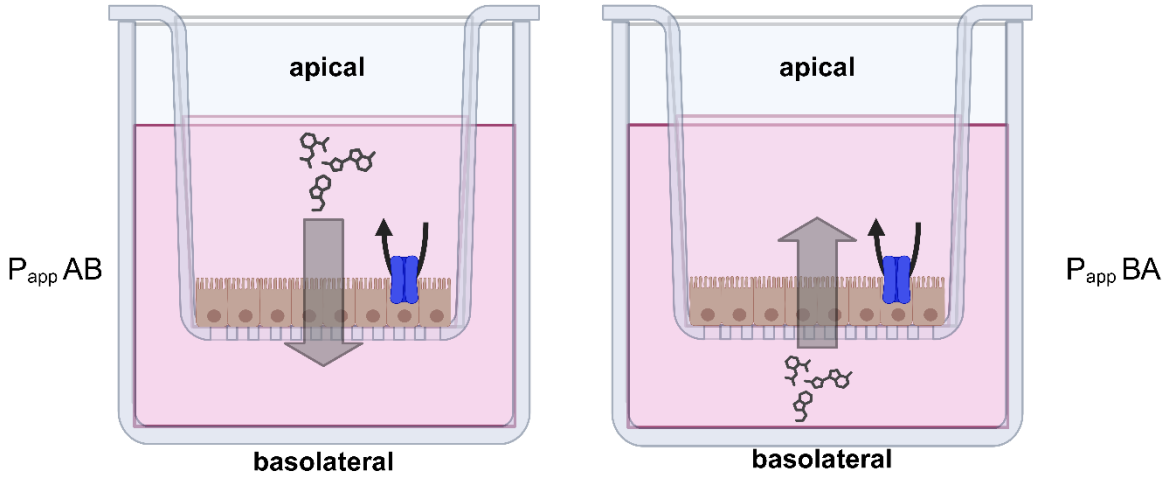

Figure 8. Experimental setting of bidirectional transport studies aiming to assess, whether a compound is a substrate of active efflux transporters. The cells are seeded onto semi-permeable filter membranes, where they form a polarised and tight monolayer. The blue icon symbolises an active efflux transporter on the apical site of the cell membrane, pumping its substrates to the apical compartment. The test compound is either added to the apical compartment to measure its apparent permeability from apical to basolateral compartment (P_{app} AB) and vice versa to the basolateral side for assessing its apparent permeability from basolateral to apical side (P_{app} BA). The Figure was created with BioRender.com and adapted from [182].

To flag a compound as substrate of active efflux transporters, which are expressed on the basolateral side of the cell membrane, an inverse of the ER can be determined. This uptake ratio (UR) can be calculated by dividing the P_{app} AB by the P_{app} BA. This concept has been applied to investigate the functional expression of MRP1 on the basolateral side of the pulmonary epithelium *in vitro* [87, 108].

A further experimental approach to assess the functional activity of efflux transporters measures the intracellular accumulation of a transporter substrate in the absence and presence of a transporter inhibitor. For these kind of experiments, the cells do not necessarily need to be cultivated on semi-permeable inserts but can be cultured in well plates [183, 184]. This method has been used to measure ABC transporters efflux within the A549 cell line, that is not capable of forming a tight barrier and thus not suitable to be tested in bidirectional transport studies [185, 186].

1.9 ABC transporters within the Lung Epithelium – *In vitro* & *In vivo*

Both MDR1 and BCRP are expressed in various tissues of the human body and are well characterised to interact with many drugs, leading to DDIs - therefore, the investigation of new drug molecules for their substrate and inhibition potential against MDR1 and BCRP is required by health authorities [18]. However, the contribution of MDR1 and BCRP on pulmonary

pharmacokinetic processes in humans is not well known [177]. Interestingly, MRP1 has shown higher protein expression levels than MDR1 and BCRP within the human lung epithelium [187]. No clinically relevant interactions of drugs with MRP1 were reported in terms of drug absorption or elimination pathways, although a number of drugs appears to be transported by MRP1 (mainly chemotherapeutics). There is currently no recommendation from health authorities on screening new drugs for their interaction with MRP1 [18, 188].

In terms of spatial expression in the human lung epithelium, both MDR1 and BCRP have been reported to be expressed on the apical ELF-facing side [146, 177]. In contrast, MRP1 has been localised on the basolateral blood vessel-facing side [177], as depicted in Figure 9.

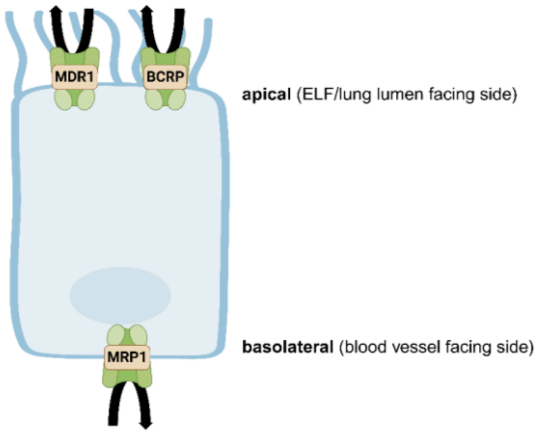

Figure 9. Graphical representation of the proposed spatial expression of ABC transporters within the human lung epithelium. Multidrug resistance protein 1 (MDR1) and Breast cancer resistance protein (BCRP) have been reported to be expressed on the apical lung lumen-facing side, whereas Multidrug resistance associated protein 1 (MRP1) has been described to be expressed on the basolateral blood vessel-facing side of the cell membrane [177]. The Figure was created with BioRender.com and adapted from [182].

The following subsection provides some background on MDR1, MRP1 and BCRP and summarises their expression and functional activity within cells derived from the human upper and lower airway epithelium. It focuses on summarising the literature findings for the lung epithelial cells, that were in scope of this thesis, and which have been described in section 1.4 (cell lines and primary cells). Furthermore, the data from *in vivo* studies, which investigated the presence of active efflux by ABC transporters in the pulmonary epithelium of rodents are presented.

1.9.1 Multidrug Resistance Protein 1 (MDR1)

The MDR1 protein is by far the most investigated and characterised ABC transporter, relevant to drug disposition [18]. MDR1 was discovered in 1976 in a Chinese hamster ovary cell line that showed cross-resistance to a number of amphiphilic drugs. It was revealed that a 170 kDa-heavy glycoprotein, embedded in the cell membrane, led to an altered drug

permeability of its substrates [189]. MDR1 has a broad substrate specificity, mainly for lipophilic and amphiphilic molecules [190]. It shows a ubiquitous expression in various human tissues including the intestine, liver, kidney, blood-brain barrier. Therefore, MDR1 is a key contributor in the body's defence against xenobiotics [174]. The expression of MDR1 has also been observed in tumours, contributing to cancer chemoresistance as several chemotherapeutics are substrates of MDR1 [191, 192].

In the human lung, lower expression levels of MDR1 compared to other organs such as liver, kidney or intestine were reported [193]. MDR1 has been described to be expressed in various cell lines and primary cells of the human upper and lower airways. This includes 16HBE14o-, Calu-3, NHBE, NCI-H441, A549 and hAEpC cells [177]. Interestingly, no MDR1 could be detected in the alveolar cell lines hAELVi and Arlo [107, 108].

It needs to be noted that differences in expression levels of MDR1 have been found across studies, even when characterising the same *in vitro* cell model. A proteomics-based mass spectrometry approach has reported the absence of MDR1 in the tumour-derived cell lines Calu-3 and NCI-H441 [194]. Whereas further studies, using Polymerase Chain Reaction or Western Blotting, confirmed the expression in both cell lines at gene and protein level [87, 94, 195]. This could arise from differences in cell culture due to non-standardised practise or the use of different detection methods that come with different sample preparation protocols and resulting different sensitivity levels [79, 196]. In order to affect the drug disposition of its substrates across the lung epithelium, MDR1 needs to be functionally active [196]. Bidirectional transport studies, as described in section 1.8.3, have usually been conducted and confirmed the presence of active MDR1 efflux within the majority of lung epithelial cells. A summary of selected *in vitro* studies is shown in Table 1. For A549, no bidirectional efflux study has been reported in literature, thus data from a cellular accumulation assay is shown.

If applying the criteria from regulatory authorities in terms of classifying a compound as a substrate of MDR1, there needs to be an at least two-fold difference in absorptive and secretory permeability (i.e. net flux ratio). For MDR1 being expressed on the apical side, this would translate to an ER ≥ 2. Moreover, in presence of a MDR1-specific inhibitor, the ER needs to reduce by a minimum of 50 % [18]. These criteria have typically not been applied, when assessing the presence of active efflux within cells of the human lung epithelium.

Considering the health authority's guidance rules for ABC transporter substrates [18], MDR1 was found to be active in the majority of lung epithelial cells, with the exception of hAELVi and a borderline result for NHBE. The fluorophore Rhodamine 123 (Rh123) has often been used as a model substrate for MDR1. This compound is not selective for MDR1 and has been described to interact with further drug transporters such as OCTs [197]. Further, verapamil used as MDR1 inhibitor, was described in literature to inhibit in addition OCTs and OCTNs

[198, 199]. Therefore, the combined use of a non-selective substrate like Rh123 in combination with a non-selective inhibitor (such as verapamil) hinders a clear understanding on the contribution of a single transporter protein [200]. This is especially a concern for cells, that are known to express a multitude of ABC and SLC transporters, like cells derived from the lung epithelium [146, 177]. In the studies summarised in Table 1, where both Rh123 and Verapamil were used in combination, the observed efflux might not solely be mediated by MDR1.

Table 1. Summary of selected *in vitro* studies assessing the presence of MDR1 efflux in cells derived from the human lung epithelium. The efflux ratio (ER) is calculated by dividing the secretory (P_{app} BA) by the absorptive permeability (P_{app} AB). The icon in the right column summarises whether the data indicates the presence of active efflux (+), the absence (-) or inconclusive data (?), based on the reported ER in absence and presence of inhibitor according to guidance rules from [18]. If no ER could be calculated (i.e. in cellular accumulation studies), non-applicable (N.A.) was added as comment. Rh123 stands for Rhodamine 123.

Cell type	Substrate	Inhibitor	Result	Presence of Efflux according to [18]
16HBE14o- [85]	Rh123	Verapamil	ER ~ 3.0, ER ~ 1.0 (+ inhibitor)	+
Calu-3 [201]	[^{3}H]-Digoxin	PSC833	ER ~ 11.4, ER ~ 1.2 (+ inhibitor)	+
NHBE [89]	Rh123	Verapamil	ER ~ 3.0, ER ~ 1.7 (+ inhibitor)	?[a]
NCI-H441 [94]	Rh123	LY335979	ER ~ 3.6, ER < 1.0 (+ inhibitor)	+
A549 [100]	Rh123	Verapamil	Intracellular concentration of Rh123 reduced within 30 min after loading by 50 %, not observed in presence of inhibitor	N.A.[b]
hAELVi [87]	Rh123	PSC833	ER ~ 1.0, ER ~ 1.0 (+ inhibitor)	-
hAEpC [111]	Rh123	Verapamil	ER ~ 3.1, ER ~ 1.0 (+ inhibitor)	+

[a] Efflux is classified as inconclusive, as the presence of MDR1 inhibitor led to a reduction in ER less than 50 %. Moreover, verapamil is no specific inhibitor of MDR1 and was reported to inhibit OCTs and OCTNs [199].

[b] Results were derived from a cellular release study, comparing the intracellular concentration of Rh123 in absence and presence of verapamil in plated cells. No intracellular release of Rh123 was observed in presence of verapamil compared to samples at t = 0 h, whereas release was observed in absence of inhibitor - thus, hinting to the presence of active MDR1 efflux in these cells. As it is no bidirectional transport study, an ER cannot be calculated.

In rats, Mdr1 is encoded by two isoforms: Mdr1a and Mdr1b [202]. Based on gene expression data, Mdr1b showed higher expression levels in the lung compared to Mdr1a (~ 6.4-fold), whereas the Mdr1a isoform appeared to be more prevalent in tissues such as the intestine, brain or kidney [203, 204]. An *ex vivo* study using the IPL model, has assessed the role of Mdr1 on the pulmonary drug disposition of four known Mdr1 substrates (Rh123, loperamide, digoxin and saquinavir). The substrates were administered via intratracheal solutions and elacridar (GF120918) was pre-dosed to chemically inhibit Mdr1. Only for Rh123 and loperamide, the concentration in the perfusate (i.e. the area under the curve of the percentage of the absorbed dose per minute) was significantly increased in presence of the Mdr1 inhibitor (3.4-fold for Rh123 and 1.9-fold for loperamide), i.e. suggesting the involvement of Mdr1 efflux of Rh123 and loperamide at the lung epithelium. Since elacridar is also a known Bcrp inhibitor, although at lower potency than for Mdr1, knock-out mice (Mdr1a/Mdr1b -/-) have been incorporated into the study and confirmed the results from the chemical knock-out experiments. It has been concluded that certain physicochemical properties might affect susceptibility to pulmonary Mdr1-mediated active efflux in rodents, with Rh123 and loperamide being more lipophilic than digoxin and saquinavir [128]. A follow-up study has tested a larger compound set using the IPL model in Mdr1a/1b knockout and wild type mice. Based on the results, the authors subdivided the compound panel in group A and B, whereas group A compounds (including digoxin) were unaffected by Mdr1a/1b knock-out and showed a similar pulmonary absorption in genetically modified and wild type animals. The group B compounds (such as Rh123) showed a significant increase in pulmonary absorption in knockout animals compared to the wild type. Analysis of the physicochemical properties has revealed that group A drugs appear to be more polar and showed a lower binding affinity to phospholipid membranes. It has been proposed that paracellular transport appears to be more pronounced in the lung and thus polar compounds (such as group A drugs) likely have a higher passive permeability (mainly paracellular). Therefore, they are less susceptible to pulmonary Mdr1 mediated efflux [205]. Further studies, that used PET tracer imaging in genetic and chemical Mdr1-knockout mice confirmed the presence of functional active Mdr1 within the rodent pulmonary epithelium and reported an expression on the apical side [206, 207].

1.9.2 Multidrug Resistance Associated Protein 1 (MRP1)

There is evidence that several members of the MRP transporter family are involved in affecting drug disposition processes within the human body [18]. MRP2, MRP3 and MRP4 were listed as potential contributors, however the clinical evidence is limited. Their expression has been reported in the intestine, liver, kidney and blood brain barrier [170].

In the human lung epithelium, especially MRP1 showed high expression levels at both gene and protein level [187, 194, 195]. MRP1 is a 190 kDa-heavy transmembrane protein and expressed in various tissues of the human body, with high expression levels reported in the lung compared to other organs like the liver or the kidney [208]. It has been described that MRP1 plays a pivotal role in the multidrug resistance of tumours due to its expression in tumour cells and the recognition (i.e. efflux) of many anti-cancer drugs, contributing to the development of chemoresistance [209]. Unlike other ABC transporter such as MDR1 and BCRP, its efflux is dependent on glutathione, that can be co-transported. Moreover, MRP1 is involved in the transport of a variety of endogenous substrates across the cell membrane. This includes glutathione, as well as glutathione conjugates such as cysteinyl leukotriene C_4, which is an inflammation mediator. Further substrates include glucuronide and sulphate conjugates, resulting from the phase II metabolism of xenobiotics. Therefore, MRP1 contributes to cells' homeostasis and protection against oxidative stress [210-212]. It has further been reported that MRP1 expression within the bronchial epithelium was reduced in patients with moderate/severe chronic obstructive pulmonary disease (COPD) compared to healthy ex-smoking individuals. The MRP1 expression was even more diminished in patients with severe COPD compared to mild/moderate COPD cases [213]. It has also been shown that the presence of cigarette smoke extract had a modulatory effect on MRP1 functionality [214].

The expression of MRP1 has been reported in a multitude of cells lines and primary cells derived from the human lung epithelium and included 16HBE14o-, Calu-3, NHBE, NCI-H441, A549, hAELVi, Arlo and hAEpC [107, 108, 177]. This indicates a ubiquitous expression across the whole lung epithelium.

Both bidirectional transport and cellular accumulation studies has been conducted to assess the functional activity of expressed MRP1, with the exception of Arlo cells that have not yet been characterised regarding the presence of MRP1 efflux. Table 2 summarises a number of selected *in vitro* studies, where bidirectional transport studies are shown if available. As MRP1 has been described to be expressed on the basolateral side of the cell membrane, the UR concept can be applied to assess, whether active efflux is present by dividing the absorptive permeability by the secretory (as an inverse of the ER) [87]. If translating the recommendations of regulatory authorities in classifying a substrate of active efflux (i.e. net flux ratio ≥ 2, [18]) to the UR concept, this would imply that active efflux is present on the basolateral side if the UR is ≥ 2. Further the UR would need to decrease by 50 % in presence of a MRP1-inhibitor.

Table 2. Summary of selected *in vitro* studies assessing the presence of MRP1 efflux in cells derived from the human lung epithelium. The uptake ratio (UR) is calculated by dividing the absorptive (P_{app} AB) by the secretory permeability (P_{app} BA). The icon in the right column summarises whether the data indicates the presence of active efflux (+) or the absence (-), based on the reported UR in absence and presence of inhibitor if adapting the guidance rules from [18]. If no UR could be calculated (i.e. in cellular accumulation studies), non-applicable (N.A.) was added as comment. 5,6-CF stands for 5,6-Carboxyfluorescein.

Cell type	Substrate	Inhibitor	Result	Presence of Efflux according to [18]
16HBE14o- [214]	5,6-CF	MK-571	~ 12.5-fold increase in intracellular concentration of 5,6-CF in presence of inhibitor	N.A.[a]
Calu-3 [87]	[^{3}H]-Estrone-3-sulphate	MK-571	UR ~ 5.0, UR ~ 2.0 (+ inhibitor)	+
NHBE[b] [87]	[^{3}H]-Estrone-3-sulphate	MK-571	UR ~ 4.0, UR ~ 2.0 (+ inhibitor)	+
NCI-H441 [74]	5,6-CF	MK-571	UR ~ 1.5, UR ~ 1.0 (+ inhibitor)	-[c]
A549 [185]	Calcein	Probenecid	~ 1.5-fold increase in intracellular concentration of Calcein in presence of inhibitor	N.A.[d]
hAELVi [108]	[^{3}H]-Estrone-3-sulphate	MK-571	UR ~ 1.2, UR ~ 0.6 (+ inhibitor)	-[e]
hAEpC [74]	5,6-CF	MK-571	UR ~ 3.1, UR ~ 1.1 (+ inhibitor)	+

[a] Results were derived from a cellular accumulation study, comparing the intracellular concentration of 5,6-CF in absence and presence of MK-571 in plated cells. Due to the significant increase in intracellular concentration of 5,6-CF in presence of inhibitor, the authors concluded a functional expression of MRP1. As it is no bidirectional transport study, an UR cannot be calculated.

[b] In this study, commercially available NHBE cells were characterised (EpiAirway® model).

[c] The observed asymmetry between absorptive and secretory permeability was less than two-fold, therefore if applying the criteria from [18], this indicates rather the absence of MRP1 efflux. However, due to the statistically significant differences in absorptive and secretory permeability and the reduction of UR in presence of inhibitor, the presence of active MRP1 efflux in NCI-H441 was reported in literature.

[d] Results were derived from a cellular accumulation study, comparing the intracellular concentration of Calcein in absence and presence of MK-571 in plated cells. Due to the significant increase in intracellular concentration of Calcein in presence of inhibitor, the authors concluded a functional expression of MRP1. As it is no bidirectional transport study, an UR cannot be calculated.

[e] The observed asymmetry between absorptive and secretory permeability was less than two-fold, therefore if taking the criteria from [18], this indicates rather the absence of MRP1 efflux. However, due to the statistically significant decrease of UR in presence of inhibitor, the presence of MRP1 efflux in hAELVi was reported in literature.

All listed *in vitro* studies in Table 2, reported the functional expression of MRP1 within the respective cell lines and primary cells. However, if applying the guidance rules for ABC transporter substrate assessment according to health authorities [18], the acceptance criteria were only fulfilled for Calu-3, NHBE and hAEpC. For NCI-H441 and hAELVi, the net flux ratio was below two (UR < 2) and according to the decision tree from the International Transporter Consortium, this indicates the absence of active efflux (or if applicable, poor efflux). However, the term 'poor' is not clearly specified in this context [18]. It would be highly beneficial to evaluate, whether these guidance rules should also be applied in future bidirectional studies, which are aiming to characterise active efflux within polarised human lung epithelial cells.

The fluorophore 5,6-Carboxyfluorescein (5,6 -CF) has been used as probe substrate for MRP1 in a number of experiments, as shown in Table 2. It is formed by intracellular cleavage of non-fluorescent carboxyfluorescein diacetate [74]. A recent study reported that 5,6-CF is rather not an appropriate substrate to evaluate MRP1 efflux. No differences in 5,6-CF transport were observed when comparing wild type NCI-H441 and MRP1-knockout NCI-H441 cells. The authors have shown that the MRP1-knockout cells formed a tight barrier, MRP1 was successfully knocked out and that the gene modification did not result in an upregulation of other transporters that could potentially recognise 5,6-CF as substrate. Thus, it was concluded that 5,6-CF does not seem to be a suitable substrate for MRP1 and that observed efflux in wild type and MRP1-knockout cells might arise from base line activity of expressed MRPs and OATs [215]. Further, estrone-3-sulphate has been used a substrate for assessing MRP1 efflux in some of the conducted bidirectional transport studies, as depicted in Table 2. In addition to MRP1, estrone-3-sulphate has been described in literature to be a substrate of OATP transporters [216]. However, gene and protein analyses reported the absence or weak expression of OATP transporters within the human lung epithelium, thus an interaction of estrone-3-sulphate with OATP is less likely in lung epithelial cells [177]. These examples emphasise the difficulty of choosing a probe substrate that is selective only for the transporter protein of interest, which was already discussed for MDR1 in 1.9.1.

In the rodents' lung, an *in vivo* study has reported the functional expression of Mrp1 on the basolateral side of the rat lung epithelium. The study applied PET imaging to investigate the pulmonary elimination of S-(6-(7-[^{11}C]-methylpurinyl))glutathione, that is formed by intracellular glutathione conjugation of 6-bromo-7-[^{11}C]-methylpurine within the pulmonary epithelial cells. The prodrug is highly cell permeable, whereas the conjugate depends on MRP1 efflux to cross the epithelial membrane. After intratracheal administration of the prodrug, the elimination of the glutathione-conjugate from the lung was significantly decreased in Mrp1-knockout rats compared to wild type animals [217].

1.9.3 Breast Cancer Resistance Protein (BCRP)

The BCRP protein is a so-called half transporter with a molecular weight of 72 kDa [218]. It has been first discovered in 1998 in a breast cancer cell line that showed resistance to several cancer drugs (mitoxantrone, daunorubicin and doxorubicin) without overexpressing MDR1 and MRP1 [219]. BCRP is expressed in various tissues of the human body, with high expression levels reported in the intestinal enterocytes and the canicular membrane of the hepatocytes. Further, it is found in the kidney proximal epithelial cells and at the level of the blood brain barrier, thus impacting absorption, distribution and elimination processes of its substrates [218]. BCRP has been described to transport a wide range of structurally diverse compounds including both hydrophobic and hydrophilic molecules such as chemotherapeutic drugs, sulphate conjugates and dietary flavonoids [220].

The expression of BCRP has been reported in various cells derived from the human pulmonary epithelium and included 16HBE14o-, Calu-3 , NHBE, NCI-H441, A549 and hAEpC [177, 195]. It has been shown that the expression levels of BCRP decreased significantly, when alveolar pneumocytes type II trans-differentiated into alveolar type I-like pneumocytes *in vitro*. Further, BCRP showed a strong expression within the nucleus of the primary alveolar cells [221]. This is aligned with findings in the alveolar-derived immortalised cell lines hAELVi and Arlo (having an alveolar pneumocytes type I phenotype), where only a negligible amount of BCRP has been detected at gene level [107, 108]. Therefore, BCRP appears to be rather expressed in the bronchial and bronchiolar region.

Overall, there is only a small number of *in vitro* studies available across literature, which assessed BCRP efflux in cells mimicking the human lung epithelium. A selection of available *in vitro* studies is summarised in Table 3. If available, data from bidirectional transport studies is shown. No *in vitro* studies that have characterised BCRP efflux within 16HBE14o- and Arlo were found. The presence of efflux was considered if there was a net flux ratio ≥ 2 in accordance with the guidance criteria from the health authorities. Further the net flux needed to be reduced by a minimum of 50 % in presence of a BCRP inhibitor [18]. Due to the proposed apical expression of BCRP within the lung epithelium, ER values were extracted from literature.

Table 3. Summary of selected *in vitro* studies assessing the presence of BCRP efflux in cells derived from the human lung epithelium. The efflux ratio (ER) is calculated by dividing the secretory (P_{app} BA) by the absorptive permeability (P_{app} AB). The icon in the right column summarises whether the data indicates the presence of active efflux (+) or the absence (-), based on the reported ER in absence and presence of inhibitor according to guidance rules from [18]. If no ER could be calculated (i.e. in cellular accumulation studies), non-applicable (N.A.) was added as comment. H33342 stands for Hoechst 33342.

Cell type	Substrate	Inhibitor	Result	Presence of Efflux according to [18]
Calu-3 [222]	H33342	Elacridar	~ 1.7-fold increase in intracellular concentration of H33342 in presence of inhibitor	N.A.[a]
NHBE[b] [87]	[^{3}H]-Mitoxantrone	Febuxostat	ER ~ 1.0, ER ~ 1.3 (+ inhibitor)	-
NCI-H441 [221]	BODIPY™-Prazosin FL	Ko143	ER ~ 1.7, ER ~ 1.0 (+ inhibitor)	-[c]
A549 [186]	H33342	Fumetrimorgin C	~ 1.5-fold increase in intracellular concentration of H33342 in presence of inhibitor	N.A.[d]
hAELVi [108]	BODIPY™-Prazosin FL	Ko143	ER ~ 0.9, ER ~ 0.7 (+ inhibitor)	-
hAEpC [221]	BODIPY™-Prazosin FL	Ko143	UR ~ 2.0, UR ~ 2.3 (+ inhibitor)[e]	-

[a] Results were derived from a cellular accumulation study, comparing the intracellular concentration of H33342 in absence and presence of Ko143 in plated cells. Due to the significant increase in intracellular concentration of H33342 in presence of inhibitor, the authors concluded a functional expression of BCRP. As it is no bidirectional transport study, an ER cannot be calculated.

[b] In this study, commercially available NHBE cells were characterised (EpiAirway® model).

[c] The observed asymmetry between absorptive and secretory permeability was less than two-fold, therefore if taking the criteria from [18], this indicates rather the absence of MRP1 efflux. However, due to the statistically significant differences in absorptive and secretory permeability and the reduction of ER in presence of inhibitor, the presence of active BCRP efflux in NCI-H441 was reported in literature.

[d] Results were derived from a cellular accumulation study, comparing the intracellular concentration of H33342 in absence and presence of Fumetrimorgin C in plated cells. Due to the significant increase in intracellular concentration of H33342 in presence of inhibitor, the authors concluded a functional expression of BCRP. As it is no bidirectional transport study, an ER cannot be calculated.

[e] As a net absorption from apical to basolateral side was measured, the uptake ratio (UR) was reported instead of an ER.

As shown in Table 3, no BCRP efflux was present in NHBE, NCI-H441, hAELVi and hAEpC based on reported net flux ratios of bidirectional transport studies, if applying the guidance criteria [18]. For NHBE, this was to be expected as BCRP was detected on both apical and basolateral side of the cell membrane, using an immunostaining approach [87]. The absence of an asymmetry in BODIPY™-prazosin FL permeability in the hAELVi cells was also expected as only a week expression of BCRP at gene level has been reported [108].

For NCI-H441 cells, an ER of ~ 1.7 has been reported in absence of inhibitor, that reduced to an ER of ~ 1.0 in presence of inhibitor [221]. According to the guidance criteria, this classifies BODIPY™-prazosin FL as non/poor substrate of BCRP. As already mentioned in the section on MRP1 (see 1.9.2), no clear definition to distinguish between a poor and non-substrate is given in the guidance document [18]. The hAEpC cells showed a net absorption of BODIPY™-prazosin FL from apical to basolateral side in absence of inhibitor, that was not changed in presence of BCRP inhibitor Ko143. Therefore, the authors concluded that another active transporter protein is likely responsible for the observed asymmetry in permeability of BODIPY™-prazosin FL in hAEpC [221].

All substrates (Hoechst 33342 (H33342), mitoxantrone and BODIPY™-prazosin FL), used to assess BCRP efflux as shown in Table 3, have been reported in literature to be shared substrates of MDR1 [78, 223, 224]. As reported in section 1.9.1, MDR1 is expressed in the majority of human lung epithelial cells, where it showed functional efflux. Therefore, a potential interaction of the chosen BCRP substrates with expressed MDR1 cannot be excluded. Moreover, the model BCRP inhibitor Ko143 has been shown to inhibit MDR1 and MRP1 efflux to a certain degree at concentrations within the low micromolar range [225]. As already raised, the use of both non-selective substrates and inhibitors impedes a clear understanding of the contribution of a single transporter [200, 226].

In terms of rodents, a recent PET imaging study assessed the presence of functional Bcrp1 within the lung of rats. A shared Mdr1/Bcrp1 substrate ([^{11}C]-erlotinib) was administered via an aerosoliser into the trachea. Moderately increased lung area under the curve values (AUC, expressed as percentage of inhaled dose per mL and min) were measured for [^{11}C]-erlotinib when comparing Mdr1a-knockout and Bcrp1-knockout rats to wild type animals. Only the pre-administration of the Mdr1 inhibitor tariquidar in Bcrp1-knockout rats led to a significant increase in lung AUC of [^{11}C]-erlotinib (‘dual’ inhibition of Mdr1a/b and Bcrp1). Therefore, the authors have concluded a functional redundancy of Mdr1a/1b and Bcrp1 in limiting the absorption of inhaled [^{11}C]-erlotinib across the lung epithelium with both transporters being expressed on the apical side of the epithelium [227].

1.10 Antibiotics and their Interaction with Pulmonary ABC Transporters *in vitro*

The number of bacteria that are resistant to known antibiotics is rising [228]. This is seen especially for tuberculosis but also for commonly known bacterial pathogens such as Staphylococcus aureus or Pseudomonas aeruginosa. Around 700 000 patients worldwide die per year due to antimicrobial resistance [229]. Given the fact that antibiotics are typically administered by oral or parental dosing [230], it becomes important to understand the drivers of their pulmonary drug disposition after systemic administration.

Data from clinical studies has reported that certain antibiotic classes show a tremendously higher concentration in the ELF compared to the unbound plasma concentration (>> 1), after an administration via the systemic circulation [4]. This has been mainly observed for macrolide and fluoroquinolone antibiotics, with extremely high ratios (> 50) seen for macrolides. It needs to be noted that there is a great variability in ratios across compounds of the same antibiotic class [15]. As both fluroquinolone and macrolide antibiotics have been described as substrates of ABC transporters *in vitro*, it was speculated whether the presence of ABC transporters at the lung epithelium could contribute to increased ELF concentrations [4, 16, 17]. Still little is known about the role that ABC transporters play in pulmonary drug disposition of antibiotics and if/how they affect the pharmacokinetics of systemically administered antibiotics. Calu-3 cells are the most commonly used *in vitro* model to assess the permeability and contribution of drug transporters at the level of the pulmonary epithelium [20]. The following subsections provide an overview on conducted *in vitro* bidirectional transport studies in lung epithelial cells (Calu-3) that included fluoroquinolone and macrolide antibiotics as test compounds. Further, additional processes, which were described to affect the pulmonary distribution of certain fluoroquinolone and macrolide antibiotics are discussed.

1.10.1 Fluroquinolones

Fluroquinolone antibiotics were described to be substrates of MDR1, MRPs and BCRP [231]. Their passive permeability across Calu-3 cells was described to be related to their lipophilicity, but active transport processes appear to be involved [17]. Table 4 provides an overview of the conducted *in vitro* studies in Calu-3 using fluoroquinolones as substrates. As described above, an ER ≥ 2 indicates the presence of active efflux, which is further confirmed if the ER reduced by at least 50 % in presence of an ABC-transporter inhibitor [18].

As shown in Table 4, the majority of tested fluoroquinolones had an ER ≥ 2, which indicates their interactions with active efflux transporters, expressed in Calu-3 cells. Only for lascufloxacin and pefloxacin, an ER < 2 was derived. The presence of PSC-833 as inhibitor of MDR1, led to a more than 50 % reduction in ER, which was observed for all fluoroquinolones

that showed an ER ≥ 2 in absence of inhibitors. The presence of MRP inhibitor probenecid had no impact on observed ER values [163, 232]. The BCRP inhibitor Ko143 reduced the ER of lascufloxacin by half, however the reported ER in absence of inhibitor was 1.6, hinting to the absence or presence of only poor efflux, according to the guidance criteria from the health authorities [18, 163]. Therefore, likely MDR1 is responsible for observed efflux of fluoroquinolone antibiotics across Calu-3 [17, 163]. This is aligned with literature data, that reported a high expression of functional active MDR1 within Calu-3 cells [87, 201].

Table 4. Overview of bidirectional *in vitro* studies in Calu-3 cells using fluoroquinolone antibiotics as substrates. Both the absorptive apparent permeability (P_{app} AB) and secretory apparent permeability (P_{app} BA) are reported based on which the efflux ratio (ER) is calculated by dividing secretory by absorptive permeability. The ER in presence of inhibitor is referred to as ER,i and is calculated by dividing the secretory by absorptive permeability in presence of inhibitor. Further the used inhibitors are listed including the ABC transporter, which they inhibit as described in the respective *in vitro* study.

Antibiotic	P_{app} AB [nm/s]	P_{app} BA [nm/s]	ER	Inhibitor	Inhibited ABC Transporter	ER,i	Reference
Ciprofloxacin	7	27	4.0	PSC-833	MDR1	0.9	[17]
Grepafloxacin	31	118	3.8	PSC-833	MDR1	1.0	[17]
Lascufloxacin	115	185	1.6	Verapamil[a]	MDR1, MRP	1.0	[163]
				PSC-833	MDR1	1.0	
				Elacridar	MDR1/BCRP	0.7	
				Ko143	BCRP	0.8	
				Probenecid[b]	MRP	1.54	
Levofloxacin	24	62	2.6	PSC-833	MDR1	1.0	[17]
Moxifloxacin	50	104	2.1	PSC-833	MDR1	0.9	[17]
	53	105	2.0	Verapamil[a]	MDR1, MRP	1.0	[232]
				PSC-833	MDR1	0.9	
				Probenecid[b]	MRP	2.2	
Norfloxacin	6	20	2.6	PSC-833	MDR1	1.0	[17]
Pefloxacin	71	98	1.4	PSC-833	MDR1	1.0	[17]

[a] Verapamil is not a selective inhibitor and was described in literature to inhibit also OCT and OCTN transporters [199].

[b] Probenecid is not a selective inhibitor and was described in literature to inhibit also OAT and OATP transporters [233, 234].

Compared to other fluoroquinolones, lascufloxacin showed a relative high ELF to unbound plasma ratio ranging from 57.5 to 86.4 within 24 h after a single oral dose in healthy volunteers [235]. As shown in Table 4, *in vitro* measurements in Calu-3 cell revealed that lascufloxacin is highly permeable and active transporters appear to play a negligible role in limiting its membrane permeability (ER< 2). Therefore, it was concluded that efflux by active transporters at the apical site of the lung epithelium is likely not responsible for the high observed ELF concentrations. The authors elucidated that lascufloxacin shows strong binding to bovine pulmonary surfactant, with extensive binding to phosphatidylserine. This degree of strong

binding to phosphatidylserine has not been observed for other fluoroquinolones like levofloxacin or grepafloxacin, therefore the authors concluded that the binding of lascufloxacin to phosphatidylserine is potentially responsible for its high ELF exposure [163].

1.10.2 Macrolides

Literature reported that macrolides are substrates of MDR1 [16, 236]. Furthermore, they appear to be inhibitors of MDR1 at higher micromolar concentrations, when using digoxin as probe substrate [78]. There was only one *in vitro* study available, that assessed the permeability of macrolides across pulmonary epithelial cells (Calu-3) in absence and presence of ABC transporter inhibitors [16]. The values are summarised in Table 5.

All three macrolides show an ER ≥ 2 in Calu-3, that was reduced by more than 50 % in presence of verapamil and cyclosporine A (as MDR1 inhibitors), whereas the MRP inhibitor probenecid did not have any impact on the ER. The authors concluded that observed efflux is therefore mediated by MDR1, which is known to be expressed in Calu-3 cells [16, 196]. As described before, neither verapamil nor cyclosporine A are selective inhibitors for MDR1 [199, 237], and thus the concurrent inhibition of other transporters cannot be excluded.

Table 5. Overview of bidirectional *in vitro* studies in Calu-3 cells using macrolide antibiotics as substrates. Both the absorptive apparent permeability (P_{app} AB) and secretory apparent permeability (P_{app} BA) are reported based on which the efflux ratio (ER) is calculated by dividing secretory by absorptive permeability. The ER in presence of inhibitor is referred to as ER,i and is calculated by dividing the secretory by absorptive permeability in presence of inhibitor. Further the used inhibitors are listed including the ABC transporter, which they inhibit as described in the respective *in vitro* study. Exact P_{app} were not provided, but estimated used a Web plot digitaliser (apps.automeris.io).

Antibiotic	P_{app} AB [nm/s]	P_{app} BA [nm/s]	ER	Inhibitor	Inhibited ABC Transporter	ER,i	Reference
Azithromycin	5	22	4.4	Verapamil[a]	MDR1	1.1	[16]
				Cyclosporine A[b]	MDR1	1.1	
				Probenecid	MRP	3.8	
Clarithromycin	13	110	8.5	Verapamil[a]	MDR1	1.1	
				Cyclosporine A[b]	MDR1	1.1	
				Probenecid	MRP	8.3	
Telithromycin	12	63	5.3	Verapamil[a]	MDR1	1.1	
				Cyclosporine A[b]	MDR1	0.9	
				Probenecid	MRP	4.5	

[a] Verapamil is not a selective inhibitor and was described in literature to inhibit also OCT and OCTN transporters [199].

[b] Cyclosporine A is a pan-inhibitor of various drug transporters [237].

Further studies reported that macrolides show an extensive accumulation in alveolar macrophages [238]. This was observed for a rat macrophage cell line (NR8383), where azithromycin, clarithromycin and telithromycin showed an at least 40-fold higher concentration in the intracellular compartment (cell) compared to extracellular compartment (medium). The intracellular concentrations were significantly reduced if the compounds were co-incubated with ammonium chloride, which abolished the pH gradient in the lysosomes compared to the cytoplasm. It was therefore concluded that the high intracellular concentrations of macrolides within the alveolar macrophages are the result of their lysosomal sequestration [51, 239, 240]. Similar observations were made for clarithromycin in human macrophages [53]. Lysosomal trapping is mainly observed for lipophilic/amphiphilic molecules that carry a strong basic amine group (pKa > 6). Due to the pH gradient in lysosomes (~ 5) compared to a pH of 7.2 in the cytoplasm, the compounds get ionised in the lysosomes and their membrane permeability decreases compared to their neutral form, thus being trapped within the lysosomes [241, 242]. Due to the strong degree of accumulation of macrolides within alveolar macrophages, it was speculated that lysis of alveolar macrophages during the collection of ELF might contribute to the high ELF to plasma ratios of these antibiotics in the clinic [15].

All macrolide and fluoroquinolone antibiotics were shown to be substrates of active efflux (ER ≥ 2) in Calu-3, likely mediated by MDR1, with the exception of lascufloxacin and pefloxacin. Therefore, it is reasonable to speculate that active efflux within the lung epithelium could contribute to the elevated ELF to plasma concentrations of these compounds in the clinic. However additional parameters such as drug binding to ELF components or potential lysis of alveolar macrophages during ELF collection, resulting in a release of intracellularly accumulated drug, need to be considered.

2. Aims and Objectives of this Thesis

There have been many efforts over the last decades to investigate the contribution of efflux transporters on pulmonary drug disposition, but their role within the human lung epithelium is not yet fully elucidated [146]. In contrast, the contribution of ABC transporters on affecting pharmacokinetic processes in tissues like the intestine, kidney or liver are well known [243]. Therefore, it is of great interest to investigate if ABC transporters play a similar role in the lung epithelium, especially in the context of drugs targeting the lung like antibiotics. For certain antibiotic classes (i.e. macrolides & fluoroquinolones), it has been hypothesised that efflux transporters at the apical side of the lung epithelium could contribute to high ELF to plasma ratios (>> 1), after a systemic administration [4]. However, further parameters like strong binding of antibiotics to ELF components could contribute to elevated ELF concentrations over time [163].

The aim of this thesis is to provide a better understanding of the potential contribution of ABC transporters on driving the pulmonary bioavailability of antibiotics after an administration via the systemic route.

Within the scope of this thesis, the initial focus was on three ABC transporters: MDR1, MRP1 and BCRP. Both MDR1 and BCRP play a significant role in affecting the disposition of their xenobiotic substrates across biological barriers like the intestine mucosa or the blood brain barrier [18]. MRP1 was included as it was described to be the ABC transporter with the highest expression levels in the pulmonary epithelium and is known to transport a variety of endogenous and exogenous substrates [209, 244]. The expression and functional activity of MDR1, MRP1 and BCRP was investigated in cell lines and primary cells mimicking the human pulmonary epithelium *in vitro*.

A further aim was to elucidate the impact of additional pharmacokinetic parameters (permeability and binding to plasma proteins and ELF components) on the transport of antibiotics across the human lung epithelium. It was also investigated whether antibiotics show active efflux mediated by ABC transporters in human lung epithelial cell lines (Calu-3 and hAELVi).

The measured *in vitro* parameters were then incorporated into a PBPK model to investigate whether observed clinical and *in vivo* ELF concentration over time profiles of two antibiotics can be reasonably predicted.

Overall, the work of this thesis contributes to deepen our mechanistic understanding on pharmacokinetic parameters, likely to affect the pulmonary exposure of antibiotics after systemic administration.

The main objectives of this thesis are summarised below, combining *in vitro* and *in silico* methodologies:

1. Characterise the expression and functional activity of MDR1, MRP1 and BCRP in various cell lines and primary cells derived from the human upper and lower airways (Chapter 3.1)
    - Are there differences in the ABC transporter expression patterns at gene and protein level between cell lines and primary cells?
    - Are the expressed ABC transporter proteins functionally active?
    - Does the culture interface (ALI vs LCC) have an impact on ABC transporters' expression and functional efflux?

2. Investigate the rate and extent of antibiotics' transport across the lung epithelium *in vitro*, focussing on permeability, active efflux and unbound fractions in plasma and ELF (Chapter 3.2)
    - Are there differences in the permeability of antibiotics across human lung epithelial cell lines (Calu-3, hAELVi) compared to cell lines, that are typically used for permeability assessment in early drug development (LLC-PK1 WT and Caco-2)?
    - Are antibiotics subject of active efflux transporters in lung epithelial cells? Are they substrates of ABC transporters in general (MDR1 and BCRP)?
    - Are there differences in the unbound fraction of antibiotics in plasma and ELF?

3. Employ PBPK modelling to quantitatively simulate the ELF concentration-time profiles of two antibiotics (moxifloxacin and telithromycin) in human and rat (Chapter 3.3)
    - How well can the literature-reported ELF concentration-time profiles be predicted if using PBPK modelling?
    - Does the ELF simulation improve/change if incorporating MDR1/Mdr1 efflux to the lung epithelium? Are there potential species differences between human and rat?
    - What impact has the binding to ELF components on predicted total ELF concentrations?

3. Results

3.1 Mapping the ABC Transporter Landscape in the Human Lung - A Comprehensive Characterisation of MDR1, MRP1 and BCRP Expression and Functional Activity in Human Lung Epithelial Cells

This chapter has been published as a research article:

Simon, S., Shanmugalingam, T., Neu, T., Schneider-Daum, N., Cantrill, C. and Lehr, C-M. (2025), Mapping the ABC Transporter Landscape in the Human Lung: A Comprehensive Characterisation of MDR1, MRP1 and BCRP Expression and Functional Activity in Human Lung Epithelial Cells, *European Journal of Pharmaceutical Sciences*, DOI: 10.1016/j.ejps.2025.107333

Contributions to this chapter:

Sina Simon was mainly responsible for the methodological experimental design of the study, performed the cell culture (apart from the alveolar cell isolation), conducted the experiments, run the LC-MS/MS for the samples from the permeability marker studies and evaluated the data. She wrote the manuscript (apart from the below mentioned exceptions in the methodology of the LC-MS/MS and the isolation of primary alveolar cells) and created all the figures. Moreover, she was mainly involved in editing the revised manuscript.

Thanusa Shanmugalingam established and validated the LC-MS/MS methods, analysed the samples from the bidirectional efflux studies and contributed to the writing of the original manuscript (methodology of LC-MS/MS analysis). Tobias Neu and Dr. Nicole Schneider-Daum isolated the primary human alveolar epithelial cells, contributed to the writing of the original manuscript (methodology of alveolar cell isolation) and critically evaluated the final manuscript. Dr. Carina Cantrill and Prof. Dr. Claus-Michael Lehr supervised the project and supported the conceptualisation of the experimental methodology, the data evaluation and critically evaluated the final manuscript.

3.1.1 Introduction

ATP-binding-cassette (ABC) drug transporters are a family of transmembrane proteins that transport a variety of xenobiotic and endogenous molecules across the cell membrane. Efflux processes are mediated against a concentration gradient, for which energy is needed, provided by adenosine triphosphate hydrolysis [245]. In drug development, ABC transporters play a pivotal role due to their impact on drug disposition of their substrates, i.e. reducing intestinal absorption, or enhancing hepatobiliary/urinary excretion. In this context, multidrug resistance protein 1 (MDR1, also known as P-glycoprotein (P-gp)) and breast cancer resistance protein (BCRP) are mentioned, for which numerous clinically relevant drug-drug interactions have been reported [18, 174]. Multidrug resistance-associated protein 1 (MRP1) is a further ABC transporter with reported ubiquitous tissue expression. MRP1 has been described to transport a variety of drugs including, but not limited to, chemotherapeutics, as well as translocating endogenous substrates such as glutathione across the cell membrane [246, 247].

The role and clinical significance of MDR1 and BCRP for drug disposition in tissues such as the intestine or liver is well known, whereas their role in the human lung remains less clear. Numerous *in vitro* studies using cell lines and primary cells derived from the human pulmonary epithelium showed the expression of MDR1, MRP1 and BCRP. This suggests a potential contribution of these transporters as drivers of pulmonary drug distribution. There are a number of reports detailing, differences in ABC transporter expression levels across *in vitro* lung epithelial cell models. However, these studies do not always assess the functionality of the expressed transporter proteins. To date, it remains unclear, whether *in vitro* models accurately characterise pulmonary disposition processes and to what extent bronchial and alveolar models differ in ABC transporter activity [19, 20, 177, 248].

To study pulmonary drug transport processes *in vitro*, human lung epithelial cell lines such as Calu-3, 16HBE14o- or NCI-H441 are commonly used [61, 94, 249]. However, due to their cancerous origin or genetic modification for the purposes of immortalisation, their genotype and phenotype may not fully reflect the healthy lung epithelium. Primary lung epithelial cells could be used as an alternative, but it remains unclear, whether they show a distinct difference in mimicking pulmonary ABC transporters' processes *in vitro* compared to cell lines [20, 41, 61, 249, 250]. Several studies characterised the ABC transporter protein expression in human pulmonary epithelial cell lines and compared them to primary cells, revealing both, similarities and differences in expression profiles [74, 87, 108, 221].

To investigate pulmonary drug disposition processes, epithelial cells are cultured on permeable membrane inserts. Once they reach confluence, an air-liquid interface (ALI) can be established by removing the liquid from the apical side and reducing the basolateral medium volume.

In general, lung epithelial cells cultured at ALI tend to differentiate into a more native-like epithelium compared to those maintained under liquid-covered condition (LCC). However, 16HBE14o- cells appear to be an exception to this. This cell line requires a certain liquid volume on the apical side to develop a tight barrier [66, 77, 79, 82, 251]. Regarding ABC transporter expression, a study in Calu-3 revealed that ALI culture led to an increased gene expression of MDR1, MRP1 and BCRP when compared to LCC culture [79].

To study permeability and active transport processes *in vitro*, it is crucial that the cells form a tight monolayer, which is commonly monitored by measuring transepithelial electrical resistance (TEER) [20]. Depending on the lung epithelial cell model and culture condition, TEER values ranging from < 100 $\Omega*cm^2$ to > 2000 $\Omega*cm^2$ have been reported [96, 105]. A threshold of 250 $\Omega*cm^2$ is considered as an acceptable indicator for barrier integrity [75].

This study aimed to investigate the *in vitro* expression and functional activity of MDR1, MRP1 and BCRP in various cells derived from the upper and lower human lung epithelium for a direct comparison. The transporters' expressions at gene and protein levels were characterised in cell lines (16HBE14o-, Calu-3, NCI-H441, A549, hAELVi, Arlo) and directly compared to findings in human primary cells, i.e. normal bronchial epithelial cells (NHBE) and alveolar type I-like epithelial cells (hAEpC). Furthermore, it was analysed whether the culture interface (ALI vs. LCC) had an impact on ABC transporter expression and barrier formation. Functional activity of transporters was then tested using known substrates, including fluorophores and drugs.

3.1.2 Material & Methods

3.1.2.1 Cell Culture

Cells were cultured in Nunc™ EasYFlasks™ (75 cm^2, Thermo Fisher Scientific, Waltham, MA, USA) and maintained in incubators with saturated humidity, a constant temperature of 37 °C and 5 % CO_2. For culture on Transwell® inserts, lung epithelial cells were seeded onto PET membrane inserts (3470, Corning, Corning, NY, USA) and reference Caco-2 cells on polycarbonate membranes (3397, Corning), having a pore size of 0.4 µm and a surface area of 0.33 cm^2. For cells at ALI, medium on the apical side of the insert was removed upon reaching confluence (typically after three days) and medium was kept only on basolateral side (500 µL). For cells cultured at LCC, medium was maintained on both sides of the insert throughout the entire cultivation time (200 µL apical and 1000 µL basolateral). Medium was exchanged three to four times per week, without addition of antibiotics. The cultivation time of the cells on Transwell® inserts was adjusted based on literature recommendation.

16HBE14o- (SSC150) were purchased from Merck KGaA (Darmstadt, Germany) and cultured in α-MEM medium (Merck KGaA) supplemented with 10 % (v/v) foetal bovine serum (FBS) and 2 mM L-Glutamine (Thermo Fisher Scientific). Flasks and Transwell® inserts were pre-coated with a mixture of 0.5 mg/mL human fibronectin, 1 mg/mL BSA Fraction V and 3 mg/mL bovine collagen (Merck KGaA) according to cell supplier's instructions. Cells were seeded at a density of 1 x 10^5 cells/cm^2 on Transwell® inserts and cultured for 14 days.

Calu-3 cells, purchased from ATCC (HTB-55; Manassas, VA, USA) were grown in Gibco DMEM/F12 medium, supplemented with 10 % (v/v) FBS, 2 mM L-Glutamine and 1 % (v/v) non-essential amino acids (Thermo Fisher Scientific). Cells were seeded onto Transwell® at a density of 3 x 10^5 cells/cm^2 and maintained for 21 days.

Normal bronchial epithelial cells (NHBE) were purchased from Lonza Bioscience (CC-2540; Basel, Switzerland). Cells were cultivated in PneumaCult™-Ex Plus Medium kit (Stemcell™ Technologies, Vancouver, Canada) supplemented with 0.1 % (v/v) hydrocortisone (Stemcell™ Technologies). Once cells were seeded on Transwell® inserts, medium was switched to PneumaCult™-ALI Medium kit to which 0.1 % (v/v) hydrocortisone and 0.2 % (v/v) heparin solution was added (Stemcell™ Technologies). NHBE were seeded on Transwell® inserts at a density of 1 x 10^5 cells/cm^2 and maintained for 21 days.

NCI-H441, purchased from ATCC (HTB-174), were cultured in ATCC-modified Gibco RPMI-1640 medium (Thermo Fisher Scientific) supplemented with 10 % (v/v) FBS. Cells were seeded onto Transwell® inserts at 1 x 10^5 cells/cm^2 and maintained for 14 days. Once cells reached confluence on Transwell® inserts, growth medium was further supplemented with

200 nM dexamethasone (Merck KGaA) and 1 % (v/v) insulin-transferrin-selenium (Thermo Fisher Scientific) [94].

A549 cells were purchased from ATCC (CCL-185) and cultivated in Gibco Ham's F12 nutrient mixture medium (Thermo Fisher Scientific) supplemented with 10 % (v/v) FBS. Cells were seeded onto Transwell® inserts at a density of 2 x 10^5 cells/cm^2 and maintained for 14 days.

hAELVi (CI-hAELVi, INS-CI-1015) and Arlo (CI-huArlo, INS-CI-1031) were purchased from InSCREENeX GmbH (Braunschweig, Germany) and were maintained in huAEC medium (InSCREENeX). Cells were seeded at a density of 1 x 10^5 cells/cm^2 onto huAEC-coated Transwell® inserts, prepared according to manufacturer's protocol. Cells were maintained on Transwells® for 14 days.

Human alveolar epithelial primary cells (hAEpC) were isolated from lung tissue obtained from SHG clinics Völklingen and Clinic Saarbrücken according to the protocol described in Daum et al. [110]. The use of patient material for this biomedical research was approved by the Ethics Committee of the State of Saarland, Germany (Reference No. 113/19 for SHG Clinics Völklingen and Reference No. 97/21 for Clinic Saarbrücken). The isolated cells were directly seeded onto Transwell® inserts (to allow trans-differentiation into alveolar type I cells). Transwell® plates were pre-coated with a mixture of 30 µg/mL bovine collagen (Merck KGaA) and 10 µg/mL human fibronectin (Corning) as described in Hittinger et al. [252]. Medium used for seeding was SAGM BulletKit™ (CC-3118; Lonza Bioscience), prepared according to manufacturer's instructions and additionally supplemented with 1 % (v/v) FBS. hAEpC were seeded at a density of 3 x 10^5 cells/cm^2 and maintained for up to 7 d. For experiments investigating monolayer integrity via TEER and to determine if the peak resistance is reached within 7 days, cells were cultured for up to 14 days (see 3.3.5).

Caco-2 (HTB-37; ATCC) were cultured in Gibco MEM medium (Thermo Fisher Scientific) that was supplemented with 10 % (v/v) FBS, 1 % (v/v) non-essential amino acids and 1 mM sodium pyruvate (all from Thermo Fisher Scientific). Cells were seeded at a density of 2 x 10^5 cells/cm^2 and maintained for 21 d. Caco-2 cells were included as positive control, as they are known to functionally express MDR1, MRP1 and BCRP and are furthermore accepted by health authorities to study intestinal absorption processes including transporter mediated efflux [181, 253].

All following experiments, apart from TEER measurements, were conducted after the cultivation time specified above.

3.1.2.2 Quantitative Polymerase Chain Reaction (qPCR) Analysis

Cells analysed by qPCR were either cultured in flasks or maintained on Transwell® inserts at ALI or LCC at seeding densities and cultivation times as described in 3.1.2.1.

Cells were lysed by using RLT lysis buffer (Qiagen, Hilden, Germany) according to supplier's protocol. Total RNA was isolated using the RNeasy Mini Kit (Qiagen), following the manufacturer's instructions. In brief, thawed RLT-lysates were diluted at a ratio of 1:1 with 70 % (v/v) ethanol (in ultrapure water) and transferred to the silica membrane of a spin column. Several washing steps were performed and to remove residual DNA, a DNA digestion step was included, using a DNase kit (Qiagen). The final RNA was eluted from the column by centrifugation with RNase-free water (Qiagen). RNA was quantified based on Beer-Lambert law by measuring the absorbance at 260 nm with a Nanophotometer (Implen, Munich, Germany) [254]. Each 500 ng of RNA were then converted to cDNA by using an iScript™ cDNA synthesis kit (Biorad, Hercules, CA, USA) according to manufacturer's recommendation. Gene expression of MDR1, MRP1 and BCRP was measured by qPCR using TaqMan™ Fast Advanced Master Mix and TaqMan™ gene expression FAM assays (Thermo Fisher Scientific, see Table 6 for TaqMan™ assay references), according to manufacturer's instructions. For each qPCR reaction, 25 ng of cDNA was used. Relative expression of ABC transporter genes was calculated with the comparative cycle threshold (C_t) method based on expression of housekeeping gene ACTB [255]. The software 'design and analysis' (Version 2.6.0; Thermo Fisher Scientific) was used to calculate individual C_t values. If C_t for transporter genes exceeded 34 out of 40 cycles, values were not reported.

Table 6: Overview of primers used in qPCR.

Gene	Protein	TaqMan® Gene Expression Assay ID
ABCB1	MDR1	Hs00184500_m1
ABCC1	MRP1	Hs01561483_m1
ABCG2	BCRP	Hs00245154_m1
ACTB	β-actin	Hs01060665_g1

3.1.2.3 Western Blot Analysis

Cells analysed by Western Blot were either cultured in flasks or maintained on Transwell® inserts at ALI or LCC at seeding densities and cultivation times as described in 3.1.2.1.

Proteins were isolated from cells by using Cell extraction buffer (Thermo Fisher Scientific) that was supplemented with 1 % (v/v) of Halt™ protease and phosphatase inhibitor cocktail (Thermo Fisher Scientific), according to supplier instructions. Total protein concentration of lysates was determined by using a Pierce bicinchoninic acid protein assay kit (Thermo Fisher Scientific). The working reagent was prepared by mixing 1 part of reagent B with 50 parts of

reagent A. To each 1.5 µL of protein lysate, 200 µL of working reagent was added and incubated for 30 min at 37 °C. A calibration curve of bovine serum albumin (BSA, Merck KGaA) ranging from 0 to 25 mg/mL was used as standard with pure working reagent as blank. Protein content was calculated based on absorbance measured at 562 nm against a calibration curve.

Western Blotting was performed using a Jess™ device (Protein Simple™, San Jose, CA, USA) [256]. Western Blots were run with the RePlex™ feature, i.e. the protein of interest and house-keeping gene were detected within the same capillary (two-step immunoassay). To minimise cross-interference when measuring the signal of two proteins within the same lane, the house-keeping control (β-actin) was detected via near-infrared (NIR) fluorescence, while the protein of interest was detected using chemiluminescence. The assay was run according to the recommended settings by the manufacturer while using a 12 – 250 kDa separation module. All consumables, except primary antibodies, were ordered directly from Protein Simple™ and volumes used according to respective product sheets.

Table 7: List of primary antibodies and their dilutions used in Western Blotting with Jess™.

Protein	Dilution (in antibody diluent 2, Protein Simple™)	Antibody type	Product ID & Manufacturer
MDR1	1:75	Rabbit polyclonal	22336-1-AP (proteintech®, Rosemont, IL, USA)
MRP1	1:500	Rabbit polyclonal	PA5-30594, Thermo Fisher Scientific
BCRP	1:10	Rabbit monoclonal	NBP3-15559, Bio-Techne (Minneapolis, MN, USA)
β-actin	1:50	Mouse monoclonal	MAB8929, Bio-Techne

In brief, protein lysates were diluted in fluorescent master mix (1:5¸ Protein Simple™) and the respective amount of sample buffer (0.1x in DPBS -/-, Protein Simple™) to achieve a final protein concentration of 0.5 µg/µL. The samples were then incubated at 95 °C for 5 minutes while shaking at 300 rpm. After the incubation, the lysates were transferred to the separation plate. Followed by antibody diluent 2 for blocking, primary antibodies (for dilutions, see Table 7), anti-rabbit secondary horseradish peroxide (HRP)-labelled antibody (to detect transporter proteins via chemiluminescence), anti-mouse NIR-labelled secondary antibody (to detect house-keeping gene via fluorescence), washing buffer, luminol-peroxide and Replex™ reagent that were added to the separation plate. A biotinylated ladder (detected by NIR-labelled streptavidin) with known molecular weights served as reference and an internal fluorescent standard was included in every run. Chemiluminescence and fluorescence images were visualised with the Compass for SW software (Version 6.1.0, Protein Simple™) and signals height & area were automatically calculated for respective proteins at defined molecular

weights. For relative assessment of protein expression, the peak area of transporter protein was normalised to the respective peak area of housekeeping protein β-actin.

3.1.2.4 Intracellular Fluorophore Accumulation Studies

Functional activity of MDR1, MRP1 and BCRP was assessed by measuring the intracellular concentration of fluorescent transporter substrates in the absence and presence of transporter-specific inhibitors (see Table 8). All chemicals were purchased from Merck KGaA and stock solutions were prepared in DMSO (Merck KGaA).

Table 8: Overview of used ABC transporter fluorescent substrates and respective inhibitors and their final incubation concentration.

Transporter protein	Substrate (concentration)	Inhibitor (concentration)
MDR1	Rhodamine 123 (1 µM)	Zosuquidar (1 µM)
MRP1	5(6)-Carboxyfluorescein (10 µM)	MK-571 (10 µM)
BCRP	Hoechst 33342 (10 µM)	Ko143 (1 µM)

Cells were seeded in 250 µL medium onto 96-well black plates (Corning, 0.32 cm^2) according to seeding densities and cultivation time as described in 3.1.2.1. If applicable, wells were coated with appropriate extracellular matrices prior to seeding.

On day of the experiment, medium was aspirated and cells were washed twice with warm 1x Dulbecco's Phosphate Buffered Saline with calcium and magnesium (DPBS +/+) (Thermo Fisher Scientific). All following incubation steps were performed at 37 °C. First, wells were incubated for 30 min with 125 µL of either of DPBS +/+ (vehicle control with DMSO as solvent match) or DPBS+/+ containing one of the inhibitors (see Table 5). Following the inhibitor preincubation, 125 µL of respective fluorophore solution was added (dissolved in DPBS +/+) and spiked with respective inhibitor or equivalent volume of DMSO (to solvent match) and incubated for 30 min. Final DMSO content was 0.25 % (v/v) in all conditions. To stop the experiment, wells were aspirated and cells were washed three times with ice-cold DPBS+/+. Then intracellular fluorescence of ABC transporter substrates within cells was measured with vehicle control cells serving as blank. Fluorescence was measured with a plate reader (iD3, Molecular Devices, San Jose, CA, USA). Excitation and emission wavelengths were as the follows: Rhodamine 123 (450/540 nm), 5(6)-Carboxyfluorescein (485/525 nm) and Hoechst 33342 (350/550 nm).

ABC transporter activity was assessed by comparing intracellular accumulation of fluorophore in absence and presence of inhibitor. Efflux was considered present if intracellular accumulation increased by more than 50 % in presence of inhibitor. This threshold was set based on guidelines from health authorities regarding classifying a compound as a substrate

of an active efflux transporter, where the efflux needs to change by at least 50 % in presence of a transporter-specific inhibitor [18].

3.1.2.5 Assessment of Monolayer Integrity

To verify whether cells cultured on Transwell® inserts formed a tight monolayer, TEER was measured using an epithelial volt-ohm-meter (EVOM-2, World precision instruments) and chopstick electrodes. TEER was assessed every two to three days for up to 14 or 21 days (depending on the respective cell line) for ALI- and LCC-cultured cells.

In brief, the medium was aspirated and 200 µL or 500 µL of 1x DPBS+/+ at 37 °C was added to apical and basolateral sides, respectively. Cells were placed on a thermoblock set to 37 °C and the resistance was measured. TEER was then calculated as described in Equation 1.

$$TEER = (TEER_{cell} - TEER_{blank}) * A$$

Equation 1. Formula to calculate the transepithelial electrical resistance (TEER) in Ω*cm^2. TEER is calculated by subtracting resistance of an empty Transwell® ($TEER_{blank}$ in Ω) from the resistance measured across monolayers ($TEER_{cell}$ in Ω) and corrected for surface area A (0.33 cm^2).

3.1.2.6 Assessment of the Permeability of Control Markers

To further investigate monolayer integrity of cells cultured on Transwell® inserts, the apparent permeability (P_{app}) of molecules with low or high passive permeability was tested. Atenolol was selected as low P_{app} marker (< 25 nm/s). Both carbamazepine and budesonide are considered high P_{app} markers (P_{app} > 100 nm/s). Moreover, LY, a known paracellular marker to assess membrane tightness, was included [78, 257]. Chemicals were prepared as DMSO stock solutions, except for LY, which was dissolved in distilled water (Thermo Fisher Scientific). Compounds were purchased from Merck KGaA except of budesonide that was purchased from Cayman Chemical (Ann Arbor, MI, USA).

Cells used in these experiments were cultured on Transwell® at ALI or LCC (for details regarding seeding density and cultivation time refer to 3.1.2.1).

The permeability of the markers substances was assessed in a bidirectional manner. For the experiment, each test compound was diluted in phenol red-free medium-199 (M-199; Bioconcept, Allschwil, Switzerland), supplemented with 0.1 % (w/v) BSA and 10 µM LY to achieve the following concentrations: atenolol (25 µM), carbamazepine (1 µM) or budesonide (10 µM). DMSO content was kept at 0.25 % in all conditions.

Compound solutions were spiked either to apical side (i.e. donor) and permeability to the basolateral side (i.e. acceptor) was measured (P_{app} AB) or the other way round (P_{app} BA).

A volume of 200 µL was added to apical side and 500 µL to basolateral side. The acceptor side contained pure M-199 with 0.1 % BSA and 0.25 % DMSO. Plates were incubated for 3 h at 37°C while shaking at 200 rpm. Samples were taken from both acceptor and donor compartments. Initial samples taken from compound solution (C_0) and donor samples were diluted 1:5 in assay medium. All samples were then quenched with the three-fold volume of ice-cold acetonitrile containing the internal standard oxazepam. Samples were then centrifuged at 6300 rpm for 10 min and the supernatant was collected. Compound concentration was quantified via liquid chromatography coupled to tandem mass spectrometry (LC-MS/MS) as described in 3.1.2.8. For LY, concentration was quantified by measuring its fluorescence at 425/525 nm. The P_{app} values were calculated as shown in Equation 2.

$$P_{app} = \frac{\Delta Q}{\Delta t} * \frac{1}{A * C_0}$$

Equation 2. Formula to calculate the apparent permeability P_{app} (nm/s). ΔQ/Δt describes the amount of compound (nmol) permeating the cell monolayer in a defined time (10 800 s). A is the filter surface area (0.33 cm^2) and C_0 the initial incubation concentration (µM).

3.1.2.7 Bidirectional Studies Assessing MDR1, MRP1 and BCRP Efflux

Bidirectional efflux studies were conducted to investigate active efflux mediated by MDR1, MRP1 and BCRP. Known substrates of ABC transporters were selected: edoxaban for MDR1, doxorubicin for MRP1 and prazosin for BCRP [211, 258, 259]. All chemicals were prepared as DMSO stock solutions. They were purchased from Merck KGaA, except for Edoxaban, which was purchased from Toronto Research Chemicals (Toronto, Canada).

Table 9: Overview of ABC transporter substrates and respective inhibitors and their final incubation concentration in bidirectional efflux study.

Transporter protein	Substrate (concentration)	Inhibitor (concentration)
MDR1	Edoxaban (1 µM)	Zosuquidar (1 µM)
MRP1	Doxorubicin (5 µM)	MK-571 (10 µM)
BCRP	Prazosin (1 µM)	Ko143 (1 µM)

Their permeability was tested in a bidirectional manner as described in 3.1.2.6, in the absence and presence of ABC transporter-specific inhibitors (see Table 9). In addition to P_{app} AB and P_{app} BA, respective permeability in presence of inhibitor was determined, indicated as $P_{app,inh}$ AB and $P_{app,inh}$ BA.

Cells used in these experiments were cultured on Transwell® at ALI or LCC (for details regarding seeding density and cultivation time refer to 3.1.2.1).

Substrates were diluted in phenol-red free M-199 + 0.1 % (w/v) BSA and either respective inhibitor or equivalent amount of DMSO was added. Acceptor medium consisted of M-199 with

0.1 % BSA plus respective inhibitor or matched DMSO volume. Final DMSO concentration was 0.25 % (v/v) in all conditions. The LX (10 µM) served as marker for barrier integrity and was added to each dose solution. Dose solutions were transferred to Transwell® plates and plates were incubated. After 3 h, samples were taken, diluted if needed and quenched (for details see 3.1.2.6). Substrate concentrations were then quantified via LC-MS/MS. Separate samples were taken from acceptor wells to measure LY concentration via fluorescence.

The P_{app} values were calculated according to Equation 2. Wells with LY P_{app} values > 25 nm/s were excluded for compounds' P_{app} calculation, as this indicates monolayer leakiness [78]. To assess efflux, efflux ratio (ER) was calculated by dividing the permeability P_{app} BA by P_{app} AB (see Equation 3). If the ER exceeds 2, it indicates the presence of active efflux at the apical side. Furthermore, ER needs to decrease by at least 50 % in presence of ABC transporter specific inhibitor [18]. The efflux ratio in presence of inhibitor is referred to as ER,i.

$$ER = \frac{P_{app}\ BA}{P_{app}\ AB}$$

Equation 3. Formula to calculate the efflux ratio (ER). Permeability from basolateral to apical side (P_{app} BA) is divided by permeability from apical to basolateral side (P_{app} AB).

3.1.2.8 Quantitative Analysis via LC-MS/MS

Sample analysis was conducted using LC-MS/MS. The liquid chromatography system included a CBM-20A controller, a DGU-20A5R degasser, two Shimadzu Nexera LC-30AD pumps (Shimadzu, Kyoto, Japan) connected to an HTS CTC PAL autosampler (CTC Analytics, Zwingen, Switzerland). For temperature control of the column (Ascentis Express C18, 20 × 2.1 mm, 2.7 µm, Supelco, Bellefonte, PA, USA) a column oven (HotDog 5090, Prolab Instruments, Dornach, Switzerland) was used. This setup was coupled to a Triple Quadrupole 6500+ mass spectrometer equipped with an IonDrive Turbo V source (AB Sciex, Concord, ON, Canada). The mass spectrometer was used in the multiple reaction monitoring mode. Positive ionization mode was applied for the analysis of all compounds, with ionization source parameters detailed in supplemental Table A1. Analytical readouts were based on the peak area ratio between the analyte and the internal standard (oxazepam). Further details of the applied transition parameters for each test compound can be found in the supplemental material (Table A2).

The supernatants of the precipitated samples were injected into the LC-MS/MS system using injection volumes of 2.0 µl for edoxaban, doxorubicin and atenolol and 1.0 µl for prazosin, budesonide and carbamazepine. Compound elution was achieved using the following mobile phases: A – 0.5% formic acid in water/acetonitrile (95/5) and B – acetonitrile. For atenonol, mobile phase A consisted of 20 mM ammonium bicarbonate in water/acetonitrile (95/5).

A high pressure linear gradient from 0% to 95% B was applied at a flow rate of 600 µl/min with a total runtime of 1.4 minutes (see supplemental Table A3).

Data analysis was conducted with Analyst 1.7.2 software (AB Sciex, Concord, ON, Canada) using initial samples as reference with a linear through zero regression model. Reference samples with accuracy above 20% bias were excluded.

3.1.2.9 Statistics

If not stated otherwise, presented data shows mean ± standard deviation (SD) from three independent experiments with at least three technical replicates. For data visualization and statistical analysis, GraphPad Prism software was used (Version 10.4.1, GraphPad Software, La Jolla, CA, USA). Differences between two groups were assessed with an unpaired two-tailed t test. Differences between multiple groups were analysed with a one-way ANOVA followed by a Tukey's post hoc multiple comparisons test. If $p \leq 0.05$, the difference was considered significant.

3.1.3 Results

3.1.3.1. Analysis of Gene Expression of MDR1, MRP1 and BCRP in Lung Epithelial Cells

Gene expression levels of MDR1, MRP1 and BCRP were analysed by qPCR in various human cells derived from upper (16HBE14o-, Calu-3, NHBE) and lower airways (NCI-H441, A549, hAELVi, Arlo and hAEpC) that mimic the human lung epithelium (Figures 10 & 11). Expression in flask cultured cells was compared to expression in Transwell® ALI and LCC culture.

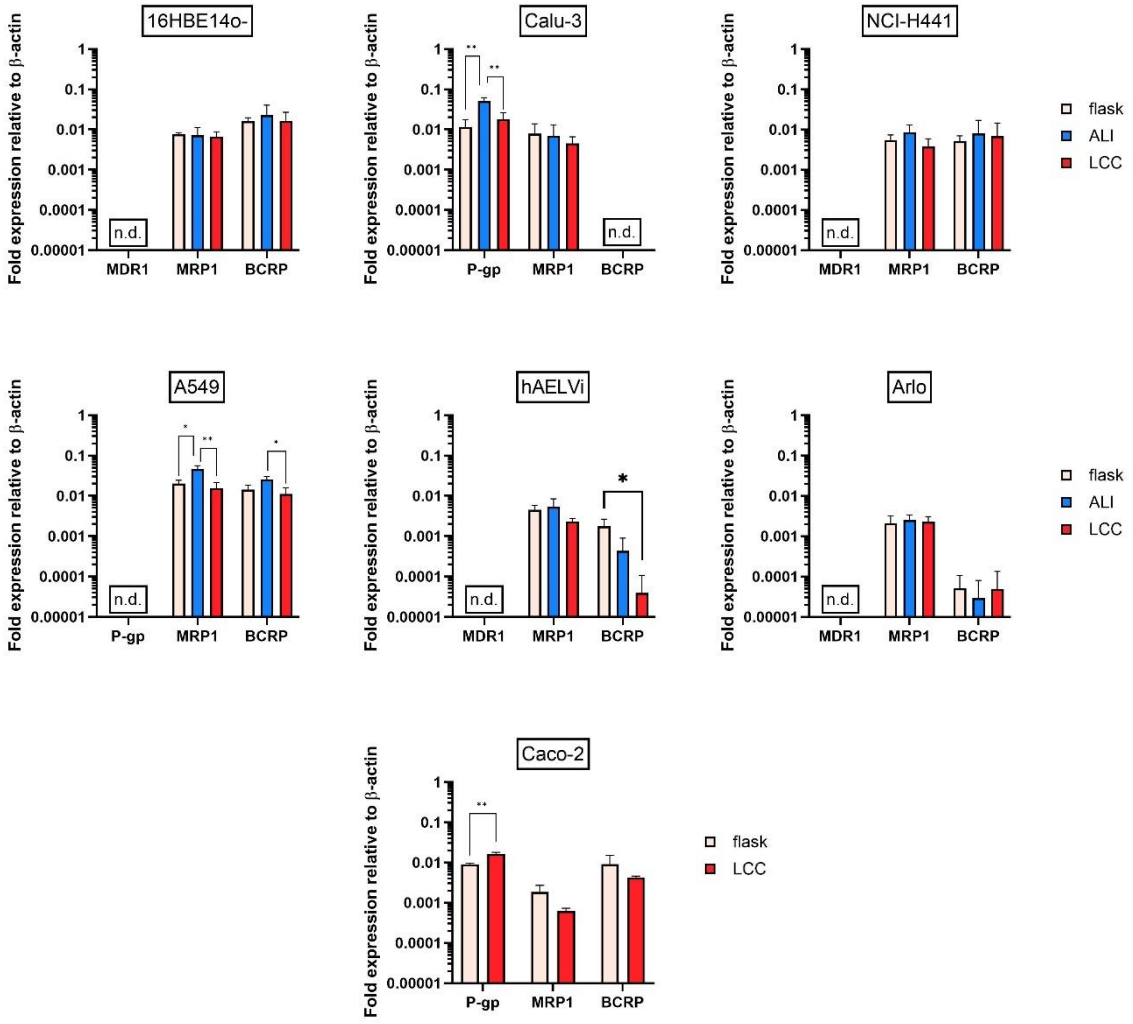

Figure 10: Gene expression of MDR1, MRP1 and BCRP in human lung epithelial cells lines and Caco-2 cells analysed by qPCR, depicted as relative expression to house-keeping gene β-actin. Expression levels of ABC transporters in lung epithelial cells cultured in flasks or on Transwell® inserts at air-liquid interface (ALI) or liquid-covered condition (LCC) were compared. Caco-2, which serve as positive control, were cultured in flasks and at LCC on Transwell® inserts. Data are presented as mean ± SD, N = 3 with n = 3. n.d. stands for non-detected. Differences in mean of three groups were analysed by One-way ANOVA followed by Tukey's multiple comparison test. Differences between two groups were analysed by un-paired two-sided t-test. *p ≤ 0.05, **p ≤ 0.01.

MRP1 expression was confirmed across all cells whereas MDR1 expression was only observed in Calu-3. BCRP was detected in some of the cells, specifically 16HBE14o-, NCI-H441 and A549 but was absent in Calu-3. Compared to these cell lines, hAELVi and Arlo showed lower expression of BCRP.

Caco-2 cells, which are known to express ABC transporter proteins and were included as positive control, showed expression of all efflux transporter proteins: MDR1, MRP1 and BCRP.

Comparative analysis of gene expression revealed that there were no statistically significant differences in ABC transporter' expression levels between lung epithelial cells cultured in flasks and those on inserts (i.e. ALI or LCC) for majority of ABC transporters (except for P-gp expression in flask vs ALI and ALI vs LCC in Calu-3, MRP1 expression in flask vs ALI and ALI vs LCC in A549, BCRP expression in flask vs LCC in hAELVi and BCRP expression in ALI vs LCC in A549).

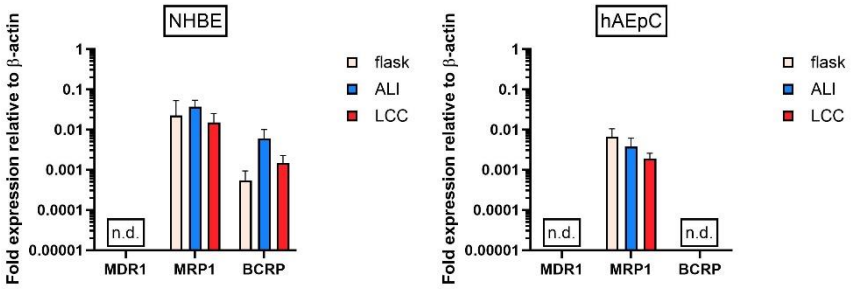

Figure 11: Gene expression of MDR1, MRP1 and BCRP in primary human lung epithelial cells analysed by qPCR, depicted as relative expression to housekeeping gene β-actin. Expression levels of ABC transporter in cells cultured in flasks or on Transwell® inserts at air-liquid interface (ALI) or liquid-covered condition (LCC) were compared. For hAEpC, the flask condition refers to cells in suspension after the isolation and prior the seeding (i.e. alveolar type II cells). Data are presented as mean ± SD, N = 3 with n = 3. n.d. stands for non-detected.

As observed in lung epithelial cell lines, MRP1 shows a ubiquitous expression in primary lung epithelial cells, whereas MDR1 was detected in neither NHBE nor in hAEpC. BCRP was not detected in hAEpC but its expression was observed in NHBE. Due to the limited number of primary cells and similar expression levels of ABC transporters at ALI and LCC (no statistically significant differences), NHBE and hAEpC cells were cultured only at ALI for further experiments.

3.1.3.2 Analysis of Protein Expression of MDR1, MRP1 and BCRP in Lung Epithelial Cells

To confirm the expression of ABC transporters at protein level, Western Blotting was performed. Relative expression of transporter proteins normalised to β-actin was compared (Figures 12 & 13). Representative Western Blots showing single bands for ABC transporter and β-actin protein expression can be found in the supplementary material (Figures A1-A9).

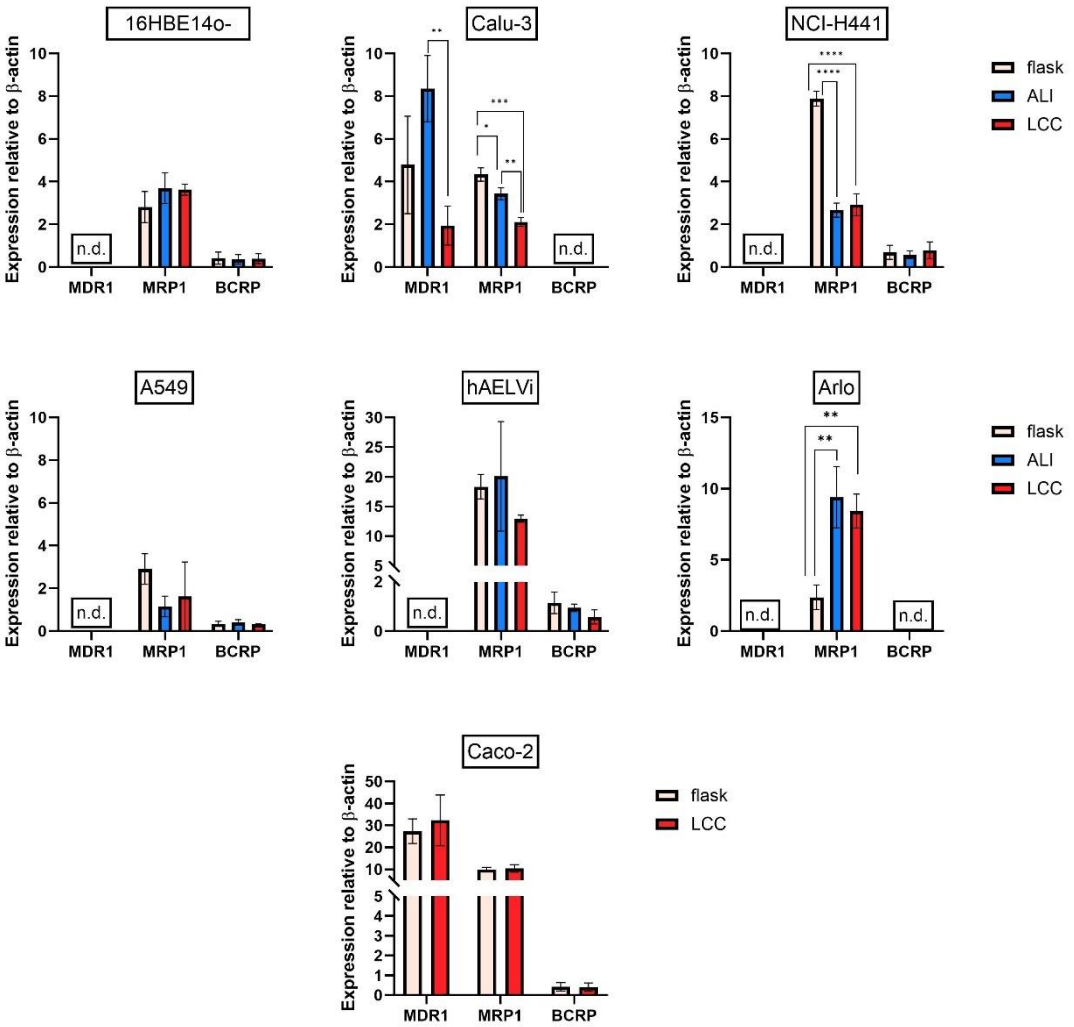

Figure 12: Protein expression of MDR1, MRP1 and BCRP in human lung epithelial cells and Caco-2 cells analysed by Western Blot and depicted as relative expression to β-actin. Expression levels of ABC transporters in cells cultured in flasks or on Transwell® inserts at air-liquid interface (ALI) or liquid-covered condition (LCC) were compared. Caco-2, which serve as positive control, were cultured in flasks and at LCC on Transwell® inserts. Data are presented as mean ± SD with N = 3. n.d. stands for non-detected. *p ≤ 0.05, **p ≤ 0.01, ***p ≤ 0.001, ****p ≤ 0.0001. Differences in mean of three groups were analysed by One-way ANOVA followed by Tukey's multiple comparison test. Differences between two groups were analysed by un-paired two-sided t-test.

Western Blotting confirmed results from previous qPCR studies (see 3.1.3.1), i.e. Caco-2 cells, which serve as positive control cells for ABC transporter expression, showed expression of MDR1, MRP1 and BCRP. In lung epithelial cells, MDR1 was detected only in Calu-3 and MRP1 was ubiquitously expressed across all cells evaluated. BCRP generally showed a weak expression in 16HBE14o-, NCI-H441, A549 and hAELVi and was absent in Calu-3 and Arlo.

Interestingly in Calu-3, MDR1 shows at protein level a more than four-fold higher expression at ALI compared to LCC. MRP1 expression appears to significantly decrease once cells are cultured on Transwell® inserts, which reductions up to two-fold in Calu-3 and up to three-fold in NCI-H441. In contrast, MRP1 expression in Arlo appeared to increase when cells were cultured onto Transwell® inserts, with an up to three-fold increase.

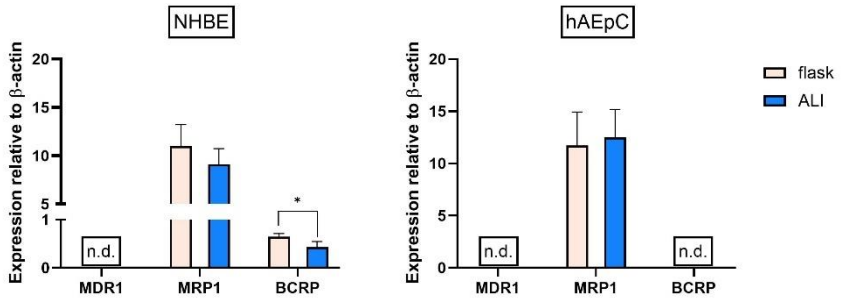

Figure 13: Protein expression of MDR1, MRP1 and BCRP in primary human lung epithelial cells analysed by Western Blot and depicted as relative expression to housekeeping protein β-actin. Expression levels of ABC transporter in cells cultured in flasks or on Transwell® inserts at air-liquid interface (ALI) were compared. For hAEpC, the flask condition refers to cells in suspension after the isolation and before the seeding (i.e. alveolar type II cells). Data are presented as mean ± SD with N = 3. n.d. stands for non-detected. Differences between two groups were analysed by un-paired two-sided t-test with *$p \leq 0.05$.

As observed for lung epithelial cell lines, protein expression analysis of MDR1, MRP1 and BCRP by Western Blot in primary lung epithelial cells NHBE and hAEpC confirmed gene expression levels. MRP1 showed expression in both cell types with MDR1 being absent. BCRP was not detected in hAEpC and being weakly expressed in NHBE.

3.1.3.3 Assessing ABC Transporter' Activity with Fluorescent Substrates

The presence of active efflux by MDR1, MRP1 and BCRP was investigated by comparing changes in the intracellular concentration of fluorescent ABC transporter substrates in the absence and presence of transporter-specific inhibitors, in cells cultured on well plates (see Figure 14).

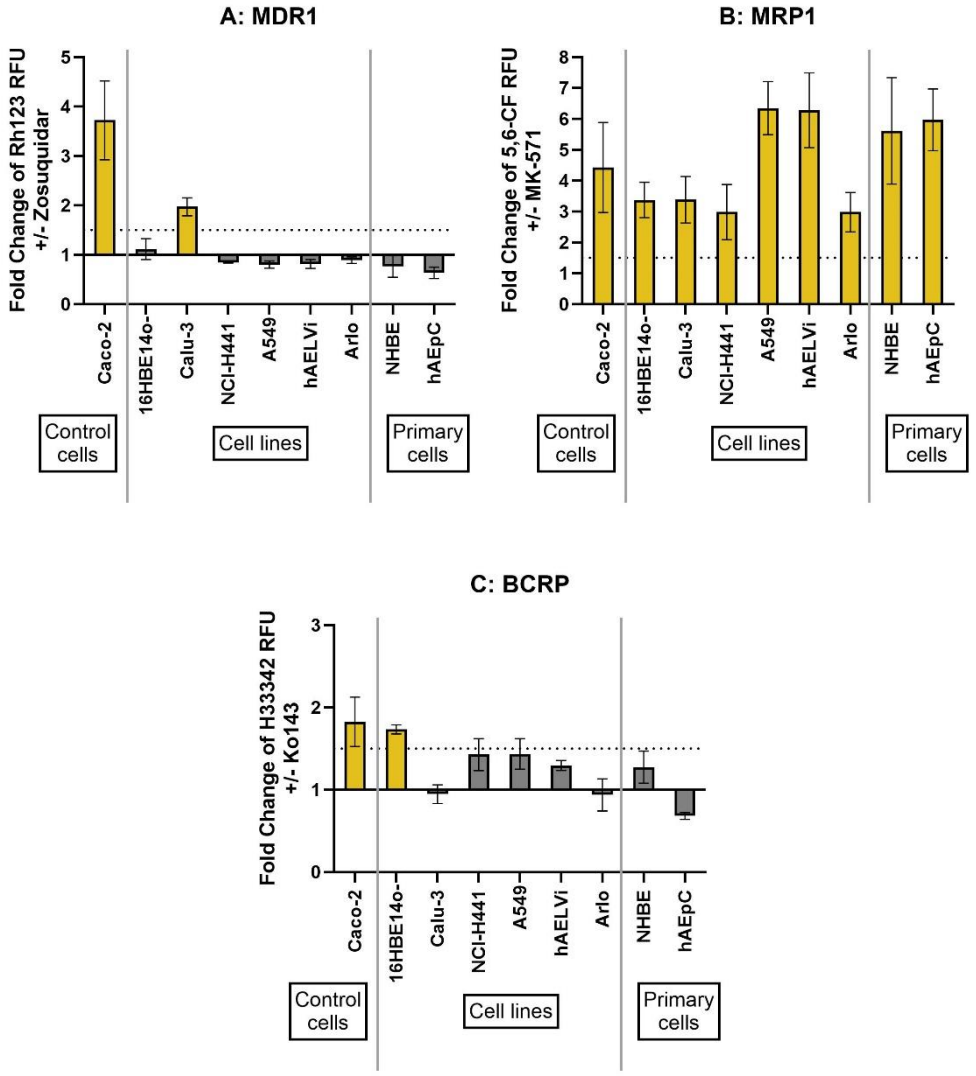

Figure 14: Relative change in intracellular concentration of fluorescent transporter substrates in presence of specific inhibitors. Data is presented as change in relative fluorescent units (RFU) as mean ± SD, N = 3 with n = 3. Active efflux was considered if intracellular concentration increased by more than 1.5-fold in presence of inhibitor (indicated via dashed line and yellow labelling of the column). A: Rhodamine 123 (Rh123) as substrate to assess **MDR1** activity; B: 5,6-Carboxyfluorescein (5,6-CF) as substrate to assess **MRP1** activity and C: Hoechst 33342 (H33342) as substrate to assess **BCRP** activity.

Rhodamine 123 (Rh123) showed a 3.7-fold and 2-fold increase in intracellular concentration in presence of zosuquidar in Caco-2 and Calu-3, respectively. This confirmed the expression of active MDR1 in both cell lines. No increase was observed in the remaining cells, which was expected as MDR1 expression was not detected via qPCR and Western Blot in these cells.

MRP1 was shown to be active in all lung epithelial cells and in Caco-2, as the intracellular concentration of 5,6-Carboxyfluorescein (5,6-CF) increased by more than three-fold in presence of MK-571 in all tested cells.

The intracellular concentration of Hoechst 33342 (H33342) increased by more than 1.5-fold in presence of Ko143 in 16HBE14o- and Caco-2, indicating the presence of active BCRP in these cells. No increase in intracellular concentration of H33342 was observed for Calu-3 and Arlo and hAEpC. In hAELVi and NHBE, the increase in H33342 intracellular concentration with inhibitor was close to 1.3-fold, whereas in NCI-H441 and A549 an increase of 1.4-fold was observed.

3.1.3.4 Assessing Monolayer Integrity of Lung Epithelial Cells

To verify the formation of a tight cell monolayer and to investigate potential differences in terms of barrier formation across the cells, TEER was measured for up to 14 or 21 days after seeding on Transwell® inserts (Figures 15 & 16). In addition to TEER, bidirectional permeability experiments, using low (atenolol and LY) and high (carbamazepine or budesonide) cellular permeability markers were conducted to further understand barrier formation properties (these experiments were conducted on day X post-seeding equivalent to the day post-seeding when bidirectional efflux studies were conducted, see 3.1.2.1 for further details). The measured P_{app} values for the low permeability markers are depicted in Figures 17 & 18.

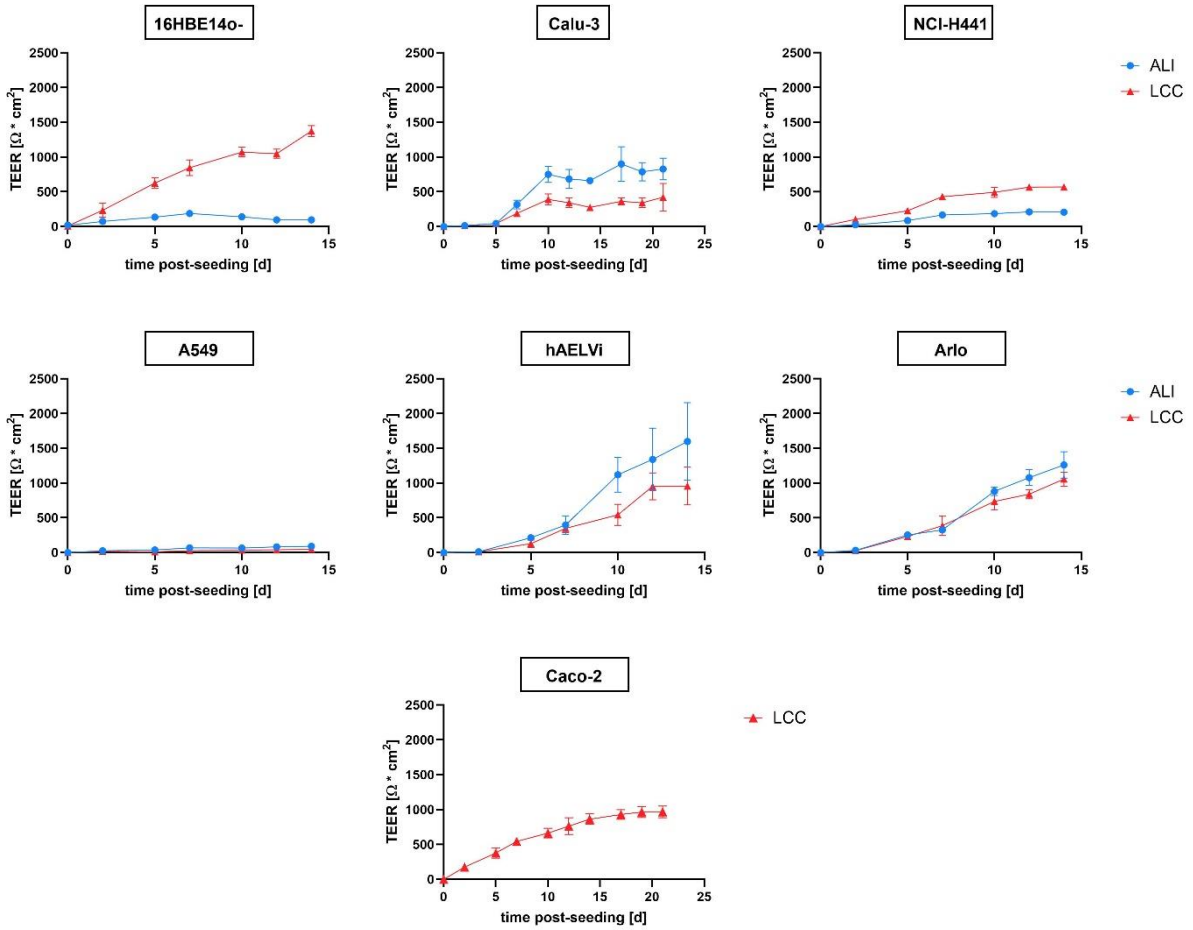

Figure 15: Time course of transepithelial electrical resistance (TEER) in lung epithelial cell lines cultured at air-liquid interface (ALI) or liquid-covered condition (LCC) and in Caco-2 at LCC. The values for ALI are shown as line chart with circles (--o--) and for LCC as line chart with triangles (--Δ--). Data is shown as mean ± SD with n ≥ 6.

TEER values < 250 Ω*cm^2 typically indicate the presence of a leaky cell layer [75]. This was observed for 16HBE14o- and NCI-H441 cells cultured at ALI (with measured TEER < 200 Ω*cm^2) and for A549 cells cultured at ALI and LCC (TEER < 100 Ω*cm^2), pointing to their inability to form an electrically tight cellular barrier. All other remaining cells showed a TEER exceeding this threshold of 250 Ω*cm^2, confirming the presence of tight cell monolayers.

Highest TEER across all cells was measured in alveolar-epithelium-derived cell lines: hAELVi and Arlo.

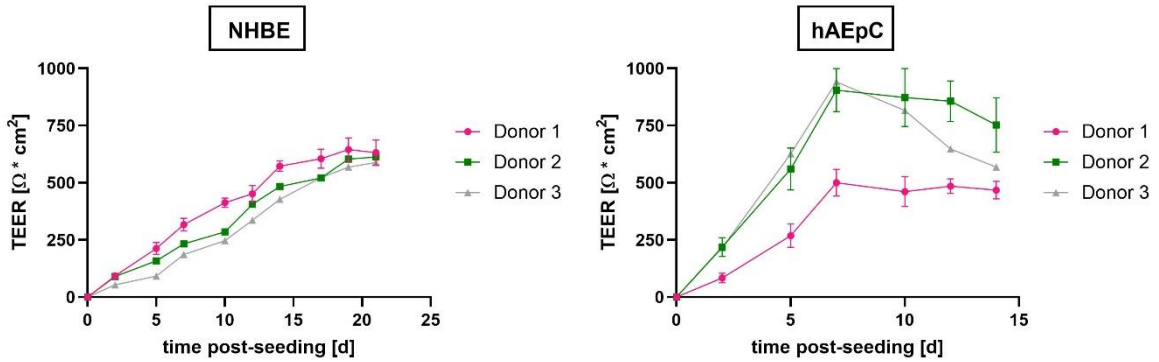

Figure 16: Time course of transepithelial electrical resistance (TEER) in each three donors of human bronchial (NHBE) and alveolar (hAEpC) primary lung epithelial cells at air-liquid interface (ALI) culture. Donor 1 is depicted as line chart with balls (--o--), donor 2 as line chart with squares (--□--), donor 3 as line chart with triangles (--Δ--). TEER values are shown as mean ± SD, n ≥ 6.

Primary NHBE cells showed an increase in TEER up to day 19, peaking around 600 Ω*cm^2 and measured values are comparable to those in Calu-3 cells at ALI (tracheo-bronchial derived cell line). Primary hAEpC cells showed a peak in TEER after 7 days (ranging from 500 to 940 Ω*cm^2), being up to two-fold lower than in their derived cell lines hAELVi and Arlo.

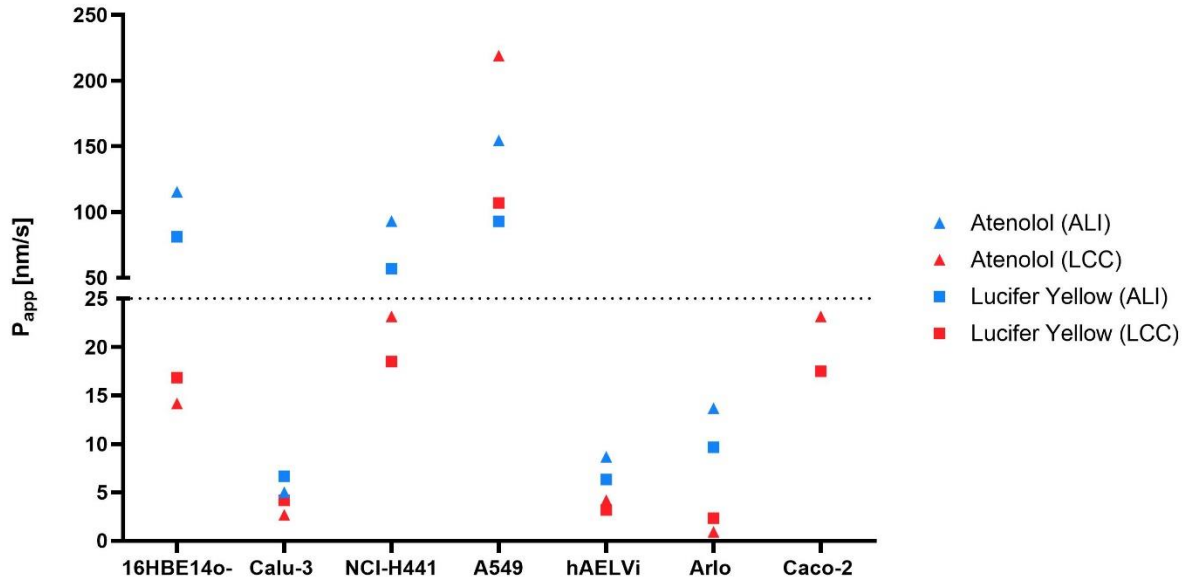

Figure 17: The mean apparent permeability (P_{app}) of low permeability control markers atenolol and Lucifer Yellow (LY) in lung epithelial cell lines cultured at air-liquid interface (ALI) or liquid-covered condition (LCC) and in Caco-2 at LCC. Values for atenolol as depicted as triangles (Δ) and for LY as squares (□). The dashed line at 25 nm/s represents the acceptance threshold for low permeability paracellular markers (atenolol and LY), typically confirmative of a tight monolayer [78]. Values are shown as mean with n = 6. P_{app} values are shown as average of P_{app} AB and P_{app} BA.

For low permeability markers, such as atenolol and LY, typically a threshold less than 25 nm/s is confirmatory of barrier integrity [78]. Measured P_{app} values for both atenolol and LY, exceed 25 nm/s in 16HBE14o- (up to five-fold) and NCI-H441 (up to four-fold) cells if cultured at ALI and in A549 (up to nine-fold), at both ALI and LCC. This indicates that those cells under these conditions did not form a tight monolayer, correlating with measured TEER values (< 250 Ω*cm^2). For remaining cells and 16HBE14o-/NCI-H441 cultured at LCC, measured P_{app} values for the two low permeability markers were below 25 nm/s, confirming the formation of an intact cell monolayer (see Figure 17). Compounds with a cellular permeability > 100 nm/s, are typically classified as highly permeable (i.e. carbamazepine) [260]. Measured permeability coefficients for carbamazepine were above this value in all lung epithelial cell lines and Caco-2 (see supplemental Figure A10).

Both NHBE and hAEpC cells showed a P_{app} of less than 25 nm/s for both low permeability markers atenolol and LY across each three donors, as shown in Figure 18. This confirms their ability to form an electrically tight barrier. Permeability data for the high permeability marker budesonide ranged from 62 nm/s to 100 nm/s in NHBE and from 88 nm/s to 112 nm/s (with data depicted in the supplemental Figure A11).

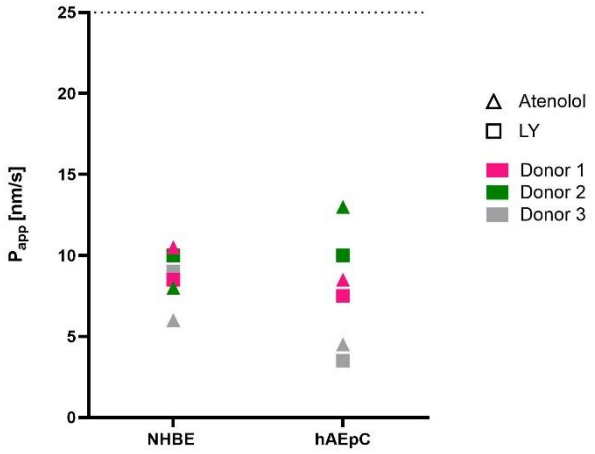

Figure 18: The mean apparent permeability (P_{app}) of low permeability control markers atenolol and Lucifer Yellow (LY) in each three donors of human bronchial (NHBE) and alveolar (hAEpC) primary lung epithelial cells cultured at air-liquid interface. Values for atenolol as depicted as triangles (Δ) and for LY as squares (□). The dashed line at 25 nm/s represents the acceptance threshold for low permeability paracellular markers (atenolol and LY), typically confirmative of a tight monolayer [78]. Values are shown as mean with n = 6. P_{app} values are shown as average of P_{app} AB and P_{app} BA.

3.1.3.5 Bidirectional Permeability Studies to Assess ABC Transporters Efflux

Bidirectional efflux studies with drug molecules as substrates were conducted to investigate if active efflux mediated by MDR1, MRP1 and BCRP is present in lung epithelial cells. Calculated efflux ratios (ER) in absence and presence of specific transporter' inhibitors are shown in Figure 19.

Edoxaban showed asymmetry of permeability in Caco-2 cells (ER = 4.3), which was reduced by more than 50 % in presence of zosuquidar ($ER_{,i}$), pointing to active MDR1 efflux at the apical side. The same was observed for Calu-3 cultured at ALI, confirming the presence of functional active MDR1. Interestingly, no efflux was present in Calu-3, when cultured at LCC. In the remaining cells, no efflux of edoxaban was observed (ER < 2.0), as expected based on the absence of MDR1 expression in these cells.

Doxorubicin showed efflux in Caco-2 (ER = 7.0) at the apical side that was reduced in presence of MK-571, confirming MRP1 efflux in these cells. Moreover, NHBE cells showed an ER > 2, however this efflux seemed to be non-sensitive to MRP1 inhibitor MK-571 (ER,i >2). All other cells showed an ER < 2, indicating the absence of MRP1 efflux. In general, it needs to be noted that measured permeability values for doxorubicin were quite low (typically < 10 nm/s). As the ER concept captures active efflux at the apical side of the cell membrane and MRP1 was claimed to be expressed rather at the basolateral side, the uptake ratio (UR, a reciprocal of the ER) was calculated in addition for doxorubicin [87]. All calculated UR values were < 2, pointing to the absence of MRP1 efflux on the basolateral side (as illustrated in the supplemental material in Figure A12). This absence of MRP1 efflux is in contradiction to the measured expression levels of MRP1 in all cell lines and primary cells. It needs to be stated that doxorubicin is not a specific substrate for MRP1 [261] and other structurally related MRPs (such as MRP2 or MRP3) could interfere with its transport across the cell membrane, given their reported expression in the human lung epithelium [177, 248]. The RNA expression of MRP2, MRP3, MRP4, MRP5 and MRP6 has been measured by qPCR in lung epithelial cells to compare their expression levels against those of MRP1. The data is shown in the supplemental material (see Figures A13 & A14).

Prazosin showed asymmetry in permeability in Caco-2 cells (ER > 2) being sensitive to BCRP inhibitor Ko143. This phenomenon was not observed in any of the lung epithelial cells, indicating the absence of active BCRP efflux, when using prazosin as model substrate for BCRP. This is in contrast to observed protein expression of BCRP in 16HBE14o-, NHBE, NCI-H441and hAELVi.

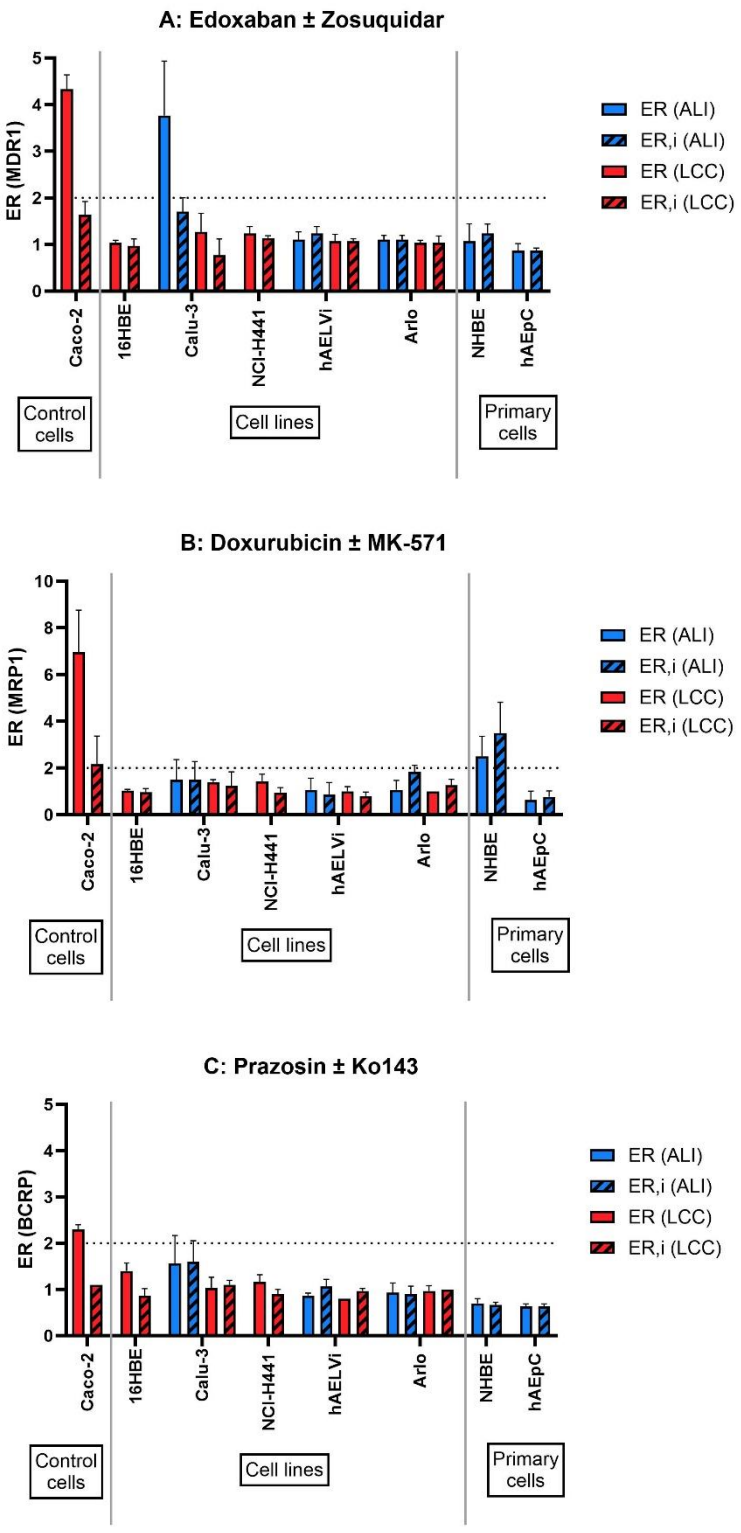

Figure 19: Calculated efflux ratios (ER) of ABC substrates in lung epithelial cells and Caco-2 in absence (ER) and presence (ER,i) of transporter-specific inhibitors. Efflux in lung epithelial cell lines was compared at both at air-liquid interface (ALI) or liquid-covered condition (LCC), but due to monolayer leakiness, no ER values are reported for 16HBE14o-/NCI-H441 at ALI and for A549 at ALI and LCC. In primary lung epithelial cells, ER was only assessed at ALI and in Caco-2 at LCC. If ER > 2, this indicates active efflux present at the apical side of the cell membrane (indicated with dashed line). Data is presented as mean ± SD, N = 3 with n = 3. A: Edoxaban efflux to assess **MDR1**; B: Doxorubicin efflux to assess **MRP1**; C: Prazosin efflux to assess **BCRP**.

3.1.4 Discussion

ABC transporters such as MDR1 or BCRP transport a wide range of exogenous molecules, including drugs, thereby influencing the pharmacokinetics of their substrates in a clinically evident manner [18]. MRP1 is described to play an important role in tumour chemoresistance [210]. Both *ex vivo* studies using isolated perfused mouse lungs and *in vivo* studies using Positron Emission Tomography tracer imaging in rats reported the presence of active Mdr1, Mrp1 and Bcrp in the rodent's lung epithelium [205, 217, 227]. In contrast, the role of these three ABC transporters as potential drivers of drug distribution in the human lung epithelium remains less clear [177].

Multiple *in vitro* studies have indicated the presence of these three ABC transporters in cell lines and primary cells from both upper and lower human airway epithelium [146, 177, 248]. However, discrepancies in expression levels, particularly for MDR1 and BCRP have been reported in further *in vitro* studies, aiming to characterise ABC transporters in the human lung. These inconsistencies may be attributed to the cellular heterogenicity of the lung epithelium across the different lung regions, the lack of clearly defined cell culture practices and variations in experimental conditions, which hinders a direct comparison across studies [20, 177].

Regarding their spatial expression in the human lung epithelium, both P-gp and BCRP were described to be expressed on the apical side (i.e. facing the lung lumen), whereas MRP1 was reported to be expressed on the basolateral side (i.e. the blood vessel-facing side) [182]. In contrast to P-gp and BCRP, the efflux of substrates (like chemotherapeutics) by MRP1 is glutathione-dependent, which is co-transported [210].

This *in vitro* study aimed to investigate ABC transporter expression and function across a number of lung epithelial cell models to allow a direct comparison and understand potential differences, particularly when using the models to evaluate drug disposition. The results of this study revealed differences in expression across tested cell lines and primary cells. While expression was confirmed, results from functionality assessments indicated limited contribution of ABC transporters in transporting drugs across the human lung epithelium, *in vitro.*

3.1.4.1 Expression of ABC Transporters at Gene and Protein Level

This study investigated the expression of MDR1, MRP1 and BCRP at both gene and protein level in six cell lines mimicking the upper and lower human lung epithelium (16HBE14o-, Calu-3, NCI-H441, A549, hAELVi and Arlo) as well as primary cells derived from bronchial (NHBE) or alveolar (hAEpC) lung epithelium.

Protein expression data confirmed presence or absence of ABC transporters as characterised by qPCR but revealed statistically significant differences in certain cell lines (i.e. expression levels in flask vs. ALI vs. LCC) that were present at protein level but not at gene level.

MDR1 Expression

In this study, MDR1 was detected only in Calu-3 cells. At gene level no significant differences in MDR1 expression across the different culture conditions was observed. Whereas, at protein level, expression was more than four-fold higher at ALI compared to LCC, which translated also into a pronounced efflux at ALI. A study that assessed MDR1 expression in Calu-3 at ALI vs. LCC at gene level by qPCR derived a similar result, where MDR1 levels were more than two-fold higher at ALI compared to LCC (when culturing cells for 21 days on Transwell® inserts) [79]. Further studies, using qPCR and Western Blot, reported a positive MDR1 expression in this cell line [87, 195, 201, 262]. However, a LC-MS/MS approach failed to detect MDR1 in Calu-3, from cells cultured in flasks [194]. Studies by Hutter et al. and Rotoli et al. have shown that protein expression of MDR1 appears to increase with increasing culture time of Calu-3 at ALI (day 7/8 vs. day 21) on Transwell® inserts [87, 201]. Additionally, the passage number was reported to influence MDR1 expression, as a stronger signal in Western Blot was observed for highly passaged Calu-3 cells (p.45-50), compared to cells at a lower passage (p.25-30). In contrast, qPCR analysis at gene level showed an opposite trend, where low passaged Calu-3 cells showed higher expression levels than highly passaged ones [201]. A study by Haghi and colleagues investigated the surface expression of MDR1 via flow cytometry and found no changes in MDR1 levels between passages 30 to 40 (if ≥ 7 days of ALI culture) [196]. Thus, it is possible that MDR1 expression levels in Calu-3 may be influenced by changes in non-standardised culture conditions. The use of different subclones could contribute to the described differences, however the individual studies do not always provide information regarding the Calu-3 clone used. Further, potential differences in sample preparation, sample extraction efficiency and sensitivity of applied characterisation methods may also play a role. Due to the fact, that Calu-3 cells are often used in pulmonary drug disposition studies and the impact of culture conditions on their differentiation, Kreft and colleagues pointed in their study to the need of standardised and optimised protocols, when working with these cells [79]. A guidance document regarding ‘Good Cell and Tissue Culture Practise’ was recently published with the aim of improving the reproducibility of experiments involving *in vitro* cell models. It pointed to factors such as choice of reagents, need of quality control of biological material and technical equipment as well as a proper documentation, which need to be accounted for to tackle the aim of an overall improvement of experimental reproducibility [263]. Aspects beyond cell culture practise were considered in guideline documents of ‘Good *in vitro*

method Practise', like the use of control items or clearly defined acceptance criteria, aiming to improve robustness and uncertainties of *in vitro* methods in the context of regulatory acceptance [264]. Standardisation attempts in terms of general cell culture and *in vitro* experimental practise could potentially contribute to reduce the variability across studies results, also in the context of differences in pulmonary ABC transporter's expression levels across literature.

In two other cell lines derived from tumours, included in this study (NCI-H441 and A549), no MDR1 was detected, neither at gene nor at protein level. However, contradicting data has been reported in the literature. MDR1 expression in NCI-H441, cultured at ALI & LCC, was detected via Western Blot in one study, whereas it was not detected using a mass spectrometric protein analysis, where cells were cultured in flasks [94, 194]. In A549, gene expression data hinted to a weak expression of MDR1 [108, 195], whereas at protein expression level, both absence and presence have been reported [108, 194, 265]. Furthermore, it is possible that other cell tumour subclones were used in this study compared to those in published studies, leading to the absence of MDR1 expression. Moreover, as described for Calu-3, differences in culture conditions and experimental settings and techniques across studies might contribute to the observed discrepancies in expression levels.

Moreover, since Calu-3, NCI-H441 and A549 are cell lines derived from lung carcinoma patients [77], they might not accurately mimic the healthy lung epithelium in terms of ABC transporter expression as their levels were described to be upregulated in tumours (i.e. multiple drug resistance) [191, 266]

Primary human bronchial epithelial cells (NHBE) did not show expression of MDR1, which aligns with the findings in this study for the immortalised human bronchial cell line 16HBE14o- but in contrast to the bronchial cancer-derived Calu-3 cells. In literature, a rather weak expression was described for NHBE at both gene and protein level, characterised by qPCR and Western Blot [89, 195, 201]. For 16HBE14o-, studies have reported conflicting results, with some describing a strong presence of MDR1 at both gene and protein level (by PCR and immunocytochemical staining), while others have reported its complete absence at gene level (using PCR) [85, 195, 267].

MDR1 was also absent in primary alveolar cells hAEpC, being in accordance with their derived immortalised cell lines hAELVi and Arlo. Literature studies have shown a weak expression in hAEpC and absence of MDR1 expression in hAELVi and Arlo [107, 108, 111, 195].

As highlighted, there are a number of conflicting reports across the literature, regarding MDR1 expression. Variability in analytical methods, which leads to differences in sensitivity and

sample processing protocols, combined with non-standardised culture conditions may contribute to the observed discrepancies.

MRP1 Expression

MRP1 is reported to have a high protein abundance in the human lung compared to other ABC transporters and its high expression levels were reported in a large number of lung epithelial cell lines, primary cells and lung tissue [187, 194, 244].

In this study, MRP1 expression was detected in all cell lines and primary cells, consistent with reports across literature [74, 87, 107, 108, 195].

At gene level, no statistically significant differences in MRP1 expression were observed, when comparing the different culture conditions, flask and Transwell® inserts (ALI/LCC). However, at protein level, MRP1 expression was significantly increased in Arlo cells cultured at ALI and LCC compared to flask-cultured cells, whereas the opposite was observed for Calu-3 and NCI-H441. Interestingly, a significant difference of MRP1 expression at ALI vs. LCC culturing was observed only in Calu-3. This is consistent with findings from Kreft et al., who reported an almost two-fold increase in MRP1 gene expression for Calu-3 at ALI compared to LCC after 21 days of Transwell® culture [79]. For other cells in this study, no impact of the culture condition (ALI vs. LCC) on expression of MRP1 was observed.

BCRP Expression

In this study, BCRP expression was confirmed at both gene and protein level in 16HBE14o-, NCI-H441 and A549. This is well aligned with literature reported expression data [194, 195, 221]. The same was observed for primary NHBE cells [87, 194, 195]

Calu-3 cells however were negative for BCRP in both qPCR and Western Blot experiments of this study. In contrast, literature findings indicated a weak to moderate expression when cells were cultured in well plates/flasks and analysed via RT-PCR, LCMS/MS or Western Blot [194, 195, 222]. Notably, when Calu-3 were cultured on Transwell® inserts at either ALI or LCC, an extremely low gene expression was reported with the absence at protein level [79, 87]. This may hint to a potential influence of culture conditions (i.e. flask vs Transwell® ALI/LCC) on expression levels of BCRP in Calu-3. As discussed for MDR1 in Calu-3, factors such as culture time, culture condition, passage number or the use of different subclones might contribute to differences in expression levels.

For hAELVi in this study, a significantly lower expression of BCRP at LCC vs. flask cultured cells was observed in qPCR, with ALI-cultured cells showing similar expression levels to flask

condition. In contrast, this significant difference was not observed at protein level, where comparable expression levels of BCRP were observed across flask, ALI and LCC. A study by Visigalli et al. demonstrated a weak gene expression at ALI and an absence of expression at protein level which contrasts with our findings [108]. A potential reason for this discrepancy could be that hAELVi cells are a heterogeneous polyclonal cell line due to the lack of a monoclonal selection during the initial immortalisation process. To overcome this limitation, a monoclonal cell line was derived from the hAELVi cells via single-cell printing: the Arlo cells [107]. This study could not detect BCRP at either the gene or protein level in Arlo and data from bulk-RNA sequencing indicated a rather weak BCRP expression [107].

Primary alveolar type-I-like cells hAEpC were negative for BCRP expression in this study, with literature reporting a weak (by PCR and Western Blot) to absent (by LC-MS/MS and Western Blot) expression [108, 194, 195, 221]. The protein expression levels of BCRP were shown to decrease once cells trans-differentiate from alveolar type II cells into alveolar type I-like cells [221].

Caco-2 cells, which served as positive control cells for both expression and functional activity of BCRP showed a rather low expression of BCRP at protein level in both flask and LCC-culture. However, the acceptance criteria in the functionality assessment of BCRP in Caco-2 were met for both tested BCRP substrates (H33342 and prazosin, see 3.1.3.3 and 3.1.3.5), therefore Caco-2 are considered a suitable control for both BCRP protein expression and efflux in the context of this study. It was further reported in literature that the protein expression of BCRP in Caco-2 cells appeared to decrease for high passage (p.59) versus low passage (p.36), when cultured on Transwell® inserts [268]. Given the use of Caco-2 cells between p.45-55 in this study, this might contribute to a rather weak expression of BCRP.

Summary ABC Transporters' Expression Levels

The results indicated both similarities and differences in expression of ABC transporters across tested lung epithelial cells. To summarise, MRP1 showed a ubiquitous expression across all tested cells. MDR1 was absent in the majority of cells, apart from Calu-3. BCRP showed expression in both cells of upper and lower airways, but was not detected in Calu-3, Arlo and hAEpC.

The culture interface (ALI vs. LCC) did not result in significant differences in expression levels (except for Calu-3). However, many more ABC transporters and solute carrier transporters (SLC) were described to be expressed in the human lung epithelium, though they were not within the scope of this study [177]. Nevertheless, whether their expression levels are affected by the choice of culture interface (i.e. ALI vs. LCC) is still an open question.

As differences in expression levels (i.e. mainly lack of MDR1 in the majority of tested cells) were observed compared to available literature data, this highlights the need for a careful characterisation of transporter expression in used cell models when conducting pulmonary distribution studies *in vitro* and comparing them to findings from other *in vitro* studies in the literature.

3.1.4.2 Cell Barrier Formation Properties

A key prerequisite to study transporter processes *in vitro* is that cells form an electrically tight monolayer. Cell layer integrity is often assessed by measuring TEER [73]. A minimum threshold of 250 Ω*cm² is proposed for TEER, however studies assessing permeability and transporter-mediated disposition in pulmonary epithelial cells typically use 500 Ω*cm² as acceptance criterion [74, 75, 87]. Another method to assess cell layer tightness is measuring P_{app} of control paracellular markers such as sodium fluorescein, mannitol or LY [105, 201, 269, 270]. For LY, a threshold of 25 nm/s was applied to indicate the formation of a tight cell barrier [78].

Measured TEER and P_{app} values for lung epithelial cell lines and primary cells revealed differences between cells and the impact of culture interface (i.e. ALI and LCC) on their ability to form a tight barrier. The P_{app} of control markers and TEER showed an inverse relationship, i.e. if TEER > 400 Ω*cm², the P_{app} of atenolol and LY was < 25 nm/s. In general, cells tended to show a higher TEER when cultured at ALI vs. LCC.

However, two cell lines were exceptions to this: the bronchial 16HBE14o- and the bronchiolar NCI-H441. For both, TEER was drastically reduced and P_{app} of atenolol and LY was strongly increased when cultured at ALI. These findings are aligned with literature, where it was reported that 16HBE14o- cells require a certain amount of liquid on the apical side (i.e. LCC culture) to form a tight barrier [82, 83]. In terms of NCI-H441, a more than three-fold higher TEER at LCC vs. ALI was reported with values > 1000 Ω*cm² for LCC [271]. In our study, measured values at LCC were lower (~550 Ω*cm²) but still more than two-fold higher than at ALI. Moreover, literature demonstrated that dexamethasone is essential to be added to culture medium of NCI-H441 to enable the presence of a tight barrier, i.e. by increasing the expression of tight junctional proteins. When NCI-H441 cells are cultured without the corticosteroid, measured TEER was < 100 Ω*cm² for both ALI and LCC [95, 272]. Tracheo-bronchial-derived Calu-3 cells showed an almost two-fold higher TEER at ALI vs. LCC in this study, whereas in literature an opposite trend was described of higher TEER at LCC [79, 86, 273, 274]. However, the P_{app} of control markers atenolol and LY was comparable at both ALI and LCC (< 25 nm/s) indicating the presence of a tight barrier. The bronchial-derived primary cells NHBE at ALI

showed a maximum TEER of ~ 600 Ω*cm² and a P_{app} of ~ 10 nm/s for control markers, which were comparable across the three tested donors and confirming the barrier tightness of cells. In literature, values ranging from 200 to 800 Ω*cm² have been reported [65, 89].

The alveolar A549 cell line showed extremely low TEER (< 100 Ω*cm²) as expected and corresponding high P_{app} of control markers (>~100 nm/s), confirmatory of a leaky monolayer. Similar values were described in literature proposing the lack of functional tight junctions in these cells. These cells should rather be used when studying, for instance, drug metabolism (such as cytochrome P450 enzymes) in the human lung or for toxicity assessments [25, 93, 99, 104, 275].

In contrast, highest TEER values (> 1000 Ω*cm²) were observed in our study for two other alveolar-derived epithelial cell lines: hAELVi and Arlo. In literature, even higher TEER values at ALI were measured up to 2000 Ω*cm² for hAELVi and 3000 Ω*cm² for Arlo [105, 107]. Interestingly, primary type I-like alveolar epithelial cells (hAEpC) showed a peak in TEER after 7 days ranging from 500 to ~ 1000 Ω*cm², showing an almost two-fold difference between donors. In literature, TEER values for hAEpC > 1500 Ω*cm² were reported, in alignment with our data that a peak in TEER was reached around 7 days post-seeding and decreased after [107, 109].

Due to their incapability to form a tight cell barrier, it is not recommendable to use 16HBE14o- at ALI as well as A549 at ALI/LCC when aiming to study drug transporter and permeation processes across the human lung epithelium *in vitro*. When using NCI-H441 in these kind of studies, a careful optimisation of the culture medium is recommended to ensure the formation of a tight barrier.

3.1.4.3 Characterisation of ABC Transporters Efflux

It is important to ascertain whether pulmonary ABC transporters are functionally active to determine their potential contribution as drivers of pulmonary exposure. Since ABC transporters often have overlapping substrate recognition combined with the use of non-selective inhibitors, readouts from these studies are not always clear. This is especially pronounced for cells that express a variety of drug transporters, where it is challenging to mechanistically evaluate the contribution of a single transporter protein only [177, 200, 226]. As an example, estrone-3-sulphate was used as substrate in a study by Rotoli et al. to investigate MRP1 efflux in the human lung epithelium, however this compound is also a well-known substrate of organic anion-transporting polypeptides (OATP) uptake transporters [87, 276].

To assess functional activity of efflux transporters, a number of methods are applied - most commonly, bidirectional transport studies are conducted using known transporter substrates in the absence and presence of a specific transporter inhibitor with cells seeded on porous filter inserts. Where, if there is a more than two-fold difference in bidirectional transport in absence of inhibitor, this is an indication for the presence of active efflux. In presence of inhibitor, this asymmetry should be reduced by at least 50 % to confirm the asymmetry is as a consequence of active transport [18]. Another approach commonly used to assess the functional activity of ABC transporters, examines the intracellular accumulation of a fluorophore in plated cells in the absence and presence of a transporter inhibitor [214]. These two approaches were implemented in this study to investigate the functional efflux of MDR1, MRP1 and BCRP.

MDR1 Efflux

All cells were evaluated for MDR1 functionality including 16HBE14o-, NCI-H441, A549, hAELVi, Arlo, NHBE and hAEpC, where MDR1 was not detected at both gene and protein level. As expected, no MDR1 efflux was evident in any cells (except Calu-3) as neither the intracellular concentration of MDR1 substrate, Rh123, increased in the presence of MDR1 inhibitor zosuquidar (< 30 %), nor edoxaban permeability in the bidirectional transport study (ER < 2).

Calu-3 showed an almost two-fold increase in Rh123 concentration in presence of zosuquidar, aligning with P-gp expression data. Rh123, however, is not a selective substrate for MDR1, although widely used as model substrate to understand MDR1 activity *in vitro* [89, 111, 196]. Studies report Rh123 is also a substrate of organic cation transporters (OCTs) such as OCT1 and OCT2. OCT1 is known to be expressed in the human lung epithelium [177, 197, 277]. The MDR1 inhibitor used in this study, zosuquidar, was shown to inhibit OCT-mediated uptake, with a reported IC_{50} of 7.5 ± 3.7 µM for OCT1, using metformin as probe substrate [278]. However, inhibitor's IC_{50} values are substrate dependant as typically several, even overlapping binding sites on the surface of the transporter protein exist [279].

When cultured under ALI, an ER of 3.8 for edoxaban was observed in Calu-3 cells, however this was not evident when cultured at LCC (ER of 1.3). Protein levels of MDR1 were more than four-fold lower once Calu-3 were cultured at LCC compared to ALI. This appears somewhat inconsistent with other reports, where one study evaluated the efflux of Rh123 in Calu-3 under both ALI and LCC conditions, using Calu-3 cells from the same origin as in this study. The authors found similar ER (> 7.5) at both ALI and LCC, indicating no potential changes in expression, however, they did not include an assessment of MDR1 expression levels [61]. In this study, the reduction in MDR1 expression caused by culture conditions, could explain the

lack of asymmetry in edoxaban permeability at Calu-3 when cultured at LCC. Western Blot was used to quantify MDR1 expression at protein level, reporting total MDR1 expression levels. However, only MDR1 that is expressed at the cell membrane, contributes to efflux. A combination of immunolabeling and flow cytometry could be used to measure MDR1 expression levels at the cell surface [196].

MRP1 Efflux

In all tested cells, 5,6-CF showed a significant increase in intracellular accumulation in presence of inhibitor MK-571, indicating the presence of active MRP1. This is well aligned with literature where 5,6-CF was used as probe substrate to assess MRP1 activity in the human lung epithelium [74, 214].

It has, however, been described that 5,6-CF is not a selective substrate of MRP1 but also of other MRPs (such as MRP3) [280, 281]. Nonetheless, MRP1 is described to show the highest expression levels across all MRPs in the human lung epithelium, therefore the interaction observed with 5,6-CF can be attributed to MRP1 [194]. Recently, a study recommended that 5,6-CF is not a suitable substrate for studying MRP1 since they observed no difference in 5,6 -CF efflux when comparing a wild-type NCI-H441 cells to their MRP1-knockout NCI-H441 clone (that showed no expression of MRP1 at protein level) [215].

In contrast to the positive results observed in the fluorophore accumulation study for MRP1 activity, no asymmetry in permeability of our MRP1 substrate doxorubicin was measured in the bidirectional efflux study in majority of lung epithelial cells. An UR< 2 was calculated, which indicates the absence of efflux at the basolateral side. In terms of apical efflux of doxorubicin, an ER of 2.5 was observed in NHBE without being reduced in presence of MRP1 inhibitor MK-571, thus questioning the transport of doxorubicin by MRP1 in these cells. Potentially another active transport system could be involved. Only for the positive control Caco-2, a strong efflux of doxorubicin was shown, being effectively reduced in presence of MK-571. A study by Prime-Chapman and colleagues reported that MRP2 shows higher expression levels than MRP1 at protein level in Caco-2 and appeared to be expressed on the apical side [282]. As doxorubicin was described in literature to interact with MRP2 [283], it might be possible that observed efflux of doxorubicin in Caco-2 is mediated by MRP2. The expression of MRP2 in lung epithelial cells was reported in literature but showing lower expression levels than MRP1, at both gene and protein level, with MRP2 hypothesised to be expressed at the apical side and MRP1 on the basolateral side [146, 177, 194, 195].

To further investigate the expression of MRP2, MRP3, MRP4, MRP5 and MRP6 in lung epithelial cells (at flask, ALI and LCC culture), a qPCR was conducted as part of this *in vitro*

study (see Figures A13 & A14 in the supplement). Interestingly, the gene expression of MRPs differed across the lung epithelial cells, and certain MRPs showed comparable expression levels to MRP1. However, there is still uncertainty regarding the spatial localisation of MRPs in in vitro models of the human lung epithelium [177, 248]. An expression of MRPs interacting with doxorubicin on both apical and basolateral side of the lung epithelial membrane, could be a potential reason why no efflux was observed for doxorubicin. Moreover, literature showed that doxorubicin appears to be recognised as well by organic cation transporters (e.g. OCT1) [284]. These transporters were described to be expressed in the human lung epithelium [177], thus a potential cross-interaction cannot be excluded, which could explain the absence of doxorubicin efflux in the lung cells. Literature showed no evidence of MK-571 as an inhibitor of OCTs. This emphasises the difficulty of finding a selective transporter substrate for assessing the activity of one single transporter protein in cells known to express a variety of different efflux and uptake transporters.

BCRP Efflux

In the fluorophore accumulation assay, using H33342 as substrate for BCRP, a more than 1.5-fold increase was observed for 16HBE14o-, being slightly below this threshold for NCI-H441, A549, NHBE and hAELVi. Compared to positive Rh123 and 5,6-CF accumulation data, the increase was less pronounced (less than two-fold change), which could be attributed to the overall lower protein expression levels of BCRP.

This is consistent with data from bidirectional efflux studies, where a weak efflux of prazosin was observed in the control cell line Caco-2 (ER ~> 2) but not in any of the lung cell lines. The rather weak BCRP expression in combination with the high cellular permeability of prazosin (> 100 nm/s) might render the involvement of active efflux by BCRP less pronounced.

Summary on ABC Transporters' Functional Activity

This study reported substantial functional activity of ABC transporters in lung epithelial cells, using fluorophores as substrates, being aligned with respective transporter expression profiles. However, in bidirectional efflux studies using drug molecules as substrates, no functional activity of ABC transporters' efflux was observed in lung cells, aside from MDR1 efflux in Calu-3 at ALI. This discrepancy could be influenced by differences in cellular permeability between fluorophores and drugs, that were selected as model substrates, as shown in Table 10.

Table 10. Overview of predicted AlogP and measured apparent permeability (P_{app}) of ABC transporter substrates used in fluorophore accumulation and bidirectional efflux studies. The AlogP values were calculated with the Biovia Pipeline pilot 2019 software (Version 24.1, Dassault Systems, Paris, France) using the method published by Ghose and Crippen [285]. Permeability values for fluorophores (*) were retrieved from literature for each one lung cell line as reference if available and compared to respective permeability values measured in this cell line for either edoxaban or doxorubicin in our study. Permeability values measured in presence of ABC transporter inhibitor in this study were compared. [a] For H33342, no measured P_{app} across lung epithelial cell was found in literature. The reported value was measured in MDCK-II cells overexpressing MDR1 in presence of elacridar, showing an asymmetry in permeability (ER = 4.1). Thus, reported P_{app} might be overestimated.

Transporter	Cell line	Drug substrate	AlogP	P_{app} [nm/s]	Fluorophore	AlogP	P_{app}* [nm/s]	Reference
MDR1	hAELVi	Edoxaban	0.844	~ 40	Rh123	2.83	< 2	[108]
MRP1	NCI-H441	Doxorubicin	-0.444	~ 9	5,6-CF	3.60	< 2	[74]
BCRP	hAELVi	Prazosin	2.11	~70 - 90	H33342	5.16	< 8[a]	[224]

The cellular permeability of fluorophores is significantly lower compared to those of drug molecules, whereas in contrast their lipophilicity (AlogP) is increased. It is well known that lipophilic compounds (i.e. AlogP >~ 3) with low cellular permeability are more prone to be affected by active efflux processes than those showing a high cellular permeability [59]. This could explain why a strong functional activity was observed in this study when using fluorophore substrates, as their cellular permeation is heavily affected by the presence of active efflux transporters.

3.1.5 Conclusion

This study investigated the expression and functional efflux of three ABC transporters (MDR1, MRP1 and BCRP) in cells typically used to study distribution and transport processes across the human lung epithelium.

Data revealed that MRP1 is ubiquitously expressed in all investigated cells, whereas BCRP showed a low expression and MDR1 was only found to be expressed in Calu-3. Expression data at protein level revealed that ALI vs. LCC culture did not affect ABC transporters expression, except for MDR1 in Calu-3. Due to their lack of forming an electrically tight barrier, not all cells in scope of this study are considered appropriate to study drug transport processes *in vitro*. Moreover, it has been shown that expressed pulmonary ABC transporters interact with fluorophore substrates but not with drug substrates (apart from MDR1 in Calu-3 at ALI).

This raises questions about the relevance of ABC transporters as potential drivers of pulmonary drug distribution or the suitability of tested cells to adequately capture these processes. Besides, the difficulty of finding a substrate that is not recognised by several transporter proteins in combination with non-specific inhibitors impedes a clear assessment of the contribution of a single transporter protein.

3.2 Transport of 20 Marketed Anti-Infectives Across the Human Lung Epithelium *In Vitro*

A peer-reviewed version of this chapter has been published as a research article:

Simon, S., Westwood, M-A., Shanmugalingam, T., Cantrill, C. and Lehr, C-M. (2026), Transport of 20 Marketed Anti-Infectives Across the Human Lung Epithelium *In Vitro*, *International Journal of Pharmaceutics*, DOI: 10.1016/j.ijpharm.2026.126721

Contributions to this chapter:

Sina Simon was mainly responsible for the methodological experimental design of the study, performed the cell culture, conducted the experiments and run the LC-MS/MS (apart from the mentioned plasma protein and sELF binding experiments) and evaluated the data. She wrote the manuscript (apart from the mentioned exception in the methodology of the LC-MS/MS) and created all the figures.

Marie-Anne Westwood and Thanusa Shanmugalingam established and validated the LC-MS/MS methods and contributed to the writing of the original manuscript (methodology of LC-MS/MS analysis). Dr. Carina Cantrill and Prof. Dr. Claus-Michael Lehr supervised the project and supported the conceptualisation of the experimental methodology, the data evaluation and critically reviewed the final manuscript.

The experiments to determine the unbound fraction of antibiotics in plasma and sELF were conducted and analysed at the CRO Selvita Ltd. in Zagreb (Croatia).

NB: The compound set in this chapter consisted of 18 antibiotics and included in addition the anti-malarial drug hydroxychloroquine as well as the antifungal drug voriconazole. For the ease of read and consistency across the other chapters of the thesis, they are referred to as ‘antibiotics’ within the scope of this chapter.

3.2.1 Introduction

The epithelial lining fluid (ELF), which covers the human lung surface is often considered as the target compartment for antibiotics to treat bacterial infections, such as Streptococcus pneumoniae. In addition, alveolar macrophages, patrolling the alveolar surface, are targets for intracellular pathogens like Legionella pneumophila [4, 52, 286]. In both cases, antibiotics administered systemically either via the oral or parental route need to cross the human lung epithelium to reach their site of action. The rate and extent for antibiotics to appear in the ELF, i.e. pulmonary bioavailability depends on a number of pharmacokinetic factors such as their epithelial permeability, the presence of active efflux transporters and the unbound fraction in plasma and ELF [4, 15].

For certain antibiotics (i.e. macrolides, ketolides and fluoroquinolones), clinical studies have reported a high drug concentration in the ELF compared to plasma [15]. These drugs have been described as substrates of human ATP-binding cassette (ABC) efflux transporters such as multidrug resistance protein 1 (MDR1, also known as P-glycoprotein) and breast cancer resistance protein (BCRP) [16, 287]. These are transmembrane proteins, extruding their substrates out of the cell membranes and are well understood to impact local drug exposure in a clinically relevant manner in tissue such as the intestine, brain, liver and kidney [18]. Thus, it has been proposed that active ABC transporters expressed in the lung epithelium, could contribute to higher ELF exposure. In the addition to the potential contribution of active mechanisms, a recent clinical study investigating a novel fluroquinolone, has revealed that other factors such as strong binding to constituents of the ELF, can also potentially result in higher ELF to plasma concentrations [163]. However, due to the technical challenging process of ELF collection by bronchoalveolar lavage, a rigorous quantitative evaluation of drug disposition is difficult for clinical studies. This is a consequence of variability from potential lysis of collected cells in the ELF, blood contamination of ELF samples, increased dwell time (length of time where the saline solution is left within lung) and resulting uncertainties in sampled ELF volume (due to the need for using urea or alternative correction techniques) need to be considered [15]. This could be a specific concern for molecules of certain physicochemical properties like macrolides, since these drug classes are weakly basic and are known to accumulate in alveolar macrophages [53, 288, 289].

In addition to binding to plasma/ELF components and potential interaction with pulmonary efflux transporters, passive permeability is another important parameter to consider, affecting the overall transport of antibiotics across the lung epithelium. In drug development, the cellular permeability of chemical entities is often measured in cell lines such as the porcine kidney epithelial LLC-PK1 cells or the canine kidney epithelial cells MDCK. If focussing on intestinal permeability, human Caco-2 cells is typically the *in vitro* model of choice [58, 290, 291].

The LLC-PK1 cells were described to express low levels of endogenous ABC transporters, whereas Caco-2 are well-known to express functional active ABC transporters such as MDR1 and BCRP [268, 292, 293].

In terms of evaluating lung disposition *in vitro*, the human tracheo-bronchial epithelial cell line Calu-3 is widely reported for investigating pulmonary permeability and active transport processes including MDR1 mediated efflux [61, 196, 294]. When comparing drug permeability measured in Calu-3 and Caco-2, a good correlation was found, using a diverse drug set summarised from individual studies. Overall, a trend of lowered permeability measured in Calu-3 was observed, which was especially pronounced for antibiotics [20, 61]. As a potential limitation, Calu-3 cells are of tumorous origin and derived from the upper airways [295]. However, the surface area of the human upper airways (trachea, bronchi and bronchiole) comprises only ~ 1 to 2 m^2, which is tremendously smaller than that of the human alveolar lung epithelium with an estimated surface area of ~ 140 m^2. In consequence, the alveolar epithelium of the lower airways offers an up to 140-fold larger area for distribution processes, including drugs transport in either absorptive or secretory direction [27]. The immortalised hAELVi cell line was recently developed to mimic the human alveolar epithelium *in vitro* [105]. However, there has been limited investigation into drug disposition in this cell line, and it is of great interest to investigate how permeability and efflux data from these cells compare to further cell lines used in pulmonary permeability testing.

This aim of this study was to investigate pulmonary transport of antibiotics *in vitro* by selecting a test set of 20 marketed molecules. Their bidirectional cellular permeability was measured in lung epithelial cells (Calu-3 & hAELVi) and compared to values in cell lines typically used for permeability studies in general (Caco-2 & LLC-PK1). In addition to investigate mechanistically, the interaction of antibiotics with human MDR1 and BCRP in overexpressing cells, and unbound fraction in both human plasma and simulated ELF (sELF) was evaluated. Since rodents are the preclinical species for assessing antibiotics disposition and efficacy [296], a smaller compound set was tested for its interaction with rodents' efflux transporters (Mdr1a and Bcrp1) and their binding to rodent plasma proteins to evaluate any potential species differences. This compound test set consisted of macrolide and fluoroquinolone antibiotics as these drug classes showed high ELF to plasma ratios (>> 1) in rodent *in vivo* studies [288, 289, 297]. This study contributes to an improved mechanistic understanding of human pulmonary drug distribution processes *in vitro* by revealing lung-regional specific characteristics and hinting to potential species differences.

3.2.2 Material & Methods

3.2.2.1 Chemicals

Antibiotics tested in this study included: amoxicillin, azithromycin dihydrate, cefdinir, cefepime dihydrochloride monohydrate, ciprofloxacin, clarithromycin, dapsone, erythromycin, hydroxychloroquine sulphate, isoniazid, levofloxacin, linezolid, moxifloxacin hydrochloride, rifampicin, tazobactam sodium salt, telithromycin, vancomycin hydrochloride and voriconazole that were purchased from Merck KGaA (Darmstadt, Germany). Omadacycline was purchased from Cayman Chemicals (Ann Arbor, MI, USA) and lascufloxacin from Toronto Research Chemicals (Toronto, Canada). Atenolol, propranolol hydrochloride, zosuquidar hydrochloride, MK-571 sodium salt hydrate, Ko143 hydrate and Lucifer Yellow (LY) were purchased from Merck KGaA, edoxaban and 2-Amino-1methyl-6-phenyllimidazol[4,5-b]pyridine (PhiP) from Toronto Research Chemicals.

All chemicals were prepared as 10 mM stock in DMSO (Merck KGaA). Only LY was prepared as 2 mM stock in distilled water (Thermo Fisher Scientific, Waltham, MA, USA).

3.2.2.2 Plasma Protein Binding

The unbound fraction in plasma was determined by high throughput equilibrium dialysis (HTDialysis, Gales Fery, CT, USA) using separation membranes with a cutoff of 12 to 14 kDa, according to manufacturer's instructions. All plasma was purchased from BioIVT (Westbury, NY, USA).

In brief, plasma was thawed, then centrifuged (2500 x g for 10 min) and pH was adjusted to 7.4, with either orthophosphoric acid or sodium hydroxide. Test compounds, 10 mM diluted in DMSO, were spiked into plasma to achieve a final concentration of 1 µM. The internal control, diazepam was cassette-dosed at a concentration of 1 µM, resulting in a final DMSO content of 1 % (v/v). Spiked plasma was then dialysed against Sørensen buffer (pH 7.4) for 5 h at 37 °C while shaking at 300 rpm in an incubator. Compounds were tested in triplicate determinations. Final buffer and plasma samples, as well as plasma samples from t = 0 h, were then matrix-matched with either plasma or blank buffer, followed by quenching with ice-cold acetonitrile containing the internal standard. Compounds' concentration was then quantified via liquid chromatography tandem mass spectrometry (LC-MS/MS). The fraction unbound ($f_{u,plasma}$) was calculated according to Equation 4.

$$f_{u,plasma} = \frac{concentration_{\,buffer,final}}{concentration_{\,plasma,final}}$$

Equation 4. Formula to calculate the unbound fraction in plasma ($f_{u,plasma}$). The concentration measured in buffer in buffer after 5 h is divided by the concentration in plasma after 5 h.

The data was accepted if the f_u of diazepam was between 0.007 to 0.03.

Fluroquinolone and macrolide antibiotics were tested in addition for their binding to rat (Wistar) and mouse (C57BL/6J) plasma under same conditions as described for human plasma experiments. The data was accepted if diazepam f_u was within 0.067 – 0.171 or 0.085 – 0.179 for mouse and rat plasma, respectively.

3.2.2.3 Simulated ELF (sELF) Binding Assay

To investigate the unbound fraction of antibiotics in the human ELF, they were tested in a simulated epithelial lining fluid (sELF) binding assay. The unbound fraction was measured by using a high throughput equilibrium dialysis device, as described by Keemink and colleagues [156].

Test compounds (in DMSO) were spiked at a final concentration of 1 µM into sELF and dialysed against Sørensen buffer (pH 7.4) for 6 h at 37 °C while shaking at 300 rpm, in an incubator. Three control compounds (ranging from 0.05 to 1 unbound fraction in sELF, based on historical in-house data) were cassette-dosed, resulting in final total DMSO concentration of 1 % (v/v). Test compounds were tested in triplicates. Initial sELF samples (t = 0 h) and final sELF and buffer samples were matrix-matched with either blank buffer or sELF. After all samples were quenched with acetonitrile/methanol (2:1 v/v) containing the internal standard and then quantified via LC-MS/MS. The unbound fraction in sELF was calculated according to Equation 5.

$$f_{u,sELF} = \frac{concentration_{\,buffer,final}}{concentration_{\,sELF,final}}$$

Equation 5. Formula to calculate the unbound fraction in sELF ($f_{u,sELF}$). The concentration measured in buffer in buffer after 6 h is divided by the concentration in sELF after 6 h.

Data was accepted if values for three control compounds were within range (according to internal validation data).

3.2.2.4 Cell Culture

All cells were maintained in Nunc™ EasYFlasks™ (75 cm^2, Thermo Fisher Scientific) in incubators with constant temperature of 37 °C, 5 % CO_2 and under saturated humidity. Cells were passaged once a week, using splitting ratios recommended from suppliers and fresh medium was supplied three times a week.

Calu-3 cells were purchased from ATCC (HTB-55; Manassas, VA, USA) and cultured in Gibco DMEM/F12 medium supplemented with 10 % (v/v) fetal bovine serum (FBS), 1 % (v/v) non-essential amino acids and 2 mM L-Glutamine (Thermo Fisher Scientific).

hAELVi cells (CI-hAELVi, INS-CI-105), purchased from InSCREENeX GmbH (Braunschweig, Germany) were cultured in huAEC basal medium, a low serum medium optimised for culturing immortalised human alveolar epithelial cells with the supplement mix to derive the complete medium (InSCREENeX).

Caco-2 were purchased from ATCC (HTB-37) and cultured in Gibco MEM medium (Thermo Fisher Scientific), supplemented with 10 % (v/v) FBS and 1 mM sodium pyruvate (Thermo Fisher Scientific).

Lilly Laboratories porcine kidney-1 wild type epithelial cells (LLC-PK1 WT) were purchased from ATCC (CL-101) and the transfected LLC-PK1 cells with human MDR1 (L-MDR1) or mouse Mdr1a (L-Mdr1a) were received from Dr. Alfred Schinkel's group from 'The Netherlands Cancer Institute' (Amsterdam, Netherlands) and used under licence agreement. Cells were cultured in Medium 199 (M-199; Bioconcept Ltd., Allschwil, Switzerland), which was supplemented with 10 % (v/v) FBS and 150 ng/mL colchicine (serving as selective agent for MDR1 expression, SERVA Electrophoresis GmbH, Heidelberg, Germany).

Madin-Darby canine kidney cells (MDCK-II), transfected with either human BCRP (M-BCRP) or mouse Bcrp1 (M-Bcrp1) were received from the Netherlands Cancer Institute and used under licence agreement. Gibco DMEM (Thermo Fisher Scientific) supplemented with 10 % (v/v) FBS was used as a growth medium.

3.2.2.5 Cell Seeding

For bidirectional experiments, cells were seeded onto porous filter membrane inserts with a surface area of 0.11 cm^2 and a pore size of 0.4 µm. Calu-3 and hAELVi were seeded onto polyethylene terephthalate membranes (7369, Corning, Corning, NY, USA), whereas polycarbonate insert membranes (PSHT004R1, Merck KGaA) were used for Caco-2, LLC-PK1 WT, L-MDR1, L-Mdr1a, M-BCRP and M-Bcrp1. Table 11 summarises the seeding densities and cultivation times.

Table 11. Overview of the seeding density and the culturing time for cells maintained on membrane insert plates.

Cell line	Seeding density [x 10^5 cells/cm^2]	Cultivation time on inserts [days]
Calu-3	3.0	21
hAELVi	1.0	14
Caco-2	2.0	21
LLC-PK1 WT	2.5	4
L-Mdr1	2.5	4
L-Mdr1a	2.5	4
M-BCRP	6.0	3
M-Bcrp1	6.0	3

Before seeding hAELVi cells onto inserts, the inserts were pre-coated with huAEC-coating solution according to manufacturer's instructions (InSCREENeX). Calu-3 and hAELVi were cultured under air-liquid interface (ALI) by removing the medium on the apical side of the insert upon cell reached confluence (after ~ 3 d), for other cell lines, medium was kept on both sides of the inserts for the whole culture time (i.e. liquid-covered culture, LCC).

3.2.2.6 Bidirectional Permeability Studies in Calu-3, hAELVi, Caco-2 and LLC-PK1 WT Cells

To investigate the apparent permeability (P_{app}) and efflux of antibiotics in lung epithelial cell lines and reference cell lines, the bidirectional permeability was evaluated in absence and presence of an ABC transporter inhibitor cocktail mix. This cocktail inhibitor included Zosuquidar (1 µM), MK-571 (10 µM) and Ko143 (1 µM) to effectively inhibit MDR1-, MRP1- and BCRP-mediated efflux, respectively.

Molecules were tested at 10 µM except for ciprofloxacin, erythromycin and azithromycin (25 µM) and cefepime, cefdinir, amoxicillin, tazobactam and vancomycin (50 µM). The incubation concentration of these antibiotics was increased for analytical purposes. LY was included as paracellular marker to indicate cell layer integrity [78]. Moreover, atenolol (25 µM) and propranolol (1 µM) were included in each experiment serving as low or high permeability marker, respectively. Edoxaban (1 µM) was included as another high permeability marker and served in addition as substrate for MDR1 mediated efflux [258].

Test compounds were diluted in medium 199 without phenol red at pH 7.4 (M-199; Bioconcept, Allschwil, Switzerland) containing 0.1 % (w/v) of bovine serum albumin (BSA), 10 µM LY and inhibitor cocktail mix or equivalent amount of DMSO. For the acceptor medium, 0.1 % (w/v) BSA, inhibitor cocktail or respective amount of DMSO was added to M-199. Final DMSO content was 0.5 % (v/v) in all conditions. Dose solutions were added either to apical side

(donor) and their permeability to basolateral side (acceptor) was measured (P_{app} AB) or in the opposite direction (P_{app} BA). In addition, the permeability of compounds in presence of inhibitor cocktail was measured ($P_{app,inh}$ AB and $P_{app,inh}$ BA). For each insert, 100 µL were added to the apical side and 240 µL to the basolateral side. The plates were then incubated at 37 °C while shaking at 200 rpm. After 3 h, samples were taken from acceptor and donor compartments. For analysis, donor samples and samples taken from initial dose solution (C_0) were diluted 1:5 in assay medium. Then, a three-fold volume of ice-cold acetonitrile containing the internal standards was added to each sample and samples were centrifuged at 6300 rpm for 10 min at 4 °C. After centrifugation, each 50 µL of supernatant was transferred to a 384-well plate and diluted 1:1 (v/v) with distilled water. The compound concentration was quantified via LC-MS/MS. Separate samples from acceptors were taken and their fluorescence at 425/525 nm was measured to quantify LY concentration. The P_{app} was then calculated according to Equation 6.

$$P_{app} = \frac{\Delta Q}{\Delta t} * \frac{1}{A * C_0}$$

Equation 6. Formula to calculate the apparent permeability P_{app} (nm/s), where ΔQ/Δt describes the amount of compound (nmol, concentration corrected for the volume in receiver) that permeates the cell monolayer in a defined time (i.e. 10 800 s). A is the filter surface area (0.11 cm^2) and C_0 the initial incubation concentration (µM).

If the P_{app} of LY exceeded the value of 25 nm/s, wells were excluded as this indicated monolayer leakiness [78]. Based on their measured permeability, compounds were classified as low permeable (< 25 nm/s), moderately permeable (25 – 100 nm/s) or highly permeable (> 100 nm/s).

To investigate whether antibiotics are substrates of active efflux mediated by ABC transporters, their efflux ratio (ER) was calculated according to Equation 7.

$$ER = \frac{P_{app}\ BA}{P_{app}\ AB}$$

Equation 7. Formula to calculate the efflux ratio (ER). The permeability from the basolateral to apical side (P_{app} BA) is divided by the permeability from the apical to basolateral side (P_{app} AB).

An ER ≥ 2 indicates the presence of active efflux at the apical side of the cell membrane. To confirm ABC transporters' efflux, the ER must decrease by ≥ 50 % in presence of inhibitor (ER_i) [18]. An ER ~ 1 typically indicates the absence of active transport processes.

Moreover, the mass balance recovery was calculated according to Equation 8.

$$\%\, recovery = \frac{(C_{Acc} * V_{Acc}) + (C_{Don} * V_{Don})}{(C_0 * V_0)} * 100$$

Equation 8. Formula to calculate the mass balance recovery. Where C_{Acc} is the concentration [µM] of the test compound in the acceptor compartment, C_{Don} the concentration [µM] in the donor compartment and C_0 the initial concentration [µM] in the dose solution in the donor compartment. The V_{Acc} and V_{Don} represent the volumes [mL] of acceptor and donor, respectively.

Due to their partially low recovery (< 50 %) in lung epithelial cells, potentially due to lysosomal trapping [241], hydroxychloroquine and propranolol were co-incubated in presence of Bafilomycin A1, an ionophore, to reduce potential lysosomal sequestration (1 µM, Merck KGaA) under same conditions as described in this section.

3.2.2.7 Bidirectional Studies Assessing MDR1 and BCRP Efflux

To assess, whether antibiotics are substrates of human efflux transporters MDR1 and BCRP, bidirectional efflux studies using cells that were transfected to overexpress either MDR1 (L-MDR1) or BCRP (M-BCRP) were tested.

Experiments were conducted as described in section 3.2.2.6 with minor modifications. To assess MDR1 efflux, antibiotics were tested in absence and presence of MDR1 inhibitor zosuquidar (1 µM). Edoxaban, a MDR1 substrate, (1 µM) was included as a positive control. For investigating BCRP mediated-efflux, antibiotics bidirectional permeability was tested in absence and presence of BCRP inhibitor Ko143 (1 µM) with PhiP, a BCRP substrate, (1 µM) used as positive control.

To confirm functional activity, the ER of positive control substrates (Edoxaban or PhiP) needed to exceed 10 and be reduced in presence of respective inhibitor and resulting in an ER_i < 2.

The P_{app} and ER of antibiotics was calculated according to Equations 6 & 7. The data was only accepted if the P_{app} of LY < 25 nm/s.

Macrolide and fluoroquinolone antibiotics were in addition tested for their interaction with rodent Mdr1a and Bcrp1 in respective overexpressing cell lines (L-Mdr1a or M-Bcrp1) under same conditions as described for human MDR1 and BCRP substrate assessment.

3.2.2.8 Quantitative Analysis via LC-MS/MS

Sample analysis was conducted using liquid chromatography-tandem mass spectrometry (LC-MS/MS). The LC system included a CBM-20A controller, a DGU-20A5R degasser, two Shimadzu Nexera LC-30AD pumps (Shimadzu, Kyoto, Japan) connected to an HTS CTC PAL autosampler (CTC Analytics, Zwingen, Switzerland). For temperature control of the columns (column 1: Ascentis Express C18, 20 × 2.1 mm, 2.7 µm, Supelco, Bellefonte, PA, USA and column 2: Atlantis T3 C18, 2.1 x 30 mm, 3.0 µm, Waters, Milford, MA, USA) a column oven (HotDog 5090, Prolab Instruments, Dornach, Switzerland) was used. This setup was coupled to a Triple Quadrupole 6500 mass spectrometer equipped with an IonDrive Turbo V source (AB Sciex, Concord, ON, Canada). The mass spectrometer was used in the multiple reaction monitoring mode. Positive or negative ionization modes were applied for the analysis of all compounds. Analytical readouts were based on the peak area ratio between the analyte and the internal standard (oxazepam for positive mode and Roche internal compound for negative mode). Further details of the applied transition parameters for each test compound can be found in the supplemental Table B1. Supernatants of the precipitated samples were dilated two-fold with water and injected into the LC-MS/MS system using injection volumes of 1.0 µL or 2.0 µL. Compound elution was achieved using the following mobile phases: A1 (0.5% formic acid in water) or A2 (Ammonium Formate 10mM in water), and B1 (0.5% formic acid in acetonitrile) or B2 (acetonitrile). A high-pressure linear gradient from 0% to 95% B was applied at a flow rate of 600 µl/min with a total runtime of 1.4 minutes.

Data analysis was conducted with the Analyst 1.7.2 software (AB Sciex, Concord, ON, Canada) using initial samples as reference with a linear through zero regression model. Reference samples with accuracy above 20% bias were excluded.

3.2.2.9 Determination of Physico-Chemical Properties

The octanol/water distribution coefficient (AlogP) values were calculated using Biovia Pipeline pilot 2019 (Version 24.1, Dassault Systems, Paris, France) according to the Ghose and Crippen method [285]. The molecular weight (MW) was also calculated using the Biovia software. The octanol/water distribution coefficient values at pH 7.4 (ML_logD) were predicted by using an inhouse developed Roche machine learning (ML) property model based on historical data [298]. The acid dissociation constants (pK_a) were calculated with an *in silico* pK_a model from Simulations Plus Inc. (Lancaster, CA, USA) [299]. Based on the pK_a values, the ionization category at pH 7.4 was derived.

3.2.2.10 Data Analysis

Unless stated otherwise, three independent experiments with each three technical replicates were performed. Data is presented as mean ± standard deviation (SD). GraphPad Prism software was used to visualise data (Version 10.4.1, GraphPad Software, La Jolla, CA, USA). The coefficient of determination (r^2) was calculated using a simple linear expression taking the data variability (i.e. SD) into account. Differences between two groups were analysed with an unpaired two-tailed t test. The difference was considered significant if $p \leq 0.05$.

3.2.3 Results

3.2.3.1 Compound Selection

The compound set comprised of 20 marketed antibiotics from different antibiotic classes and diverse in physicochemical properties, shown in Table 12. A summary of antibiotics' pKa values can be found in the supplemental material (Table B2).

Table 12. Overview of test compounds' physicochemical properties. The information on drug classes was taken from [4, 15, 235, 258, 300, 301].

	Antibiotic class	Compound	Molecular weight [Da]	AlogP	ML_logD (pH 7.4)	Ionisation category (pH 7.4)
ANTIBIOTICS	fluoroquinolone	Ciprofloxacin	331	-1.27	-0.35	zwitter
		Lascufloxacin	439	-0.40	0.37	zwitter
		Levofloxacin	361	-1.37	-0.16	zwitter
		Moxifloxacin	401	-0.70	0.01	zwitter
	macrolide	Azithromycin	749	2.08	0.62	basic
		Clarithromycin	748	2.20	1.76	basic
		Erythromycin	734	1.79	1.23	basic
		Telithromycin	812	4.17	1.91	zwitter
	penicillin	Amoxicillin	365	-0.70	-0.59	zwitter
	cephalosporin	Cefdinir	395	-0.17	-0.82	acidic
		Cefepime	481	-2.98	-0.48	zwitter
	β-lactamase inhibitor	Tazobactam	300	-1.19	-0.64	acidic
	sulphonamide	Dapsone	248	1.44	1.09	neutral
	oxazolidinone	Linezolid	337	0.9	0.65	neutral
	tetracycline	Omadacycline	557	1.10	0.16	zwitter
	glycopeptide	Vancomycin	1449	-3.15	0.31	zwitter
	anti-tuberculosis	Isoniazid	137	-0.81	-0.02	neutral
		Rifampicin	823	3.26	1.64	zwitter
	antimalarial	Hydroxychloroquine	336	3.46	0.82	basic
	antifungal	Voriconazole	349	2.07	1.76	neutral
Low P_{app} marker	β-blocker	Atenolol	266	0.70	-0.7	basic
High P_{app} marker		Propranolol	259	2.54	1.35	basic
MDR1 Substrate control	Factor Xa inhibitor	Edoxaban	548	0.84	1.91	Basic

3.2.3.2 Plasma Protein and sELF Binding Assessment of Antibiotics

The free drug hypothesis states that only the unbound drug fraction can cross biological barriers [302]. Therefore, the free fraction of antibiotics was measured in human plasma and sELF using the high throughput equilibrium dialysis. The unbound fraction of antibiotics in human plasma was then compared to their unbound fraction in a human sELF as shown in Figure 20. Measured values can be found in the supplemental Table B3.

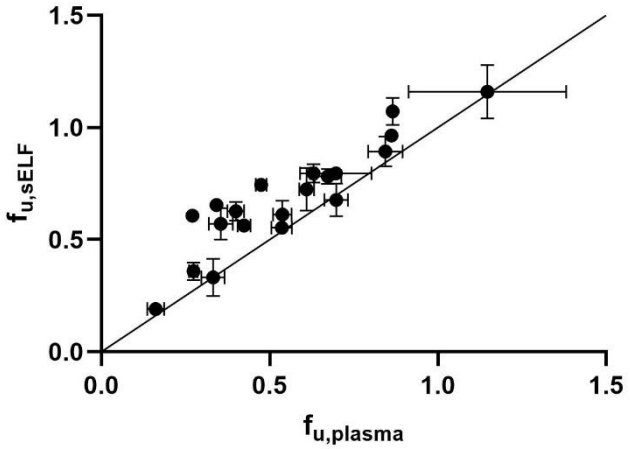

Figure 20. Comparison of unbound fraction of antibiotics in human sELF ($f_{u,sELF)}$ vs. human plasma ($f_{u,plasma}$). The line represents the line of unity. Values are shown as mean ± SD with n =3 from three independent experiments except for three compounds (Cefdinir, Isoniazid and Tazobactam), where $f_{u,plasma}$ was extracted from literature (see Supporting Table B3). The r^2 value was calculated by a simple linear regression with $r^2 = 0.784$.

The antibiotics showed a similar unbound fraction in both plasma and sELF, with a trend of a slightly higher binding to plasma proteins ($f_{u,plasma}$ ranging from 0.161 – 1.15) than constituents of the sELF ($f_{u,sELF}$ ranging from 0.190 – 1.16).

The impact of physicochemical parameters such as AlogP, logD and ionisation on the fraction unbound of antibiotics in human plasma and sELF were investigated and are shown in supplemental Figures B1 and B2. The results indicated an inverse relationship between the fraction unbound in plasma and sELF and the lipophilicity of antibiotics.

To investigate potential species differences (between human and rodents) in terms of protein binding, a smaller set of antibiotics (macrolides, ketolide and fluroquinolones) were tested for their unbound fraction in mouse and rat plasma. Overall, a similar fraction unbound was found across the species, with the exception of telithromycin, which showed an up to 4.5-fold lower fraction in mouse plasma (see supplemental Figure B3 and Table B4).

3.2.3.3 Apparent Permeability of Antibiotics in Lung Epithelial Cells versus Reference cell lines

As it was the aim to further investigate the permeation of antibiotics across the human lung epithelium from a systemic exposure, the focus was on comparing measured permeability coefficients from basolateral to apical side (i.e. P_{app} BA and $P_{app,inh}$ BA). The P_{app} BA represents the permeability in presence of active efflux processes, whereas $P_{app,inh}$ BA in absence of active ABC transporters' efflux, therefore the passive permeability. In bidirectional transport studies, the basolateral side represented the blood-vessel facing membrane and the apical side the ELF facing side. The individual permeability values are detailed in supporting Tables B5 – B8.

In a first step, the measured basolateral to apical permeability values of antibiotics in the two reference cell lines were compared (LLC PK1 WT vs Caco-2) in absence and presence of ABC transporter inhibitor cocktail, as shown in Figure 21.

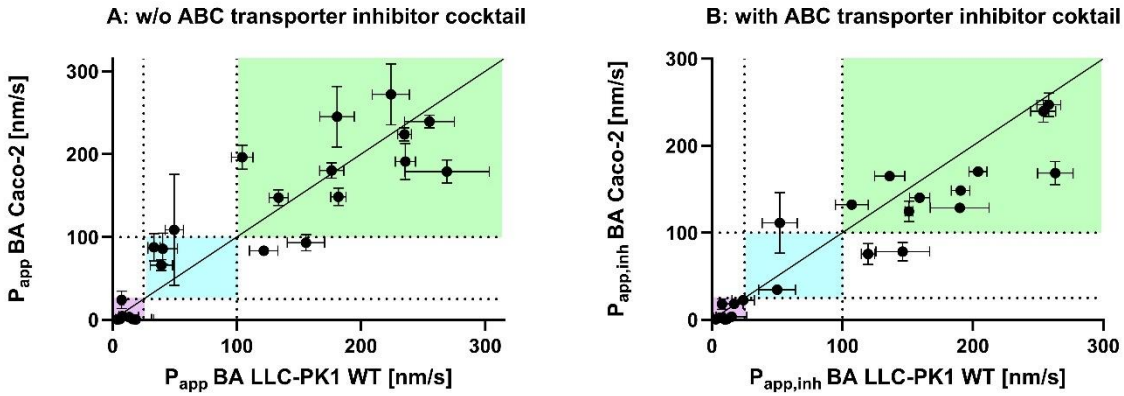

Figure 21. Comparison of basolateral to apical permeability of antibiotics and permeability markers in absence (P_{app} BA) (A) or presence of ABC transporter inhibitor cocktail ($P_{app,inh}$ BA) (B) in Caco-2 vs. LLC-PK1 WT cells. Compounds were colour-coded in violet if low permeable in both cell lines (< 25 nm/s), in blue if moderately permeable in both cell lines (25 -100 nm/s) or in green if high permeable in both cell lines (> 100 nm/s). The straight line represents the line of unity. Values are shown as mean ± SD, N = 3 with n = 3. The r^2 values were calculated by a simple linear regression with r^2 = 0.766 (A) and r^2 = 0.868 (B). w/o stands for without.

Overall, a good correlation in P_{app} BA and $P_{app,inh}$ BA categorisation of antibiotics was observed when comparing values in the LLC-PK1 WT and Caco-2 cells. Two antibiotics showed a slightly lower permeability in Caco-2 than LLC-PK1 WT: levofloxacin and hydroxychloroquine, thus being classified as moderately or high permeable, respectively. Rifampicin shows a more than two-fold increase in permeability in Caco-2 compared to LLC PK1 WT. This is most likely due to active transport mediated by other proteins than ABC transporter (as ER & ER_i > 5 in Caco-2), which appear to be absent in LLC PK1 WT (ER & ER_i < 2).

Azithromycin, ciprofloxacin and erythromycin showed an around two-fold higher P_{app} BA in Caco-2, likely due to their interaction with ABC transporters active in Caco-2 cells as this discrepancy disappeared in presence of ABC inhibitors ($P_{app,inh}$ BA).

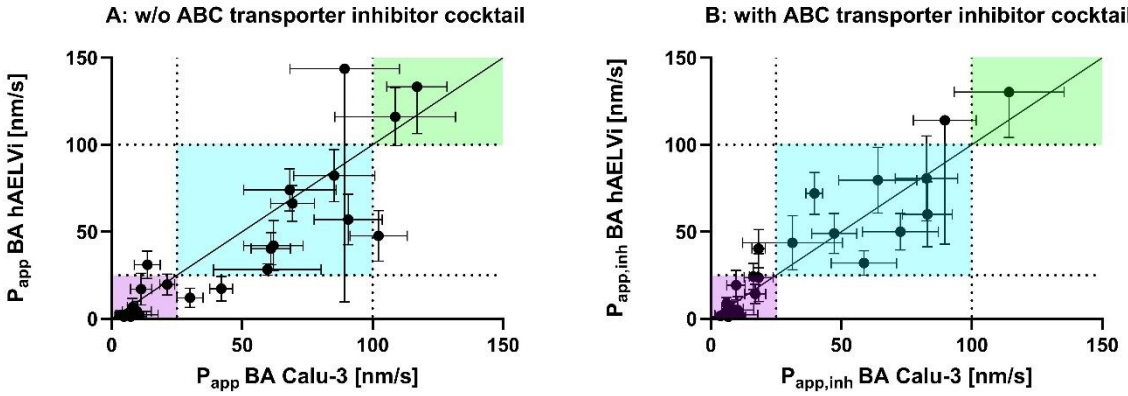

Figure 22. Comparison of basolateral to apical permeability of antibiotics and permeability markers in absence (P_{app} BA) (A) or presence of ABC transporter inhibitor cocktail ($P_{app,inh}$ BA) (B) in hAELVi vs. Calu-3 cells. Compounds were colour-coded in violet if low permeable in both cell lines (< 25 nm/s), in blue if moderately permeable in both cell lines (25 -100 nm/s) or in green if high permeable in both cell lines (> 100 nm/s). The straight line represents the line of unity. Values are shown as mean ± SD, N = 3 with n = 3. The r^2 values were calculated by a simple linear regression with r^2 = 0.571 (A) and r^2 = 0.753 (B). w/o stands for without.

In Figure 22, the P_{app} BA and $P_{app,inh}$ BA of antibiotics was compared in hAELVi vs. Calu-3 cells. The majority of compounds are classified within the same permeability category, whereas isoniazid showed an increased P_{app} BA in hAELVi but at the same time a large standard deviation (P_{app} BA of 143 ± 134 nm/s in hAELVi vs. 89.3 ± 21.0 nm/s in Calu-3). The latter may reflect some peculiar analytical difficulties of this compound, which were already encountered in the protein and sELF binding experiments. In comparison to LLC-PK1 WT and Caco-2, only few antibiotics are classified as highly permeable (> 100 nm/s, green quadrant) in lung epithelial cell lines.

Azithromycin, erythromycin and edoxaban showed a more than two-fold higher P_{app} BA in Calu-3 than in hAELVi (30.0 nm/s vs. 12 nm/s for azithromycin; 42.0 nm/s vs. 17.3 nm/s for erythromycin and 102 nm/s vs. 47.7 nm/s for edoxaban). This disconnect disappeared in presence of ABC transporter inhibitor cocktail ($P_{app,inh}$ BA), thus hinting to the presence of active efflux mediated by ABC transporters in Calu-3 that is absent in hAELVi.

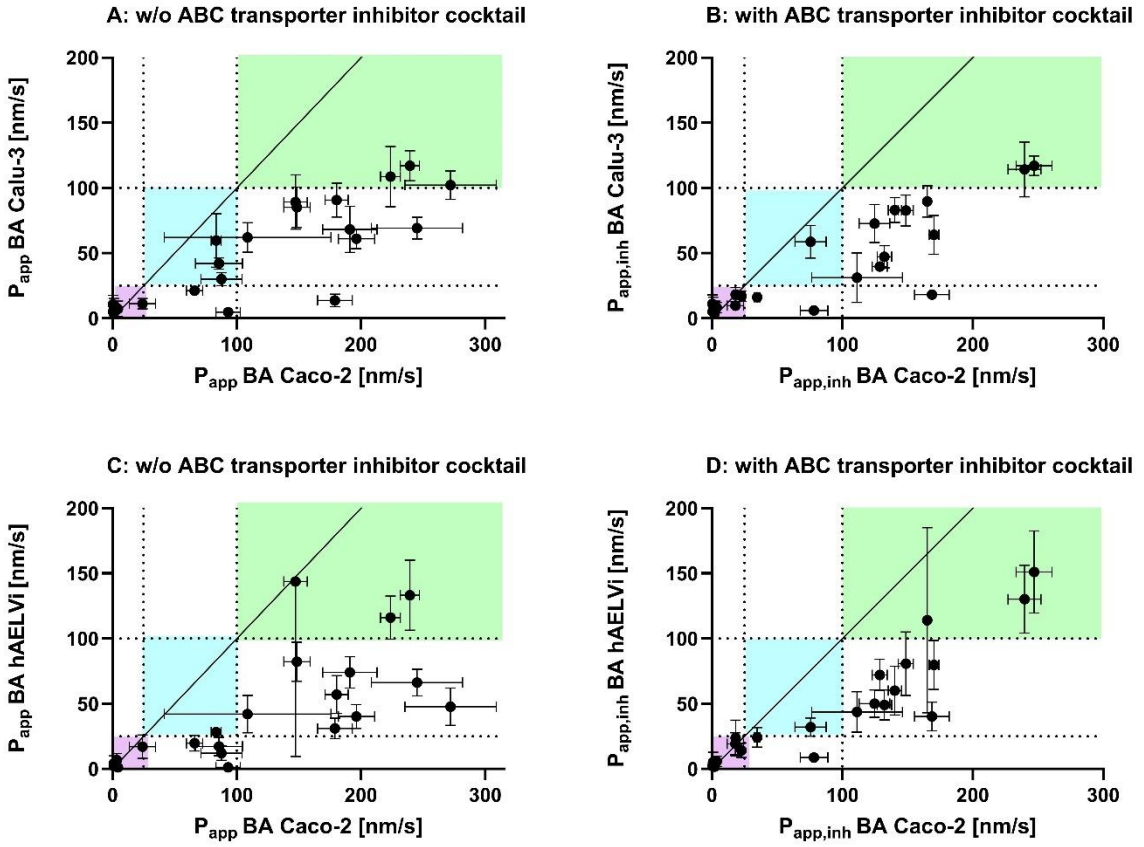

Figure 23. Comparison of basolateral to apical permeability of antibiotics and permeability markers in absence (P_{app} BA) or presence of ABC transporter inhibitor cocktail ($P_{app,inh}$ BA) in Calu-3 vs. Caco-2 (A & B) or in hAELVi vs. Caco-2 (C & D). Compounds were colour-coded in violet if low permeable in both cell lines (< 25 nm/s), in blue if moderately permeable in both cell lines (25 -100 nm/s) or in green if high permeable in both cell lines (> 100 nm/s). The straight line represents the line of unity. Values are shown as mean ± SD, N = 3 with n = 3. The r^2 values were calculated by a simple linear regression with r^2 = 0.674 (A) , r^2 = 0.728 (B), r^2 = 0.399 (C) and r^2 = 0.743 (D). w/o stands for without.

In Figure 23, the basolateral to apical permeability of antibiotics was compared in lung epithelial cells to Caco-2. As an overall trend, both P_{app} BA and $P_{app,inh}$ BA were decreased in Calu-3 and hAELVi in comparison to values measured in Caco-2, especially pronounced for antibiotics being classified as moderate to high permeable in Caco-2. In contrast, this disconnect was less evident for low permeable compounds. A similar observation was made when comparing P_{app} BA and $P_{app,inh}$ BA measured in LLC-PK1 WT to those in Calu-3 and hAELVi (see supplemental Figure B4).

3.2.3.4 Co-incubation of Hydroxychloroquine and Propranolol with Bafilomycin A1, a Disruptor of Lysosomal Acidification, in Lung Epithelial Cells

Due to their extremely low permeability in lung epithelial cells in part due to a poor mass balance recovery < 50 % and being basic and lipophilic, hydroxychloroquine and propranolol appeared to be affected by lysosomal trapping [241]. Therefore, their permeability was measured in presence of Bafilomycin A1 , a known ionophore, which disrupts the lysosomal pH gradient, thus abolishing lysosomal trapping processes [303].

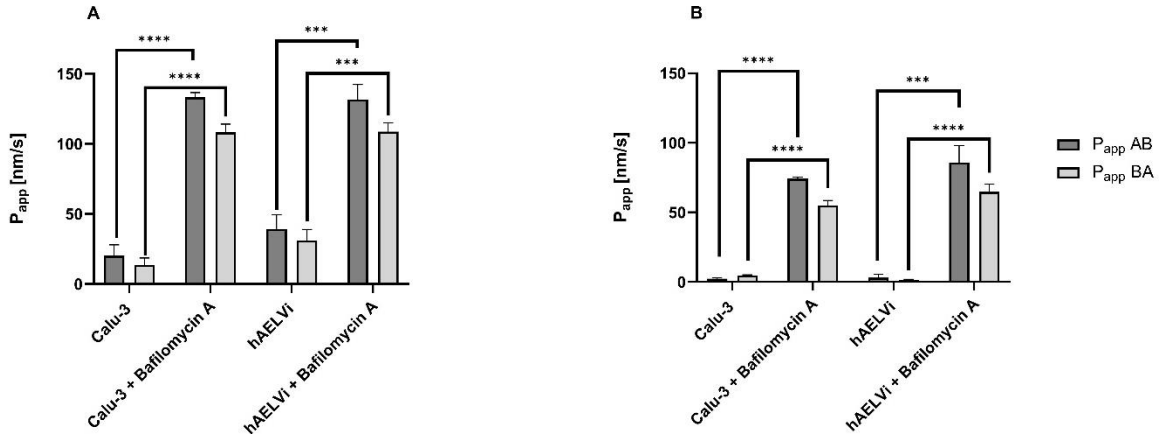

Figure 24. Apparent Permeability (P_{app}) of propranolol (A) and hydroxychloroquine (B) in lung epithelial cells Calu-3 and hAELVi and absence and presence of lysosomal trapping inhibitor Bafilomycin A1 (1 µM). Both permeability from apical to basolateral (P_{app}AB) and permeability from basolateral to apical side (P_{app}BA) are shown. Data is shown as mean ± SD, N = 3 with n = 3. Differences between two groups were analysed by un-paired t-test. ***p ≤ 0.001, ****p ≤ 0.0001

As demonstrated in Figure 24, the permeability of both hydroxychloroquine and propranolol significantly increased in presence of Bafilomycin A1, indicating the presence of lysosomal trapping processes in lung epithelial cells. The permeability of paracellular marker LY was similar in Calu-3 and hAELVi in both absence and presence of Bafilomycin A1, confirming the presence of an intact cell monolayer in both conditions (data shown in supplemental Figure B5). Moreover, the measured mass balance recovery of hydroxychloroquine and propranolol was within the acceptance range (with values ranging from 70 to 100 %) when co-incubating Bafilomycin A1 in Calu-3 and hAELVi.

3.2.3.5 Active Efflux of Antibiotics by ABC Transporters

To investigate whether antibiotics are transported by ABC efflux transporters, their ER was evaluated and compared in the lung epithelial cell lines (Calu-3 and hAELVi) vs. the reference cell lines (LLC-PK1 WT and Caco-2), as shown in Figure 25. All plotted ER values and the ER_i (in presence of ABC transporter inhibitor cocktail) are detailed in supporting Tables B5 – B8.

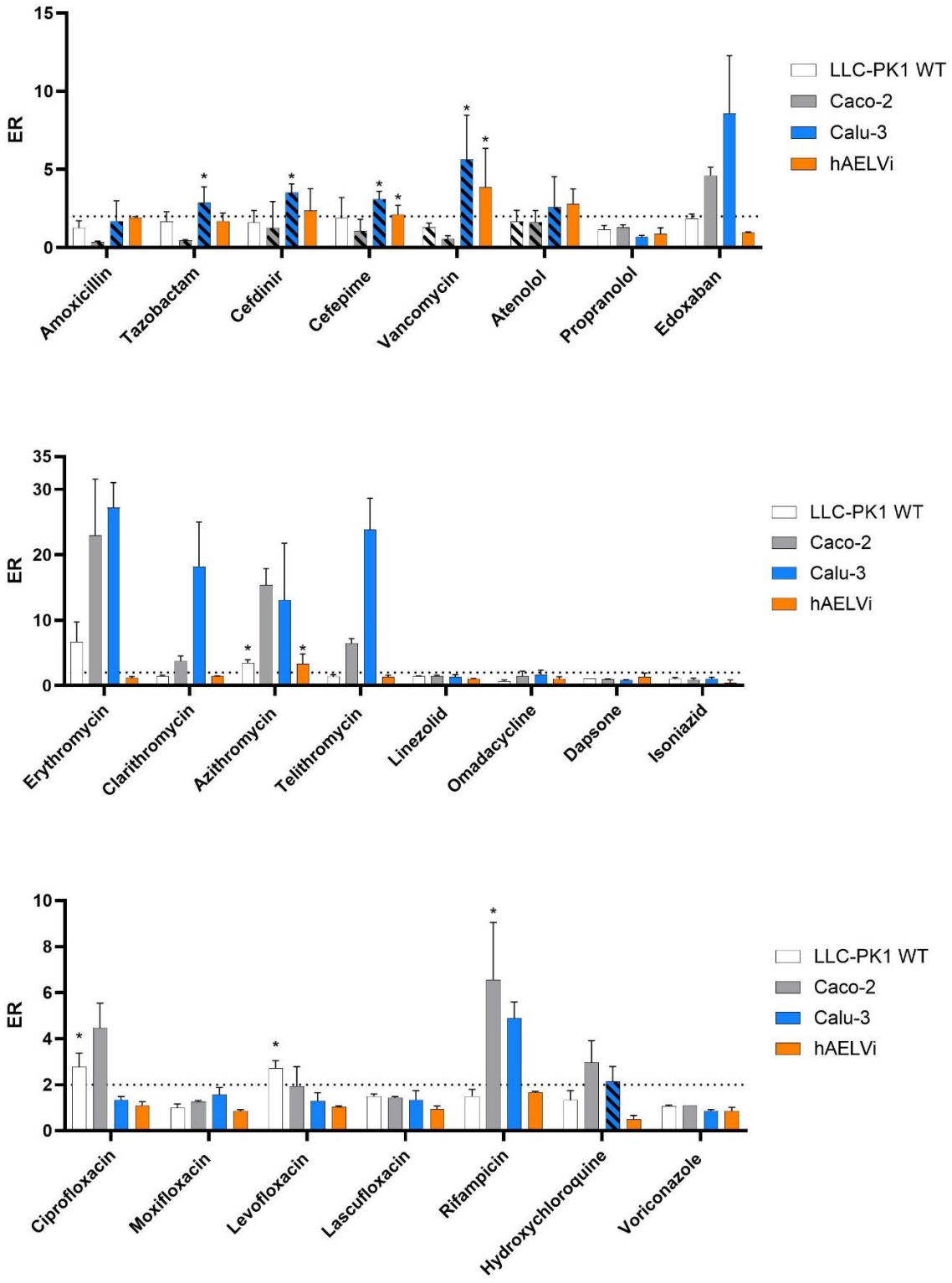

Figure 25. Efflux ratio (ER) of antibiotics and permeability markers in LLC-PK1 WT, Caco-2, Calu-3 and hAELVi cells. The dashed line indicates the ER threshold value of 2 over which it indicates active efflux (ER > 2). If both permeability coefficients used to calculate the ER were ≤ 5 nm/s (i.e. P_{app} AB and P_{app}BA), columns were striped to indicate uncertainty in ER due to extremely low permeability. If columns are marked with an asterisk (*), the ER was not changed in presence of ABC transporter inhibitor cocktail. Data is shown as mean ± SD, N = 3 with n = 3.

An ER ≥ 2 typically indicates the presence of active efflux. This was observed predominantly in Calu-3 and Caco-2 cells, where macrolide antibiotics (erythromycin, clarithromycin, azithromycin and telithromycin) showed high efflux ratio (ER 6.5 – 27.2). This efflux was also reduced by more than 50 % in presence of ABC transporter inhibitor mix. In terms of fluroquinolones, only ciprofloxacin showed efflux in Caco-2 (ER 4.5), whereas others did not show any efflux in both Calu-3 and Caco-2 (ER < 2). The high permeability marker edoxaban, that is a known substrate for MDR1, showed active efflux in both Calu-3 and Caco-2 (ER > 4.5), confirming the presence of active MDR1 in these cells with being absent in hAELVi and LLC-PK1 WT.

An ER ranging from 1.70 to 5.63 in Calu-3 and hAELVi was observed for amoxicillin, tazobactam, cefdinir, cefepime and vancomycin. However, the permeability measured for these compounds was extremely low (< 5 nm/s), indicating high uncertainty in reported ER due to being within a very low dynamic range. However, ER was largely not impacted by presence of ABC transporter inhibitor mix, indicating the ER was likely a consequence of low dynamic range.

Overall active efflux mediated by ABC transporters appeared to be present in Calu-3 but absent in hAELVi.

Few antibiotics (azithromycin, erythromycin, ciprofloxacin and levofloxacin) showed weak efflux in LLC-PK1 WT cells (ER 2.0 - 4.0) but being not reduced in the presence of ABC transporter inhibitor mix (except erythromycin).

3.2.3.6 MDR1/Mdr1a and BCRP/Bcrp1 Substrate Assessment

Investigating the Interaction of Antibiotics with Human MDR1 and BCRP *in vitro*

To investigate whether antibiotics are substrates of human active efflux transporter proteins MDR1 or BCRP, bidirectional efflux studies using ABC transporter overexpressing cell lines were evaluated (Figure 26).

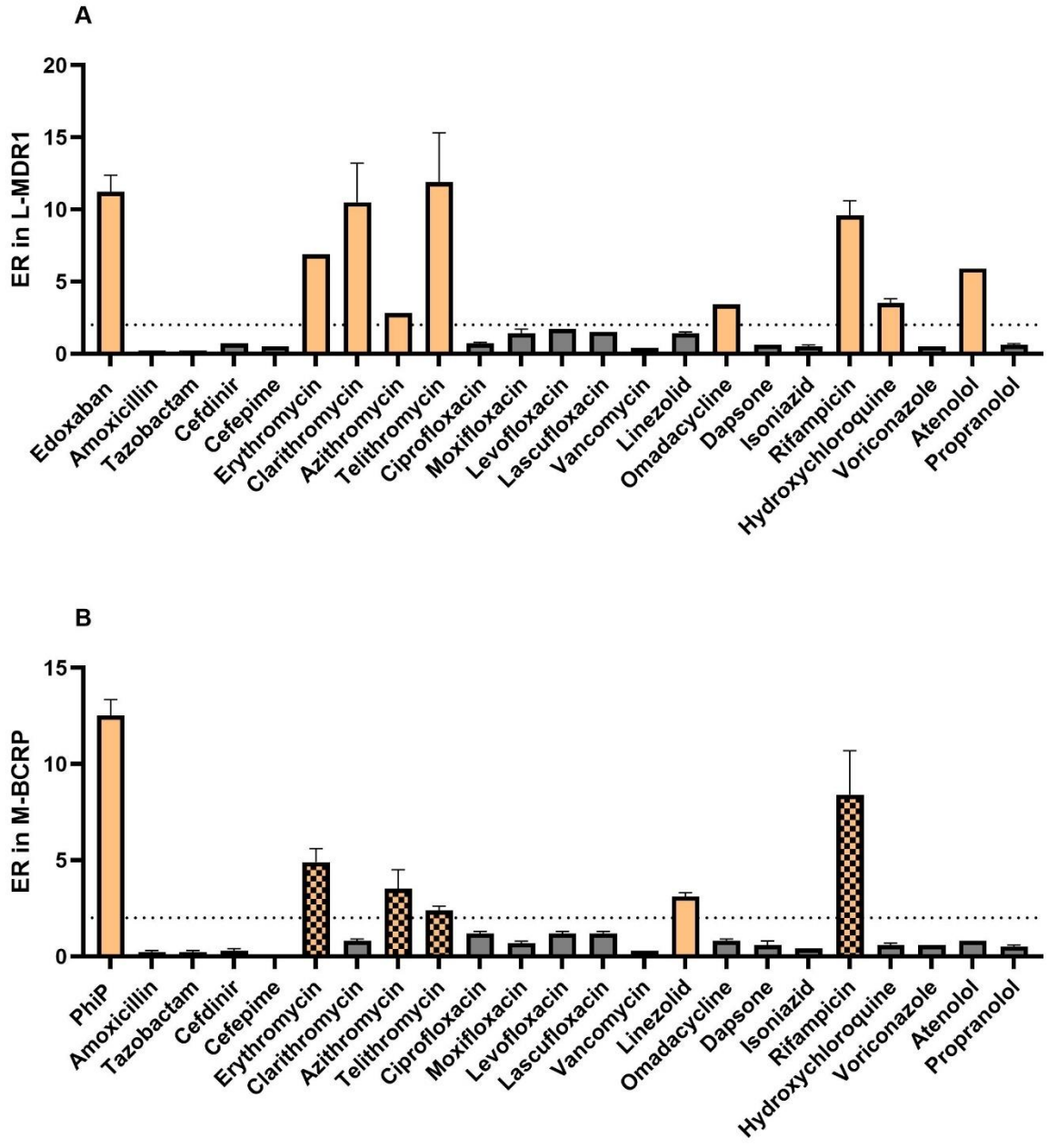

Figure 26. Efflux ratio (ER) of antibiotics and permeability markers in human MDR1 (A) and BCRP (B) overexpressing LLC-PK1 (MDR1) or MDCK-II (BCRP) cells. The dashed line indicates the threshold value of 2, over which it indicates the presence of active efflux by either MDR1 or BCRP. If ER > 2, the column is highlighted in orange. If efflux did not reduce in presence of inhibitor, the columns are marked in orange with black squares. Data is shown as mean ± SD if n =3, otherwise only mean is shown. A: Edoxaban (1 µM) served as positive control. B: PhiP (1 µM) served as positive control.

All macrolide antibiotics show an ER greater than 2 in L-MDR1 cells, confirming their interaction with human MDR1, whereas the fluroquinolone antibiotics showed less than 2. In addition, omadacycline, rifampicin and hydroxychloroquine were actively transported by MDR1 as well as the low permeability marker atenolol (ER > 2). For all these compounds, the efflux was abolished in presence of MDR1-inhibitor zosuquidar (data not shown), confirming efflux mediated by MDR1.

Only one antibiotic (linezolid) showed an ER exceeding the threshold of 2 in M-BCRP cells (ER = 3.1) and was sensitive to presence of BCRP inhibitor (ER reduced to 0.80), thus being classified as substrate of human BCRP. All other antibiotics that had an ER > 2 (erythromycin, azithromycin, telithromycin and rifampicin) in M-BCRP, showed the same degree of efflux in presence of BCRP inhibitor Ko143 (data not shown). Therefore, their active efflux does not seem to be mediated by BCRP.

Investigating the Interaction of Macrolide and Fluoroquinolone Antibiotics with Mouse Mdr1a and Bcrp1 *in vitro*

A smaller compound test set consisting of fluoroquinolone and macrolides antibiotics and the permeability markers atenolol and propranolol was tested for their active efflux in mouse Mdr1a or Bcrp1 overexpressing cells (Figure 27).

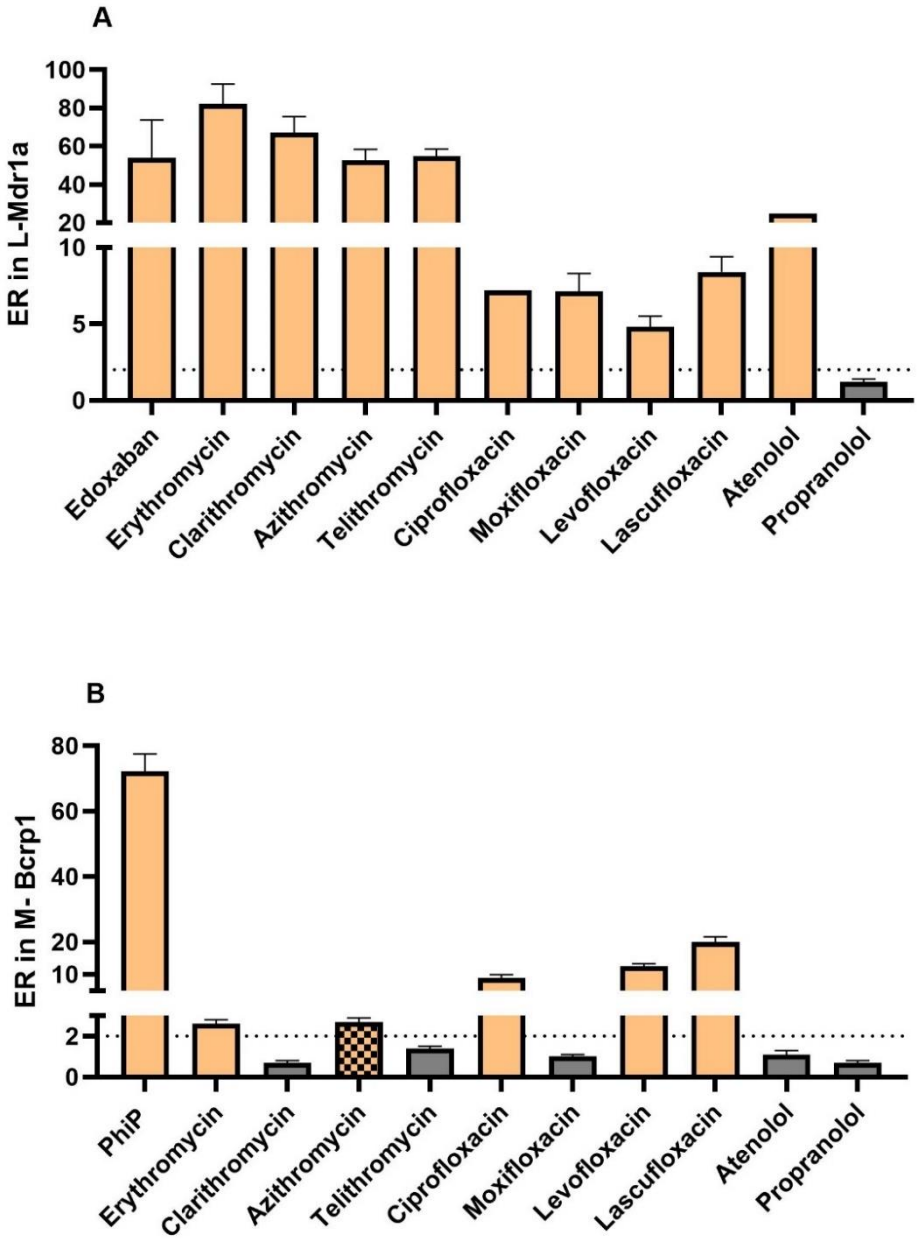

Figure 27. Efflux ratio (ER) of macrolides, fluoroquinolones and permeability markers in mouse Mdr1a (A) and Bcrp1 (B) overexpressing LLC-PK1 (Mdr1a) or MDCK-II (Bcrp1) cells. The dashed line indicates the threshold value of 2, over which it indicates the presence of active efflux by either Mdr1a or Bcrp1. If ER > 2, the column is highlighted in orange. If efflux did not reduce in presence of inhibitor, the columns are marked in orange with black squares. Data is shown as mean ± SD if n =3, otherwise only mean is shown. A: Edoxaban (1 µM) served as positive control. B: PhiP (1 µM) served as positive control.

All macrolide and fluoroquinolone antibiotics showed efflux in mouse Mdr1a overexpressing cells (ER > 2), whereas efflux was more pronounced for macrolides (ER 52.6 – 82.0) than for fluoroquinolones (ER 4.78 – 8.36). Also, the low permeability marker atenolol appeared to be recognised by Mdr1a (ER of 24.3). Overall, 4.6 to 18.8-fold higher ER values were measured in mouse Mdr1a cells compared to human MDR1 for macrolide antibiotics.

In terms of mouse Bcrp1, ciprofloxacin, levofloxacin and lascufloxacin showed an ER > 5, whereas erythromycin showed an ER of 2.58. For azithromycin, the efflux was still present with Ko143 (ER = 2.64 and ER_i = 2.65), thus questioning the transport of azithromycin by Bcrp1.

3.2.4 Discussion

To elicit their therapeutic effect, antibiotics need to permeate across the lung human epithelium to reach the ELF or alveolar macrophages [15]. Clinical studies, which have measured antibiotics exposure in plasma and ELF have reported that certain classes (i.e. macrolide and fluoroquinolones) often have an ELF to plasma ratio > 1, indicating a potentially active mechanism at the apical site of the lung epithelium against a concentration gradient, driving a higher ELF than plasma exposure [4]. However, other mechanisms such as strong binding to constituents of the ELF could also contribute to high ELF to plasma ratios of certain antibiotics [163].

This *in vitro* study aimed to shed some more light on the mechanisms how anti-infectives are transported across the human lung epithelium, which essentially determines their pulmonary bioavailability after systemic exposure by e.g. oral or parenteral administration. A compound set of twenty marketed anti-infectives was selected, and their unbound fraction in human plasma and in a simulated ELF was compared. Subsequently their permeability was investigated in human lung epithelial cells (Calu-3 and hAELVi) and compared to reference cell lines (LLC-PK1 WT and Caco-2) to ascertain if physiologically relevant systems would be more representative of lung disposition than standard models used for ADME profiling in early development. Since active efflux was observed for certain molecules in the test set, their interaction with human efflux transporters MDR1 and BCRP was also evaluated. Last, a smaller number of anti-infectives was assessed for their interaction with rodent efflux transporters Mdr1a and Bcrp1, as well as their binding to rodent plasma proteins to investigate potential species differences.

3.2.4.1 Plasma Protein and sELF Binding of Antibiotics

To estimate the extent of drug distribution, it is of importance to measure the unbound fraction in plasma, since only the unbound drug can cross biological barriers. For antibiotics treating a pneumonia, the site of action lays within the ELF [156, 302]. Due to the low abundance of proteins in ELF compared to plasma, it was often assumed that antibiotics show an unbound fraction of 1 in the ELF (i.e. completely unbound) [161]. However, a recent study using a human simulated ELF fluid revealed that especially basic antibiotics showed strong binding, with an average unbound fraction of 0.17, to ELF constituents via acidic lipids, thus reducing free drug concentrations in the ELF [156]. Moreover, for the novel fluoroquinolone lascufloxacin, it was proposed that strong binding to the ELF component phosphatidylserine is responsible for its high accumulation in human ELF compared to plasma, since the contribution of pulmonary active efflux transporter is negligible [163]. Lascufloxacin showed an ELF to free plasma ratio ranging from 57.5 to 86.4 [235].

Therefore in this study, the unbound fraction of antibiotics in sELF as described previously [156] and compared it to their unbound fraction in plasma. For the test set, we observed a moderate correlation in unbound fractions in both matrices with an r^2 of 0.784, and a trend of higher unbound fractions in sELF than plasma was observed. A similar moderate correlation between $f_{u,plasma}$ and $f_{u,sELF}$ was reported in a study by Keemink et al., however showing strong differences in binding for basic compounds [156]. If taking the ionisation at pH 7.4 into account, the average unbound fraction of basic antibiotics was lowest in both sELF and plasma compared to acidic, neutral and zwitterions. Nevertheless, the test set in this study was small and only 20 % of antibiotics were basic (50 % zwitterions, 20 % acidic and 10 % neutral). A potential limitation of sELF is that it consists of the nine main components of human ELF, but further ELF constituents like phosphatidylserine might affect drug binding in this matrix, as proposed for lascufloxacin [156, 162, 163]. Furthermore, pulmonary surfactant associated proteins like SP-A, SP-B, SP-C and SP-D are present in the ELF to which drugs could bind and thus potentially reducing the free fraction in ELF [156, 304, 305]. Moreover, the sELF assay assesses the binding at the physiological pH of 7.4, which does not represent the pH of the lung surface fluid that has been described to be more acidic (~ 6.6) [306]. Therefore, the measured unbound fraction in ELF might be mispredicted for compounds, whose ionisation state changes significantly at a lower pH.

Overall, this data supports previous findings that the unbound fraction of antibiotics in ELF is < 100 % and should be considered when estimating local free pulmonary drug concentrations [30].

3.2.4.2 Comparing the Permeability of Antibiotics in Human Lung Epithelial Cell Lines and Reference Cell Lines

The epithelial permeability of molecules can vary across cell models if accounting for differences in efflux transporter expression or differences in tight junction expression (i.e. monolayer integrity) [307]. When comparing the basolateral to apical ('secretory' or plasma to ELF) permeability of antibiotics in human lung epithelial cells Calu-3 and hAELVi to Caco-2 and LLC-PK1 WT, a clear trend of lower permeability derived in the lung cells was observed. This was especially pronounced for antibiotics being classified as highly permeable in the reference cell lines LLC-PK1 WT and Caco-2 (P_{app} BA > 100 nm/s), where an average two- to three-fold higher permeability was measured.

A study by Sibinovska and colleagues measured the permeability of a panel of low, moderate, and high permeable drugs in Calu-3 cells under ALI conditions and compared these to literature data from Caco-2. The study showed a good correlation across models, irrespective of the tissue-of-origine including for highly permeable compounds (r^2 = 0.93). One caveat of the study

of Sibinovska with regards to a direct comparison of this study is that only one antibiotic was included in the test set (oxacillin), which was found to have an extremely low permeability in both cell lines (< 2 nm/s) [61]. A further study by Selo et al. conducted a literature analysis on P_{app} AB values for forty-eight drugs comparing Calu-3 and Caco-2. Depending on the incorporated data (i.e. if several studies were available for one compound in one cell line) a weak correlation (r^2 = 0.51) to moderate correlation was found (r^2 = 0.79) for the data set. However, a similar rank order of the compounds regarding their permeability in both cell lines was seen. In this comparison study, nine antibiotics were included (aztreonam, ciprofloxacin levofloxacin, norfloxacin, oxacillin, pefloxacin, sulphamethoxazole, sulphapyridine and tobramycin), where most showed a tremendously lower permeability in Calu-3, compared to Caco-2 ranging from 1.7- to 35-fold with the exception of sulfamethoxazole which had a comparable P_{app} AB between the two cell lines. Overall, a trend of lower permeability in Calu-3 was reported for the majority of the compound set. The authors hypothesised that this may arise from the formation of a tighter barrier of pulmonary epithelial Calu-3 cells compared to intestinal epithelial Caco-2 cells [20]. This might not explain the disconnect observed in this study, since the low permeability marker Atenolol showed no significant differences in P_{app} BA across tested cell lines, thus indicating a similar monolayer tightness (see Supporting Figure B6).

It could be suggested that lung-specific mechanisms might be responsible for the observed lower permeability of antibiotics in the Calu-3 and hAELVi *in vitro* models. One factor described to affect compounds' permeability across the lung epithelium is the presence of mucus, as a potential barrier for drug permeation of basic and lipophilic drugs by binding to negatively charged mucins [308]. Calu-3 cells have been shown to have enhanced mucus production when cultured at ALI compared to LCC [86]. A study by Sibinovska and colleagues assessed the permeability of twenty-two drugs in Calu-3 at ALI and LCC and reported similar values across both conditions and concluded that the presence of mucus at the ALI condition did not have any impact on drug's permeability [61]. However, it has also been reported that drugs with a high lipophilicity (logP > 3) appear to show reduced permeability in Calu-3 at ALI vs. LLI, whereas permeability of hydrophilic compounds was similar across both culture conditions [309]. Since the compound set in this study consists of rather hydrophilic drugs (see Table 12), the interaction with mucus proteins might be less pronounced.

Another physiological aspect to consider is a potential difference in expression levels of active transporters, such as solute carrier (SLC) uptake transporters across cell lines, with which antibiotics could interact and thus impact permeability. Particularly, (novel) organic cation transporters (OCT and OCTN) and peptide transporters (PEPT) have been shown to be expressed in the lung epithelium in a functionally active manner [271, 310]. Literature reported

the recognition of fluoroquinolones like ciprofloxacin and levofloxacin by OCTs, whereas beta-lactams and cephalosporines were described to interact with OCTN and PEPT transporters [311-315].

The lung is a lysosomally rich organ. The lysosomes are acidic organelles, found in the cytosol of every living cell, which have the potential to trap basic drugs in the intracellular compartment, termed lysosomal trapping [316]. Lysosomal trapping describes the sequestration of lipophilic basic compounds in cellular lysosomes, where they become protonated due to acidic lysosomal pH (~ 5), resulting in decreased permeability *in vitro* [241]. The consequence of lysosomal trapping in the lung results in enhanced lung retention of drugs, which has been reported for propranolol and β-2 adrenergic bronchodilators, such as formoterol and salmeterol, both *in vitro* and *in vivo* [317, 318]. Further, lysosomal trapping has been shown to be present in human and rat alveolar macrophages [53, 239]. The impact of lysosomal trapping on cellular permeability *in vitro* was investigated by Bednarczyk and colleagues using MDCK cells where they reported that every 10 % loss in mass balance recovery due to lysosomal trapping led to an underestimation of permeability by ~ 22 nm/s, mainly observed for lipophilic, basic drugs [241]. Therefore, this should be considered when using *in vitro* models to evaluate disposition in terms of permeability estimation.

The compound set in this study consisted of four basic antibiotics (azithromycin, clarithromycin, erythromycin and hydroxychloroquine) with predicted logD values of 0.62 to 1.76, indicating a certain degree of lipophilicity. However, only for hydroxychloroquine, an extremely low recovery less than 50 % was observed, when tested *in vitro* in lung epithelial cells compared to mass balance recovery values above 80 % in LLC-PK1 WT. Hydroxychloroquine showed also an extremely low permeability across Calu-3 and hAELVi (< 10 nm/s), whereas more than 15-fold higher values were measured across LLC-PK1 WT. Similar findings were made for propranolol, which is basic and lipophilic (logD of 1.35) and showed a more than 10-fold lower permeability across Calu-3 compared to LLC-PK1 WT. Thus, the permeability of hydroxychloroquine and propranolol was measured in presence of Bafilomycin A1, a V-type H^+-ATPase inhibitor and thus a disruptor of the lysosomal acidification [303], to evaluate the potential impact of lysosomal trapping on the permeability of these two molecules across Calu-3 and hAELVi. In presence of Bafilomycin A1, the permeability of both hydroxychloroquine and propranolol across Calu-3 and hAELVi increased significantly to values similarly measured across Caco-2 and LLC-PK1 WT. Bednarczyk and colleagues have reported the relevance of lysosomal trapping in underestimating the *in vitro* permeability of basic, lipophilic compounds with amine groups [241]. As both hydroxychloroquine and propranolol carry amine groups and their permeability across Calu-3 and hAELVi significantly increased in presence pf Bafilomycin A1, this hints to the presence of lysosomal sequestration. This appears to be less pronounced in

cells like LLC-PK1 WT, potentially due to a lower cellular content of lysosomes. However, there are no studies available that quantified the lysosomal content in Calu-3, hAELVi to enable a direct comparison to other cell lines. Overall, this data emphasises the risk of a potential permeability underestimation in bidirectional transport studies if mass balance recovery is low, especially when testing basic and lipophilic compounds. This highlights the importance of calculating recovery values in these studies, which might be a special concern for lipophilic and basic antibiotics with a positive charge (e.g. via an amine group), that is an important prerequisite for targeting gram-negative bacteria [164]. In contrast to hydroxychloroquine, the mass balance recovery for the three other basic antibiotics azithromycin, clarithromycin and erythromycin was within acceptance range (~ 70 – 100 %) under normal conditions in both Calu-3 and hAELVi. These antibiotics show a similar or higher lipophilicity (logD) compared to hydroxychloroquine. It is possible that they are also affected by lysosomal trapping, but to a lower degree. In this context it needs to be mentioned that lysosomal trapping is a reversible, concentration-dependant, slowly equilibrating process [318]. Both azithromycin and erythromycin were tested at 2.5-fold higher incubation concentration than hydroxychloroquine due to analytical purposes, which might contribute to a partial saturation of lysosomal trapping. The vast majority of tested antibiotics in this study are zwitterions. Literature reported that zwitterions do not seem to be significantly impacted by lysosomal trapping [242], thus this phenomenon may likely not contribute significantly to their reduced permeability in the lung cell lines.

A further mechanism described to increase lung retention time *in vitro* and *in vivo* and thus potentially decreasing *in vitro* cellular permeability is non-specific binding to lung tissue, i.e. phospholipids of the cell membrane [318]. Especially binding of moderate to strong basic compounds (pKa ≥ 7) via electrostatic interactions to acidic phospholipids, such as phosphatidylserine has been described as key factor of their tissue distribution [319]. Similar behaviour was described for zwitterions that carry a basic group with a pKa ≥ 7 [320]. The human tracheal lung epithelium membrane was described to constitute mainly of phosphatidylcholine (PC, 50 mol%), followed by phosphatidylethanolamine (PE, 28 mol%), phosphatidylinositol (PI, 8 mol%), phosphatidylserine (PS, 6 mol%) and phosphatidylglycerol (PG, 1 mol%) and further lipids. Both neutral PC and PE found in all cell membranes of mammalians and are the most abundant phospholipids, whereas PS, PI and PG are acidic phospholipids [321-323]. Strong binding of bases like propranolol to acidic phospholipids PS, PI and PG has been reported in rats, with a pronounced binding to PS. In rats, PS showed highest expression levels in the lung, being almost three-fold higher than in intestine or kidney. Furthermore, highest tissue to plasma distribution rates were observed for propranolol in the rat's lung showing a direct relationship with PS tissue expression levels [324]. In human, highest expression levels of PS have been reported in brain with accounting for 20 % of total

phospholipids, whereas in human kidney and intestine, PS accounts for around 6 or 2 % of total phospholipids, respectively [325-327]. This points to potential species differences in PS tissue distribution between rat and human. However, a study by Small and colleagues incorporated the binding of basic drugs (like propranolol) to acidic phospholipids, like PS, into the prediction of the total volume of distribution in humans. They reported a more accurate prediction if accounting for PS binding, highlighting of the importance of PS binding to the tissue distribution of basic compounds also in humans [328]. As most of the tested antibiotics are strong bases or zwitterions that carry a strong basic group, binding to acidic phospholipids in the membrane of lung epithelial cells is likely. In terms of human cell lines, a study by Treyer et al. compared the membrane phospholipid composition of human cell lines including Caco-2 and A549 (an alveolar tumour cell line with characteristics of alveolar pneumocytes type II) and reported similarities in content levels of acidic phospholipids PS and PG and slightly higher PI in Caco-2. The same study also assessed the unbound fraction to cells for a variety of drugs in homogenates of Caco-2, A549, LLC-PK1 WT and further cell lines. Interestingly, two of the basic test compounds (diltiazem and metoprolol with a basic pKa > 7) showed up to four-fold stronger binding to A549 homogenate that to Caco-2 and LLC-PK1 WT [329].. To date, there is no study currently available that performed a lipidomic assessment of the phospholipid composition of the cell membrane than to Calu-3 and hAELVi cells (in flask or ALI culture), which would allow a comparison to the membrane phospholipid composition of LLC-PK1 WT and Caco-2 cells.

To conclude, the lowered *in vitro* permeability of antibiotics in lung epithelial cells might arise from strong binding to acidic phospholipids due to potential differences in membrane acidic phospholipid levels in Calu-3 and hAELVi vs. human intestine (Caco-2) and porcine kidney (LLC-PK1 WT) cells. Further, an enhanced presence of lysosomal trapping in Calu-3 and hAELVi could contribute to observed differences in permeability for antibiotics like hydroxychloroquine.

3.2.4.3 Active Efflux of Antibiotics by ABC Transporters

Bidirectional transport studies revealed that few antibiotics showed an asymmetry in transport in Calu-3 (ER ≥ 2) that was reduced by more than 50 % in presence of ABC transporter inhibitors (i.e. zosuquidar, MK-571 and Ko143), hinting to the presence of active ABC transporter-mediated efflux. This was mainly observed for the macrolide antibiotics (erythromycin, clarithromycin, azithromycin and telithromycin) and rifampicin. Testing these compounds in the human MDR1-overexpressing cells (L-MDR1) revealed that they are all substrates of MDR1. Several *in vitro* studies have reported the expression of functionally active MDR1 in Calu-3 as well as its interaction with macrolide antibiotics [16, 86, 196, 288].

Moreover, the permeability marker edoxaban (a known substrate of MDR1 [258]) showed active efflux in Calu-3 that was reduced in presence of inhibitors. This confirms active efflux mediated by MDR1 in Calu-3 cells. Similar observations were made for the Caco-2 cells, which have been described to express functional MDR1 due to the cells being of intestinal origine [293]. In these cells, efflux (ER ≥ 2), was observed for the MDR1 model substrate Edoxaban, as well as for macrolides. As these antibiotics were classified as substrates of human MDR1 in this study, MDR1 is likely responsible for measured efflux in Caco-2.The efflux of rifampicin was not reduced in presence of ABC inhibitors (ER_i = 6.5), thus potential other active transporters in Caco-2 may contribute to its efflux.

Fluoroquinolone antibiotics ciprofloxacin, levofloxacin and moxifloxacin have been reported to be substrates of MDR1 efflux in Calu-3, with rather low ER values of 4.0, 2.6 and 2.1, respectively [17]. Whereas for lascufloxacin an ER < 2 was observed, classifying the compound as non/poor substrate of MDR1 according to guideline rules from health authorities [18, 163]. In this study, no active efflux of fluroquinolones was observed in Calu-3 or Caco-2 (ER < 2), except ciprofloxacin that showed a weak efflux in Caco-2 (ER = 4.5). In addition, none of the fluoroquinolones showed an ER ≥ 2 in the MDR1- and BCRP-overexpressing cells, suggesting they are no substrates of both human MDR1 and BCRP. This was an interesting finding, since fluoroquinolone antibiotics often show an ELF to unbound plasma ratio > 1 and the involvement of active efflux transporters in human lung epithelium was proposed, driving a higher ELF concentration in an active manner [4, 15].

In contrast to Calu-3, a tracheo-bronchial cell line, no considerable active efflux of antibiotics was observed in the alveolar epithelium-derived hAELVi cell line, generated by lentivirus-mediated immortalisation. This can be explained by the absence of MDR1 and BCRP expression in these cells as reported in literature [108]. Only azithromycin showed some kind of efflux in hAELVi but without being sensitive to ABC transporter inhibitors (i.e. ER_i > 2). This asymmetry in transport of azithromycin might be considered an artefact due to its extremely low permeability in the hAELVi cells with a high standard deviation (i.e. 5.0 ± 5.3 nm/s for P_{app} AB and 12.0 ± 5.6 for P_{app} BA) and a similar range in permeability measured in presence of ABC transporter inhibitor cocktail.

Few antibiotics (azithromycin, ciprofloxacin, and levofloxacin) showed weak ABC transporter-independent efflux in the LLC-PK1 WT (i.e. efflux still present while co-incubation with ABC transporter inhibitor cocktail). This porcine kidney epithelial cell line has been described to express functionally active endogenous uptake transporters, like organic cation transporters (OCT) [330, 331]. Levofloxacin was reported to show an increased influx clearance at the basolateral side of LLC-PK1 cells, likely mediated by an organic cation transporter [311].

Linezolid was the only antibiotics that was classified as human BCRP substrate in BCRP-overexpressing cells (ER > 2). Also, erythromycin, azithromycin, telithromycin and rifampicin showed an ER > 2 in M-BCRP. However, their efflux was not reduced in presence of BCRP inhibitor Ko143, thus they cannot be classified as BCRP substrates. In contrast, they were all classified as substrates of human MDR1 within this study Furthermore, literature reported a high expression of endogenous Mdr1 in the MDCK-II cells [292]. As all these antibiotics were classified as MDR1 substrates, their efflux in M-BCRP is most likely mediated by endogenously expressed canine Mdr1.

In summary, only few anti-infectives were found to be substrates of human MDR1, which is likely responsible for mediated efflux in Calu-3 cells. This efflux was not observed in the hAELVi cells, which raises the question whether active efflux plays a substantial role in the human lung epithelium of the alveolar region. Given the larger surface area in the alveolar region (140 m^2 versus 1-2 m^2 in upper airways [27]) and the resulting much larger surface area of the lower airways, the contribution of active efflux transporters within the bronchial region might be negligible on total pulmonary drug disposition. Furthermore, Calu-3 cells are derived from a tumour patient and thus might not be representative of the healthy lung physiology due to the general multidrug resistance phenotype (i.e. elevated expression of ABC efflux transporters) often observed in cells of cancerous origin [332].

3.2.4.4 Potential Species Differences in Rate and Extent of Antibiotics' Transport across the Lung Epithelium in Human and Rodents

Rodents are often used as preclinical species to study the pharmacokinetics, efficacy and tissue exposure of novel antimicrobials in drug development [333]. However, species differences in pharmacokinetic processes need to be considered [114]. Therefore, a small test set of antibiotics (macrolides and fluoroquinolones) was tested for their interaction with mouse Mdr1a and Bcrp1 (as potential impact on rate of distribution) and their binding to rodents' plasma proteins (as potential impact on extent of distribution).

In vivo, fluroquinolones such as moxifloxacin and ciprofloxacin showed an increased concentration in ELF compared to unbound plasma at distribution equilibrium after intravenous administration in rats (i.e. four-fold for ciprofloxacin or 13-fold for moxifloxacin). The authors concluded that the presence active efflux transporters such as P-glycoprotein (i.e. Mdr1) on the apical side of the lung epithelium might be responsible [297, 334]. Similar results were reported for azithromycin, clarithromycin and telithromycin after oral administration to rats, suggesting the involvement of active transport by Mdr1 to high ELF concentrations [288, 289]. The presence of functionally active Mdr1 and Bcrp in the rodent lung epithelium has been described in literature [205, 227]. In rodents, P-glycoprotein is coded by two isoforms: Mdr1a

and Mdr1b. Mdr1a is predominantly expressed in mouse lung and Mdr1b in rat lung [203, 335]. As a potential caveat of our study, we only assessed antibiotics in mouse Mdr1a-overexpressing cells. However, a sequence homology of 83 % was described between the two isoforms of Mdr1 in mice and a more than 90 % sequence identity between the respective mouse and rat Mdr1 isoforms. Therefore, no significant substrates differences between mouse and rat Mdr1 are expected [336, 337].

Erythromycin, clarithromycin, azithromycin and telithromycin showed a strong efflux in the mouse Mdr1a-overexpressing cells (ER > 50), that is up to 18-fold higher than the ER in human MDR1-overexpressing cells. Ciprofloxacin, moxifloxacin, levofloxacin and lascufloxacin showed efflux in the mouse Mdr1a cells (ER >~ 5), without being recognised as substrates of human MDR1 (ER < 2). A similar observation was made for BCRP. None of the fluoroquinolones and macrolides could be classified as substrate of human BCRP (ER < 2), whereas ciprofloxacin, levofloxacin and lascufloxacin showed an ER > 5 in mouse Bcrp1-overexpressing cells and erythromycin and azithromycin an ER of 2 - 3 for mouse Bcrp1.

This data points to a potential stronger impact of efflux transporters on drug distribution in rodents compared to humans. This phenomenon was observed at the level of the blood brain barrier, where P-glycoprotein had a stronger impact on limiting the brain exposure of its substrates in rodents compared to humans [338]. Thus, the potential active secretion of antibiotics (like macrolides or fluoroquinolones) from the pulmonary epithelium into the ELF (and resulting higher ELF concentration than plasma in steady state) might be more pronounced in rodents, than in humans.

Species differences in plasma protein binding are known and a recent study testing β-lactam antibiotics revealed a stronger plasma protein binding in rat than human [339, 340]. In this study, we did not observe any species differences as measured unbound fractions for the macrolides and fluoroquinolone antibiotics were comparable across human, mouse and rat. Telithromycin was an exception by showing four- to five-fold stronger binding to mouse ($f_{u,plasma}$ = 0.074) than rat (0.251) or human (0.342) plasma, respectively. A similar unbound fraction of 0.054 was reported for telithromycin in mice, when testing at 2.5 µM (compared to 1.0 µM in this study). This unbound fraction increased with elevating telithromycin concentration with a unbound fraction of 0.312 when tested at ~ 30.7 µM, which indicates some degree of concentration-dependent protein binding [341]. The unbound fraction in rodent plasma was not compared to those measured in sELF, since the sELF was based on human composition and thus may not represent the rodent ELF [156]. However, a strong binding of antibiotics to ELF in rodents can likely impact the extent of antibiotics distribution across the rodent lung epithelium.

Overall, the data indicates that there are some species differences in the interaction of macrolide and fluroquinolone antibiotics with ABC transporter proteins, resulting a higher efflux ratio for mouse Mdr1a/Bcrp1 compared to human MDR1/BCRP *in vitro*. This raises the question whether rodents are a suitable model to investigate the contribution of ABC transporters on the pulmonary drug disposition of antibiotics. In terms of binding to plasma proteins, species differences appear to less be pronounced for the selected compound set.

3.2.5 Conclusion

This in vitro study investigated the pharmacokinetic parameters affecting pulmonary transport and bioavailability of anti-infectives into the ELF after systemic administration with the aim to deepen our mechanistic understanding of these processes. The majority of anti-infectives showed a reduced permeability across Calu-3 and hAELVi monolayers compared to values with LLC-PK1 WT and Caco-2 cells, respectively. These differences might be ascribed to enhanced binding to acidic phospholipids in the membrane of the lung epithelial cells and the impact of lysosomal trapping for certain drugs. Active efflux by ABC transporters was observed in the bronchial Calu-3 cells but absent in the alveolar hAELVi cells. If accounting for the larger surface area of the alveolar epithelium compared to the bronchial epithelium, this raises the question about the relevance of ABC transporters on overall pulmonary drug disposition. A somewhat stronger interaction with rodent Mdr1 and Bcrp than with the analogous human proteins was seen for macrolide and fluoroquinolones, hinting to potential species differences and a likely more pronounced impact of active efflux on drug distribution across the lung epithelium in rodents. Integrating some physiology-based pharmacokinetic modelling (PBPK) approach might help to translate these in vitro findings to the clinic.

3.3 A Mechanistic PBPK Framework to Simulate Moxifloxacin and Telithromycin ELF Concentration-time Profiles in Human and Rat

3.3.1 Introduction

Antibiotics are typically administered via the systemic circulation to patients, either intravenously or via an oral application [9]. Therefore to treat a bacterial pneumonia, the antibiotics need to permeate across the human lung epithelial via the pulmonary endothelium to reach their side of action in the epithelial lining fluid (ELF) [15]. The ELF is a thin and aqueous layer, covering upper and lower airways and consists of proteins, lipids, antioxidants and further components [38, 156]. The composition of the ELF changes from upper to lower airways, with the presence of mucins or surfactant proteins [342].

Clinical studies have reported that certain antibiotic classes, principally fluoroquinolones and macrolides, show a higher concentration in ELF than plasma (>> 1) at steady state [4]. Similar observations of high ELF to plasma ratios were also observed in rodents [288, 297]. Furthermore, certain macrolides and fluoroquinolones have been described in literature to be substrates of active efflux transporters, such as multi drug resistance protein 1 (MDR1 or P-glycoprotein) and breast cancer resistance protein (BCRP) [16, 17, 231]. Thus, it has been hypothesised that the presence of active efflux transporters at the lung epithelium could be an explanation for the higher ELF concentrations in both human and rodent compared to simultaneously measured concentrations in plasma [4, 297].

A point to consider when assessing ELF to plasma ratios is that reported ratios are rarely corrected for the unbound fraction in plasma and might not necessarily represent a physiological relevant ratio, as only the unbound drug can pass biological barriers [4, 15]. A review by Kiem and Schentag corrected clinical ELF-to-plasma ratios for the unbound fraction in plasma and the reported ratios were > 1 for macrolides (up to 304) and for fluoroquinolones (up to 110) [15]. A previous hypothesis assumed that ELF drug concentrations are likely 100 % free due to the low abundance of proteins in ELF compared to plasma [161]. Therefore, the measured ELF concentrations were not corrected for potential binding to ELF components. Recent studies have, however, shown that drug binding to proteins, lipids or surfactants within ELF occurs and consequently, reduces free local drug concentrations [156, 162, 163].

To investigate the impact of active efflux in the lung epithelium and the degree of binding to ELF components on total ELF concentration-time profiles, physiologically based pharmacokinetic modelling (PBPK) can be employed. The PBPK modelling allows the prediction of drug concentration-time profiles across in various tissues and across species

in silico, through incorporation of ADME processes [131]. The PBPK models usually consist of several compartments including intestine, kidney, liver, brain, lung and heart that are defined by anatomical parameters. A blood circulation connects all the compartments with each other [133]. Plasma and local tissue concentrations are estimated by informing a mechanistic system with appropriate physicochemical properties of the compound of interest as well as physiological parameters according to the species/individual. Mathematical differential equations that take these parameters into account are used to predict pharmacokinetic processes [131, 343]. These PBPK models can also be used to investigate the impact of drug transporters on absorption, distribution and elimination processes [135].

Gaohua and colleagues have employed PBPK modelling to simulate the concentration of anti-tuberculosis drugs in plasma and ELF, using a multicompartment lung model. The initial model has assumed that lung distribution is driven by passive diffusion only. The passive permeability values used as input parameters were derived from an *in vitro-in vivo* extrapolation from permeability coefficients in Calu-3 cells (human bronchial epithelial cell line) and corrected for the respective surface area in upper and lower airways. Seven antibiotics were screened and for four out of these seven, the simulated ELF-to-plasma ratios were comparable (within 2.5-fold) to available clinical data, such as the macrolide erythromycin. For the remaining antibiotics including the macrolide clarithromycin, ELF-to-plasma ratios were underestimated up to 26-fold. Sensitivity analysis revealed that factors such as active transporters or a change in pH of the lung fluid might improve simulations for these three antibiotics. The study further showed that the establishment of a lung-specialised PBPK model appears to be a powerful tool to estimate pulmonary drug concentrations in the early phase of drug discovery [141]. Moreover, PBPK models were used to estimate pulmonary and systemic drug absorption profiles after administration via inhalation [137, 344].

This *in silico* study described in this report aimed to simulate the plasma and ELF concentration-time profiles of two antibiotics that showed high ELF to plasma ratios (>> 1): the fluoroquinolone moxifloxacin and the macrolide telithromycin [4, 289, 297]. The profiles were simulated in both human and rat to investigate potential differences across species, since rodents are often used as preclinical models [333]. It was explored whether the presence of MDR1 efflux at the apical side of the pulmonary epithelium had any impact on predicted ELF concentrations. The focus laid on MDR1 due to the availability of kinetic data for moxifloxacin and telithromycin with MDR1 *in vitro* [345, 346]. Further, the impact of the unbound drug fraction in ELF was simulated to investigate any potential influence of binding on the ELF concentration-time profiles.

3.3.2 Methods

3.3.2.1 General Points and Study Workflow

The GastroPlus™ software (Version 9.9, Simulations Plus Inc., Lancaster, CA, USA) was used to simulate the concentration-time profiles of moxifloxacin and telithromycin in plasma and ELF of human and rat. Simulated profiles were always verified against data from clinical or *in vivo* studies, which are summarised in the supplemental Tables C1 & C2.

The input parameters used for the simulations were either measured experimentally, retrieved from literature or predicted by GastroPlus™. A detailed list of all parameters, which were manually added to set up the PBPK models can be found in Supplemental tables C3 & C4.

An approach consisting of three steps was used to set up and validate the PBPK models for moxifloxacin and telithromycin in both human and rat (see Table 13).

Table 13. Study workflow to set up and validate PBPK models for moxifloxacin and telithromycin in human and rat. The table provides an overview of clinical studies and *in vivo* studies used for the validation of established PBPK models and summarises the dose, dosing frequency and route of administration.

		Moxifloxacin		**Telithromycin**	
	Simulation matrix	Human	Rat	Human	Rat
Step 1	Plasma	400 mg SD po [347]	9.2 mg/kg SD iv [348]	800 mg SD po [349]	50 mg/kg SD po [350]
Step 2	Plasma	400 mg SD po [351] 400 mg PO q24h x 5 doses [352]	5 mg/kg SD iv [297]	800 mg PO q24h x 5 doses [353] 800 mg PO q24h x 5 doses [354]	50 mg/kg SD po [289]
Step 3	ELF	400 mg SD po [351] 400 mg PO q24h x 5 doses [352]	5 mg/kg SD iv [297]	800 mg PO q24h x 5 doses [353] 800 mg PO q24h x 5 doses [354]	50 mg/kg SD po [289]

In a first step, the PBPK model was built, and the plasma concentration-time profiles were simulated after a single dose in healthy volunteers or control animals. If needed, models were further refined, as described in section 3.3.2.3 In a second step, the established models were used to estimate the plasma concentration profile of clinical/*in vivo* studies that measured both plasma and ELF concentrations. The antibiotics were either administered as a single or

multiple dose. For moxifloxacin and telithromycin, two studies were considered in human and one in rat. In a third step, the respective ELF concentration-time profiles in human and rat were simulated and compared to respective observed clinical and *in vivo* data.

3.3.2.2 General PBPK Model Set Up

In GastroPlus™, there are three modules to be evaluated and if needed to be adapted before running the simulation.

The first module is called 'Compound' and contains the physicochemical and pharmacokinetic parameters, especially important for predicting the absorption profile. These include amongst others, the molecular weight, distribution/partition coefficient (logD or logP), solubility, biorelevant solubility (in simulated intestinal fluids), and effective intestinal permeability (P_{eff}). In this study, logD/logP, solubility and P_{eff} were taken from inhouse experiments or predictions (see supplemental Tables C3 & C4). All other parameters were predicted by the software. This tab allows further to enter the dosage information, where immediate release tablet was selected for oral administration in human, immediate release solution for oral administration in rat and intravenous bolus for intravenous injections in rat. For the human simulations, it was assumed that study subjects take the tablet with 250 mL of water (default by GastroPlus™). This tab was further used to enter respective transporter and enzyme kinetics, if applicable.

The second module 'gut physiology' contains all information regarding the intestinal absorption model based on the advanced compartmental absorption and transit™ model. This models subdivides the intestine into nine compartments from stomach to ascending colon. For modelling the absorption profiles in human, either the physiological fasted or fed condition was chosen, depending on the set-up of the clinical study. For rats, the physiological fed condition was chosen. The absorption scaling factors for the individual gut compartments were predicted by the Opt logD Model SA/V 6.1 (default selection).

The pharmacokinetic tab was used to set up the actual PBPK model. For human, the default healthy male model (30 years, 85.53 kg) was chosen. For rat, the default model was selected (0.250 kg). In this tab, the experimentally derived plasma protein binding values were added, on which basis the adjusted plasma protein binding was calculated that takes binding to plasma lipids into account. The tissue to plasma partition coefficients (K_p) were calculated according to Lukacova-Rodgers – Single method (further details can be found in GastroPlus™ user manual [355]). Clerance values were either scaled in GastroPlus™ based on in-house available hepatocyte stability data or taken from literature (see supplemental Tables C3 & C4). All tissues were set to perfusion-limited if not stated otherwise.

The simulations were run in single simulation mode. The simulated profiles were then compared to the observed ones, with special focus on the maximal plasma concentration (C_{max}), the time of C_{max} (t_{max}) and the area under the plasma concentration-time curve for the respective simulation time (AUC_{0-t}). These pharmacokinetic parameters were compared to the observed values for orally administered drugs, whereas for intravenously administered drugs, the volume of distribution (V_{ss}) and the half-life ($t_{1/2}$) were compared in addition to the AUC_{0-t}.

3.3.2.3 Simulation of Plasma Concentration-Time Profiles

Moxifloxacin

For modelling the plasma concentration of moxifloxacin, the following parameters were used as input parameters by measured/predicted in-house or literature-retrieved values: logD, P_{eff}, solubility, unbound fraction in plasma ($f_{u,plasma}$), unbound fraction in simulated ELF ($f_{u,sELF}$), hepatic clearance (CL_h) and renal clearance (CL_r). The values can be found in the supplemental table C3. All other parameters were maintained as predicted from GastroPlus™.

For human, both fasted and fed conditions were simulated. For rat, no absorption parameters were considered as moxifloxacin was administered via an intravenous injection.

Telithromycin

The PBPK model for telithromycin to simulate its plasma concentration-time profiles was set by using GastroPlus™ predicted values apart from logP, P_{eff}, solubility, $f_{u,plasma}$, $f_{u,sELF}$, CL_h, biliary clearance (CL_b) and CL_r that were taken from inhouse data or retrieved from literature (see Supplemental Table C4). The logP was taken instead of the logD due to a more accurate estimation of V_{ss} and $t_{1/2}$.

Further, intestinal metabolism by CYP3A4 was incorporated into the human model to increase its predictiveness [346]. Kinetic parameters (Michaelis-Menten constant (K_m) and maximal velocity (V_{max})) of the interaction of telithromycin with human CYP3A4 were taken from literature and can be found in Supplemental Table C4. Intestinal MDR1 was not included in the model, as literature indicated that the transporter is likely saturated due to the high oral dose given in humans (i.e. 800 mg) [346].

Since Mdr1a was described in literature to limit the intestinal absorption of telithromycin in rats at doses similar to those given in *in vivo* studies used for this *in silico* study [356], the P_{eff} was reduced four-fold (to 0.5×10^{-4} cm/s) compared to the human model to account for this. This approach showed a good fit between observed and simulated plasma curve shape and was taken due to the unavailability of measured interaction kinetics of telithromycin with rat Mdr1a.

Intestinal metabolism of telithromycin was also incorporated into the rat PBPK model, where literature-retrieved K_m and V_{max} values were first attributed to Cyp3A, as metabolism of telithromycin within rat was determined to be largely mediated by this enzyme [350, 357]. This allowed a good fit for the plasma concentration profile to the observed values from the first *in vivo* study (step 1, see Table 13). However, for the second *in vivo* study (step 2, see Table 13), this resulted in a more than two-fold overestimation of the observed plasma concentration, therefore K_m and V_{max} values were transferred to lumped gut enzymes, as the reported values referred to intestinal microsomes and not a specific enzyme [357]. The gut expression levels of lumped enzymes were set to 0.25 across all gut compartments, based on results from a performed sensitivity analysis.

3.3.2.4 Population Simulation of Human Plasma Concentration-Time Profiles

The population simulator module in GastroPlus™ was used to estimate the plasma concentration in human subjects, where each subject was mimicked by a random combination of physiological and pharmacokinetic parameters (based on a log normal distribution). This allowed an estimation of the variation within a population. If the gender and range of age and weight were known for the individual clinical studies, these parameters were incorporated. Results showed the mean, minimal and maximal values as well as a 90 % confidence interval for C_{max}, t_{max} and $AUC_{0\text{-}t}$.

3.3.2.5 Simulation of ELF Concentration-Time Profiles

The PBPK models used to predict the ELF concentrations were based on parameters and conditions set when estimating the respective plasma concentration profiles (see 3.3.2.3).

Within GastroPlus™, the lung is not separated into the individual regions (i.e. trachea, bronchial, bronchiolar and alveolar compartment), but taken as a whole tissue compartment. There are different options to simulate total ELF concentrations within GastroPlus™, as shown below. All options consider lung-specific physiological parameters like pH of ELF, the ELF volume and the mucociliary clearance (MCL). The ELF volume and MCL rate are species-dependent and the pH of ELF was set to 6.69 across species [355]. All these parameters were maintained at default values.

Perfusion-Limited Model

If a compound is highly permeable, only the tissue blood flow/perfusion rate can limit its partition into the tissue. The compound concentration within the tissue is then estimated based on respective K_p. The compound concentration in ELF can then be calculated by using the ELF to unbound plasma partition coefficient ($K_{ELF/p,u}$) with the assumption of an instant partition of drug from lung tissue into ELF (see Figure 28). In this scenario, only passive diffusion processes are considered. This $K_{ELF/p,u}$ coefficient is predicted by GastroPlus™ from the chemical structure, based on a machine learning model that was trained with data from clinical studies [140, 355, 358]. This coefficient is consistent across species in GastroPlus™.

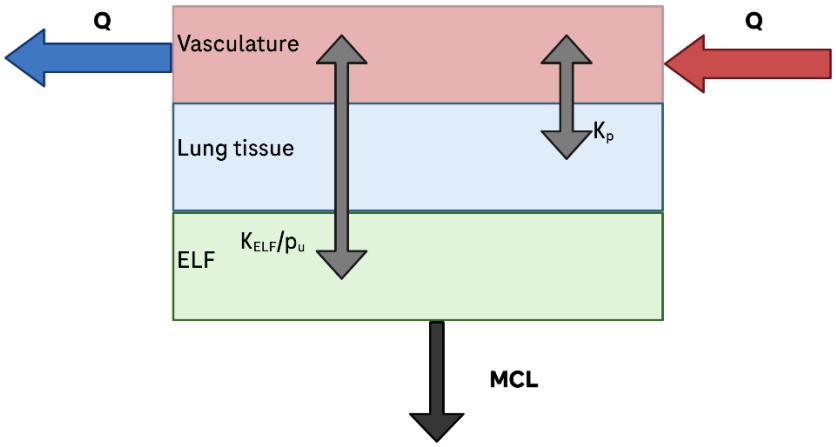

Figure 28. Lung perfusion-limited model in GastroPlus™. In this model, only the tissue blood flow (Q) can limit the distribution of a compound from the vasculature (plasma) into the tissue. The partition coefficient K_p represents the partition from plasma into tissue and $K_{ELF/P,u}$ the partition from plasma into the epithelial lining fluid (ELF). The mucociliary clearance (MCL) represents the removal of compound via the ELF flow. The schematic was adapted and simplified from the GastroPlus™ user manual [355]. Image was created with BioRender.com.

If the compounds' lung tissue partition is dependent on blood flow only (high permeable) but the partition from lung tissue into ELF is limited by a slow diffusion or the presence of a saturable drug transporter on the apical ELF-facing side of the lung epithelium, the above-mentioned perfusion model can be adapted accordingly, see Figure 29. The tissue concentration is still estimated based on calculated K_p. However, the partition from the tissue into the ELF is defined by an active transporter-mediated component (via the K_m and V_{max} of the drug interaction with the transporter) and/or a passive component defined by the apical permeability surface area product (Ap PStc). The software assumes that the passive permeability of a compound across the membrane is the same in all tissues, thus the passive diffusion needs to be corrected for the tissue surface area if scaling from one tissue to the others. By default, the liver passive diffusion clearance (CL_{diff}) was used to estimate tissue specific PStc values.

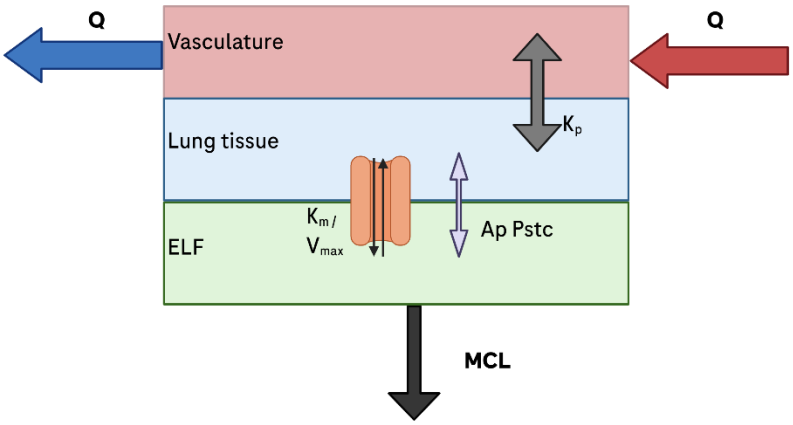

Figure 29. Lung perfusion-limited model in GastroPlus™ with a saturable clearance mechanism (i.e. Transporter protein) on the apical ELF facing side of the lung membrane. In this model, only the tissue blood flow (Q) can limit the distribution of compound from the vasculature (plasma) into the lung tissue. The partition coefficient K_p represents the partition from plasma into tissue. The partition from tissue into the epithelial lining fluid (ELF) is characterised via the active transporter clearance (either efflux or influx and defined with the Michaelis-Menten constant (K_m) and maximal velocity (V_{max})) and/or the passive diffusion across the apical membrane (Ap PStc). The mucociliary clearance (MCL) represents the removal of compound via the ELF flow. The schematic was adapted and simplified from the GastroPlus™ user manual [355]. The image was created with BioRender.com.

Permeability-Limited Model

For drugs that are poorly permeable the partition from the vasculature into the tissue is rate-limiting, the available tissue surface area and by the potential presence of active transport mechanisms. In the permeability-limited model, the model is extended by a fourth compartment, the extracellular space, whereas the tissue is referred to as intracellular space. The partition from vasculature (plasma) into the extracellular space is estimated via the K_p. The partition from the extracellular space into the intracellular one (tissue) is then limited by the presence of a saturable transporter (via K_m and V_{max}) on the basolateral side of the lung tissue (vasculature-facing side) and/or the passive diffusion that is defined by the basolateral permeability surface area (Ba PStc). The further partition form intracellular space into the ELF is defined via an active transporter mechanism (via K_m and V_{max}) and/or a passive component (Ap PStc), as shown in Figure 30.

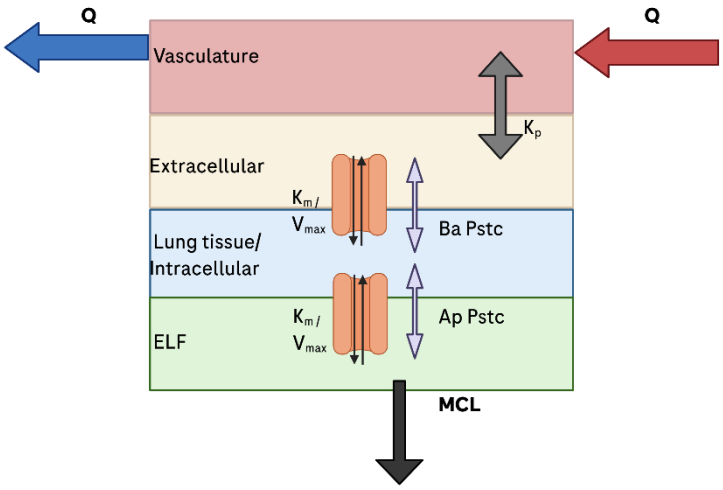

Figure 30. Lung permeability-limited model in GastroPlus™ with saturable clearance mechanisms (i.e. Transporter protein) on the apical and basolateral side of the lung membrane. The partition coefficient K_p represents the partition from plasma into the extracellular space. In this model, the distribution of drug from the vasculature (plasma) into the tissue is limited by tissue surface area, active transporter clearance (either efflux or influx and defined with the Michaelis-Menten constant (K_m) and maximal velocity (V_{max}) and/or the passive diffusion across the basolateral membrane (Ba PStc). The partition from tissue into ELF is then characterised via the active transporter clearance (either efflux or influx and defined with the Michaelis-Menten constant (K_m) and maximal velocity (V_{max})) and/or the passive diffusion across the apical membrane (Ap PStc). The mucociliary clearance (MCL) represents the removal of compound via the ELF flow. The schematic was adapted and simplified from the GastroPlus™ user manual [355]. The image was created with BioRender.com.

Since both moxifloxacin and telithromycin showed a moderate to high permeability *in vitro* (P_{app} > 50 nm/s), setting the lung tissue to the perfusion-limited model appeared reasonable. However, as antibiotics showed overall a reduced permeability across lung epithelial cells *in vitro* (see chapter 3.2), the simulations were also run with setting the lung tissue to a permeability-limited model to investigate if this has any impact on received simulations of ELF concentration-time profiles.

3.3.2.6 Incorporation of MDR1 Efflux into the Lung Tissue

In the default lung PBPK tissue within GastroPlus™, no transporter expression is defined. Since this study aimed to investigate the potential impact of MDR1 on ELF exposure of moxifloxacin and telithromycin, MDR1 expression levels were added manually. The transporter was defined as efflux transporter on the apical side (i.e. ELF-facing side). The transporter expression within GastroPlus™ is defined as 'transporter amount in mg per 1 g of tissue. The respective expression levels were estimated from available gene expression data in literature.

A study by Nishimura and colleagues measured the gene expression of MDR1 in a variety of human tissues. The expression levels of MDR1 within the human lung were approximately a tenth of those in the human kidney [193]. As the expression of MDR1 in the human kidney is defined as 1.80E-02 mg enzyme/g tissue within GastroPlus™, the MDR1 expression in the human lung tissue was assumed to be 1.80E-03 mg enzyme/g tissue.

In rodents, Mdr1 is defined by two isoforms Mdr1a and Mdr1b [121]. A study by Brady and colleagues reported that Mdr1b showed a roughly two-fold higher expression at gene level within the rat lung compared to Mdr1a [203]. GastroPlus™ does not differentiate between Mdr1a and Mdr1b expression. As the total Mdr1 in the rodent lung is roughly two-fold higher than the total Mdr1 expression within the rat kidney, this was taken as an estimate of rodent pulmonary Mdr1 expression [203]. In GastroPlus™, Mdr1 has a defined expression level of 1.10E-02 mg enzyme/g tissue within the rat kidney, thus lung Mdr1 expression was set to 2.20E-02 mg enzyme/g tissue.

The parameters describing the interaction of MDR1 with moxifloxacin and telithromycin (i.e. K_m and V_{max}) were taken from literature and are stated in supplemental table C3 & C4. No K_m and V_{max} were found for describing the interaction of both antibiotics with rat Mdr1, thus the human MDR1 kinetic values were taken as estimate for the simulations.

3.3.2.7 Parameter Sensitivity Analysis

The parameter sensitivity analysis (PSA) was used to assess a potential change in predicted ELF concentrations if critical input parameters are changed. This included $f_{u,plasma}$, $f_{u,sELF}$, PStc, MDR1 pulmonary expression levels, as well as K_m and V_{max} of reported interaction kinetics of moxifloxacin and telithromycin with MDR1.

These analyses allowed an assessment on which parameters are critical when predicting ELF concentration-time profiles and where an accurate experimental determination would be beneficial. This is of particular importance in this study, as many parameters were estimated due to the unavailability of experimentally derived data.

3.3.2.8 Visualisation

Graphics were visualised using the GraphPad Prism software (Version 10.4.1, GraphPad Software, La Jolla, CA, USA). Population simulation graphics were adapted and taken from GastroPlus™.

3.3.3 Results

3.3.3.1 Prediction of Plasma Concentration-Time Profiles (Model Validation step 1)

Moxifloxacin – Human

The plasma concentration-time profiles of moxifloxacin in human were simulated under both fasted and fed states after an oral single dose of 400 mg, as the antibiotic was given to both fasted and fed study subjects to examine a potential effect of food on absorption profiles. The simulated and measured plasma concentration-time profiles are shown in Figure 31.

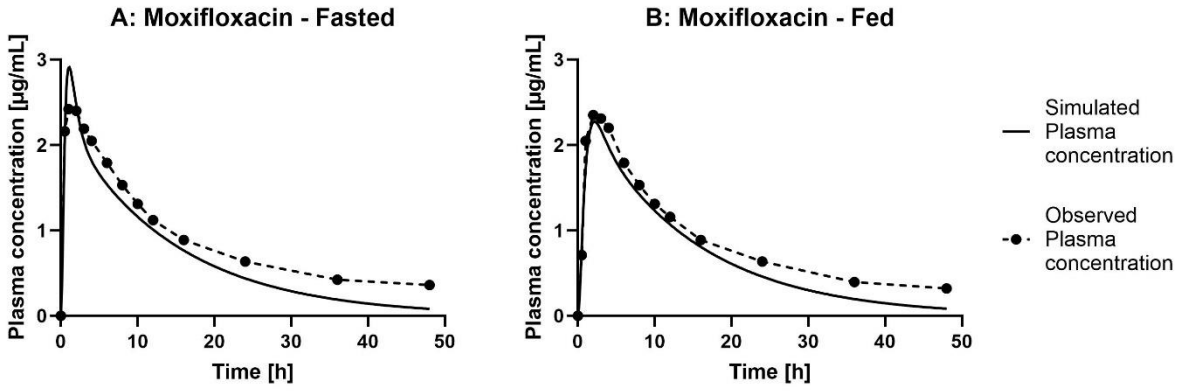

Figure 31. Simulated and observed plasma concentration-time profiles of **Moxifloxacin** in human after a single oral dose of 400 mg in fasted (A) or fed (B) state. The predicted plasma profiles are depicted as solid line (-) and observed profiles from clinical study [347] as dotted line with measured means as dots (--·--).

A good fit between the simulated and reported clinical plasma concentration profiles was observed for both fasted and fed condition. This was confirmed, when comparing pharmacokinetic parameters C_{max}, t_{max} and $AUC_{0\text{-}48h}$ between predicted and observed data which were within 1.15-fold of each other (Table 14).

Table 14. Overview of predicted and observed maximal plasma concentration (C_{max}), time of C_{max} (t_{max}) and area under the curve over the simulated time ($AUC_{0\text{-}48h}$) for **Moxifloxacin** when dosed at 400 mg as oral single dose in humans, either at fasted or fed state.

	Fasted		*Fed*	
Parameter	Predicted	Observed [347]	Predicted	Observed [347]
C_{max} [µg/mL]	2.93	2.80	2.27	2.50
t_{max} [h]	1.10	1.00	2.18	2.50
$AUC_{0\text{-}48h}$ [µg*h/mL]	32.9	36.6	32.8	35.3

As described in literature, the intake of food did not seem to have an impact on the absorption of Moxifloxacin as the absorption phase of plasma concentration-time profiles was similar at fasted and fed state [347].

The population simulation analysis showed that there are no significant differences between fasted and fed conditions, as the plasma concentration-time profiles were similar to each other. The only difference is a slightly higher predicted C_{max} at fasted and a delayed t_{max} at fed state, as shown in Figure 32.

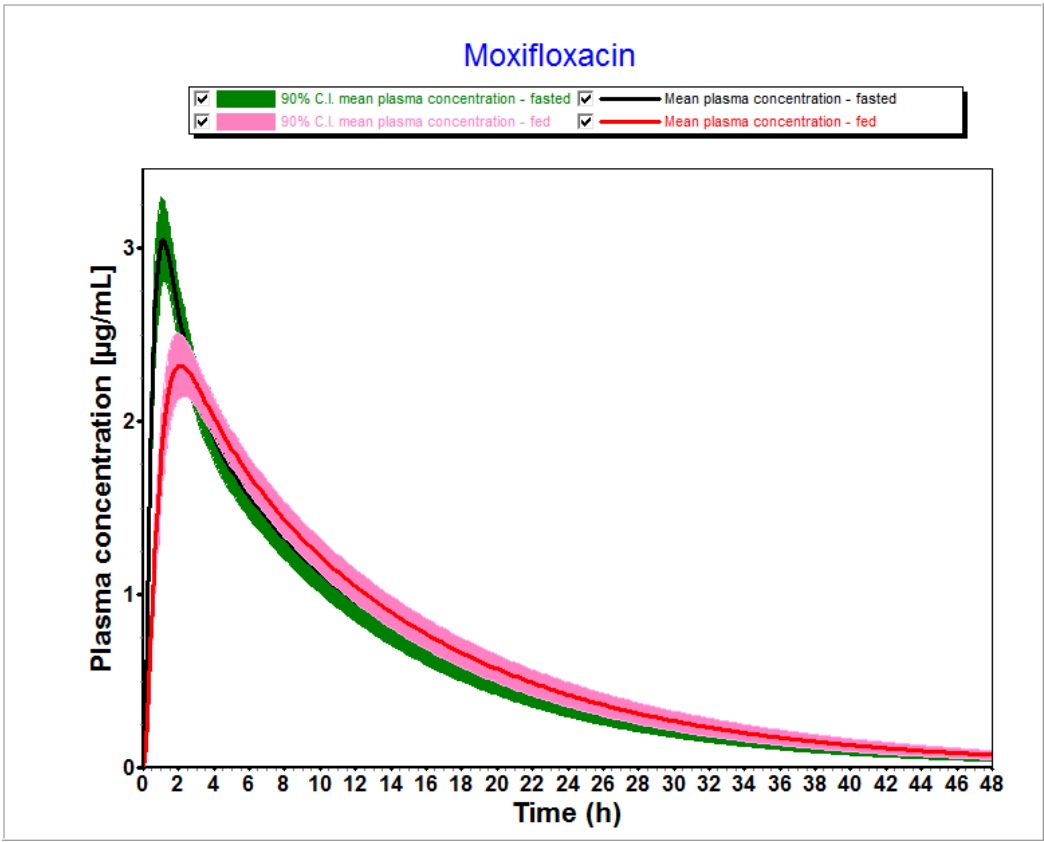

Figure 32. Predicted mean plasma concentration-time profile of **Moxifloxacin** in human after a single oral dose of 400 mg in fasted and fed condition, showing the 90 % confidence interval (CI), based on a virtual population trial with 18 individuals.

Table 15 summarises the predicted mean and the 90% confidence interval (CI) for C_{max}, t_{max} and $AUC_{0\text{-}48h}$. Clinically observed values, that are shown in Table 14, are either within or close to the threshold of the 90 % CI. Overall, this confirmed the good predictiveness of the established human PBPK model for moxifloxacin.

Table 15. Predicted mean and 90 % confidence interval (CI) of the maximal plasma concentration (C_{max}), time of C_{max} (t_{max}) and area under the curve over the simulated time ($AUC_{0\text{-}48h}$) for **Moxifloxacin** when dosed at 400 mg as oral single dose in fasted and fed condition using the virtual population simulation with 18 individuals.

	Fasted		*Fed*	
	Mean	90% CI	Mean	90% CI
C_{max} [µg/mL]	3.15	[2.86, 3.33]	2.41	[2.24, 2.58]
t_{max} [h]	1.17	[1.00, 1.26]	2.30	[1.98, 2.60]
$AUC_{0\text{-}48h}$ [µg*h/mL]	31.6	[27.5, 35.2]	32.1	[29.0, 35.2]

Moxifloxacin – Rat

The plasma concentration of moxifloxacin in rats was modelled after a single intravenous dose of 9.2 mg/kg. A good fit between the observed and predicted plasma exposure profiles was found, as shown in Figure 33.

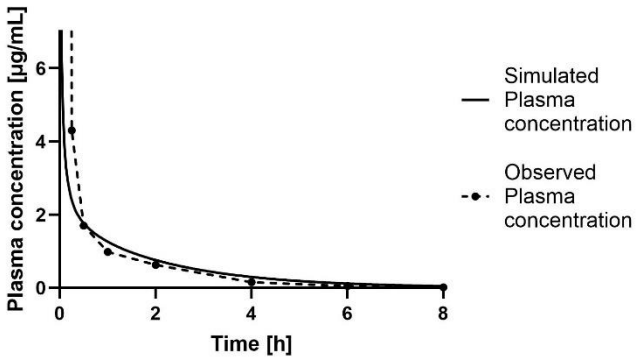

Figure 33. Simulated and observed plasma concentration-time profiles of **Moxifloxacin** in rats after a single intravenous dose of 9.2 mg/kg. The predicted plasma profiles are depicted as solid line (-) and observed profiles from the *in vivo* study [348] as dotted line with individual means as dots (--·--).

As moxifloxacin was administered via an intravenous injection to rats, the V_{ss} and the $t_{1/2}$ were considered more suitable to be compared than the C_{max} and t_{max} (as C_{max} and t_{max} would be achieved immediately after the injection due to an instant distribution, which cannot be adequately measured in an experimental setting). Therefore, the pharmacokinetic parameters V_{ss}, $t_{1/2}$ and $AUC_{0\text{-}8h}$ from the simulated and *in vivo* plasma concentration-time profile for moxifloxacin were compared. The results are depicted in Table 16. A good capture of the observed pharmacokinetic parameters was found using the established PBPK model.

Table 16. Overview of predicted and observed volume of distribution (V_{ss}), half-life ($t_{1/2}$) and area under the curve over the simulated time ($AUC_{0\text{-}8h}$) for **Moxifloxacin** when dosed at 9.2 mg/kg by an intravenous bolus in rats.

Parameter	Predicted	Observed [348]
V_{ss} [L/kg]	2.2	2.0
$T_{1/2}$ [h]	1.2	1.2
$AUC_{0\text{-}8h}$ [µg*h/mL]	5.46	3.61[a]

[a] Values were reported normalised to dose in literature and were back calculated in this table to a dose-independent value to allow a direct comparison to the simulated data.

Telithromycin – Human

The plasma concentration-time profile of Telithromycin was simulated after a single oral dose of 800 mg to healthy participants, in both fasted and fed state and compared to clinical data [349], as shown in Figure 34.

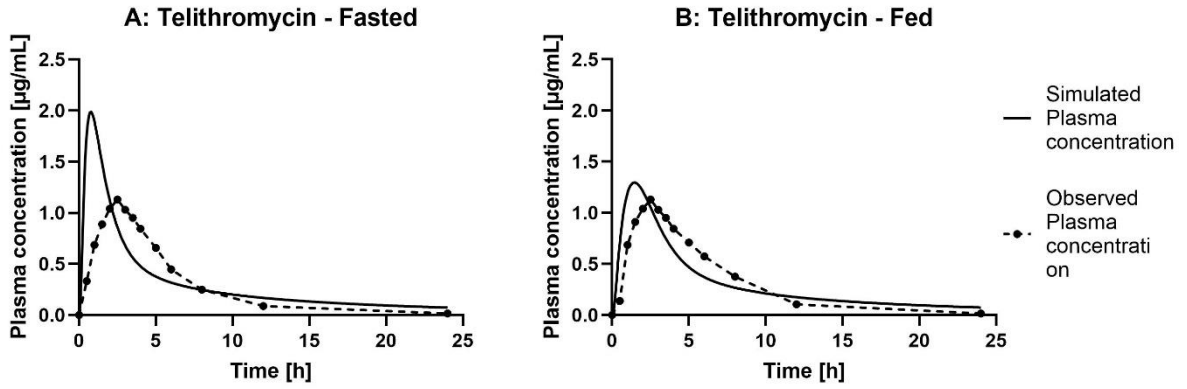

Figure 34. Simulated and observed plasma concentration-time profiles of **Telithromycin** in human after a single oral dose of 800 mg in fasted (A) or fed (B) state. The predicted plasma profiles are depicted as solid line (-) and observed profiles from clinical studies [349] as dotted line with measured means as dots (--·--).

The fasted predicted plasma profile shows an almost two-fold higher C_{max} and a more than two-fold earlier t_{max} compared to the observed one. However, if taking the standard deviation/range of reported clinical data into account (see Table 17), both predicted values are within a reasonable range. The plasma profile predicted for the fed condition showed a good fit to the observed one.

Table 17. Overview of predicted and observed maximal plasma concentration (C_{max}), time of C_{max} (t_{max}) and area under the curve over the simulated time ($AUC_{0\text{-}24h}$) for **Telithromycin** when dosed at 800 mg as oral single dose in humans, either at fasted or fed state. Observed C_{max} and $AUC_{0\text{-}24h}$ are shown as mean ± SD, whereas for observed t_{max}, the median and range is shown.

	Fasted		*Fed*	
Parameter	Predicted	Observed [349]	Predicted	Observed [349]
C_{max} [µg/mL]	1.99	1.44 ± 0.73	1.30	1.46 ± 0.77
t_{max} [h]	0.8	2.50 [1.0 – 5.0]	1.44	2.25 [1.0 – 6.0]
$AUC_{0\text{-}24h}$ [µg*h/mL]	7.81	6.69 ± 2.91	7.564	7.32 ± 3.00

A virtual population simulation was run for telithromycin with fasted and fed state and revealed minor differences between the two conditions. In fasted humans, an earlier t_{max} and a higher C_{max} was observed compared to fed individuals (see Figure 35). However, the elimination profiles showed a good overlay.

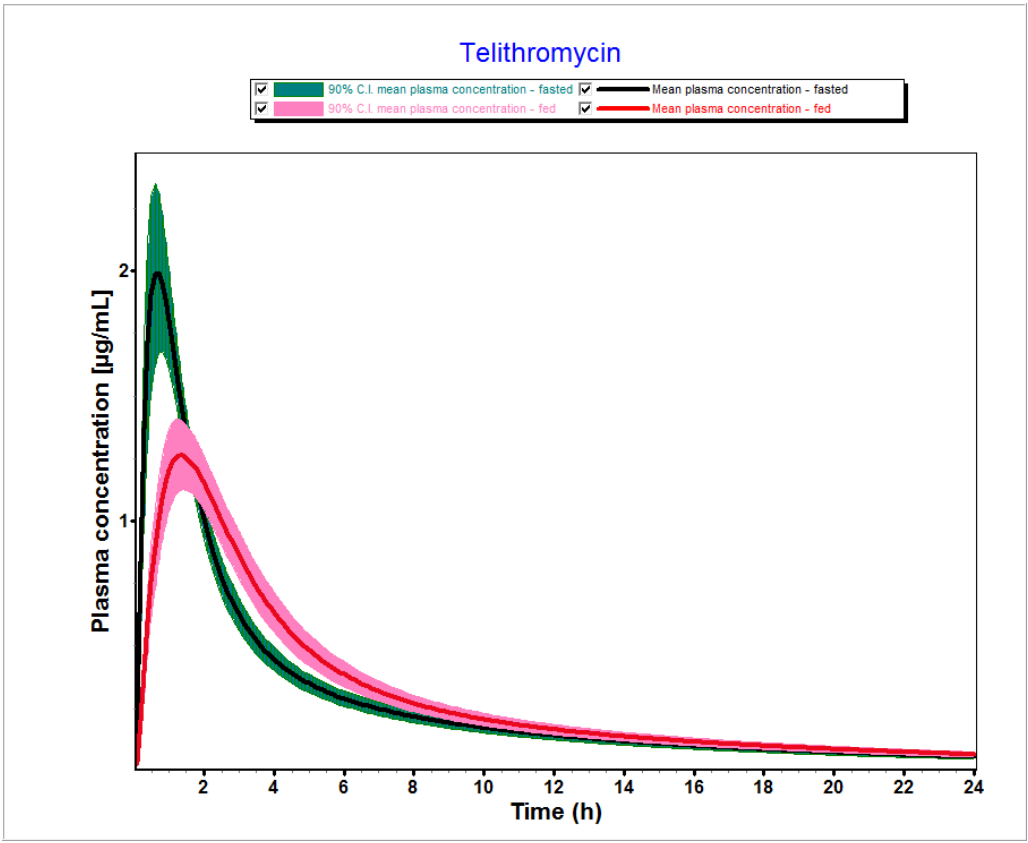

Figure 35. Predicted mean plasma concentration-time profile of **Telithromycin** in human after a single oral dose of 800 mg in fasted and fed condition, showing the 90 % confidence interval (CI), based on a virtual population trial with 18 individuals.

The predicted mean and the 90% confidence interval for C_{max}, t_{max} and $AUC_{0\text{-}24h}$ that were simulated for Telithromycin are summarised in Table 18. Comparing these values to those reported ones of the clinical study (as shown in Table 17), observed mean values are within or close to the 90% CI, if taking the subject variability into account.

Table 18. Predicted mean and 90 % confidence interval (CI) of the maximal plasma concentration (C_{max}), time of C_{max} (t_{max}) and area under the curve over the simulated time ($AUC_{0\text{-}24h}$) for **Telithromycin** when dosed at 800 mg as oral single dose in fasted and fed condition using the virtual population simulation with 18 individuals.

	Fasted		*Fed*	
	Mean	90% CI	Mean	90% CI
C_{max} [µg/mL]	2.12	[1.78, 2.47]	1.32	[1.18, 1.46]
t_{max} [h]	0.783	[0.684, 0.882]	1.51	[1.32, 1.69]
$AUC_{0\text{-}24h}$ [µg*h/mL]	7.18	[6.49, 7.87]	7.41	[6.71, 8.10]

Telithromycin – Rat

The telithromycin plasma concentration-time profile in rats was simulated after a single oral dose of 50 mg/kg and plotted against observed *in vivo* values, as depicted in Figure 36.

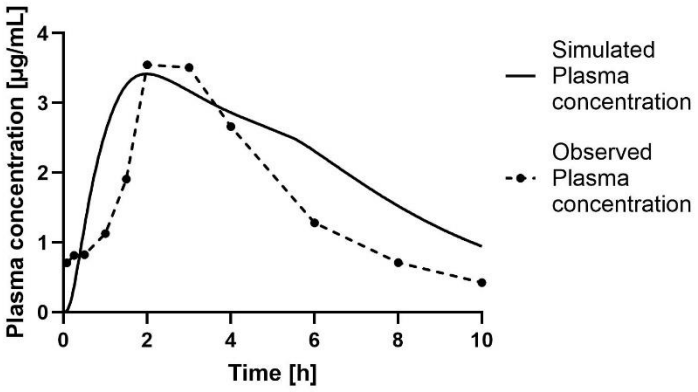

Figure 36. Simulated and observed plasma concentration-time profiles of **Telithromycin** in rats after a single oral dose of 50 mg/kg. The predicted plasma profiles are depicted as solid line (-) and observed profiles from the *in vivo* study [350] as dotted line with measured means as dots (--·--).

Overall, the simulated plasma concentration-time profile looked reasonable to the observed one, with the elimination clearance being slightly underestimated, resulting in a slightly higher predicted $AUC_{0\text{-}10h}$ (as shown in Table 19). The absorption processes are captured well, as both C_{max} and t_{max} are close to the observed values.

Table 19. Overview of predicted and observed maximal plasma concentration (C_{max}), time of C_{max} (t_{max}) and area under the curve over the simulated time ($AUC_{0\text{-}8h}$) for **Telithromycin** when dosed at 50 mg/kg by a single oral dose in rats. Observed C_{max} and $AUC_{0\text{-}10h}$ are shown as mean ± SD, whereas for observed t_{max} the median and range is shown.

Parameter	Predicted	Observed [350]
C_{max} [µg/mL]	3.42	3.73 ± 1.23
t_{max} [h]	2.0	2.5 [2.0 – 3.0]
$AUC_{0\text{-}10h}$ [µg*h/mL]	22.6	16.4

3.3.3.2 Prediction of Plasma Concentration-Time Profiles (Model Validation Step 2)

Before estimating the ELF concentration profiles, the plasma concentration-time profiles of the respective studies were simulated first and compared to observed data to validate the PBPK models performance.

Moxifloxacin – Human

Moxifloxacin was given as a single oral dose of 400 mg to patients undergoing a bronchoscopy, [351]. No information was provided regarding the intake of food, thus both fasted and fed conditions were modelled, as shown in Figure 37. Furthermore, no average age of study participants was reported.

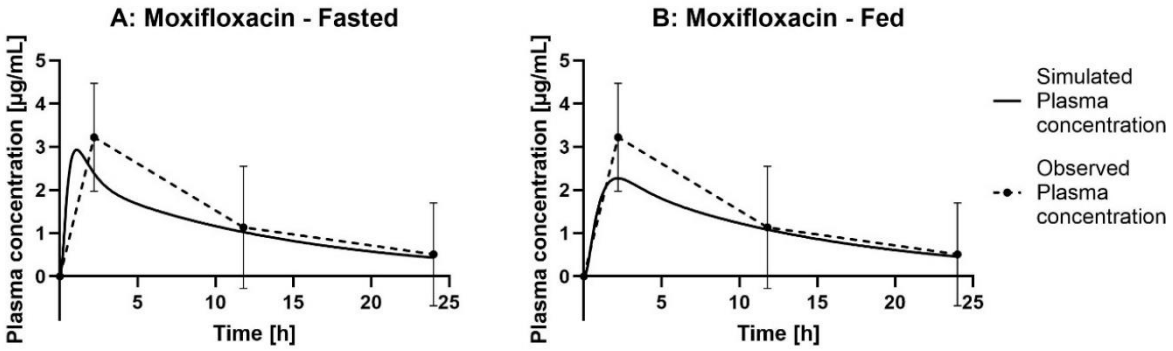

Figure 37. Simulated and observed plasma concentration-time profiles of **Moxifloxacin** in human after a single oral dose of 400 mg in fasted (A) or fed (B) state. The predicted plasma profiles are depicted as solid line (-) and observed profiles from clinical studies [351] as dotted line with measured means ± SD as dots (--·--).

The elimination profiles of moxifloxacin were nicely captured in both fasted and fed condition, whereas the predicted t_{max} in fasted state is slightly underestimated, as well as the C_{max} in fed state. However, the predicted $AUC_{0\text{-}24h}$ is within ~1.3-fold of the observed value (see Table 20).

Table 20. Overview of predicted and observed maximal plasma concentration (C_{max}), time of C_{max} (t_{max}) and area under the curve over the simulated time ($AUC_{0\text{-}24h}$) for **Moxifloxacin** when dosed at 400 mg as oral single dose in humans, either at fasted or fed state.

Parameter	Predicted		Observed *[351]*
Condition	Fasted	Fed	-[a]
C_{max} [µg/mL]	2.93	2.27	3.22[b]
T_{max} [h]	1.12	2.16	2.2[b]
$AUC_{0\text{-}24h}$ [µg*h/mL]	27.9	27.5	36.5

[a] In the clinical study, there is no information provided whether patients were fasted or fed.

[b] No values for C_{max}, t_{max} and $AUC_{0\text{-}24h}$ were reported in this study. Therefore, predicted values from GastroPlus™ based on the clinical data is reported.

In the second clinical study, moxifloxacin was administered orally at 400 mg QD x 5 days to patients undergoing diagnostic bronchoscopy. The patients were fasted six hours before bronchoscopy [352]. However, both fasted and fed condition was simulated. The graphs are shown in Figure 38.

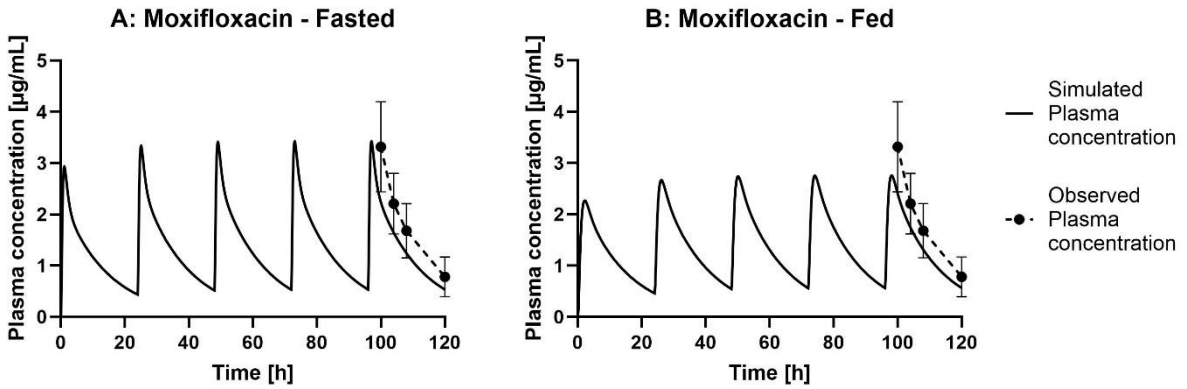

Figure 38. Simulated and observed plasma concentration-time profiles of **Moxifloxacin** in human after multiple oral doses of 400 mg (q24h x 5 doses) in fasted (A) or fed (B) state. The predicted plasma profiles are depicted as solid line (-) and observed profiles from clinical studies [352] as dotted line with measured means ± SD as dots (--·--).

The simulated total plasma concentrations reasonably captured the observed values, being within the standard deviation of the individual sampling points. The elimination profiles showed a good fit to the observed ones. If taking the $AUC_{0\text{-}120h}$ into account, both fasted and fed predictions are within 1.3-fold of the observed clinical data (see Table 21).

Table 21. Overview of predicted and observed maximal plasma concentration (C_{max}), time of C_{max} (t_{max}) and area under the curve over the simulated time ($AUC_{0\text{-}120h}$) for **Moxifloxacin** when dosed at 400 mg as oral multiple dose in humans (q24h x 5 doses), either at fasted or fed state.

Parameter	Predicted		Observed [352]
Condition	Fasted	Fed	Fasted
C_{max} [µg/mL]	3.42	2.76	3.23[a]
T_{max} [h]	97.1	98.1	100[a]
$AUC_{0\text{-}120h}$ [µg*h/mL]	162.61	162.13	205

[a] No values for C_{max} and t_{max} were reported in this study. Therefore, predicted values from GastroPlus™ based on the clinical data is reported.

As the patients average age was 67 years, the parameters C_{max}, t_{max} and $AUC_{0\text{-}120h}$ were estimated for the elderly population and values can be found in Table 22. Predicted values were similar to those predicted for the default 30 years old population (see Table 21).

Table 22. Overview of predicted and observed maximal plasma concentration (C_{max}), time of C_{max} (t_{max}) and area under the curve over the simulated time ($AUC_{0\text{-}120h}$) for **Moxifloxacin** when dosed at 400 mg as oral multiple dose in humans (q24h x 5 doses), either at fasted or fed state. The population age in PBPK model was set to 67 to mimic the average age of study participants.

Parameter	Predicted		Observed [352]
Condition	Fasted	Fed	Fasted
C_{max} [µg/mL]	3.35	2.69	3.23[a]
T_{max} [h]	97.1	98.1	100[a]
$AUC_{0\text{-}120h}$ [µg*h/mL]	159.1	158.63	205

[a] No values for C_{max} and t_{max} were reported in this study. Therefore, predicted values from GastroPlus™ based on the clinical data is reported.

Moxifloxacin – Rat

The rat PBPK model's predictiveness for moxifloxacin was further evaluated by simulating the plasma concentration-time profile after a single i.v. bolus of 5 mg/kg to rats [297], as depicted in Figure 39.

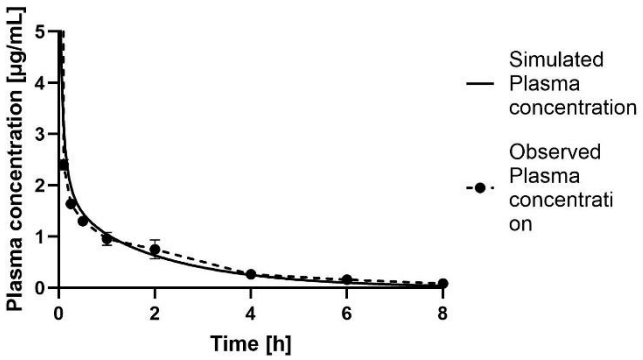

Figure 39. Simulated and observed plasma concentration-time profiles of **Moxifloxacin** in rats after a single i.v. dose of 5 mg/kg. The predicted plasma profiles are depicted as solid line (-) and observed profiles from the *in vivo* study [297] as dotted line with measured means ± SD as dots (--·--).

A good fit of the simulated and observed plasma concentration-time profiles was observed, with the individual derived pharmacokinetic parameters shown in Table 23.

In summary, the established PBPK models for moxifloxacin in both human and rat showed a good prediction of the observed plasma concentration-time profiles from several studies and can thus be used as basis for estimating the respective ELF concentration-time profiles.

Table 23. Overview of predicted and observed volume of distribution (V_{ss}), half-life ($t_{1/2}$) and area under the curve over the simulated time (AUC_{0-8h}) for Moxifloxacin when dosed at 5 mg/kg by an intravenous bolus in rats.

Parameter	Predicted	Observed [297]
V_{ss} [L/kg]	2.2	1.2
$T_{1/2}$ [h]	1.2	-[a]
AUC_{0-8h} [µg*h/mL]	4.50	4.04[b]

[a] No value for $t_{1/2}$ was reported in the respective in vivo study.

[b] No values for the AUC_{0-8h} were reported in the respective *in vivo* study. Therefore, predicted values from GastroPlus™ based on the *in vivo* data is reported for the AUC_{0-8h}.

Telithromycin – Human

The sparse plasma concentration-time profiles of telithromycin were simulated and compared to those of patients undergoing bronchoscopy who took multiple oral doses of each 800 mg QD for 5 days. No information was provided whether the patients were fasted or fed during the drug intake and further no average age was reported [353]. The respective simulations are shown in Figure 40.

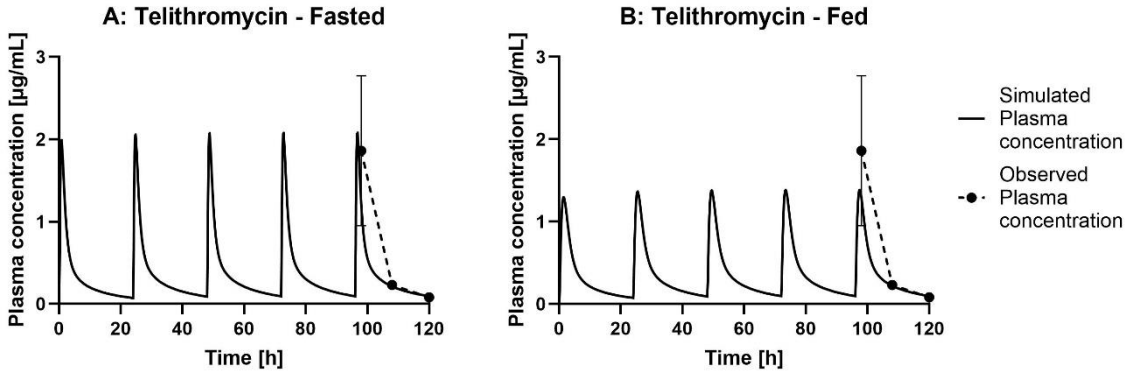

Figure 40. Simulated and observed plasma concentration-time profiles of **Telithromycin** in human after multiple oral doses of 800 mg (q24h x 5 doses) in fasted (A) or fed (B) state. The predicted plasma profiles are depicted as solid line (-) and observed profiles from clinical studies [353] as dotted line with measured means ± SD as dots (--·--).

A good fit was observed for the fasted and fed condition, if accounting for the standard deviation of the clinical data. The respective values for C_{max}, t_{max} and AUC_{0-120h} are shown in Table 24.

Table 24. Overview of predicted and observed maximal plasma concentration (C_{max}), time of C_{max} (t_{max}) and area under the curve over the simulated time ($AUC_{0\text{-}120h}$) for **Telithromycin** when dosed at 800 mg as oral multiple dose in humans q24h x 5 doses), either at fasted or fed state.

Parameter	Predicted		Observed [353]
Condition	Fasted	Fed	-[a]
C_{max} [µg/mL]	2.08	1.38	1.86[b]
T_{max} [h]	96.8	97.4	98.0[b]
$AUC_{0\text{-}120h}$ [µg*h/mL]	43.5	42.2	104[b]

[a] In the clinical study, there is no information provided whether patients were fasted or fed.

[b] No values for C_{max}, t_{max} and $AUC_{0\text{-}120h}$ were reported in this study. Therefore, predicted values from GastroPlus™ based on the clinical data are reported.

In the second clinical study, telithromycin was administered at multiple oral doses of 800 mg (5 times every 24 h) to patients undergoing bronchoscopy. Patients were asked to be fasted 6 hours before the bronchoscopy. The average participant age was 65 years [354]. The respective graphs are shown in Figure 41 and values for C_{max}, t_{max} and $AUC_{0\text{-}120h}$ in Table 25.

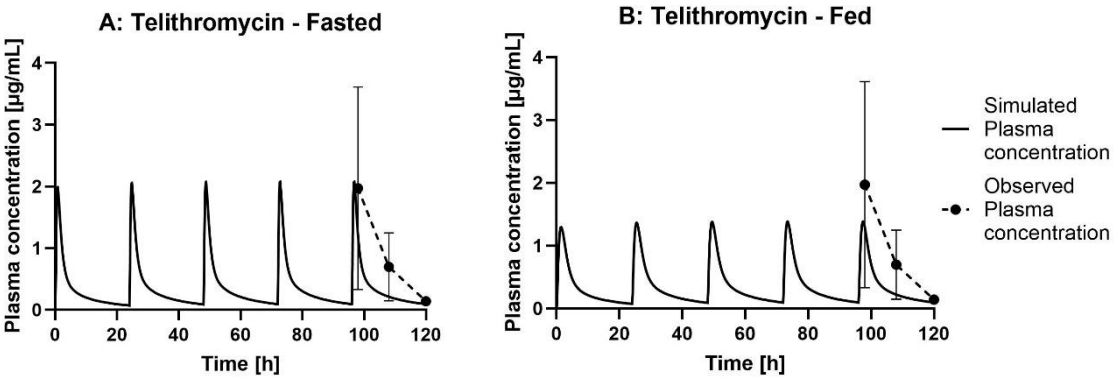

Figure 41. Simulated and observed plasma concentration-time profiles of **Telithromycin** in human after multiple oral doses of 800 mg (q24h x 5 doses) in fasted (A) or fed (B) state. The predicted plasma profiles are depicted as solid line (-) and observed profiles from clinical studies [354] as dotted line with measured means ± SD as dots (--·--).

The simulated profiles of fasted and fed condition showed a reasonable fit of the observed plasma concentration-time profiles if accounting for the reported standard deviation. The elimination was slightly overestimated if comparing to clinically reported means, however due to the sparse data available, this is difficult to ascertain as a real difference.

Table 25. Overview of predicted and observed maximal plasma concentration (C_{max}), time of C_{max} (t_{max}) and area under the curve over the simulated time ($AUC_{96\text{-}120h}$) for **Telithromycin** when dosed at 800 mg as oral multiple dose in humans (q24h x 5 doses) [354], either at fasted or fed state.

Parameter	Predicted		Observed [354]
Condition	Fasted	Fed	Fasted
C_{max} [µg/mL]	2.08	1.38	1.97[a]
T_{max} [h]	96.8	97.4	98.0[a]
$AUC_{96\text{-}120h}$[b] [µg*h/mL]	9.0	8.8	15.0[b]

[a] No values for C_{max} and t_{max} were reported in this study. Therefore, predicted values from GastroPlus™ based on the clinical data are reported.

[b] The reported AUC was accounting for the plasma exposure within 24 h after the fifth dose. Therefore, the predicted AUC capturing the plasma profile within this time period was calculated (i.e. starting at 96 h after the initial dose $AUC_{96\text{-}120h}$)

As the average age of the study participants was 65 years, the PBPK model was adapted accordingly and simulated values for C_{max}, t_{max} and $AUC_{0\text{-}120h}$ in this elderly population are depicted in Table 26. The values were similar to those obtained when using the 30-year old population PBPK model (see Table 25).

Table 26. Overview of predicted and observed maximal plasma concentration (C_{max}), time of C_{max} (t_{max}) and area under the curve over the simulated time ($AUC_{96\text{-}120h}$) for **Telithromycin** when dosed at 800 mg as oral multiple dose in humans (q24h x 5 doses) [354], either at fasted or fed state. The average age of the PBPK model was set to 65 years to mimic average of study subjects.

Parameter	Predicted		Observed [354]
Condition	Fasted	Fed	Fasted
C_{max} [µg/mL]	1.99	1.38	1.97[a]
T_{max} [h]	96.8	97.4	98.0[a]
$AUC_{96\text{-}120h}$[b] [µg*h/mL]	8.9	8.7	15.0[b]

[a] No values for C_{max} and t_{max} were reported in this study. Therefore, predicted values from GastroPlus™ based on the clinical data are reported.

[b] The reported AUC was accounting for the plasma exposure within 24 h after the fifth dose. Therefore, the predicted AUC capturing the plasma profile within this time period was calculated (i.e. starting at 96 h after the initial dose $AUC_{96\text{-}120h}$)

Telithromycin – Rat

The plasma concentration-time of telithromycin was simulated in rats receiving an oral single dose of 50 mg/kg [289]. The observed and simulated plasma concentration-time profiles are shown in Figure 42.

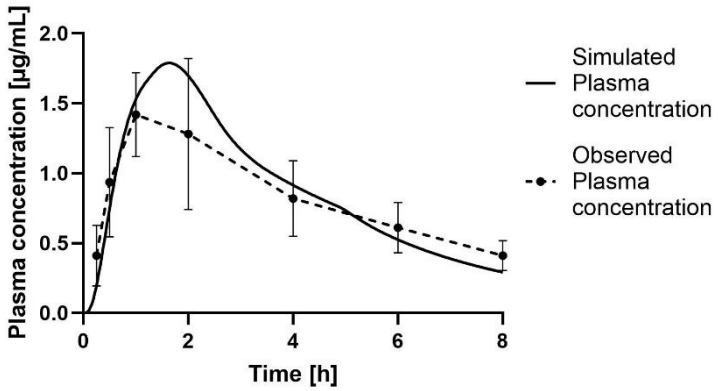

Figure 42. Simulated and observed plasma concentration-time profiles of **Telithromycin** in rats after a single oral dose of 50 mg/kg. The predicted plasma profiles are depicted as solid line (-) and observed profiles from the *in vivo* study [289] as dotted line with measured means ± SD as dots (--·--).

Overall, a good fit between the observed and simulated plasma concentration-time profile was seen. This is also reflected in simulated and observed values for C_{max}, t_{max} and $AUC_{0\text{-}8h}$ as shown in Table 27.

Table 27. Overview of predicted and observed maximal plasma concentration (C_{max}), time of C_{max} (t_{max}) and area under the curve over the simulated time ($AUC_{0\text{-}8h}$) for **Telithromycin** when dosed at 50 mg/kg by a single oral dose in rats.

Parameter	Predicted	Observed [289]
C_{max} [µg/mL]	1.79	1.42
T_{max} [h]	1.65	1.00
$AUC_{0\text{-}8h}$ [µg*h/mL]	7.80	6.68

The established PBPK models show a good prediction of telithromycin's plasma concentration-time profiles in human and rat and can thus be used to model the respective ELF concentrations.

3.3.3.3 Prediction of Moxifloxacin and Telithromycin Concentrations in ELF (Step 3) and Parameter Sensitivity Analysis (PSA)

The established PBPK models were used to estimate total ELF concentration-time profiles of both moxifloxacin and telithromycin in human and rat. For modelling the ELF concentration in humans, the fasted condition was chosen, since a good fit was observed for both moxifloxacin and telithromycin (see 3.3.3.2) and patients were typically fasted six hours or more before bronchoscopy and bronchoalveolar lavage (BAL) collection. Rat PBPK models were set to fed condition due to food ad libitum in *in vivo* studies [359]. Each one clinical study and one *in vivo* study for moxifloxacin and telithromycin will be presented in the following chapter and their observed data will be compared to simulated ELF profiles. For each one additional clinical study, the observed ELF concentration-time profiles of moxifloxacin and telithromycin were compared to the profiles from the simulation, which can be found in the supplement (Figures C1 – C5). The obtained results are similar to those, described for the clinical studies within this chapter. Given the complexity of obtaining ELF samples, only a sparse amount of observed data points is available.

Lung Perfusion-limited Model – Simulation of ELF Concentration based on ELF-to-free Plasma Partition Coefficient ($K_{ELF/p,u}$)

In the perfusion-limited model, the partition into the lung tissue is limited by the blood flow only and an instant partition from the tissue into the ELF is assumed. The lung partition is characterised by the $K_{ELF/p,u}$ (coefficient of partition between ELF and free plasma).

Figure 43 shows the prediction of ELF concentration-time profile of moxifloxacin in human and rat using the perfusion-limited model based on $K_{ELF/p,u}$.

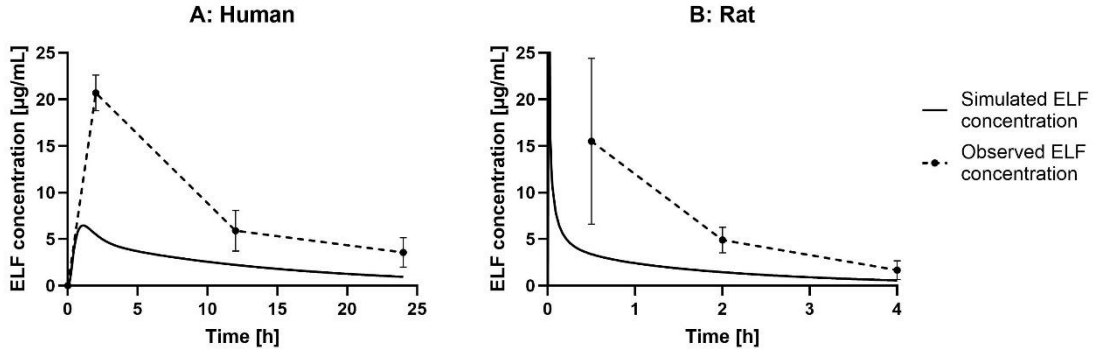

Figure 43. Simulated and observed ELF concentration-time profile of **Moxifloxacin** in human (A) and rat (B) using the perfusion-limited model on the basis of the ELF over unbound plasma partition coefficient ($K_{ELF/p,u}$). Moxifloxacin was given as single oral dose of 400 mg to human and as single i.v. bolus of 5mg/kg to rats [297, 347]. The predicted ELF profiles are depicted as solid line (-) and observed profiles are shown as dotted line with measured means ± SD as dots (--·--).

For both human and mouse, there was a more than three-fold underestimation of the observed total ELF concentration.

Figure 44 shows the results of the ELF concentration-time profile simulation of telithromycin using the perfusion limited model, based on $K_{ELF/p,u}$. For human, a similar observation was made as for moxifloxacin that the total ELF concentration was more than three-fold underpredicted, however the simulated profile is within or close to the standard deviation of the observed data. Interestingly, the opposite was observed for rat, where a more than two-fold higher ELF concentration-time profile was predicted compared to the observed *in vivo* data.

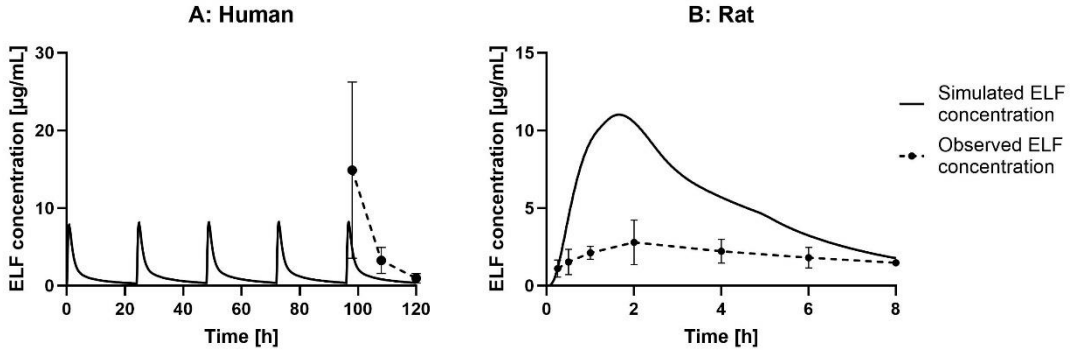

Figure 44. Simulated and observed ELF concentration-time profile of **Telithromycin** in human (A) and rat (B) using the perfusion-limited model on the basis of the ELF over unbound plasma partition coefficient ($K_{ELF/p,u}$). Telithromycin was given as a multiple oral dose of 800 mg to human (q24h x 5 doses) and as single oral dose of 50 mg/kg to rats [289, 353]. The predicted ELF profiles are depicted as solid line (-) and observed profiles are shown as dotted line with measured means ± SD as dots (--·--).

A parameter sensitivity analysis (PSA) was performed to investigate how the predicted ELF concentration-time profiles would change if the $K_{ELF/p,u}$ or the $f_{u,plasma}$ would vary, as the ELF prediction using the perfusion-limited model in this setting mainly relies on these two parameters. The results are shown in Figures 45 - 48. The $K_{ELF/p,u}$ is considered consistent across species, whereas the $f_{u,plasma}$ is species-dependent [355]

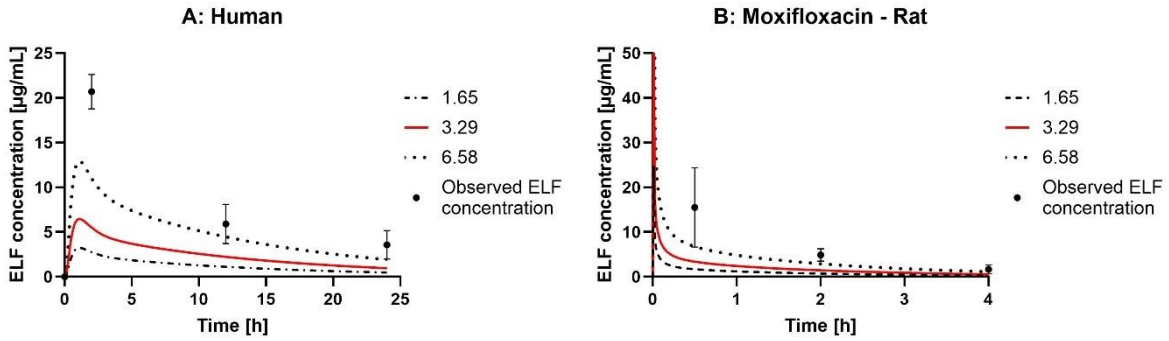

Figure 45. Parameter sensitivity analysis (PSA) of the predicted ELF concentration-time profiles of **Moxifloxacin** in human (A) and rat (B) if changing the ELF over unbound plasma partition coefficient ($K_{ELF/p,u}$) and using the perfusion-limited model. The simulated ELF concentration profile using the estimated $K_{ELF/p,u}$ by GastroPlus™ is shown a solid red line, with a two-fold lower $K_{ELF/p,u}$ as dashed line (---) and with a two-fold higher $K_{ELF/p,u}$ as dotted line (⋯). Observed ELF concentrations are shown as measured means ± SD as dots (·) [297, 347].

The data from the PSA analysis when changing the $K_{ELF/p,u}$ for moxifloxacin showed that modifying this parameter had a significant impact on simulated ELF concentration-time profiles (Figure 45). Doubling the $K_{ELF/p,u}$ led to a two-fold increase of simulated ELF concentration in both rat and human. This was expected as in this scenario, as the partition from the plasma into the ELF is defined only by $K_{ELF/p,u}$ and thus if changing $K_{ELF/p,u}$ by x-fold, the simulated ELF concentration will increase by x-fold if the $f_{u,plasma}$ remains constant.

For telithromycin, the ELF concentration profile in human was well captured, when the predicted $K_{ELF/p,u}$, was increased by two-fold. Whereas in rat, a reasonable simulated ELF profile was found when lowering the predicted $K_{ELF/p,u}$ by two-fold (Figure 46).

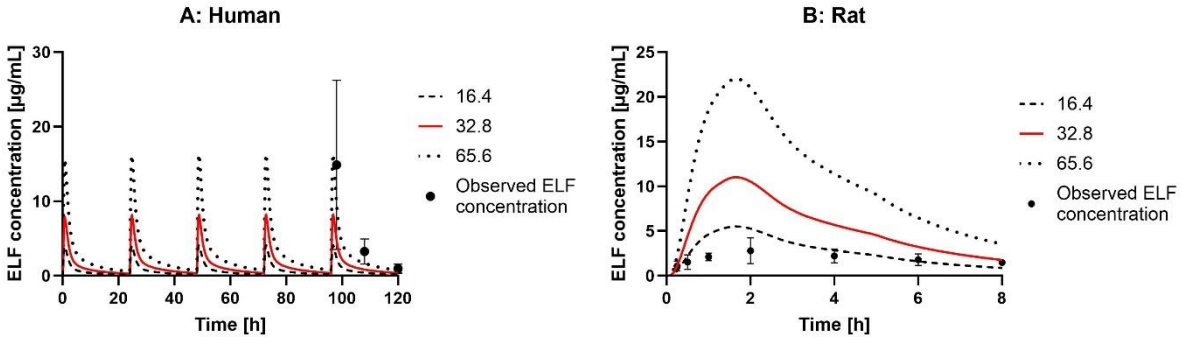

Figure 46. Parameter sensitivity analysis (PSA) of the predicted ELF concentration-time profiles of **Telithromycin** in human (A) and rat (B) if changing the ELF over unbound plasma partition coefficient ($K_{ELF/p,u}$) and using the perfusion-limited model. The simulated ELF concentration profile using the estimated $K_{ELF/p,u}$ by GastroPlus™ is shown a solid red line, with a two-fold lower $K_{ELF/p,u}$ as dashed line (---) and with a two-fold higher $K_{ELF/p,u}$ as dotted line (⋯). Observed ELF concentrations are shown as measured means ± SD as dots (·) [289, 353].

When using the $f_{u,plasma}$ as parameter in the PSA, a 10-fold lower value (of the experimentally derived $f_{u,plasma}$) was taken and the maximal unbound fraction possible, 100 %.

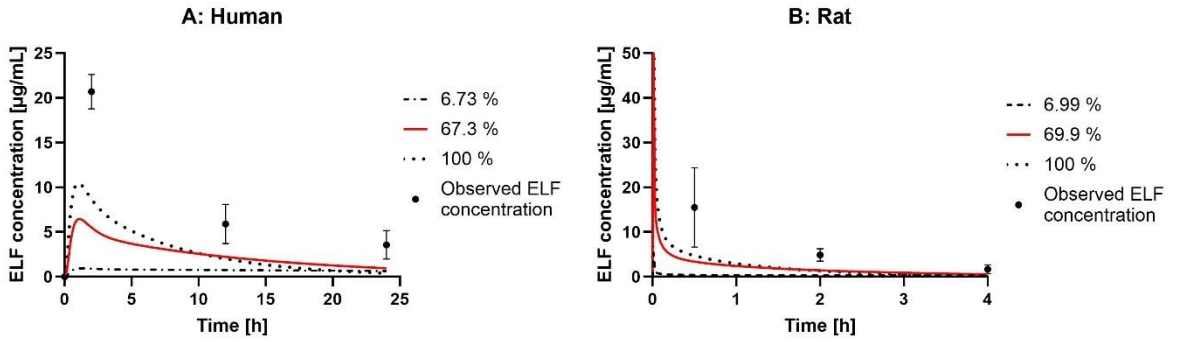

Figure 47. Parameter sensitivity analysis (PSA) of the predicted ELF concentration-time profiles of **Moxifloxacin** in human (A) and rat (B) if changing the unbound plasma fraction ($f_{u,plasma}$) and using the perfusion-limited model. The simulated ELF concentration profile using the experimental $f_{u,plasma}$ is shown a solid red line, with a 10-fold lower $f_{u,plasma}$ as dashed line (---) and with the maximal $f_{u,plasma}$ as dotted line (⋯). The entered value for $f_{u,plasma}$ was corrected for plasma lipid binding in GastroPlus™ by accounting for moxifloxacin's lipophilicity. Observed ELF concentrations are shown as measured means ± SD as dots (·) [297, 347].

As seen in Figures 47 and 48, only for moxifloxacin in human, an around two-fold increase in predicted ELF concentration was observed, when increasing $f_{u,plasma}$ to its maximal value of

100 %. In contrast, the 10-fold reduction of experimental derived $f_{u,plasma}$ resulted in negligible ELF concentration for moxifloxacin in human and rat, and an around two-fold reduced ELF concentration of telithromycin in human and rat.

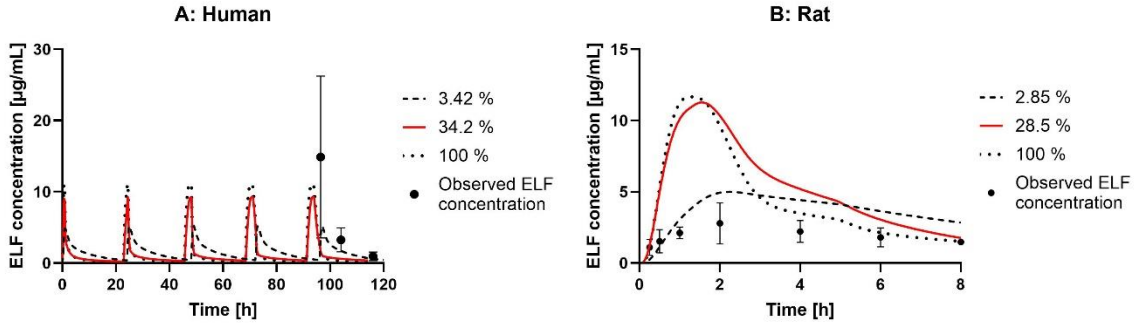

Figure 48. Parameter sensitivity analysis (PSA) of the predicted ELF concentration-time profiles of **Telithromycin** in human (A) and rat (B) if changing the unbound plasma fraction ($f_{u,plasma}$) and using the perfusion-limited model. The simulated ELF concentration using the experimental $f_{u,plasma}$ is shown a solid red line, with a 10-fold lower f $f_{u,plasma}$ as dashed line (---) and with the maximal $f_{u,plasma}$ as dotted line (⋯). The entered value for $f_{u,plasma}$ was corrected for plasma lipid binding in GastroPlus™ by accounting for telithromycin's lipophilicity. Observed ELF concentrations are shown as measured means ± SD as dots (·) [289, 353].

Lung Perfusion-limited Model – Simulation of ELF Concentration based on Passive Permeability (PStc) and Fraction Unbound in ELF ($f_{u,ELF}$)

Similar to the perfusion-limited model based on $K_{ELF/p,u}$, the adapted perfusion limited model assumes that the tissue partition is limited only by the blood flow, whereas the partition from the tissue into the ELF is limited by a slow passive diffusion (as defined by Ap PStc) and/or the presence of an active transporter.

In a first simulation, the ELF concentrations of moxifloxacin and telithromycin were estimated using only the Ap PStc as an input parameter without incorporating any active transport process. The Ap PStc was scaled by GastroPlus™, using the passive hepatic clearance per default [355]. The simulated ELF-concentration time profiles are shown in Figures 49 and 50.

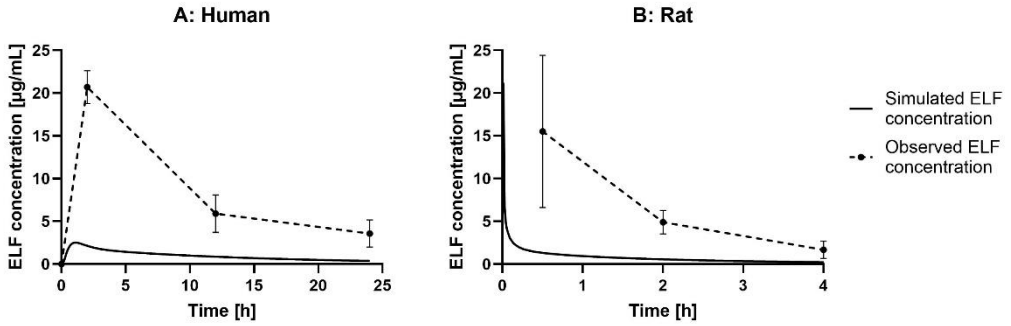

Figure 49. Simulated and observed ELF concentration-time profiles of **Moxifloxacin** in human (A) and rat (B) using the perfusion-limited model with a scaled permeability surface area product on the apical side (Ap PStc). Moxifloxacin was given as single oral dose of 400 mg to human and as single i.v. bolus of 5mg/kg to rats [297, 347]. The predicted ELF profiles are depicted as solid line (-) and observed profiles are shown as dotted line with measured means ± SD as dots (--·--).

Compared to the perfusion-limited model based on $K_{ELF/p,u}$, a lower total ELF concentration was predicted for moxifloxacin in both human (10-fold) and rat (12-fold), see Figure 49. This underestimation of the observed data was also pronounced for telithromycin (60-fold for human and six-fold for rat), as shown in Figure 50.

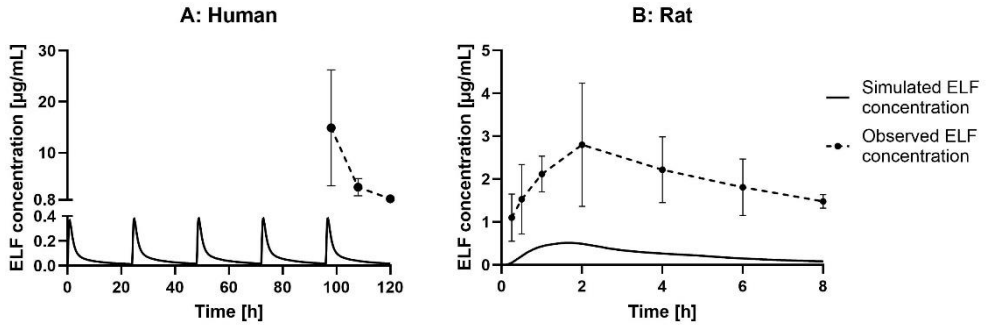

Figure 50. Simulated and observed ELF concentration-time profiles of **Telithromycin** in human (A) and rat (B) using the perfusion-limited model with a scaled permeability surface area product on the apical side (Ap PStc). Telithromycin was given as multiple oral dose of 800 mg to human (q24h x 5 doses) and as single oral dose of 50 mg/kg to rats [289, 353]. The predicted ELF profiles are depicted as solid line (-) and observed profiles are shown as dotted line with measured means ± SD as dots (--·--).

In a next step, a PSA was performed investigating whether changing the Ap PStc (increase or decrease by 10-fold of the initial scaled value) had any impact on the predicted concentrations of moxifloxacin and telithromycin in the ELF (see Figures 51 and 52).

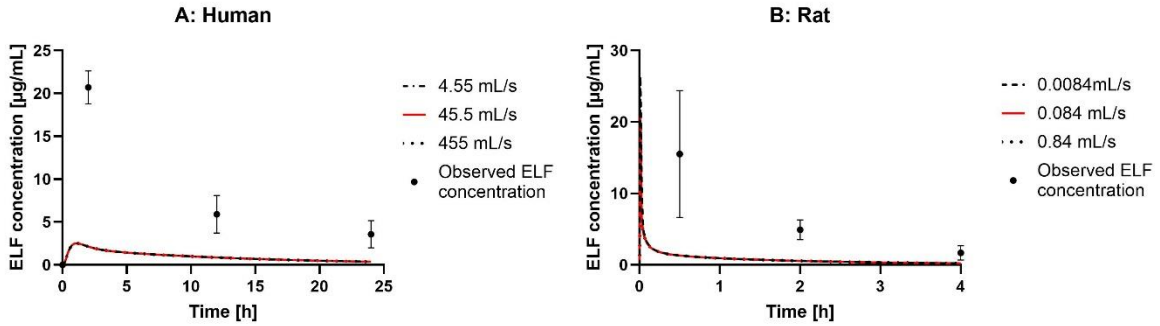

Figure 51. Parameter sensitivity analysis (PSA) of the predicted ELF concentration-time profiles of **Moxifloxacin** in human (A) and rat (B) if changing the apical permeability surface area product (Ap PStc) and using the perfusion-limited model. The simulated ELF concentration using the experimental Ap PStc is shown a solid red line, with a 10-fold lower Ap PStc as dashed line (---) and with a 10-fold higher Ap PStc as dotted line (⋯). Observed ELF concentrations are shown as measured means ± SD as dots (·) [297, 347].

For both moxifloxacin and telithromycin in human and rat, increasing or decreasing the scaled Ap PStc by 10-fold did not have any impact on predicted ELF concentrations, still resulting in a strong underestimation of the observed values.

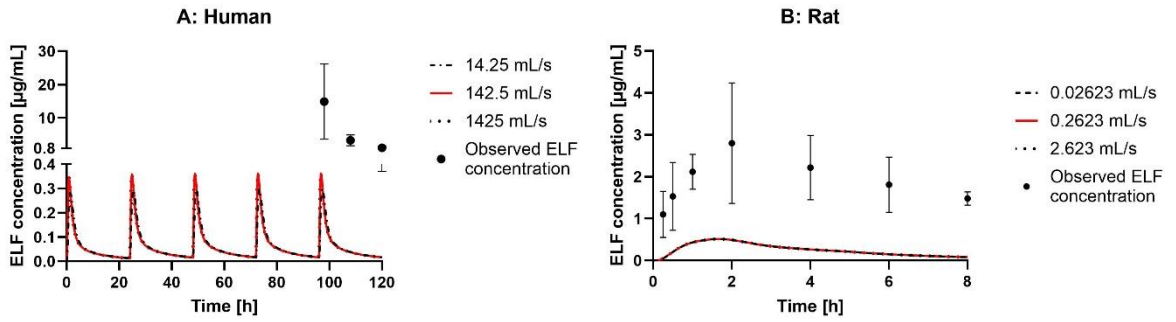

Figure 52. Parameter sensitivity analysis (PSA) of the predicted ELF concentration-time profiles of **Telithromycin** in human (A) and rat (B) if changing the apical permeability surface area product (Ap PStc) and using the perfusion-limited model. The simulated ELF concentration using the experimental Ap PStc is shown a solid red line, with a 10-fold lower Ap PStc as dashed line (---) and with a 10-fold higher Ap PStc as dotted line (⋯). Observed ELF concentrations are shown as measured means ± SD as dots (·) [289, 353].

GastroPlus™ predicted based on the chemical structure of moxifloxacin and telithromycin, a lower unbound fraction in ELF ($f_{u,ELF}$) compared to the experimentally derived values in sELF *in vitro*: 35.7 % instead of 78.2 % for Moxifloxacin and 2.92 % instead of 65.4 % for Telithromycin. Thus, a PSA was performed comparing the impact on ELF prediction if taking the predicted, the experimentally derived $f_{u,sELF}$ or a 10-fold lower value of the experimental one.

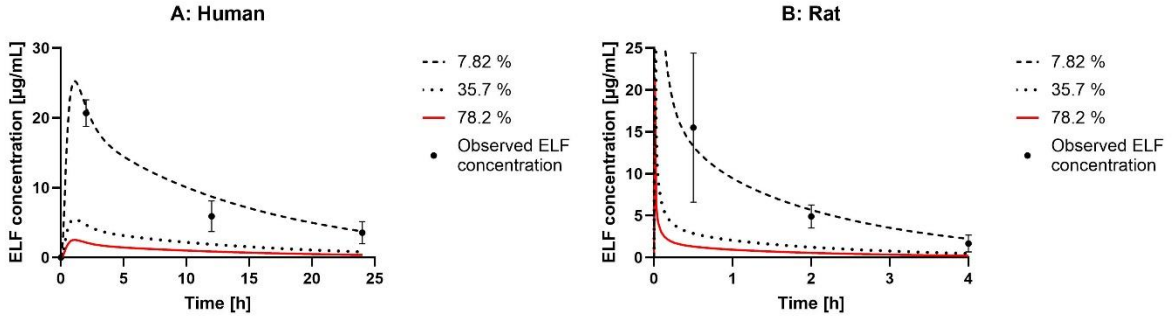

Figure 53. Parameter sensitivity analysis (PSA) of the predicted ELF concentration-time profiles of **Moxifloxacin** in human (A) and rat (B) if changing the unbound fraction in ELF ($f_{u,ELF}$) and using the perfusion-limited model. The simulated ELF concentration using the experimental $f_{u,ELF}$ is shown a solid red line, with a 10-fold lower $f_{u,ELF}$ as dashed line (---) and with the predicted $f_{u,ELF}$ from GastroPlus™ as dotted line (⋯). Observed ELF concentrations are shown as measured means ± SD as dots (·) [297, 347].

As depicted in Figure 53, the simulated total ELF concentration of moxifloxacin increased when lowering the $f_{u,ELF}$. If taking a 10-fold lower $f_{u,ELF}$ compared to the experimentally derived value (i.e. 7.82 %), an almost perfect capture of the observed ELF concentration-time profiles in both human and rat was found.

For telithromycin, changing the $f_{u,ELF}$ to the predicted value of 2.92 %, led a more accurate prediction of the observed ELF data within human (within the standard deviation of two sampling time points), whereas in rat, the ELF concentration was more than two-fold overestimated, as depicted in Figure 54. However, lowering the experimentally derived value for $f_{u,ELF}$ by 10-fold (i.e. 6.54 %) resulted in a reasonable capture of the rat *in vivo* profile.

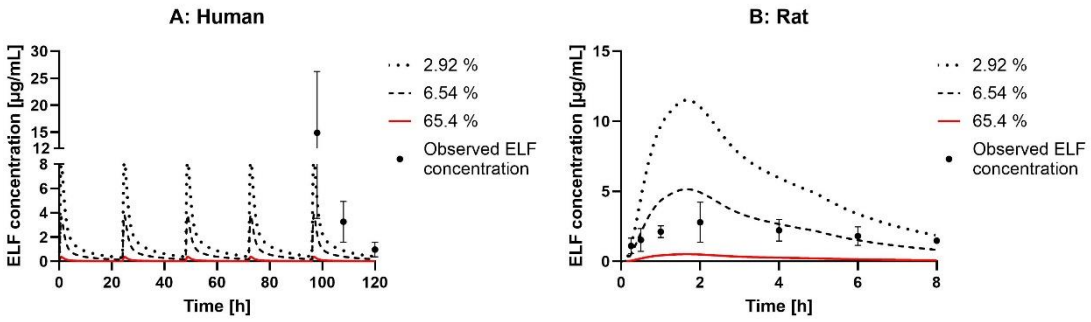

Figure 54. Parameter sensitivity analysis (PSA) of the predicted ELF concentration-time profiles of **Telithromycin** in human (A) and rat (B) if changing the unbound fraction in ELF ($f_{u,ELF}$) and using the perfusion-limited model. The simulated ELF concentration using the experimental $f_{u,ELF}$ is shown a solid red line, with a 10-fold lower $f_{u,ELF}$ as dashed line (---) and with the predicted $f_{u,ELF}$ from GastroPlus™ as dotted line (⋯). Observed ELF concentrations are shown as measured means ± SD as dots (·) [289, 353].

Lung Perfusion-limited Model – Influence of Pulmonary MDR1 Efflux on Simulated ELF Concentrations

In a further step, the expression of the efflux transporter MDR1 was incorporated into the PBPK at the apical ELF-facing side of the lung tissue. The Ap PStc was maintained at the initially scaled value. The respective ELF concentration-time plots for moxifloxacin and telithromycin are shown in Figures 55 & 56.

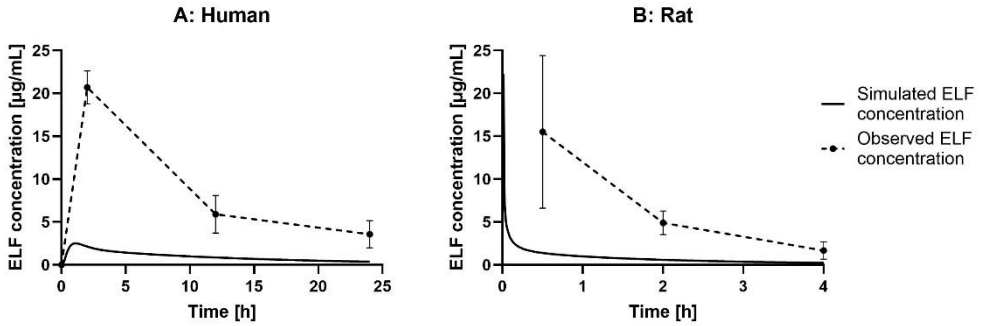

Figure 55. Simulated and observed ELF concentration-time profiles of **Moxifloxacin** in human (A) and rat (B) using the perfusion-limited model with a scaled permeability surface area product on the apical side (Ap PStc) and incorporated MDR1 efflux at the apical side. Moxifloxacin was given as single oral dose of 400 mg to human and as single iv. bolus of 5mg/kg to rats [297, 347]. The predicted ELF profiles are depicted as solid line (-) and observed profiles are shown as dotted line with measured means ± SD as dots (--·--).

The presence of MDR1 efflux within the lung did not result in any significant change of the predicted ELF concentrations in both human and rat, if comparing to Figures 49 and 50, where the ELF concentrations were estimated based on the Ap PStc only. Observed ELF concentrations were strongly underestimated for moxifloxacin (10- and 12-fold) and telithromycin (60- and six-fold) in human and rat, respectively (if accounting for pulmonary MDR1 efflux).

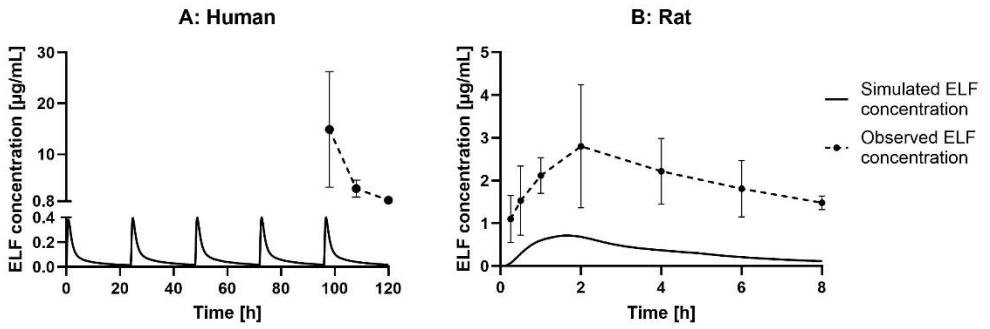

Figure 56. Simulated and observed ELF concentration-time profiles of **Telithromycin** in human (A) and rat (B) using the perfusion-limited model with a scaled permeability surface area product on the apical side (Ap PStc) and incorporated MDR1 efflux at the apical side. Telithromycin was given as multiple oral dose of 800 mg to human (q24h x 5 doses) and as single oral dose of 50 mg/kg to rats [289, 353]. The predicted ELF profiles are depicted as solid line (-) and observed profiles are shown as dotted line with measured means ± SD as dots (--·--).

As the MDR1 expression within the human and rat lung was estimated based on available gene expression data in literature, a PSA was performed by adjusting the expression levels of pulmonary MDR1 (either increased or decreased by 10-fold based on the value used in the baseline simulation). The results are depicted in Figures 57 and 58.

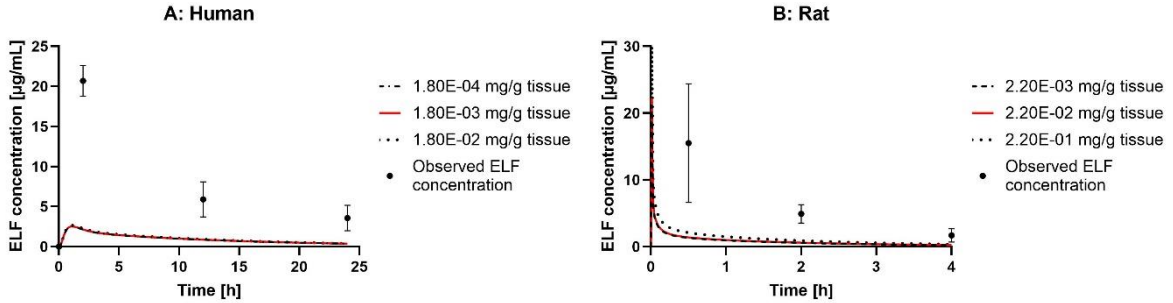

Figure 57. Parameter sensitivity analysis (PSA) of the predicted ELF concentration-time profiles of **Moxifloxacin** in human (A) and rat (B) if changing the MDR1 expression level in the lung and using the perfusion-limited model. The simulated ELF concentration using the estimated MDR1 expression is shown as solid red line, with a 10-fold lower MDR1 expression as dashed line (---) and with a 10-fold higher MDR1 expression as dotted line (⋯). Observed ELF concentrations as measured means ± SD as dots (·) [297, 347].

Changing the pulmonary MDR1 expression levels did not have any impact on the simulated ELF concentrations of moxifloxacin in both human and rat and for telithromycin in human (Figure 57). However, as shown in Figure 58, increasing the MDR1 expression in the rodent lung by 10-fold led to a five-fold increase of the simulated ELF concentration of telithromycin. Thus, this indicates that MDR1 could potentially contribute to active efflux of telithromycin into the rodent ELF after a single dose.

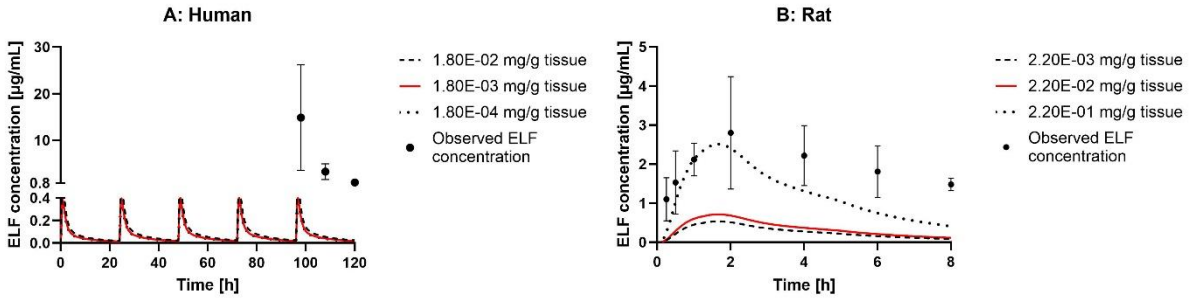

Figure 58. Parameter sensitivity analysis (PSA) of the predicted ELF concentration-time profiles of **Telithromycin** in human (A) and rat (B) if changing the MDR1 expression level in the lung and using the perfusion-limited model. The simulated ELF concentration using the estimated MDR1 expression is shown as solid red line, with a 10-fold lower MDR1 expression as dashed line (---) and with a 10-fold higher MDR1 expression as dotted line (⋯). Observed ELF concentrations are shown as measured means ± SD as dots (·) [289, 353].

In a last step, a potential change in simulated ELF concentration-time profiles was investigated if changing the Michaelis-Menten kinetics of moxifloxacin and telithromycin against MDR1, i.e. the K_m and V_{max}. For the conducted PSA, the literature-retrieved K_m values were either decreased by 10- or 100-fold or increased by 100-fold, whereas the literature-derived V_{max} were increased or decreased by 10-fold.

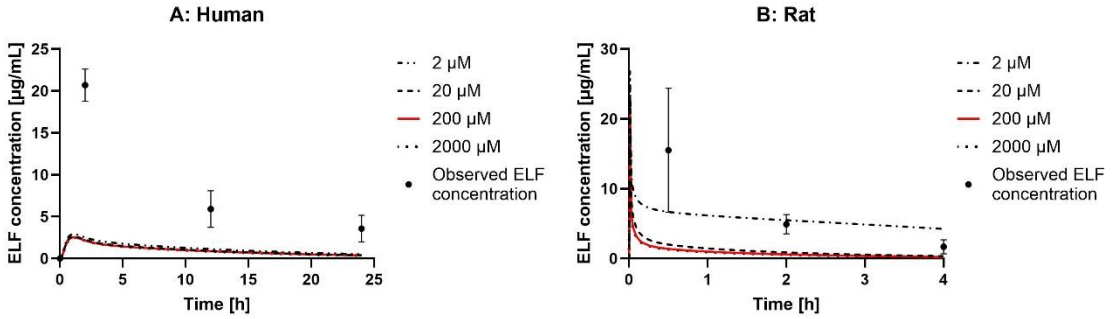

Figure 59. Parameter sensitivity analysis (PSA) of the predicted ELF concentration-time profiles of **Moxifloxacin** in human (A) and rat (B) if changing the Michaelis-Menten constant (K_m) of MDR1 interaction and using the perfusion-limited model. The simulated ELF concentration using the literature-retrieved K_m is shown as solid red line, with a 100-fold lower K_m as patterned line (-·-), with a 10-fold lower K_m as dashed line (---) and with a 10-fold higher K_m as dotted line (⋯). Observed ELF concentrations as measured means ± SD as dots (·) [297, 347].

As depicted in Figure 59, a change in K_m had no impact on the simulated ELF concentrations of moxifloxacin in human. Whereas in rat, a 100-fold lower K_m led to an a more than five-fold increase of simulated ELF concentration with two out of three observed time points being nicely predicted.

Similar observations were made for telithromycin in rat, where lowering the literature-retrieved K_m by 10-fold, resulted in a more than three-fold higher simulated ELF concentration profile that is close to the observed profile. The lowering of literature K_m by 100-fold in human ELF predictions of telithromycin resulted in a around two-fold increase of ELF concentrations, but still significantly underestimating observed values (around 15-fold), see Figure 60. A 10-fold lower K_m resulted in a good prediction of telithromycin's observed ELF concentration in rat.

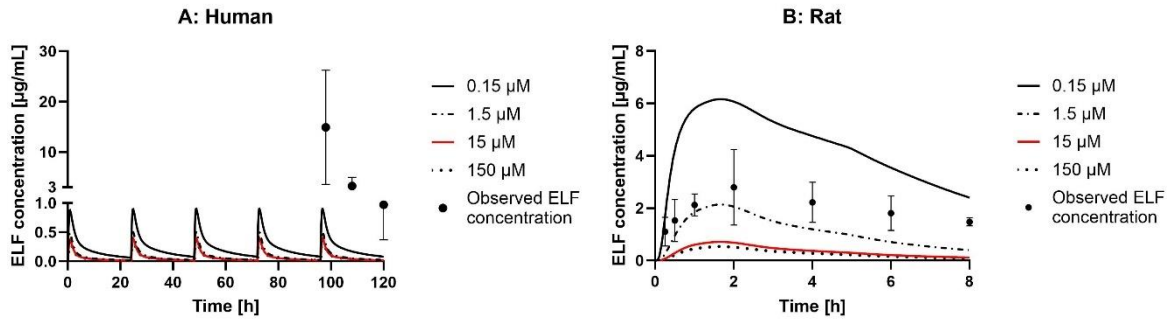

Figure 60. Parameter sensitivity analysis (PSA) of the predicted ELF concentration-time profiles of **Telithromycin** in human (A) and rat (B) if changing the Michaelis-Menten constant (K_m) of MDR1 interaction and using the perfusion-limited model. The simulated ELF concentration using the literature-retrieved K_m is shown as solid red line, with a 100-fold lower K_m as black solid line, with a 10-fold lower K_m as patterned line (-·-), and with a 10-fold higher K_m as dotted line (⋯). Observed ELF concentrations as measured means ± SD as dots (·) [289, 353].

Figure 61 shows the results from the PSA when changing the literature-retrieved V_{max} of moxifloxacin's interaction with MDR1. For the simulated ELF concentration-time profiles in human and rat, no change was observed when increasing or decreasing the V_{max} by 10-fold.

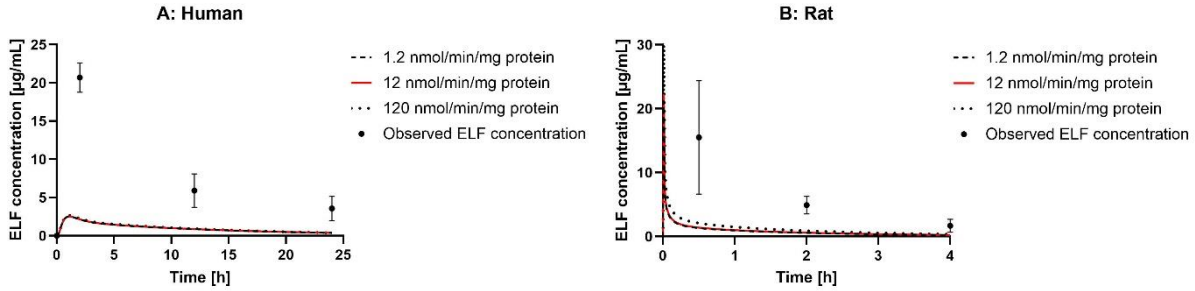

Figure 61. Parameter sensitivity analysis (PSA) of the predicted ELF concentration-time profiles of **Moxifloxacin** in human (A) and rat (B) if changing the maximal velocity (V_{max}) of MDR1 interaction and using the perfusion-limited model. The simulated ELF concentration using the literature-retrieved V_{max} is shown as solid red line, with a 10-fold lower V_{max} as dashed line (---) and with a 10-fold higher V_{max} as dotted line (⋯). Observed ELF concentrations as measured means ± SD as dots (·) [297, 347].

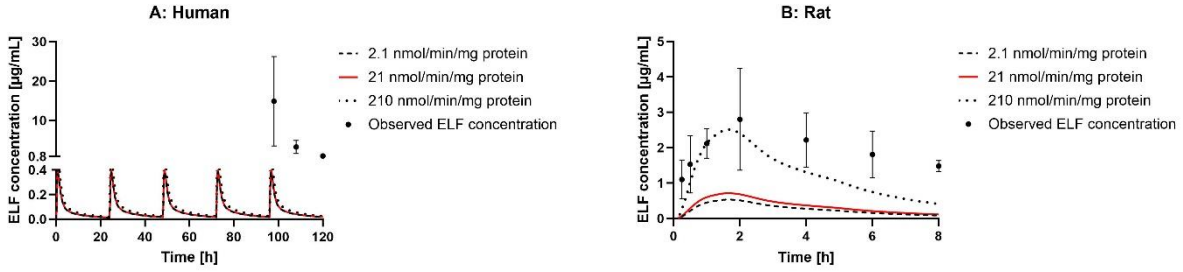

Figure 62. Parameter sensitivity analysis (PSA) of the predicted ELF concentration-time profiles of **Telithromycin** in human (A) and rat (B if changing the maximal velocity (V_{max}) of MDR1 interaction and using the perfusion-limited model. The simulated ELF concentration using the literature-retrieved V_{max} is shown as solid red line, with a 10-fold lower V_{max} as dashed line (---) and with a 10-fold higher V_{max} as dotted line (⋯). Observed ELF concentrations as measured means ± SD as dots (·) [289, 353].

A similar result was observed when changing the literature-retrieved V_{max} of telithromycin's interaction with MDR1. In human, a change in predicted ELF concentration-time profile was not observed when increasing or decreasing the V_{max} by 10-fold. For rat, an almost perfect

capture of the observed ELF concentration profile was found when increasing the literature-retrieved V_{max} by 10-fold (see Figure 62).

Lung Permeability-limited Model – Simulation of ELF Concentrations based on Passive Permeability (Ap & Ba PStc)

In the permeability limited model, the drug partition from the extracellular space into the lung tissue and from lung tissue into ELF is characterised by a slow diffusion and/or the presence of active transport.

In a first simulation, the ELF concentration was estimated by incorporating only the passive diffusion processes, using the Ba PStc and Ap PStc, respectively. The PStc was calculated based on the passive hepatic liver clearance (default by GastroPlus™) and the same value was used for Ap and Ba PStc.

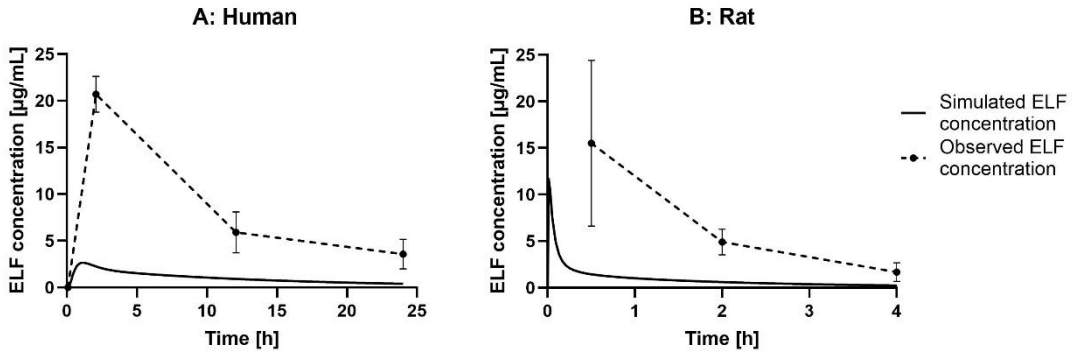

Figure 63. Simulated and observed ELF concentration-time profiles of Moxifloxacin in human (A) and rat (B) using the permeability-limited model with a scaled permeability surface area product on the basolateral (Ba PStc) and on the apical side (Ap PStc). Moxifloxacin was given as single oral dose of 400 mg to human and as single i.v. bolus of 5mg/kg to rats [297, 347]. The predicted ELF profiles are depicted as solid line (-) and observed profiles are shown as dotted line with measured means ± SD as dots (--·--).

As seen in Figure 63, the observed ELF concentration-time profiles of moxifloxacin were underestimated for both human (10-fold) and rat (12-fold), when using the permeability-limited model. This was also evident when predicting the ELF concentration-time profiles of telithromycin in both species (six- to 60-fold in rat and human) using the permeability-limited model (see Figure 64). The simulated ELF profiles are similar to those received when using the perfusion-limited model with a defined apical diffusion by the Ap PStc (as shown in Figures 49 and 50).

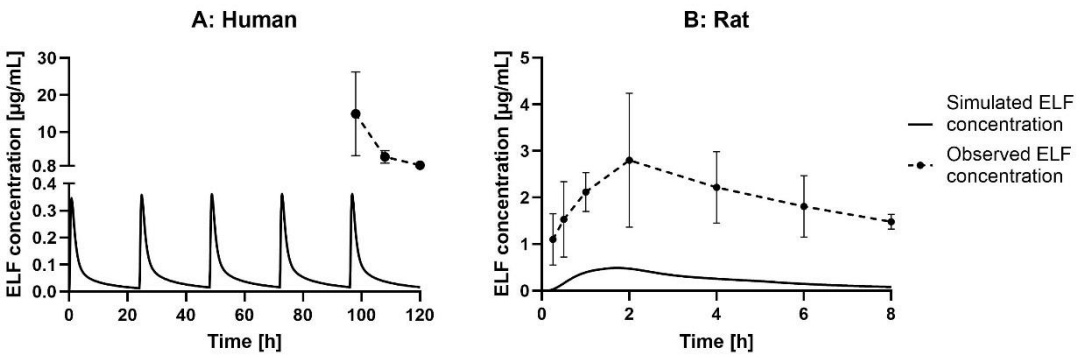

Figure 64. Simulated and observed ELF concentration-time profiles of Telithromycin in human (A) and rat (B) using the permeability-limited model with a scaled permeability surface area product on the basolateral (Ba PStc) and on the apical side (Ap PStc).Telithromycin was given as multiple oral dose of 800 mg to human (q24h x 5 doses) and as single oral dose of 50 mg/kg to rats [289, 353]. The predicted ELF profiles are depicted as solid line (-) and observed profiles are shown as dotted line with measured means ± SD as dots (--·--).

Several PSA were performed to investigate the impact of a change of Ba PStc & AP PStc and $f_{u,ELF}$ on the simulated ELF concentration-time profiles of both moxifloxacin and telithromycin, using the permeability-limited model. The respective graphics can be found in the supplemental material (Figure C6 – C9) and similar observations were made as described for the PSA, when using the lung perfusion limited model.

Lung Permeability-limited Model – Influence of Pulmonary MDR1 Efflux on Simulated ELF Concentrations

In a last step, the permeability model was adapted by adding MDR1 as active efflux transporter to the apical side of the lung tissue in addition to the Ap PStc. The ELF concentration-time profiles of moxifloxacin and telithromycin were simulated and shown in Figures 65 & 66.

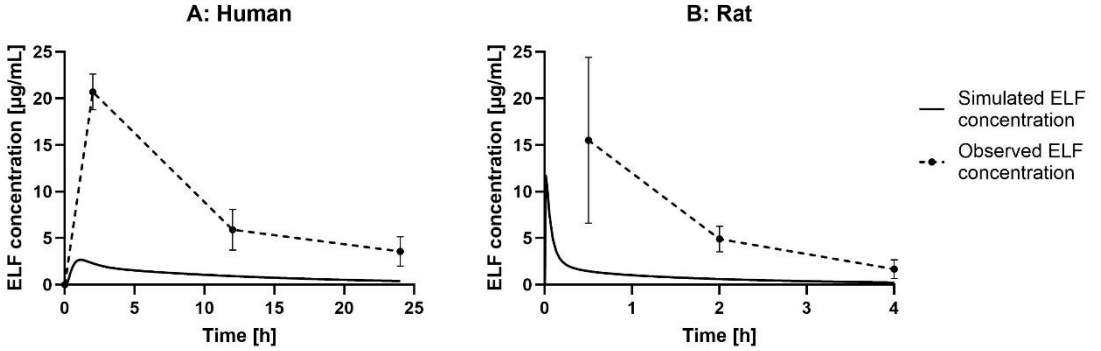

Figure 65. Simulated and observed ELF concentration-time profiles of **Moxifloxacin** in human (A) and rat (B) using the permeability limited model with a scaled permeability surface area product on the basolateral (Ba PStc) and on the apical side (Ap PStc) and MDR1 efflux at the apical side. Moxifloxacin was given as single oral dose of 400 mg to human and as single iv. bolus of 5mg/kg to rats [297, 347]. The predicted ELF profiles are depicted as solid line (-) and observed profiles are shown as dotted line with measured means ± SD as dots (--·--).

The resulting ELF simulations did not show any significant change to those using the permeability limited model without the incorporation of MDR1 to the lung tissue (see Figures 63 & 64). The simulated ELF concentrations were strongly underestimated compared to the

observed profiles for both antibiotics (10- to 12-fold for moxifloxacin and 60- to six-fold for telithromycin in human and rat, respectively).

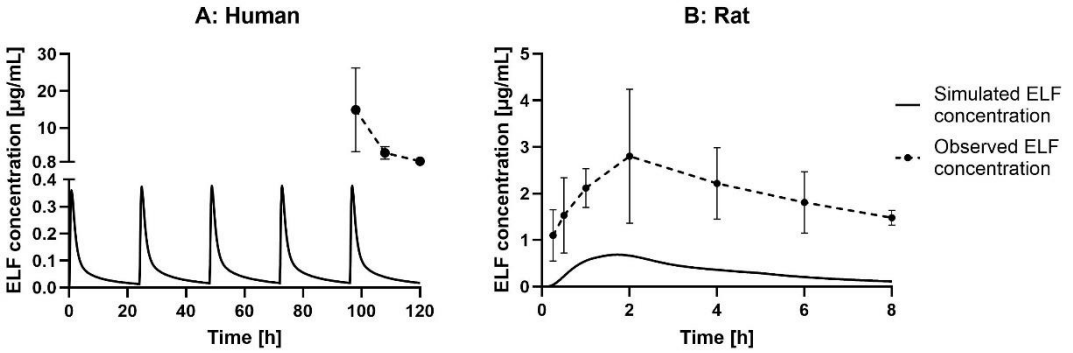

Figure 66. Simulated and observed ELF concentration-time profiles of **Telithromycin** in human (A) and rat (B) using the permeability limited model with a scaled permeability surface area product on the basolateral (Ba PStc) and on the apical side (Ap PStc) and MDR1 efflux on the apical side. Telithromycin was given as multiple oral dose of 800 mg to human (q24h x 5 doses) and as single oral dose of 50 mg/kg to rats [289, 353]. The predicted ELF profiles are depicted as solid line (-) and observed profiles are shown as dotted line with measured means ± SD as dots (--·--).

Further PSA were performed to investigate whether the predicted ELF concentration-time profiles change if adapting the MDR1 expression levels within the lung or the K_m and V_{max}, while using the permeability-limited model. The respective graphics can be found in the Supplemental material (Figure C10 – C15) and simulated ELF profiles are similar to those, when using the lung perfusion-limited model.

3.3.4 Discussion

The aim of this *in silico* study was to simulate the ELF concentration-time profiles of two antibiotics (moxifloxacin and telithromycin) in human and rat using the PBPK modelling software GastroPlus™. The two antibiotics were selected as they showed high ELF to plasma ratios (>> 1) in both clinical and *in vivo* studies, after an administration via the systemic circulation [4, 289, 297]. Literature has reported that the two compounds are substrates of active efflux transporter MDR1, therefore it was speculated that the presence of this transporter at the apical side of the pulmonary epithelium could contribute to the observed increased ELF over plasma ratios [16, 232]. Nevertheless, recent studies pointed out that enhanced binding of drugs to components of the ELF, such as lipids, surfactant proteins or the lung tissue itself likely contribute to elevated total ELF over plasma concentrations for certain antibiotics [156, 162, 163].

The different options in GastroPlus™ to simulate ELF concentration-time profiles were employed (see 3.3.2.5). In a first step, the perfusion limited model was used, where the ELF concentration was estimated based on the predicted ELF to unbound plasma partition coefficient ($K_{ELF/P,u}$). Further, the ELF concentration was simulated using the perfusion limited model, where the partition from the lung tissue into the ELF was characterised by the passive apical permeability surface area product (Ap PStc), followed by the permeability limited model, where both the basolateral and apical permeability across the lung epithelial were defined by the basolateral/apical PStc (Ba/Ap PStc). Further, active efflux mediated by MDR1 was incorporated into the PBPK models to the apical side of the lung epithelium to investigate the potential impact on predicted ELF concentrations. This was followed by several parameter sensitivity analyses (PSA), where it was investigated how/if the simulated ELF concentrations change if one key pharmacokinetic parameter was modified.

However, before estimating the ELF profiles, the individual PBPK models were established within GastroPlus™ and respective plasma concentration-time profiles were simulated and only when a good fit to the observed plasma values was achieved, the model was used to predict local ELF concentrations.

3.3.4.1 General Model Assumptions

When no experimental or literature information was available, the physicochemical and pharmacokinetic parameters used within the established PBPK models were predicted by GastroPlus™ based on the molecule's chemical structure (see supplemental Tables C3 & C4 for modified input parameters). This could add some uncertainty to predictions, however the PBPK models showed good predictions of the observed plasma concertation-time profiles from

two independent clinical/*in vivo* studies, adequately capturing both the absorption and elimination profiles of moxifloxacin and telithromycin in both species. Therefore, the models are considered suitable to simulate ELF concentration-time profiles.

Clinical studies used to initially validate the established PBPK models, were assessing the plasma concentration profiles of moxifloxacin and telithromycin in healthy young male participants (overview provided in supplemental Table C1). In contrast, participants were typically elderly and had a medical indication for bronchoscopy in the clinical studies where ELF and plasma were sampled. However, the PBPK simulations in human were run using the default 30-years healthy male model, as during the PBPK model establishment no significant differences in profile shape and individual pharmacokinetic parameters (C_{max}, t_{max} and $AUC_{0\text{-}th}$) of both moxifloxacin and telithromycin were observed, when changing the model age to an elderly population (65 or 67 years, respectively). This is aligned with available literature, where it was reported that moxifloxacin and telithromycin showed a similar pharmacokinetic profile in elderly compared to a young population after an oral administration [360, 361].

3.3.4.2 Simulation of Plasma Concentration-Time Profiles

The established PBPK models showed a good prediction of the observed plasma concentrations of moxifloxacin and telithromycin in human and rat.

To obtain a good fit of moxifloxacin's elimination kinetics, both hepatic and renal clearance was incorporated into the human and rat PBPK model. This is aligned with literature, where it has been described, that moxifloxacin mainly undergoes phase II metabolism by sulphation and glucuronidation and is excreted both via faeces and active secretion into urine [362, 363]. Moxifloxacin was reported to be a substrate of MDR1 efflux within the intestine of humans [345]. However, due to the high oral dose of Moxifloxacin typically given to humans (400 mg) and the high solubility of the drug [364], a potential saturation of intestinal MDR1 is likely and its impact on limiting intestinal absorption is negligible (i.e. assuming a complete dissolution of moxifloxacin in the concomitantly taken amount of 250 mL water to swallow the tablet). This would result in a local intestinal concentration of around 4000 µM, clearly exceeding the literature-retrieved K_m value for moxifloxacin against MDR1 [345]. Therefore, intestinal MDR1 efflux was not incorporated into the human PBPK model. The intestinal Mdr1 efflux was not applicable to the rat PBPK model, as the moxifloxacin was dosed by intravenous injections in the *in vivo* studies, thus bypassing intestinal absorption processes.

Telithromycin has been described in literature to undergo hepatic, biliary and renal clearance in humans [365]. Therefore, in addition to the scaled hepatic clearance, both biliary and renal clearance were added to the human PBPK model to enable a good prediction of its elimination

profile. To capture the elimination profile of telithromycin in rats, only renal clearance was added to the scaled hepatic clearance and a good fit to the observed profile was received. However, literature indicated that biliary clearance mediated by Mdr1 and Mrp2 is likely contributing to its elimination in rats [366]. Moreover, telithromycin is known to undergo phase I metabolism, mainly mediated by CYP3A4 in human and Cyp3A1/2 in rats [346, 367]. Therefore, intestinal metabolism was incorporated into both human and rat PBPK models to improve the predicted absorption profile. Telithromycin was described to be a time-dependent inhibitor (TDI) of its own metabolism by CYP3A4 in human. However, a study that used PBPK modelling to estimate plasma concentration of telithromycin in humans, showed an acceptable prediction without accounting for the TDI effect, thus this factor was not taken into consideration [346]. In addition, telithromycin has been described to be a substrate of MDR1, which might impact its intestinal absorption. The contribution of MDR1 in limiting the intestinal absorption of telithromycin in humans appeared to negligible due to high oral give dose (800 mg), which was shown to likely saturate MDR1-mediated efflux [346]. If assuming the drug is taken with 250 mL of water and accounting for the limited water solubility of telithromycin, this would result in an estimated intestinal concentration of ~ 1000 µM, thus clearly exceeding the reported K_m of 15 µM [346]. Whereas in rats, Mdr1 appeared to limit the intestinal absorption of telithromycin due to the lower doses given. An *in vivo* study in Wistar rats showed that the non-metabolised, absorbed fraction in enterocytes increased by 17 % if co-dosing telithromycin with verapamil (Mdr1 inhibitor) [356]. To account for a potential contribution of Mdr1 in limiting the intestinal absorption of telithromycin in rats, the effective intestinal permeability (P_{eff}) was reduced in the rat PBPK model by four-fold (as determined via parameter sensitivity analysis of P_{eff}. This resulted in a good fit of the absorption profile, together with the incorporated intestinal metabolism of telithromycin by CYP3A in rats.

As the available clinical studies dosed moxifloxacin and telithromycin via oral administration and the plasma exposure data for fasted and fed conditions were reported [347, 349], the plasma concentration-time profiles were simulated in the two scenarios. This comparison was run as food can impact drug absorption processes ('food effect'). Concomitant intake of food while taking an oral medication can affect several physiological factors relevant for drug absorption processes, such as the gastric emptying time, gastric/intestinal pH and release of bile salts, thus potentially impacting the drug's intestinal solubility and permeability. This can result in either 'positive' effect, where the absorption is increased or in a 'negative' effect, where the opposite is observed [368, 369]. For both antibiotics, a slightly higher C_{max} and a slightly earlier t_{max} were observed when simulating the fasted condition. However, the calculated fasted and fed AUC values were close to each other, when comparing the fasted and fed state (within 1.05-fold), indicating the absence of any food effect. This was also observed when running the population trial simulation, hinting to tiny differences in the absorption profile between fasted

and fed conditions, however almost identical elimination profiles were seen. Therefore, the intake of food does not seem to have any impact on plasma concentration levels of moxifloxacin and telithromycin in humans. This is aligned with literature, where it was reported that food did not have any significant effect on the observed plasma concentration-time profiles and resulting bioavailability of the two antibiotics in humans [347, 349].

To account for the complex composition of the gastric fluid, biorelevant media (FaSSIF, FeSSIF) were developed to mimic fasted and fed state (accounting for factors such pH and bile salts), which allows a more accurate estimation of a compound's intestinal solubility [370, 371]. Within the simulation of this study, the biorelevant solubilities values were predicted from GastroPlus™, as no experimentally derived values were available for the two antibiotics in these media. Therefore, it is possible that these values do not fully capture the physiological observed solubilities and could be an explanation why slightly different values in C_{max} and t_{max} were predicted compared to observed values for the fasted and fed state.

Despite the uncertainty due the use of mainly predicted parameters, the established PBPK models showed a good prediction of the observed plasma concentration profiles of moxifloxacin and telithromycin in human and rat. Therefore, they were used to simulate the ELF concentration-time profiles of both antibiotics.

3.3.4.3 Sampling of ELF by Bronchoalveolar Lavage and Potential Limitations

To quantify the amount of drug within the ELF, sampling by bronchoalveolar lavage (BAL) is typically performed [15]. The BAL procedure is often accompanied by a bronchoscopy. Patients receive local anaesthesia, followed by the insertion of the bronchoscope to the smaller airways. Physiological, sterile saline is instilled, thereby washing the airway surface, and saline is careful retrieved. Usually, aliquots of 50 mL saline are used with a maximal volume of 300 mL [372]. The first aliquot of aspirate is often discarded to avoid a potential sample contamination with cells and liquids of the upper airways. Following aliquots are pooled and then centrifuged to separate the ELF (supernatant) from the remaining cells [351].

Overall, the ELF collection by BAL is a technically challenging procedure, which comes with some limitations [15]. Cells that are present in the ELF such as alveolar macrophages can lyse during the sample collection, through mechanical force. This might be a special concern for antibiotics, that are known to heavily accumulate within the alveolar macrophages such as telithromycin or moxifloxacin, as lysis of macrophages results in release of their intracellular content and thus could increase measured ELF concentrations. Therefore, it is of special importance that ELF samples are centrifuged before the analysis to separate the cells from the ELF [15, 351, 373]. Due to the instillation of saline for collecting the ELF, the total ELF volume

is diluted and thus needs to be corrected for this. For the correction, urea is often taken, which is a low-molecular endogenous marker, and assumed to have the same concentration across tissues, incl. plasma and ELF. It is a non-polar molecular marker, that is fast diffusing across membranes following a concentration gradient. The actual volume of sampled ELF can then be calculated from the urea concentration in the ELF sample and concomitantly taken plasma sample [4, 374]. As a limitation, the urea concentration within the ELF can be overestimated by contamination of blood during the collection procedure. Moreover, it was reported that additional urea can diffuse from the lung interstitial space into the ELF during the BAL collection if the 'dwell time' (time between saline instillation and aspiration) is too long (> 1 min) [15, 375]. A further limitation of clinical studies using BAL is that subjects usually provide only one sample of ELF at one time point due to the complexity of the procedure. This can contribute to seen high variability in reported ELF concentrations of antibiotics in clinical studies [4, 300]. Moreover, often a broad range of ELF to plasma ratios is reported for the same antibiotic across different clinical studies, i.e. for Clarithromycin, reported peak ratios range from 5 to 61, which emphasises the difficulty of receiving reproducible data, when measuring ELF concentrations by BAL [141].

As an alternative to BAL, the sampling of ELF can be performed by a bronchoscope microprobe that contains an absorptive tip for collecting the ELF. This method bears the advantage that the ELF is not diluted, and several samples can be taken from the same subject. In contrast to BAL, samples are taken from bronchial lung space [38]. A clinical study by Yamazaki and colleagues assessed the concentration of the fluoroquinolone levofloxacin in the ELF of healthy male volunteer after an oral administration comparing ELF concentration measured simultaneously by BAL and bronchoscopic microsampling (BMS). They reported an around two-fold higher ELF concentration in BAL samples. The authors concluded that the lower ELF concentration by BMS might arise from the sampling location (bronchial vs. alveolar for BAL) and as BAL sampled need to be corrected for the dilution, increasing the uncertainty in measured values by BAL [376].

All clinical studies, that were in scope of this *in silico* study, sampled the ELF via BAL. Therefore, the above limitations should be considered when interpreting measured ELF concentrations of these studies.

3.3.4.4 Simulation of ELF Concentration-time Profiles – Based on $K_{ELF/p,u}$ & $f_{u,plasma}$

The most accurate prediction of observed ELF concentration-time profiles was achieved when using the perfusion-limited model on basis of the ELF to free plasma partition coefficient ($K_{ELF/p,u}$). However, the simulated total ELF concentrations of moxifloxacin (human and rat) and telithromycin (human) were underpredicted more than three-fold, whereas the total ELF

concentration of telithromycin in rat was more than two-fold overestimated. The value of $K_{ELF/p,u}$ for both moxifloxacin and telithromycin was predicted from their chemical structure using a quantitative structure activity relationship (QSAR) model by the ADMET Predictor® module within GastroPlus™. The QSAR regression model was trained based on the clinical ELF to free plasma ratios of 56 antibiotics from different classes and 12 antibiotics were used to test the performance of the model. Both moxifloxacin and telithromycin appeared to be part of the training set (GastroPlus™ user manual V 9.9, Dec 2023, [358, 377]).

The ADMET Predictor® module predicted a $K_{ELF/p,u}$ of 3.29 for Moxifloxacin and a value of 32.8 for Telithromycin, which translates into a 3.29- or 32.8-fold higher simulated ELF concentration compared to the unbound plasma concentration, respectively. Therefore, if increasing or decreasing the $K_{ELF/p,u}$ by two-fold, as performed in the parameter sensitivity analysis (PSA), the predicted ELF concentration of moxifloxacin and telithromycin increased or decreased by two-fold accordingly. As the clinical ELF and plasma concentrations as well as the protein binding data for moxifloxacin and telithromycin are available, one could calculate the individual $K_{ELF/p,u}$ for each clinical study, using this value in predictions and likely receive an optimal prediction of the observed ELF concentration-time profiles. This approach does not answer the questions of this *in silico* study, however using ELF predictions based on $K_{ELF/p,u}$ might be a starting point to simulate the ELF concentrations of antibiotics for which clinical ELF data are not yet available or to compare the potential ELF exposure of a series of structurally different antibiotics in early discovery phase.

If taking the unbound fraction in plasma ($f_{u,plasma}$) into account, the PSA showed that a reduction by 10-fold to the experimental values (< 5 % unbound) resulted in a reduced ELF concentration, which is to be expected as only the free fraction can cross biological membranes and thus the lower the free concentration in plasma, the lower the amount that can partition into the tissue [378]. As seen for moxifloxacin (human and rat) and telithromycin (rat), the shape of the ELF profile changed when decreasing the unbound fraction. This was to be expected, since lowering the unbound fraction in plasma impacts further pharmacokinetic processes such as the volume of distribution, half-life or clearance processes [302].

The ELF simulation of telithromycin in rats, when using the predicted $K_{ELF/p,u}$ resulted in more than two-fold higher prediction compared to the observed data. This might arise from the fact that the QSAR model for predicting the $K_{ELF/p,u}$ is based on clinical data and was not trained for *in vivo* ELF predictions.

Moreover, the approach based on $K_{ELF/p,u}$ does not account for any binding to components of the ELF, as this was considered negligible due to the low abundance of proteins within the ELF [358]. However, recent studies have shown that the free fraction of antibiotics in ELF is rarely 100 % as previously assumed [161].

3.3.4.5 Simulation of ELF Concentration-time Profiles – Based on PStc & $f_{u,ELF}$

When using the perfusion limited model with an apical permeability surface area product (Ap PStc), an underestimation of the observed total ELF concentrations for both moxifloxacin (up to 10-fold) and telithromycin (more than 35-fold) was observed. In this scenario, the partition from the plasma into the lung tissue is limited only by the blood flow and the partition into the ELF is characterised by the Ap PStc. As only passive permeation processes are assumed, the free plasma concentration matches the free lung tissue concentration and equally the free ELF concentration.

Since telithromycin is highly bound to proteins/lipids within the plasma (12 %), its predicted free plasma concentration peak is ~ 0.25 µg/mL in human. Therefore, the model takes the same free concentration within the lung tissue and ELF as it assumes that the compound crosses biological membrane by passive diffusion only. If accounting for the experimentally derived unbound fraction in sELF (65.4 %), this results in a simulated total ELF concentration of ~ 0.4 µg/mL. This explains the low predicted ELF concentration of telithromycin in human. The same assumptions were made by the model when simulating the total ELF concentrations of telithromycin in rats or for moxifloxacin in human and rat. It was decided to showcase the calculation for telithromycin in human, as the disconnect between observed and predicted ELF concentration was the greatest.

The PStc is calculated by GastroPlus™ based on the hepatic passive diffusion rate. It assumes that the passive permeability through the cell membrane is the same across all tissues in the body. Therefore, the calculated PStc of the liver is used to scale the PStc of further tissues if accounting for their respective surface area. As the exact surface areas for the different tissues are not always known, the model performs the upscaling based on the total cell volume of a tissue [355]. A PSA was performed where the predicted lung PStc was increased or decreased by 10-fold compared to initially scaled PStc value. No change in predicted ELF concentration was observed for the two antibiotics in human and mouse. Both moxifloxacin and telithromycin were considered highly permeable *in vitro* (in LLC-PK1 WT and Caco-2 cells, as shown in supplemental Table B3 & B4). Therefore, a 10-fold reduction in PStc does not seem to affect total ELF concentrations.

Within the scope of this thesis, it was observed that antibiotics tend to show a lower permeability in cell lines derived from the human lung epithelium (Calu-3 and hAELVi) compared to cells, that are typically used in permeability testing such as the porcine kidney epithelial cell line LLC-PK1 or the human intestinal epithelial cell line Caco-2 (see chapter 3.2). As the modelling software assumes passive permeation is the same across tissues, it might be argued that the passive hepatic clearance is not accurately capturing passive diffusion processes in the lung. Therefore, the human passive pulmonary diffusion clearance was

calculated based on the *in vitro* apparent permeability (measured in hAELVi, a human alveolar epithelial cell line derived from alveolar type I epithelial cells [105]) and if accounting for the reported surface area of human alveolar type I epithelial cells [379]. The calculations can be found in the supplemental material in Section C5. The lung PStc value for moxifloxacin was 1.5-fold lower compared the PStc estimated by the passive hepatic clearance (28.7 vs 45.5 mL/s), whereas for telithromycin an around eight-fold lower PStc was calculated (17.9 vs 142.5 mL/s), when using the estimated pulmonary passive diffusion clearance. The estimated lung PStc values for moxifloxacin and telithromycin were within 10-fold of the PStc estimated via the hepatic diffusion clearance and thus covered by the respective PSA, showing that a lowered lung PStc within this order of magnitude did not result in a change of predicted total ELF concentration. Thus, a potential underestimation of antibiotics pulmonary passive permeability is likely not the reason for the observed disconnect in simulated and observed ELF profiles.

In terms of the rodent lung, no report in literature was found where the permeability of drugs across the rodent pulmonary epithelium was assessed in an *in vitro* setting. A study by Sapich and colleagues reported that primary alveolar murine epithelial cells form a tight barrier with a reported transepithelial electric resistance of ~ 1800 Ω x cm² and a low permeability of paracellular marker sodium fluorescein (< 25 nm/s) [380]. Thus, it is plausible to speculate that passive permeability of drugs is likely similar to that in human alveolar epithelial cells.

A further factor to consider is the binding of antibiotics to components of the ELF. The PBPK model assumes that the unbound concentration in the ELF equals the unbound concentration in the lung tissue, as partition from lung tissue into ELF is driven by passive diffusion only. Therefore, the drug binding to ELF components plays a pivotal role in driving total ELF concentrations. If a drug shows strong binding to ELF components, this results in lower free ELF concentration levels and due to the passive diffusion, following a concentration gradient, resulting in an increased total ELF concentration over time.

Due to the low abundance of proteins within the ELF, it was previously assumed that the free fraction within ELF is 100 % [161]. However, recent studies have shown that compounds can strongly bind to lipids and proteins within the ELF [156, 162]. A novel fluoroquinolone, lascufloxacin, showed an extremely high ELF to unbound plasma ratio (> 60) in clinic. An *in vitro* study elucidated that the compound showed strong binding to the phospholipid phosphatidylserine, which is present in the surfactant and thus likely driving the high ELF concentration [163, 235]. It was proposed in literature that the ELF-bound drug can be extracted during the BAL washing process and thus result in high measured total ELF concentrations, that do not reflect local free concentrations. This was described for basic, positively charged compounds [162]. Antibiotics often carry a positive charge due to the

increased effectiveness against Gram-negative bacteria [164]. Therefore, a strong binding to components of the ELF could contribute to the observed high ELF to plasma ratios of fluoroquinolones and macrolides (as they carry a basic group) [4, 381, 382].

This hypothesis was confirmed when running the PSA while changing the unbound ELF fraction ($f_{u,ELF}$) - the lower the $f_{u,ELF}$, the higher the predicted total ELF concentration. When lowering the experimentally measured $f_{u,ELF}$ by 10-fold to 7.82 % unbound for moxifloxacin, the observed ELF concentration-time profile was well predicted in human and rat. For telithromycin, lowering the experimentally derived $f_{u,ELF}$ by 10-fold resulted in a better capture of observed ELF profiles. This emphasises that strong binding of drugs to ELF components can result in high total ELF concentrations. Using the experimental value for $f_{u,ELF}$ as input parameters, determined by the simulated ELF binding assay did not result in improved predictions of observed ELF concentrations for both moxifloxacin and telithromycin. It is possible that measured $f_{u,ELF}$ values are overpredicted as the sELF consists of the main nine components of ELF, but further ELF components are likely contributing to binding *in situ*. Moreover, the sELF was designed to mimic the human ELF and might thus not necessarily being representative of the rodent ELF, further investigation would be needed to assess its relevance for preclinical species [156]. Future research should therefore focus on developing a simulated ELF fluid, that represents the physiological human ELF more closely with regards to its numerous components to allow a more accurate estimation of the unbound fraction in ELF *in vitro*. A further point to consider is the establishment of a simulated ELF fluid, which takes disease-related aspects into account. It was reported in literature, that patients suffering from a bronchiolitis showed increased concentrations of albumin within the ELF [383].

The same observations, as described in this chapter, regarding PStc and $f_{u,ELF}$ were made when using the permeability limited model, where the ELF concentration-time profiles were defined by the basolateral and apical PStc (Ba/Ap PStc).

3.3.4.6 Expression of MDR1 within the Pulmonary Epithelium

In a further step, pulmonary MDR1 expression was incorporated into the PBPK models to investigate the potential impact of active efflux on the simulated ELF concentration-time profiles of moxifloxacin and telithromycin. MDR1 was described to be expressed on the apical side of the lung epithelium [177]. The focus in this *in silico* study was on MDR1, as literature reported moxifloxacin and telithromycin being substrates of MDR1 and due to availability of human MDR1 Michaelis-Menten-kinetics (K_m and V_{max}) for both antibiotics [16, 232, 345]. Within the scope of this thesis project, the two antibiotics were tested in bidirectional transport studies, using cells overexpressing either human MDR1 or mouse Mdr1 (see chapter 3.2).

An efflux ratio (ER) ≥ 2 typically classifies a compound as substrate of MDR1 [18]. Telithromycin was classified as substrate of both human and mouse (ER of 54.7 for mouse and 11.9 for human), whereas moxifloxacin was found to be a substrate of rodent Mdr1 (ER of 7.1) but not of human MDR1 (ER of 1.4).

Within the default lung PBPK tissue in GastroPlus™, no transporter expression was defined. The pulmonary expression levels of MDR1/Mdr1 were estimated based on gene expression data and set relative to already defined MDR1/Mdr1 protein expression levels of other organs within GastroPlus™ (i.e. relative to the kidney expression of MDR1/Mdr1). This approach comes with some uncertainty as gene expression levels do not necessarily correlate with protein expression levels [384]. Moreover, the gene expression studies, based on which the pulmonary MDR1/Mdr1 expression levels were estimated from, assessed the lung as a whole, not taking the different cell types into account [193, 203]. The transporter does not seem to be expressed only in the pulmonary epithelium, as studies reported its expression as well as in the pulmonary endothelium and immune cells [206, 385, 386]. Therefore, reported total MDR1/Mdr1 expression levels might not necessarily capture those within the lung epithelium. A further point to consider is, that the human gene expression data is based on pooled RNA from three individuals (Caucasian male & female) and for the rat expression data, the RNA was measured from five male Sprague-Dawley rats [193, 203]. A study by Sakamoto and colleagues reported that MDR1 protein expression levels varied up to 44 % across human subjects [187]. As the mentioned gene expression study pooled human lung RNA from the three donors, no variability across subjects was considered [193]. This approach was taken due to the unavailability of measured protein concentrations of MDR1/Mdr1 in the human or rodent lung epithelium, respectively.

3.3.4.7 Simulation of ELF Concentration-time Profiles – Incorporation of MDR1/Mdr1 Efflux on Apical Side of the Lung Epithelium

The active efflux transporter MDR1/Mdr1 was incorporated to the PBPK model on the apical, ELF-facing side of the lung tissue. Both the perfusion and permeability limited model were used. The addition of active efflux to the lung tissue had no impact on predicted ELF concentrations of both moxifloxacin and telithromycin in human and rat. The simulated ELF concentration-time profiles were almost identical to those when running the simulations without MDR1 expression within the lung tissue. Based on this simulation data, MDR1/Mdr1 does rather not play a role in driving elevated ELF concentrations of moxifloxacin and telithromycin in the two species.

However, it needs to be noted that pulmonary MDR1/Mdr1 protein expression levels were estimated based on gene expression data and thus are subject to uncertainty. A PSA was

performed where pulmonary protein expression levels of MDR1/Mdr1 were either 10-fold decreased or increased compared to initially estimated expression level. For moxifloxacin in rat and human and telithromycin in human, a change in MDR1/Mdr1 expression did not result in any significant change of the predicted ELF concentration-time profile, whereas for telithromycin in rat a 10-fold increase of Mdr1 pulmonary expression levels resulted in overall good capture of the *in vivo* ELF concentrations. This observation could arise from the fact that the estimated human pulmonary MDR1 expression levels were 10-fold lower than those of the rat and due to an around 13-fold higher affinity of telithromycin to MDR1, than moxifloxacin (as defined by the Michaelis-Menten constant (K_m)).

In a further step, several sensitivity analyses were performed by taking the key parameters, assessing MDR1 transport kinetics into account: K_m and the maximal velocity (V_{max}). The K_m gives an idea of the affinity of the substrate (drug) to the transporter (i.e. the lower K_m, the higher the affinity to the transporter protein), whereas the V_{max} is a reflection of the transporter capacity [387]. The PSA showed that lowering the K_m 100-fold to the experimental derived one had no impact on predicted moxifloxacin ELF concentration in human, and only minor on human telithromycin ELF concentration. In contrast, lowering the K_m of moxifloxacin 100-fold in rat, resulted in well capturing the observed ELF profile, apart from the first sampling time point. For telithromycin, a 10-fold lower K_m gave a good estimation of the observed data in rat. In terms of V_{max}, only the condition, where the V_{max} of telithromycin was increased by 10-fold in the rat model, resulted in a good prediction of observed ELF data. Taken together, the results from the sensitivity analyses showed that Mdr1 could contribute, as active efflux transporter, to drive higher ELF concentrations (compared to plasma) of both moxifloxacin and telithromycin in rat, whereas its contribution in the human lung epithelium appears to be negligible based on the simulated ELF data of this study. As a potential limitation, only two antibiotics were in scope of this *in silico* study.

Further, the literature K_m and V_{max} were assessed in human MDR1 overexpression cells (moxifloxacin [345]) or in human MDR1 overexpressing membranes (telithromycin [16]). Therefore, these values might not necessarily reflect those in rodent Mdr1 overexpressing cells. Especially, the K_m values are likely to be lower, as both Moxifloxacin and Telithromycin showed stronger efflux in mouse Mdr1 overexpressing cells compared to human MDR1 overexpressing cells (4.6-fold for Telithromycin and 4.8-fold for Moxifloxacin, see chapter 3.2). Both antibiotics have likely a higher affinity to the mouse Mdr1 than the human MDR1. Thus, it is reasonable to speculate that efflux transporters might have a more pronounced impact in driving ELF exposure of these two antibiotics in rodents compared to humans. This is aligned with findings from other organs, where literature reported for instance that the brain exposure

of MDR1/Mdr1 substrates is likely more restricted in rodents than in humans, thus highlighting potential species differences [338].

In this context, it is worth mentioning that extrapolating drug transporter mechanisms from *in vitro* to *in vivo* is challenging. Reasons for this are manifold. The transporter expression levels within the chosen *in vitro* model do often not capture those of the respective tissue *in vivo*, passive permeability processes may differ between *in vitro* and *in vivo*. Moreover, free tissue intracellular concentrations are often not known (i.e. amount of drug being available for active transport processes) and thus chosen test concentrations *in vitro* might over- or underestimate transporter's contribution [388]. Further difficulties arise when exact transporter tissues expression levels are not known and if multiple transporter proteins are involved in distribution processes [135]. As the human lung epithelium was described to be rich in the expression of further ABC transporter such as MRPs, and uptake transporters from the solute carrier (SLC) family like OCTs, it is possible that antibiotics interact with these proteins, potentially impacting their permeability across the lung epithelium *in situ* [177].

3.3.4.8 Further Aspects to Consider when Estimating ELF Concentrations

Further factors can be taken into consideration when estimating drug concentrations within the ELF. One of these is the mucociliary clearance (MCL). This process is a defence mechanism of pulmonary epithelium to protect against pathogens and particles. The mucus is produced by secretory cells and by beating of ciliated cells, it gets transported from conducting airways in direction of the throat to be either expectorated or swallowed [389, 390]. This is mainly considered, when administering a drug via the inhalation or nasal route [391]. In GastroPlus™, the MCL refers to the removal of a drug from the airways via flow of the ELF and is defined as 2.75 nL/s or 6.67 nL/s by default for human and rat, respectively. This default value was not adjusted during all simulations of this study and kept at its default value.

A further point to consider is the pH of the ELF. An average pH of the 'healthy' ELF of around 6.6 was reported, being slightly acidic compared to physiological pH of the blood with pH 7.4 [139]. In GastroPlus™, the pH was set to 6.69 by default within the ELF of both human and rat. It was shown by PBPK sensitivity simulations in literature that a reduction in the pH of the ELF can increase the ELF exposure of antibiotics (e.g. lowering the ELF pH down to 6.0 resulted in a 2.7-fold higher predicted ELF concentration for the macrolide azithromycin) [139]. Similar observations were made when lowering the pH in ELF-PBPK simulations for clarithromycin [141]. In case of a severe lung injury, the pH of the ELF can be reduced down to ~ 5.5, as measured in the exhaled breath condensate of patients [392]. Since antibiotics are typically administered to patients suffering from a bacterial infection, a lowered pH in ELF

should be considered. A drop in pH can affect the ionisation charge of antibiotics within the ELF (depending on their pKa) and thus potentially impacting the binding to components of the ELF. This might be likely observed for antibiotics that carry a strong basic group (pKa of ~ 7.0), as a drop in pH would result in a higher proportion of ionised species and thus likely enhanced binding to e.g. acidic lipids within the ELF [141, 156, 319].

A limitation of this *in silico* study is that ELF concentrations were predicted within a healthy subject population, whereas the observed ELF concentrations were measured in patients that underwent a diagnostic bronchoscopy (see Supplemental Table C1). However, it was not clearly specified in the clinical studies what individual diagnosis the subjects had. The plasma concentrations of respective clinical studies were reasonably captured by the established PBPK models without taking disease-related mechanisms into account. Thus, the PBPK models are likely a solid base to predict ELF concentration-time profiles and compare to observed data of the respective clinical studies.

It is reported that severe illness can affect several pharmacokinetic parameters of absorption, distribution, metabolism and elimination processes. This can result in a change of volume of distribution, protein concentration within the plasma, clearance mechanism and beyond, which would have a direct impact on observed plasma concentration profiles and thus also resulting ELF concentrations [393]. It was further reported that severe pneumonia can result in alveolar damage and alveolar cells losing their barrier functions, thus becoming leaky [394]. This phenomenon likely affects local drug concentration within the ELF. As this was not considered in this study, the established PBPK model within this *in silico* study are likely not suitable to predict ELF concentrations of antibiotics within a severely ill population.

3.3.5 Conclusion

This *in silico* study aimed to simulate the concentrations of moxifloxacin and telithromycin in the ELF of both human and rat, using a PBPK modelling approach. The ELF concentration-time profiles were predicted after a drug administration via the systemic circulation and compared to observed data from clinical and *in vivo* studies.

Overall, an underestimation of the measured ELF concentrations was observed for both antibiotics in the two species. Parameter sensitivity analysis revealed that closer predictions of ELF concentration-time profiles were received once lowering the unbound drug fraction within the ELF, whereas a change in the passive pulmonary permeability did not affect predicted ELF concentrations. The incorporation of MDR1/Mdr1 as active efflux transporter on the apical side of the lung tissue did not result in more accurate predictions of observed ELF concentrations. However, following sensitivity analysis showed that a change in MDR1/Mdr1

interaction parameters improved ELF predictions of moxifloxacin and telithromycin in rat, without any significant change in the human simulations.

This PBPK approach is a first step to a better mechanistic understanding of the pharmacokinetic parameters driving drug's exposure into the ELF, while pinpointing to potential species differences in the contribution of active efflux transporters (MDR1/Mdr1) at the level of the lung epithelium.

Further, this study highlights the fact that drug binding to components of the ELF can significantly increase total ELF concentrations in both human and rat, a parameter being often ignored due to the previous assumption that binding of antibiotics to ELF components is negligible.

4. Summary and Outlook

The overall aim of this thesis was to deepen the mechanistic understanding on the role of ABC efflux transporters at the human lung epithelium and their potential impact on the pulmonary bioavailability of antibiotics after an administration via the systemic circulation. The experimental approach employed a combination of *in vitro* and *in silico* methods and was described in Chapters 3.1, 3.2 and 3.3.

4.1 Characterising the Expression and Functional Activity of MDR1, MRP1 and BCRP in Cell Lines and Primary Cells of the Human Upper and Lower Airways

In the first manuscript (Chapter 3.1), the expression and functional activity of MDR1, MRP1 and BCRP was characterised in several cell lines and primary cells that were derived from the human upper and lower airway epithelium. The focus was on MDR1 and BCRP due to their clinically relevant impact on the pharmacokinetics of their substrates in tissues like the intestine, kidney or liver [173]. Further, MRP1 was included due to its reported high expression levels within the human pulmonary epithelium [187]. The following cell lines were investigated: 16HBE14o-, Calu-3, NCI-H441, A549, hAELVi and Arlo and the respective primary cells of bronchial (NHBE) and alveolar (hAEpC) origin, allowing a direct comparison in terms of ABC transporters' expression and mediated efflux.

MRP1 showed ubiquitous expression, being well aligned with literature findings [177]. In contrast, MDR1 was only expressed in Calu-3 cells, whereas literature reported its expression also in the 16HBE14o-, NCI-H441 and A549 cell lines [94, 195]. The absence of widely standardised culture conditions and protocols across labs, the use different reagents and potential selective agents or the formation of subclones (which often possess different properties compared to the parent cell line) may result in variability of transporter expression levels across studies [79, 395, 396]. Further factors like the passage number, cultivation time on membrane inserts or the culture interface (ALI vs. LCC) have been described to impact the MDR1 expression levels in Calu-3 [79, 87, 201]. Findings from this thesis have revealed that culturing lung epithelial cells at ALI versus LCC resulted only for Calu-3 in significant differences in the expression of MDR1 and MRP1 at protein level, whereas this was not observed for the other cell lines. Future research would be needed to investigate to what extent additional factors, like the culture time or passage number affect transporters' expression in lung epithelial cell lines other than Calu-3. This might contribute to a better understanding of the inconsistent findings in terms of ABC transporters expression patterns in pulmonary *in vitro* models across literature [19]. In contrast to existing reports [89, 111], MDR1 was also not detected in the primary NHBE and hAEpC cells characterised in this study. Overall, there is still little known about the expression levels of ABC transporters within the human pulmonary

tissue [177]. Sakamoto and colleagues reported that factors like gender might influence total transporters' expression levels within the human lung. However, further studies with a larger number of donors would be needed to investigate this further [187]. Moreover, the potential influence of age and disease state on ABC transporters' expression is likely contributing to observed donor to donor variability of primary cells [397]. In the context of hAEpC cells isolated in this study, no information regarding the donors' age, gender and disease state was received to ensure patients' data protection. Considering the absence of MDR1 in each three independent donors of primary NHBE and hAEpC cells, as well as in the majority of pulmonary cell lines, this questions the relevance of MDR1 on pulmonary drug disposition processes *in situ*.

The expression of BCRP was mainly observed in cells derived from the bronchial and bronchiolar epithelium [87, 221], whereas its expression was less pronounced or absent in alveolar-derived hAEpC, hAELVi and Arlo, being aligned with literature findings [107, 108]. This may point to a potential lung regional-specific expression of BCRP. Given that the alveolar epithelial surface area is up to 140-fold larger than the bronchial epithelial surface area [27], it raises the question how relevant the expression of BCRP in the bronchial epithelium is to overall pulmonary drug disposition in the context of a systemic drug administration.

Nevertheless, more important than the mere expression of drug transporters is to evaluate whether they are functionally active. This is typically assessed by measuring the efflux of transporter substrates in absence and presence of transporter inhibitors [18]. In literature, the functional activity of pulmonary expressed MDR1, MRP1 and BCRP was often assessed by using fluorophores as probe substrates [74, 111, 222]. In this study, fluorescent Rh123, 5,6-CF and H33342 were used as substrates for MDR1, MRP1 and BCRP, respectively. The observed efflux was well aligned with the expression profiles of MDR1, MRP1 and BCRP in the different lung cells. However, none of these fluorophores is selective for the respective ABC transporter and an interplay with further expressed ABC and SLC transporter proteins cannot be excluded [197, 215, 224]. This is especially a concern for lung epithelial cells, which are described to express a variety of active drug transporters, including members from the SLC family [177, 271]. To confirm the presence of active efflux within the lung epithelial cells in this study, bidirectional transport studies using drugs that are known substrates of the individual ABC transporters, were performed. In contrast to fluorophore experiments, no efflux mediated by MRP1 and BCRP was observed across all the lung epithelial cells (but being present in the Caco-2 cells, which served as positive control). Only for MDR1, efflux was shown in Calu-3 in this type of experiments. It was hypothesised that the fluorophores are more prone to be affected by active transporters, since they are more lipophilic (AlogP >~ 3) and showed an extremely low membrane permeability (P_{app} < 2 nm/s) across lung epithelial cells, if comparing

to the used drug substrates. Due to the distinct physicochemical properties of fluorophores and their non-selectivity for a specific ABC transporter, their use should be avoided, when aiming to assess the contribution of a single transporter protein on overall pulmonary drug disposition.

In bidirectional transport studies conducted within the scope of this thesis, the presence of active efflux was considered if there was a more than two-fold difference in net flux ratio across polarised epithelial cells, which had to decrease at least 50 % in presence of a transporter-specific inhibitor. This is in accordance with the recommendations from the health authorities [18]. However, these acceptance criteria have so far not been applied in literature, when assessing active efflux in pulmonary epithelial cell models, where efflux was typically considered if there was a statistically significant difference in permeability (absorptive versus secretory) [87]. To standardise the readout (i.e. presence of active efflux), it is worth to debate, whether these guidance criteria from health authorities should also be applied in future bidirectional transport studies using pulmonary epithelial cells [182].

Overall, the results indicate that ABC transporters may rather not play a pivotal role in pulmonary drug disposition processes, which is in contrast to their contribution in the epithelia of other organs like the intestine, liver or kidney [18]. Further drugs, which are known ABC transporter substrates, should be tested in bidirectional transport studies across pulmonary epithelial cells to confirm this finding. The use of primary cells has often been described as benchmark, especially when focussing on pulmonary drug disposition across the alveolar airways [20]. However, in terms of ABC transporters expression and functional efflux, similar findings were made in cell lines, when comparing data from primary cells to cell lines of the respective region. Calu-3 cells appear to be an exception (due to the presence of MDR1 efflux), which might arise from their cancer phenotype [332].

4.2 Investigating the Transport of 20 marketed Antibiotics across the Human Lung Epithelium *in vitro*

The aim of the second manuscript (Chapter 3.2) was to gain a deeper mechanistic understanding on the processes driving the transport of antibiotics across the pulmonary epithelium into the ELF after an administration via the systemic circulation. The following pharmacokinetic parameters were investigated: permeability, active efflux by ABC transporters and the degree of binding to plasma proteins and components of a simulated ELF. A diverse compound set of 20 marketed antibiotics was investigated.

The basolateral to apical permeability (i.e. mimicking the drug permeation from plasma into ELF) was measured in human tracheo-bronchial Calu-3 and alveolar hAELVi epithelial cells and compared to analogous values in LLC-PK1 WT (porcine kidney epithelial) and Caco-2

(human intestinal epithelial) cells, which are typically used for permeability profiling in early drug development [58, 290]. On average, a two- to three-fold lower permeability was measured in the lung cell lines, which was mainly pronounced for antibiotics, that were classified as highly permeable (> 100 nm/s) in LLC-PK1 WT and Caco-2 cells. Since the majority of antibiotics carries a moderate to strong basic group (pKa ≥ 7), it was hypothesised that enhanced binding to acidic phospholipids like phosphatidylserine (PS) within the membrane of lung epithelial cells could contribute to their reduced permeability *in vitro* [319, 320]. This process is well known in rats, where a high expression of PS was found in the lung, directly correlating with increased lung tissue retention of basic drugs [324]. Further studies would be needed to quantify the content of acidic phospholipids like PS within the cell membrane of different human organs including the lung, to understand the significance of this process on the tissue distribution of basic drugs in humans and whether there are significant differences across organs, which could impact local drug distribution [398]. To date, there are no studies available that conducted a lipidomic characterisation of the membrane phospholipid composition of Calu-3 and hAELVi, which would provide an estimation of their content of acidic phospholipids compared to other cells lines like LLC-PK1 WT and Caco-2.

Based on the measured extremely low permeability (< 10 nm/s) and recovery values (< 50 %) for hydroxychloroquine in Calu-3 and hAELVi (but not observed in LLC-PK1 WT and Caco-2), the presence of lysosomal drug sequestration *in vitro* was suggested [241]. In presence of Bafilomycin A1, a disruptor of the lysosomal acidification [303], both permeability and recovery of hydroxychloroquine significantly increased. This pointed to the relevance of lysosomal sequestration in Calu-3 and hAELVi cells, when aiming to determine an accurate estimate of the permeability of lipophilic and weakly basic drugs (like hydroxychloroquine). Future studies should be conducted to quantify the amount of lysosomes within Calu-3 and hAELVi to investigate, whether they possess a significantly higher cellular lysosomal concentration than LLC-PK1 WT or Caco-2 cells, as the presence of lysosomal trapping appeared to be less pronounced in these renal and intestinal epithelial cells. This could be assessed by staining lysosomes with fluorophores like 'LysoTracker™ deep red' and using a flow cytometrical readout [399].

Only few antibiotics, i.e. macrolides, ketolides and rifampicin, showed active efflux within the Calu-3 cells, which was likely mediated by MDR1, as all these compounds were classified as substrates of human MDR1 in MDR1-overexpressing cells and as Calu-3 was shown to express functionally active MDR1. No active efflux of antibiotics mediated by ABC transporters was observed within the hAELVi cells. This may hint to potential lung-regional differences, as Calu-3 were derived from the tracheo-bronchial epithelium and hAELVi from the alveolar epithelium [77]. If accounting for the significantly larger surface area for drug permeation in the

alveolar region [27], this might render the potential presence of active efflux within the bronchial region *in situ* negligible, especially in the context of a systemic drug administration. Furthermore, Calu-3 cells were derived from a lung adenocarcinoma patient, thus potentially overexpressing MDR1, as part of tumours' chemoresistance, and thus not necessarily representing the naïve human epithelium [60, 332].

Since macrolides and fluoroquinolones have shown increased ELF to plasma concentrations (>> 1) in clinics and *in vivo*, it has been discussed whether the presence of active efflux at the apical side of the lung epithelium is responsible for this observation [4, 288, 289, 297]. The respective antibiotics were therefore tested in human MDR1 or BCRP and in mouse Mdr1a or Bcrp1 overexpressing cells. Due to the higher efflux observed for these antibiotics in the mouse ABC transporter-overexpressing cells and thus likely higher affinity to mouse transporter proteins compared to analogous human proteins, this may point to potential species differences with regards to the transporters' impact on drug distribution processes, as described for other biological barriers like the blood-brain-barrier [338]. Therefore, the contribution of ABC transporter on pulmonary drug disposition of antibiotics may be more pronounced in rodents than in human. Further research would be needed to investigate this hypothesis, i.e. by comparing the lung exposure of macrolides and fluoroquinolones in transporter-knockout versus wild type animals [124].

There has been growing evidence that binding of antibiotics to lipids and proteins of the ELF can significantly reduce their local free ELF concentrations, whereas previously an unbound fraction of 100 % in ELF was assumed due to the lower abundance of proteins in ELF compared to plasma [156, 161, 163]. Literature has reported that especially basic antibiotics tend to show a stronger binding to lipids present in ELF compared to plasma proteins [156]. This was not observed for the compound set in this study, although still highlighting, that unbound fraction of most antibiotics in ELF is likely less than 100 % free and thus needs to be considered when investigating pulmonary pharmacokinetic processes. As a caveat of the simulated ELF used in this study, only the nine major components of human ELF were included, but additional components like surfactant-associated proteins or additional phospholipids like PS could contribute to drug binding in ELF and thus lower the free local concentrations [156, 163, 304, 305]. Future research would also be needed to evaluate whether there are species differences in ELF composition between human and rodents, which would need to be accounted for.

4.3 Employ PBPK Modelling to Quantitatively Simulate the ELF Concentration-Time Profiles of Moxifloxacin and Telithromycin in Human and Rat

In the third part (Chapter 3.3), PBPK modelling was used to simulate the ELF concentration-time profiles of moxifloxacin and telithromycin in both human and rat. The predictions were compared to the observed ELF concentration-time profiles from clinical and *in vivo* studies. The established PBPK models showed a good prediction of the observed plasma-time profiles for both antibiotics in the two species and were therefore considered suitable for predicting the respective ELF concentrations.

The simulated ELF concentration-time profiles of moxifloxacin and telithromycin were generally underestimating the observed values in human and rat. Incorporating MDR1 efflux on the apical side of the lung epithelium did not result in any significant changes in predicted ELF concentrations of moxifloxacin and telithromycin in both species.

The conducted parameter sensitivity analyses revealed that a change in MDR1 interaction parameters, either the Michaelis-Menten constant (K_m) and/or the maximal transport velocity (V_{max}) resulted in closer prediction of observed ELF concentrations for the two antibiotics in rat but had no significant impact on ELF predictions in human. This observation hinted to potential species differences in terms of the contribution of active efflux at the pulmonary epithelium, emphasising that ABC transporters could potentially play a role in driving ELF exposure in rodents. Having a more quantitative understanding of MDR1 protein expression levels in the pulmonary epithelium of humans and rodents *in situ* would contribute to a deeper understanding of potential species differences, especially as significant differences in MDR1 expression levels were reported for human, mouse and rat lung microvessels [400]. Further, the incorporation of experimentally derived K_m and V_{max} values of antibiotics with the rodent Mdr1 into the PBPK model would be beneficial to further improve the predictions.

Additional PBPK simulations have shown that the degree of the unbound fraction in the ELF can have a tremendous impact on total ELF concentrations of moxifloxacin and telithromycin in human and rat – the smaller the unbound fraction, the higher the total ELF concentration over time. Since literature reported a strong binding of basic drugs to lipids and proteins within the ELF [156, 163], it is reasonable to speculate that enhanced binding to components of the ELF could contribute to observed elevated ELF to plasma ratios of macrolides and fluoroquinolones in human and rodent, given that these molecules possess basic groups. Future research should focus on further elucidating, which individual components of the ELF contribute to enhanced binding of drugs like macrolides and fluoroquinolones in this matrix.

4.4 Final Conclusion

The *in vitro* and *in silico* results of this thesis have provided evidence that ABC transporters play a rather minor role in affecting the pulmonary bioavailability of antibiotics after a systemic administration. The data from the PBPK modelling revealed that additional pharmacokinetic parameters, such as the unbound drug fraction in ELF, are potentially contributing to elevated ELF to plasma ratios observed in clinics for macrolides and fluoroquinolones, rather than active efflux by ABC transporters at the apical side of the lung epithelium.

Overall, the findings of this thesis provided a deeper mechanistic understanding on the role of ABC efflux transporters within the human pulmonary epithelium, pointing to a negligible contribution, which contrasts their role in other tissues of the human body like the intestinal mucosa or the blood brain barrier [18]. These findings can be used as foundation for future studies, when aiming to translate relevant pharmacokinetic parameters of pulmonary drug disposition, like epithelial permeability and the unbound fraction in ELF to a disease state such as pneumonia.

5. References

1. C. Cilloniz, et al., *World Pneumonia Day 2024: Fighting Pneumonia and Antimicrobial Resistance*. Am J Respir Crit Care Med, 2024. 210(11): p. 1283–1285.
2. W.W. Labaki and M.K. Han, *Chronic respiratory diseases: a global view*. Lancet Respir Med, 2020. 8(6): p. 531–533.
3. S. Abed, et al., *Cell-specific drug targeting in the lung*. Biochem Pharmacol, 2021. 190: p. 114577.
4. K.A. Rodvold, et al., *Penetration of anti-infective agents into pulmonary epithelial lining fluid: focus on antibacterial agents*. Clin Pharmacokinet, 2011. 50(10): p. 637–64.
5. A.L. Jung, et al., *The clinical role of host and bacterial-derived extracellular vesicles in pneumonia*. Adv Drug Deliv Rev, 2021. 176: p. 113811.
6. J.M. Borghardt, et al., *Inhaled Therapy in Respiratory Disease: The Complex Interplay of Pulmonary Kinetic Processes*. Can Respir J, 2018. 2018: p. 2732017.
7. X. Liu, et al., *The development of models for the evaluation of pulmonary drug disposition*. Expert Opin Drug Metab Toxicol, 2013. 9(4): p. 487–505.
8. S.P. Newman, *Drug delivery to the lungs: challenges and opportunities*. Ther Deliv, 2017. 8(8): p. 647–661.
9. K. McCarthy and M. Avent, *Oral or intravenous antibiotics?* Aust Prescr, 2020. 43(2): p. 45–48.
10. E. Prina, et al., *Community-acquired pneumonia*. Lancet, 2015. 386(9998): p. 1097–108.
11. S. Andrei, et al., *FDA approved antibacterial drugs: 2018-2019*. Discoveries (Craiova), 2019. 7(4): p. e102.
12. D. Li and E.K. Schneider-Futschik, *Current and Emerging Inhaled Antibiotics for Chronic Pulmonary Pseudomonas aeruginosa and Staphylococcus aureus Infections in Cystic Fibrosis*. Antibiotics (Basel), 2023. 12(3).
13. D.R. Vandevanter and D.E. Geller, *Tobramycin administered by the TOBI((R)) Podhaler((R)) for persons with cystic fibrosis: a review*. Med Devices (Auckl), 2011. 4: p. 179–88.
14. L.M. Daniels, et al., *Inhaled Antibiotics for Hospital-Acquired and Ventilator-Associated Pneumonia*. Clin Infect Dis, 2017. 64(3): p. 386–387.
15. S. Kiem and J.J. Schentag, *Interpretation of antibiotic concentration ratios measured in epithelial lining fluid*. Antimicrob Agents Chemother, 2008. 52(1): p. 24–36.
16. K. Togami, et al., *Transport characteristics of clarithromycin, azithromycin and telithromycin, antibiotics applied for treatment of respiratory infections, in Calu-3 cell monolayers as model lung epithelial cells*. Pharmazie, 2012. 67(5): p. 389–93.
17. J. Brillault, et al., *Relative contributions of active mediated transport and passive diffusion of fluoroquinolones with various lipophilicities in a Calu-3 lung epithelial cell model*. Antimicrob Agents Chemother, 2010. 54(1): p. 543–5.
18. K.M. Giacomini, et al., *Membrane transporters in drug development*. Nat Rev Drug Discov, 2010. 9(3): p. 215–36.
19. C. Ehrhardt, et al., *Current Progress Toward a Better Understanding of Drug Disposition Within the Lungs: Summary Proceedings of the First Workshop on Drug Transporters in the Lungs*. J Pharm Sci, 2017. 106(9): p. 2234–2244.
20. M.A. Selo, et al., *In vitro and ex vivo models in inhalation biopharmaceutical research - advances, challenges and future perspectives*. Adv Drug Deliv Rev, 2021. 177: p. 113862.
21. D.K. Molina and V.J. DiMaio, *Normal organ weights in men: part II-the brain, lungs, liver, spleen, and kidneys*. Am J Forensic Med Pathol, 2012. 33(4): p. 368–72.
22. D.K. Molina and V.J. DiMaio, *Normal Organ Weights in Women: Part II-The Brain, Lungs, Liver, Spleen, and Kidneys*. Am J Forensic Med Pathol, 2015. 36(3): p. 182–7.
23. J. Petersson and R.W. Glenny, *Gas Exchange in the Lung*. Semin Respir Crit Care Med, 2023. 44(5): p. 555–568.

24. B. Han and H. Hirahara, *Effect of Gas Oscillation-Induced Irreversible Flow in Transitional Bronchioles of Human Lung*. Journal of Flow Control, Measurement & Visualization, 2016. 4: p. 171–193.
25. J.L. Sporty, et al., *In vitro cell culture models for the assessment of pulmonary drug disposition*. Expert Opin Drug Metab Toxicol, 2008. 4(4): p. 333–45.
26. E.R. Weibel, *Principles and methods for the morphometric study of the lung and other organs*. Lab Invest, 1963. 12: p. 131–55.
27. H. Eixarch, et al., *Drug Delivery to the Lung: Permeability and Physicochemical Characteristics of Drugs as the Basis for a Pulmonary Biopharmaceutical ClassificationSystem (pBCS)*. Journal of Epithelial Biology & Pharmacology, 2010. 3(1).
28. N. Heinen, et al., *In Vitro Lung Models and Their Application to Study SARS-CoV-2 Pathogenesis and Disease*. Viruses, 2021. 13(5).
29. J.S. Patton and P.R. Byron, *Inhaling medicines: delivering drugs to the body through the lungs*. Nat Rev Drug Discov, 2007. 6(1): p. 67–74.
30. K.P. O'Donnell and H.D.C. Smyth, *Chapter 1 Macro- and Microstructure of the Airways for Drug Delivery*, in *Controlled Pulmonary Drug Delivery*, H.D.C. Smyth and A.J. Hickey, Editors. 2011, Springer New York. p. 1 ff.
31. J.R. Harkema, et al., *Chapter 14 - Respiratory System*, in *Fundamentals of Toxicologic Pathology (Third Edition)*, M.A. Wallig, et al., Editors. 2018, Academic Press. p. 351–393.
32. N. Yaqub, et al., *Recent advances in human respiratory epithelium models for drug discovery*. Biotechnol Adv, 2022. 54: p. 107832.
33. M. Isasi-Campillo, et al., *Pulmonary surfactant-derived antiviral actions at the respiratory surface*. Current Opinion in Colloid & Interface Science, 2023. 66.
34. E.R. Weibel, *On the tricks alveolar epithelial cells play to make a good lung*. Am J Respir Crit Care Med, 2015. 191(5): p. 504–13.
35. P. Khan, et al., *Culture of human alveolar epithelial type II cells by sprouting*. Respir Res, 2018. 19(1): p. 204.
36. H. Fehrenbach, *Alveolar epithelial type II cell: defender of the alveolus revisited*. Respir Res, 2001. 2(1): p. 33–46.
37. N. Joshi, et al., *Alveolar Macrophages*. Cell Immunol, 2018. 330: p. 86–90.
38. L. Franciosi, et al., *Proteomics of epithelial lining fluid obtained by bronchoscopic microprobe sampling*. Methods Mol Biol, 2011. 790: p. 17–28.
39. M. Hassoun, et al., *Design and development of a biorelevant simulated human lung fluid*. J Drug Deliv Sci Technol, 2018. 47: p. 485–491.
40. X.M. Bustamante-Marin and L.E. Ostrowski, *Cilia and Mucociliary Clearance*. Cold Spring Harb Perspect Biol, 2017. 9(4).
41. M. Haghi, et al., *Across the pulmonary epithelial barrier: Integration of physicochemical properties and human cell models to study pulmonary drug formulations*. Pharmacol Ther, 2014. 144(3): p. 235–52.
42. X. Murgia, et al., *The role of mucus on drug transport and its potential to affect therapeutic outcomes*. Adv Drug Deliv Rev, 2018. 124: p. 82–97.
43. K.R. Atanasova and L.R. Reznikov, *Strategies for measuring airway mucus and mucins*. Respir Res, 2019. 20(1): p. 261.
44. H.H. Sigurdsson, et al., *Mucus as a barrier to lipophilic drugs*. Int J Pharm, 2013. 453(1): p. 56–64.
45. A.W. Ng, et al., *Innate host defense of the lung: effects of lung-lining fluid pH*. Lung, 2004. 182(5): p. 297–317.
46. C.A. Ruge, et al., *The interplay of lung surfactant proteins and lipids assimilates the macrophage clearance of nanoparticles*. PLoS One, 2012. 7(7): p. e40775.
47. W. Bernhard, *Lung surfactant: Function and composition in the context of development and respiratory physiology*. Ann Anat, 2016. 208: p. 146–150.

48. J. Liekkinen, et al., *Surfactant Proteins SP-B and SP-C in Pulmonary Surfactant Monolayers: Physical Properties Controlled by Specific Protein-Lipid Interactions*. Langmuir, 2023. 39(12): p. 4338–4350.
49. A.C. Kirby, et al., *Alveolar macrophages transport pathogens to lung draining lymph nodes*. J Immunol, 2009. 183(3): p. 1983–9.
50. M.J. Reasor, et al., *Drug-induced phospholipidosis: issues and future directions*. Expert Opin Drug Saf, 2006. 5(4): p. 567–83.
51. K. Togami, et al., *Subcellular distribution of azithromycin and clarithromycin in rat alveolar macrophages (NR8383) in vitro*. Biol Pharm Bull, 2013. 36(9): p. 1494–9.
52. A.M. Copenhaver, et al., *Alveolar macrophages and neutrophils are the primary reservoirs for Legionella pneumophila and mediate cytosolic surveillance of type IV secretion*. Infect Immun, 2014. 82(10): p. 4325–36.
53. A. Ufuk, et al., *In Vitro and in Silico Tools To Assess Extent of Cellular Uptake and Lysosomal Sequestration of Respiratory Drugs in Human Alveolar Macrophages*. Mol Pharm, 2017. 14(4): p. 1033–1046.
54. P. Butler and R.J. Riley, *In Vitro ADME Assays and In Vivo Extrapolations*, in *The ADME Encyclopedia*, A. Talevi, Editor. 2022, Springer, Cham.
55. K. Schroeder, et al., *Report from the EPAA workshop: in vitro ADME in safety testing used by EPAA industry sectors*. Toxicol In Vitro, 2011. 25(3): p. 589–604.
56. P. Artursson and J. Karlsson, *Correlation between oral drug absorption in humans and apparent drug permeability coefficients in human intestinal epithelial (Caco-2) cells*. Biochem Biophys Res Commun, 1991. 175(3): p. 880–5.
57. P. Artursson, et al., *Caco-2 monolayers in experimental and theoretical predictions of drug transport*. Adv Drug Deliv Rev, 2001. 46(1-3): p. 27–43.
58. E.C. Sherer, et al., *QSAR Prediction of Passive Permeability in the LLC-PK1 Cell Line: Trends in Molecular Properties and Cross-Prediction of Caco-2 Permeabilities*. Mol Inform, 2012. 31(3-4): p. 231–45.
59. H. Atkinson, et al., *Drug Permeability and Transporter Assessment: Polarized Cell Lines*, in *The ADME Encyclopedia*, A.e. Talevi, Editor. 2022, Springer, Cham. p. 1–13.
60. H.X. Ong, et al., *Pharmaceutical applications of the Calu-3 lung epithelia cell line*. Expert Opin Drug Deliv, 2013. 10(9): p. 1287–302.
61. N. Sibinovska, et al., *Suitability and functional characterization of two Calu-3 cell models for prediction of drug permeability across the airway epithelial barrier*. Int J Pharm, 2020. 585: p. 119484.
62. M. Hittinger, et al., *Preclinical safety and efficacy models for pulmonary drug delivery of antimicrobials with focus on in vitro models*. Adv Drug Deliv Rev, 2015. 85: p. 44–56.
63. R. Bhowmick and H. Gappa-Fahlenkamp, *Cells and Culture Systems Used to Model the Small Airway Epithelium*. Lung, 2016. 194(3): p. 419–28.
64. S. Fuchs, et al., *Differentiation of human alveolar epithelial cells in primary culture: morphological characterization and synthesis of caveolin-1 and surfactant protein-C*. Cell Tissue Res, 2003. 311(1): p. 31–45.
65. R.E. Rayner, et al., *Optimization of Normal Human Bronchial Epithelial (NHBE) Cell 3D Cultures for in vitro Lung Model Studies*. Sci Rep, 2019. 9(1): p. 500.
66. P.S. Hiemstra, et al., *Airway and alveolar epithelial cells in culture*. Eur Respir J, 2019. 54(5).
67. A.J. Miller and J.R. Spence, *In Vitro Models to Study Human Lung Development, Disease and Homeostasis*. Physiology (Bethesda), 2017. 32(3): p. 246–260.
68. N.J. Darling, et al., *Bioengineering Novel in vitro Co-culture Models That Represent the Human Intestinal Mucosa With Improved Caco-2 Structure and Barrier Function*. Front Bioeng Biotechnol, 2020. 8: p. 992.

69. J.L. Harcourt and L.M. Haynes, *Establishing a liquid-covered culture of polarized human airway epithelial Calu-3 cells to study host cell response to respiratory pathogens in vitro.* J Vis Exp, 2013(72).
70. S. Upadhyay and L. Palmberg, *Air-Liquid Interface: Relevant In Vitro Models for Investigating Air Pollutant-Induced Pulmonary Toxicity.* Toxicol Sci, 2018. 164(1): p. 21–30.
71. B. Forbes, *Human airway epithelial cell lines for in vitro drug transport and metabolism studies.* Pharm Sci Technol Today, 2000. 3(1): p. 18–27.
72. L. Gonzalez-Mariscal, et al., *Critical role of tight junctions in drug delivery across epithelial and endothelial cell layers.* J Membr Biol, 2005. 207(2): p. 55–68.
73. B. Srinivasan, et al., *TEER measurement techniques for in vitro barrier model systems.* J Lab Autom, 2015. 20(2): p. 107–26.
74. M.A. Selo, et al., *Tobacco Smoke and Inhaled Drugs Alter Expression and Activity of Multidrug Resistance-Associated Protein-1 (MRP1) in Human Distal Lung Epithelial Cells in vitro.* Front Bioeng Biotechnol, 2020. 8: p. 1030.
75. B.B. Karakocak, et al., *Rethinking of TEER measurement reporting for epithelial cells grown on permeable inserts.* Eur J Pharm Sci, 2023. 188: p. 106511.
76. W. Zhao, et al., *Lucifer Yellow - A Robust Paracellular Permeability Marker in a Cell Model of the Human Blood-brain Barrier.* J Vis Exp, 2019(150).
77. S. Silva, et al., *Air-liquid interface (ALI) impact on different respiratory cell cultures.* Eur J Pharm Biopharm, 2023. 184: p. 62–82.
78. A. Poirier, et al., *Calibration of in vitro multidrug resistance protein 1 substrate and inhibition assays as a basis to support the prediction of clinically relevant interactions in vivo.* Drug Metab Dispos, 2014. 42(9): p. 1411–22.
79. M.E. Kreft, et al., *The characterization of the human cell line Calu-3 under different culture conditions and its use as an optimized in vitro model to investigate bronchial epithelial function.* Eur J Pharm Sci, 2015. 69: p. 1–9.
80. C. Richter, et al., *Chapter 3.5 - Cell-based in vitro models for pulmonary permeability studies*, in *Concepts and Models for Drug Permeability Studies (2nd Edition)*, B. Sarmento, et al., Editors. 2024, Woodhead Publishing. p. 137–168.
81. P.J. Callaghan, et al., *Epithelial barrier function properties of the 16HBE14o- human bronchial epithelial cell culture model.* Biosci Rep, 2020. 40(10).
82. C. Ehrhardt, et al., *Influence of apical fluid volume on the development of functional intercellular junctions in the human epithelial cell line 16HBE14o-: implications for the use of this cell line as an in vitro model for bronchial drug absorption studies.* Cell Tissue Res, 2002. 308(3): p. 391–400.
83. B. Forbes, et al., *The human bronchial epithelial cell line 16HBE14o- as a model system of the airways for studying drug transport.* Int J Pharm, 2003. 257(1-2): p. 161–7.
84. C. Ehrhardt, et al., *Salbutamol is actively absorbed across human bronchial epithelial cell layers.* Pulm Pharmacol Ther, 2005. 18(3): p. 165–70.
85. C. Ehrhardt, et al., *16HBE14o- human bronchial epithelial cell layers express P-glycoprotein, lung resistance-related protein, and caveolin-1.* Pharm Res, 2003. 20(4): p. 545–51.
86. C.I. Grainger, et al., *Culture of Calu-3 cells at the air interface provides a representative model of the airway epithelial barrier.* Pharm Res, 2006. 23(7): p. 1482–90.
87. B.M. Rotoli, et al., *Characterization of ABC Transporters in EpiAirway, a Cellular Model of Normal Human Bronchial Epithelium.* Int J Mol Sci, 2020. 21(9).
88. M. Mukherjee, et al., *In-cell Western detection of organic cation transporters in bronchial epithelial cell layers cultured at an air-liquid interface on Transwell((R)) inserts.* J Pharmacol Toxicol Methods, 2013. 68(2): p. 184–189.
89. H. Lin, et al., *Air-liquid interface (ALI) culture of human bronchial epithelial cell monolayers as an in vitro model for airway drug transport studies.* J Pharm Sci, 2007. 96(2): p. 341–50.

90. X. Cao, et al., *Invited review: human air-liquid-interface organotypic airway tissue models derived from primary tracheobronchial epithelial cells-overview and perspectives*. In Vitro Cell Dev Biol Anim, 2021. 57(2): p. 104–132.
91. K.A. Min, et al., *Human Airway Primary Epithelial Cells Show Distinct Architectures on Membrane Supports Under Different Culture Conditions*. Cell Biochem Biophys, 2016. 74(2): p. 191–203.
92. K.A. Min, et al., *Functional and cytometric examination of different human lung epithelial cell types as drug transport barriers*. Arch Pharm Res, 2016. 39(3): p. 359–69.
93. H. Ren, et al., *An Optimised Human Cell Culture Model for Alveolar Epithelial Transport*. PLoS One, 2016. 11(10): p. e0165225.
94. J.J. Salomon, et al., *The cell line NCI-H441 is a useful in vitro model for transport studies of human distal lung epithelial barrier*. Mol Pharm, 2014. 11(3): p. 995–1006.
95. W. Neuhaus, et al., *Lung endothelial cells strengthen, but brain endothelial cells weaken barrier properties of a human alveolar epithelium cell culture model*. Differentiation, 2012. 84(4): p. 294–304.
96. M.I. Hermanns, et al., *Lung epithelial cell lines in coculture with human pulmonary microvascular endothelial cells: development of an alveolo-capillary barrier in vitro*. Lab Invest, 2004. 84(6): p. 736–52.
97. F. Kielgast, et al., *Glucocorticoids Regulate Tight Junction Permeability of Lung Epithelia by Modulating Claudin 8*. Am J Respir Cell Mol Biol, 2016. 54(5): p. 707–17.
98. K.A. Foster, et al., *Characterization of the A549 cell line as a type II pulmonary epithelial cell model for drug metabolism*. Exp Cell Res, 1998. 243(2): p. 359–66.
99. H. Barosova, et al., *Inter-laboratory variability of A549 epithelial cells grown under submerged and air-liquid interface conditions*. Toxicol In Vitro, 2021: p. 105178.
100. J.J. Salomon and C. Ehrhardt, *Nanoparticles attenuate P-glycoprotein/MDR1 function in A549 human alveolar epithelial cells*. Eur J Pharm Biopharm, 2011. 77(3): p. 392–7.
101. J.J. Salomon, et al., *Organic cation transporter function in different in vitro models of human lung epithelium*. Eur J Pharm Sci, 2015. 80: p. 82–8.
102. E. Moschini, et al., *The modality of cell-particle interactions drives the toxicity of nanosized CuO and TiO(2) in human alveolar epithelial cells*. Toxicol Lett, 2013. 222(2): p. 102–16.
103. E.L. Roggen, et al., *Respiratory immunotoxicity: an in vitro assessment*. Toxicol In Vitro, 2006. 20(8): p. 1249–64.
104. Z. Enlo-Scott, et al., *Drug metabolism in the lungs: opportunities for optimising inhaled medicines*. Expert Opin Drug Metab Toxicol, 2021. 17(5): p. 611–625.
105. A. Kuehn, et al., *Human alveolar epithelial cells expressing tight junctions to model the air-blood barrier*. ALTEX, 2016. 33(3): p. 251–60.
106. S. Kletting, et al., *Co-culture of human alveolar epithelial (hAELVi) and macrophage (THP-1) cell lines*. ALTEX, 2018. 35(2): p. 211–222.
107. P. Carius, et al., *A Monoclonal Human Alveolar Epithelial Cell Line ("Arlo") with Pronounced Barrier Function for Studying Drug Permeability and Viral Infections*. Adv Sci (Weinh), 2023. 10(8): p. e2207301.
108. R. Visigalli, et al., *Expression and Function of ABC Transporters in Human Alveolar Epithelial Cells*. Biomolecules, 2022. 12(9).
109. K.J. Elbert, et al., *Monolayers of human alveolar epithelial cells in primary culture for pulmonary absorption and transport studies*. Pharm Res, 1999. 16(5): p. 601–8.
110. N. Daum, et al., *Isolation, cultivation, and application of human alveolar epithelial cells*. Methods Mol Biol, 2012. 806: p. 31–42.
111. S. Endter, et al., *P-glycoprotein (MDR1) functional activity in human alveolar epithelial cell monolayers*. Cell Tissue Res, 2007. 328(1): p. 77–84.
112. A. Barilli, et al., *Organic cation transporters (OCTs/OCTNs) in human primary alveolar epithelial cells*. Biochem Biophys Res Commun, 2021. 576: p. 27–32.

113. P. Mukherjee, et al., *Role of animal models in biomedical research: a review.* Lab Anim Res, 2022. 38(1): p. 18.
114. D. Andes and W.A. Craig, *Animal model pharmacokinetics and pharmacodynamics: a critical review.* Int J Antimicrob Agents, 2002. 19(4): p. 261–8.
115. C. Tang and T. Prueksaritanont, *Use of in vivo animal models to assess pharmacokinetic drug-drug interactions.* Pharm Res, 2010. 27(9): p. 1772–87.
116. L.S. Schanker, et al., *Species comparison of drug absorption from the lung after aerosol inhalation or intratracheal injection.* Drug Metab Dispos, 1986. 14(1): p. 79–88.
117. L.S. Schanker, et al., *Pulmonary absorption of drugs in the dog: comparison with other species.* Pharmacology, 1986. 32(3): p. 176–80.
118. A.V. Gontijo, et al., *Biopharmaceutical characterization of nebulized antimicrobial agents in rats: 2. Colistin.* Antimicrob Agents Chemother, 2014. 58(7): p. 3950–6.
119. M. Sakagami, *In vivo, in vitro and ex vivo models to assess pulmonary absorption and disposition of inhaled therapeutics for systemic delivery.* Adv Drug Deliv Rev, 2006. 58(9-10): p. 1030–60.
120. M. Sakagami, *In vitro, ex vivo and in vivo methods of lung absorption for inhaled drugs.* Adv Drug Deliv Rev, 2020. 161-162: p. 63–74.
121. A.H. Schinkel, et al., *Normal viability and altered pharmacokinetics in mice lacking mdr1-type (drug-transporting) P-glycoproteins.* Proc Natl Acad Sci U S A, 1997. 94(8): p. 4028–33.
122. S. Cisternino, et al., *Expression, up-regulation, and transport activity of the multidrug-resistance protein Abcg2 at the mouse blood-brain barrier.* Cancer Res, 2004. 64(9): p. 3296–301.
123. S. Mairinger, et al., *Nuclear medicine imaging methods as novel tools in the assessment of pulmonary drug disposition.* Expert Opin Drug Deliv, 2022. 19(12): p. 1561–1575.
124. I. Hernandez-Lozano, et al., *Influence of ABC transporters on the excretion of ciprofloxacin assessed with PET imaging in mice.* Eur J Pharm Sci, 2021. 163: p. 105854.
125. O. Langer, *Use of PET Imaging to Evaluate Transporter-Mediated Drug-Drug Interactions.* J Clin Pharmacol, 2016. 56 Suppl 7: p. S143–56.
126. J. Rong, et al., *Radiochemistry for positron emission tomography.* Nat Commun, 2023. 14(1): p. 3257.
127. G. Al-Jayyoussi, et al., *Absorption of ipratropium and l-carnitine into the pulmonary circulation of the ex-vivo rat lung is driven by passive processes rather than active uptake by OCT/OCTN transporters.* Int J Pharm, 2015. 496(2): p. 834–41.
128. G. Al-Jayyoussi, et al., *Selectivity in the impact of P-glycoprotein upon pulmonary absorption of airway-dosed substrates: a study in ex vivo lung models using chemical inhibition and genetic knockout.* J Pharm Sci, 2013. 102(9): p. 3382–94.
129. W.T. Poh and J. Stanslas, *The new paradigm in animal testing - "3Rs alternatives".* Regul Toxicol Pharmacol, 2024. 153: p. 105705.
130. X. Zhuang and C. Lu, *PBPK modeling and simulation in drug research and development.* Acta Pharm Sin B, 2016. 6(5): p. 430–440.
131. H. Jones and K. Rowland-Yeo, *Basic concepts in physiologically based pharmacokinetic modeling in drug discovery and development.* CPT Pharmacometrics Syst Pharmacol, 2013. 2: p. e63.
132. H.J. Ryu, et al., *A compatibility evaluation between the physiologically based pharmacokinetic (PBPK) model and the compartmental PK model using the lumping method with real cases.* Front Pharmacol, 2022. 13: p. 964049.
133. M.A. Cabrera-Perez and H. Pham-The, *Computational modeling of human oral bioavailability: what will be next?* Expert Opin Drug Discov, 2018. 13(6): p. 509–521.
134. L. Kuepfer, et al., *Applied Concepts in PBPK Modeling: How to Build a PBPK/PD Model.* CPT Pharmacometrics Syst Pharmacol, 2016. 5(10): p. 516–531.

135. H.M. Jones, et al., *Physiologically based pharmacokinetic modeling in drug discovery and development: a pharmaceutical industry perspective.* Clin Pharmacol Ther, 2015. 97(3): p. 247–62.
136. Z. Sun, et al., *Application of physiologically based pharmacokinetic modeling of novel drugs approved by the U.S. food and drug administration.* Eur J Pharm Sci, 2024. 200: p. 106838.
137. N.A. Miller, et al., *Physiologically Based Pharmacokinetic Modelling of Inhaled Nemiralisib: Mechanistic Components for Pulmonary Absorption, Systemic Distribution, and Oral Absorption.* Clin Pharmacokinet, 2022. 61(2): p. 281–293.
138. E. Karakitsios and A. Dokoumetzidis, *Extrapolation of lung pharmacokinetics of antitubercular drugs from preclinical species to humans using PBPK modelling.* J Antimicrob Chemother, 2024. 79(6): p. 1362–1371.
139. K. Rowland Yeo, et al., *Impact of Disease on Plasma and Lung Exposure of Chloroquine, Hydroxychloroquine and Azithromycin: Application of PBPK Modeling.* Clin Pharmacol Ther, 2020. 108(5): p. 976–984.
140. L.B.S. Aulin, et al., *Physiologically Based Modelling Framework for Prediction of Pulmonary Pharmacokinetics of Antimicrobial Target Site Concentrations.* Clin Pharmacokinet, 2022. 61(12): p. 1735–1748.
141. L. Gaohua, et al., *Development of a Multicompartment Permeability-Limited Lung PBPK Model and Its Application in Predicting Pulmonary Pharmacokinetics of Antituberculosis Drugs.* CPT Pharmacometrics Syst Pharmacol, 2015. 4(10): p. 605–13.
142. W. Wang and D. Ouyang, *Opportunities and challenges of physiologically based pharmacokinetic modeling in drug delivery.* Drug Discov Today, 2022. 27(8): p. 2100–2120.
143. L. Knudsen and M. Ochs, *The micromechanics of lung alveoli: structure and function of surfactant and tissue components.* Histochem Cell Biol, 2018. 150(6): p. 661–676.
144. J.K. Hennigs, et al., *Vascular Endothelial Cells: Heterogeneity and Targeting Approaches.* Cells, 2021. 10(10).
145. K. Sugano, et al., *Coexistence of passive and carrier-mediated processes in drug transport.* Nat Rev Drug Discov, 2010. 9(8): p. 597–614.
146. M. Gumbleton, et al., *Spatial expression and functionality of drug transporters in the intact lung: objectives for further research.* Adv Drug Deliv Rev, 2011. 63(1-2): p. 110–8.
147. E. Cocucci, et al., *Role of Passive Diffusion, Transporters, and Membrane Trafficking-Mediated Processes in Cellular Drug Transport.* Clin Pharmacol Ther, 2017. 101(1): p. 121–129.
148. N. Noureddine, et al., *The Role of Defective Epithelial Barriers in Allergic Lung Disease and Asthma Development.* J Asthma Allergy, 2022. 15: p. 487–504.
149. H.E. Nilsson, et al., *CFTR and tight junctions in cultured bronchial epithelial cells.* Exp Mol Pathol, 2010. 88(1): p. 118–27.
150. A. Khalil, et al., *Enhancing paracellular and transcellular permeability using nanotechnological approaches for the treatment of brain and retinal diseases.* Nanoscale Horiz, 2023. 9(1): p. 14–43.
151. S. Menard, et al., *Multiple facets of intestinal permeability and epithelial handling of dietary antigens.* Mucosal Immunol, 2010. 3(3): p. 247–59.
152. G. Camenisch, et al., *Estimation of permeability by passive diffusion through Caco-2 cell monolayers using the drugs' lipophilicity and molecular weight.* Eur J Pharm Sci, 1998. 6(4): p. 317–24.
153. L. Gaohua, et al., *Crosstalk of physiological pH and chemical pKa under the umbrella of physiologically based pharmacokinetic modeling of drug absorption, distribution, metabolism, excretion, and toxicity.* Expert Opin Drug Metab Toxicol, 2021. 17(9): p. 1103–1124.
154. S. Wilkens, *Structure and mechanism of ABC transporters.* F1000Prime Rep, 2015. 7: p. 14.

155. X. Liu, *SLC Family Transporters*. Adv Exp Med Biol, 2019. 1141: p. 101–202.
156. J. Keemink, et al., *Estimating Unbound Drug Concentrations in Simulated Human Lung Fluid: Relevance to Lung Antibiotic PKPD*. Mol Pharm, 2023. 20(7): p. 3578–3588.
157. S.G. Summerfield, et al., *Free Drug Theory - No Longer Just a Hypothesis?* Pharm Res, 2022. 39(2): p. 213–222.
158. L.M. Berezhkovskiy, *On the influence of protein binding on pharmacological activity of drugs*. J Pharm Sci, 2010. 99(4): p. 2153–65.
159. L. Di, *An update on the importance of plasma protein binding in drug discovery and development*. Expert Opin Drug Discov, 2021. 16(12): p. 1453–1465.
160. E. Hann, et al., *The importance of plasma protein and tissue binding in a drug discovery program to successfully deliver a preclinical candidate.* Prog Med Chem, 2022. 61: p. 163–214.
161. C. Bissantz, et al., *Translational PK/PD for the Development of Novel Antibiotics-A Drug Developer's Perspective*. Antibiotics (Basel), 2024. 13(1).
162. E. Backstrom, et al., *Possible Extraction of Drugs from Lung Tissue During Bronchoalveolar Lavage Suggest Uncertainty in the Procedure's Utility for Quantitative Assessment of Airway Drug Exposure*. J Pharm Sci, 2022. 111(3): p. 852–858.
163. K. Ohya, et al., *In Vitro Mechanistic Study of the Distribution of Lascufloxacin into Epithelial Lining Fluid*. Antimicrob Agents Chemother, 2019. 63(4).
164. S. Jones, *Permeability rules for antibiotic design*. Nat Biotechnol, 2017. 35(7): p. 639.
165. X. Lu, et al., *Ion channels and transporters regulate nutrient absorption in health and disease*. J Cell Mol Med, 2023. 27(18): p. 2631–2642.
166. L.M. Koehn, *ABC Transporters: An Overview*, in *The ADME Encyclopedia*, A. Talevi, Editor. 2022, Springer, Cham.
167. G. Cooper, *Transport of Small Molecules*, in *The Cell: A Molecular Approach. 2nd edition*. 2000, Sunderland (MA): Sinauer Associates.
168. A. Talevi and C.L. Bellera, *Active and Facilitated Transport in Drug Absorption*, in *The ADME Encyclopedia*, A. Talevi, Editor. 2022, Springer, Cham.
169. G. You and M.E. Morris, *Overview of Drug Transporter Families*, in *Drug Transporters: Molecular Characterization and Role in Drug Disposition, Second Edition*, G. You and M.E. Morris, Editors. 2014, John Wiley & Sons, Inc. p. 1–6.
170. A. Galetin, et al., *Membrane transporters in drug development and as determinants of precision medicine*. Nat Rev Drug Discov, 2024. 23(4): p. 255–280.
171. K.R. Lee, et al., *Findings on In Vitro Transporter-Mediated Drug Interactions and Their Follow-Up Actions for Labeling: Analysis of Drugs Approved by US FDA between 2017 and 2021*. Pharmaceutics, 2022. 14(10).
172. B. Hagenbuch and P.J. Meier, *Organic anion transporting polypeptides of the OATP/ SLC21 family: phylogenetic classification as OATP/ SLCO superfamily, new nomenclature and molecular/functional properties*. Pflugers Arch, 2004. 447(5): p. 653–65.
173. F. Muller and M.F. Fromm, *Transporter-mediated drug-drug interactions*. Pharmacogenomics, 2011. 12(7): p. 1017–37.
174. P. Borst and A.H. Schinkel, *P-glycoprotein ABCB1: a major player in drug handling by mammals*. J Clin Invest, 2013. 123(10): p. 4131–3.
175. Y. Wang, et al., *Efflux ABC transporters in drug disposition and their posttranscriptional gene regulation by microRNAs*. Front Pharmacol, 2024. 15: p. 1423416.
176. A. Sajid, et al., *Advances in the structure, mechanism and targeting of chemoresistance-linked ABC transporters*. Nat Rev Cancer, 2023. 23(11): p. 762–779.
177. S. Nickel, et al., *Transport mechanisms at the pulmonary mucosa: implications for drug delivery.* Expert Opin Drug Deliv, 2016. 13(5): p. 667–90.
178. R. Elsby, et al., *Studying the right transporter at the right time: an in vitro strategy for assessing drug-drug interaction risk during drug discovery and development*. Expert Opin Drug Metab Toxicol, 2022. 18(10): p. 619–655.

179. M. Natoli, et al., *Good Caco-2 cell culture practices.* Toxicol In Vitro, 2012. 26(8): p. 1243–6.
180. A. Doryab and O. Schmid, *Towards a gold standard functional readout to characterize In Vitro lung barriers.* Eur J Pharm Sci, 2022. 179: p. 106305.
181. I. Hubatsch, et al., *Determination of drug permeability and prediction of drug absorption in Caco-2 monolayers.* Nat Protoc, 2007. 2(9): p. 2111–9.
182. S. Simon, et al., *The role of ABC transporters in the human lung epithelium—insights from and limitations of current in vitro cell models.* In vitro models, 2025.
183. J. Pasquier, et al., *P-glycoprotein-activity measurements in multidrug resistant cell lines: single-cell versus single-well population fluorescence methods.* Biomed Res Int, 2013. 2013: p. 676845.
184. C. Ozvegy-Laczka, et al., *Fluorescence-based methods for studying activity and drug-drug interactions of hepatic solute carrier and ATP binding cassette proteins involved in ADME-Tox.* Biochem Pharmacol, 2023. 209: p. 115448.
185. O. Legrand, et al., *Pgp and MRP activities using calcein-AM are prognostic factors in adult acute myeloid leukemia patients.* Blood, 1998. 91(12): p. 4480–8.
186. M. Galetti, et al., *Effect of ABCG2/BCRP Expression on Efflux and Uptake of Gefitinib in NSCLC Cell Lines.* PLoS One, 2015. 10(11): p. e0141795.
187. A. Sakamoto, et al., *Quantitative expression of human drug transporter proteins in lung tissues: analysis of regional, gender, and interindividual differences by liquid chromatography-tandem mass spectrometry.* J Pharm Sci, 2013. 102(9): p. 3395–406.
188. K.M. Hanssen, et al., *Targeting multidrug resistance-associated protein 1 (MRP1)-expressing cancers: Beyond pharmacological inhibition.* Drug Resist Updat, 2021. 59: p. 100795.
189. R.L. Juliano and V. Ling, *A surface glycoprotein modulating drug permeability in Chinese hamster ovary cell mutants.* Biochim Biophys Acta, 1976. 455(1): p. 152–62.
190. C. Karthika, et al., *Multidrug Resistance of Cancer Cells and the Vital Role of P-Glycoprotein.* Life (Basel), 2022. 12(6).
191. C. Pilotto Heming, et al., *P-glycoprotein and cancer: what do we currently know?* Heliyon, 2022. 8(10): p. e11171.
192. M.M. Gottesman and I.H. Pastan, *The Role of Multidrug Resistance Efflux Pumps in Cancer: Revisiting a JNCI Publication Exploring Expression of the MDR1 (P-glycoprotein) Gene.* J Natl Cancer Inst, 2015. 107(9).
193. M. Nishimura and S. Naito, *Tissue-specific mRNA expression profiles of human ATP-binding cassette and solute carrier transporter superfamilies.* Drug Metab Pharmacokinet, 2005. 20(6): p. 452–77.
194. A. Sakamoto, et al., *Drug Transporter Protein Quantification of Immortalized Human Lung Cell Lines Derived from Tracheobronchial Epithelial Cells (Calu-3 and BEAS2-B), Bronchiolar-Alveolar Cells (NCI-H292 and NCI-H441), and Alveolar Type II-like Cells (A549) by Liquid Chromatography-Tandem Mass Spectrometry.* J Pharm Sci, 2015. 104(9): p. 3029–38.
195. S. Endter, et al., *RT-PCR analysis of ABC, SLC and SLCO drug transporters in human lung epithelial cell models.* J Pharm Pharmacol, 2009. 61(5): p. 583–91.
196. M. Haghi, et al., *Time- and passage-dependent characteristics of a Calu-3 respiratory epithelial cell model.* Drug Dev Ind Pharm, 2010. 36(10): p. 1207–14.
197. E. Jouan, et al., *The mitochondrial fluorescent dye rhodamine 123 is a high-affinity substrate for organic cation transporters (OCTs) 1 and 2.* Fundam Clin Pharmacol, 2014. 28(1): p. 65–77.
198. R. Ohashi, et al., *Molecular and physiological evidence for multifunctionality of carnitine/organic cation transporter OCTN2.* Mol Pharmacol, 2001. 59(2): p. 358–66.

199. H. Koepsell, *Update on drug-drug interaction at organic cation transporters: mechanisms, clinical impact, and proposal for advanced in vitro testing*. Expert Opin Drug Metab Toxicol, 2021. 17(6): p. 635–653.
200. E.M. Leslie, et al., *Multidrug resistance proteins: role of P-glycoprotein, MRP1, MRP2, and BCRP (ABCG2) in tissue defense*. Toxicol Appl Pharmacol, 2005. 204(3): p. 216–37.
201. V. Hutter, et al., *Digoxin net secretory transport in bronchial epithelial cell layers is not exclusively mediated by P-glycoprotein/MDR1*. Eur J Pharm Biopharm, 2014. 86(1): p. 74–82.
202. J.C. Taylor, et al., *The equilibrium and kinetic drug binding properties of the mouse P-gp1a and P-gp1b P-glycoproteins are similar*. Br J Cancer, 1999. 81(5): p. 783–9.
203. J.M. Brady, et al., *Tissue distribution and chemical induction of multiple drug resistance genes in rats*. Drug Metab Dispos, 2002. 30(7): p. 838–44.
204. Y.J. Cui, et al., *Tissue distribution, gender-divergent expression, ontogeny, and chemical induction of multidrug resistance transporter genes (Mdr1a, Mdr1b, Mdr2) in mice*. Drug Metab Dispos, 2009. 37(1): p. 203–10.
205. D.F. Price, et al., *The Differential Absorption of a Series of P-Glycoprotein Substrates in Isolated Perfused Lungs from Mdr1a/1b Genetic Knockout Mice can be Attributed to Distinct Physico-Chemical Properties: an Insight into Predicting Transporter-Mediated, Pulmonary Specific Disposition*. Pharm Res, 2017. 34(12): p. 2498–2516.
206. S. Mairinger, et al., *Influence of P-glycoprotein on pulmonary disposition of the model substrate [(11)C]metoclopramide assessed by PET imaging in rats*. Eur J Pharm Sci, 2023. 183: p. 106404.
207. I. Hernandez-Lozano, et al., *PET imaging to assess the impact of P-glycoprotein on pulmonary drug delivery in rats*. J Control Release, 2022. 342: p. 44–52.
208. M.J. Flens, et al., *Tissue distribution of the multidrug resistance protein*. Am J Pathol, 1996. 148(4): p. 1237–47.
209. S.P. Cole, *Targeting multidrug resistance protein 1 (MRP1, ABCC1): past, present, and future*. Annu Rev Pharmacol Toxicol, 2014. 54: p. 95–117.
210. S.P. Cole, *Multidrug resistance protein 1 (MRP1, ABCC1), a "multitasking" ATP-binding cassette (ABC) transporter*. J Biol Chem, 2014. 289(45): p. 30880–8.
211. S.P. Cole and R.G. Deeley, *Transport of glutathione and glutathione conjugates by MRP1*. Trends Pharmacol Sci, 2006. 27(8): p. 438–46.
212. P. Borst, et al., *A family of drug transporters: the multidrug resistance-associated proteins*. J Natl Cancer Inst, 2000. 92(16): p. 1295–302.
213. M. van der Deen, et al., *Diminished expression of multidrug resistance-associated protein 1 (MRP1) in bronchial epithelium of COPD patients*. Virchows Arch, 2006. 449(6): p. 682–8.
214. M. van der Deen, et al., *Cigarette smoke extract affects functional activity of MRP1 in bronchial epithelial cells*. J Biochem Mol Toxicol, 2007. 21(5): p. 243–51.
215. J.A. Sake, et al., *Knockout of ABCC1 in NCI-H441 cells reveals CF to be a suboptimal substrate to study MRP1 activity in organotypic in vitro models*. Eur J Pharm Sci, 2022. 181: p. 106364.
216. K. Alam, et al., *Regulation of Organic Anion Transporting Polypeptides (OATP) 1B1- and OATP1B3-Mediated Transport: An Updated Review in the Context of OATP-Mediated Drug-Drug Interactions*. Int J Mol Sci, 2018. 19(3).
217. S. Mairinger, et al., *Assessing the Activity of Multidrug Resistance-Associated Protein 1 at the Lung Epithelial Barrier*. J Nucl Med, 2020. 61(11): p. 1650–1657.
218. Q. Mao and J.D. Unadkat, *Role of the breast cancer resistance protein (BCRP/ABCG2) in drug transport--an update*. AAPS J, 2015. 17(1): p. 65–82.
219. L.A. Doyle, et al., *A multidrug resistance transporter from human MCF-7 breast cancer cells*. Proc Natl Acad Sci U S A, 1998. 95(26): p. 15665–70.

220. Z. Ni, et al., *Structure and function of the human breast cancer resistance protein (BCRP/ABCG2)*. Curr Drug Metab, 2010. 11(7): p. 603–17.
221. S. Nickel, et al., *Expression and Activity of Breast Cancer Resistance Protein (BCRP/ABCG2) in Human Distal Lung Epithelial Cells In Vitro*. Pharm Res, 2017. 34(12): p. 2477–2487.
222. D.K. Paturi, et al., *Identification and functional characterization of breast cancer resistance protein in human bronchial epithelial cells (Calu-3)*. Int J Pharm, 2010. 384(1-2): p. 32–8.
223. S. Dey, et al., *Evidence for two nonidentical drug-interaction sites in the human P-glycoprotein*. Proc Natl Acad Sci U S A, 1997. 94(20): p. 10594–9.
224. F. Tang, et al., *Bidirectional transport of rhodamine 123 and Hoechst 33342, fluorescence probes of the binding sites on P-glycoprotein, across MDCK-MDR1 cell monolayers*. J Pharm Sci, 2004. 93(5): p. 1185–94.
225. L.D. Weidner, et al., *The Inhibitor Ko143 Is Not Specific for ABCG2*. J Pharmacol Exp Ther, 2015. 354(3): p. 384–93.
226. Q. Wang, et al., *Application and limitation of inhibitors in drug-transporter interactions studies*. Int J Pharm, 2008. 356(1-2): p. 12–8.
227. S. Mairinger, et al., *Impact of P-gp and BCRP on pulmonary drug disposition assessed by PET imaging in rats*. J Control Release, 2022. 349: p. 109–117.
228. M.A. Salam, et al., *Antimicrobial Resistance: A Growing Serious Threat for Global Public Health*. Healthcare (Basel), 2023. 11(13).
229. B. Loretz, et al., *Drug delivery for fighting infectious diseases: a global perspective*. Drug Deliv Transl Res, 2021. 11(4): p. 1316–1322.
230. Z. Shi, et al., *A Comprehensive Overview of the Antibiotics Approved in the Last Two Decades: Retrospects and Prospects*. Molecules, 2023. 28(4).
231. A.I. Alvarez, et al., *Fluoroquinolone efflux mediated by ABC transporters*. J Pharm Sci, 2008. 97(9): p. 3483–93.
232. J. Brillault, et al., *P-glycoprotein-mediated transport of moxifloxacin in a Calu-3 lung epithelial cell model*. Antimicrob Agents Chemother, 2009. 53(4): p. 1457–62.
233. Y. Zhang, et al., *Detection of Weak Organic Anion-Transporting Polypeptide 1B Inhibition by Probenecid with Plasma-Based Coproporphyrin in Humans*. Drug Metab Dispos, 2020. 48(10): p. 841–848.
234. K. Maeda, et al., *Inhibitory effects of p-aminohippurate and probenecid on the renal clearance of adefovir and benzylpenicillin as probe drugs for organic anion transporter (OAT) 1 and OAT3 in humans*. Eur J Pharm Sci, 2014. 59: p. 94–103.
235. H. Furuie, et al., *Intrapulmonary Pharmacokinetics of Lascufloxacin in Healthy Adult Volunteers*. Antimicrob Agents Chemother, 2018. 62(4).
236. J.I. Pachot, et al., *Experimental estimation of the role of P-Glycoprotein in the pharmacokinetic behaviour of telithromycin, a novel ketolide, in comparison with roxithromycin and other macrolides using the Caco-2 cell model*. J Pharm Pharm Sci, 2003. 6(1): p. 1–12.
237. M. Qadir, et al., *Cyclosporin A is a broad-spectrum multidrug resistance modulator*. Clin Cancer Res, 2005. 11(6): p. 2320–6.
238. M. Labro, *Cellular accumulation of macrolide antibiotics. Intracellular bioactivity*, in *Macrolide Antibiotics. Milestones in Drug Therapy MDT*, W. Schönfeld and H.A. Kirst, Editors. 2022, Birkhäuser, Basel.
239. A. Ufuk, et al., *In Vitro Assessment of Uptake and Lysosomal Sequestration of Respiratory Drugs in Alveolar Macrophage Cell Line NR8383*. Pharm Res, 2015. 32(12): p. 3937–51.
240. K. Togami, et al., *Intracellular pharmacokinetics of telithromycin, a ketolide antibiotic, in alveolar macrophages*. J Pharm Pharmacol, 2010. 62(1): p. 71–5.
241. D. Bednarczyk and M.V. Sanghvi, *The impact of assay recovery on the apparent permeability, a function of lysosomal trapping*. Xenobiotica, 2020. 50(7): p. 753–760.

242. F. Kazmi, et al., *Lysosomal sequestration (trapping) of lipophilic amine (cationic amphiphilic) drugs in immortalized human hepatocytes (Fa2N-4 cells)*. Drug Metab Dispos, 2013. 41(4): p. 897–905.
243. K. Kielbowski, et al., *The Role of ABCB1, ABCG2, and SLC Transporters in Pharmacokinetic Parameters of Selected Drugs and Their Involvement in Drug-Drug Interactions*. Membranes (Basel), 2024. 14(11).
244. A. Sakamoto, et al., *Correlation of Organic Cation/Carnitine Transporter 1 and Multidrug Resistance-Associated Protein 1 Transport Activities With Protein Expression Levels in Primary Cultured Human Tracheal, Bronchial, and Alveolar Epithelial Cells*. J Pharm Sci, 2016. 105(2): p. 876–883.
245. D.C. Rees, et al., *ABC transporters: the power to change*. Nat Rev Mol Cell Biol, 2009. 10(3): p. 218–27.
246. R.G. Deeley and S.P. Cole, *Substrate recognition and transport by multidrug resistance protein 1 (ABCC1)*. FEBS Lett, 2006. 580(4): p. 1103–11.
247. E. Bakos and L. Homolya, *Portrait of multifaceted transporter, the multidrug resistance-associated protein 1 (MRP1/ABCC1)*. Pflugers Arch, 2007. 453(5): p. 621–41.
248. C. Bosquillon, *Drug transporters in the lung--do they play a role in the biopharmaceutics of inhaled drugs?* J Pharm Sci, 2010. 99(5): p. 2240–55.
249. C. Bosquillon, et al., *A Comparison of Drug Transport in Pulmonary Absorption Models: Isolated Perfused rat Lungs, Respiratory Epithelial Cell Lines and Primary Cell Culture*. Pharm Res, 2017. 34(12): p. 2532–2540.
250. F. Manford, et al., *Drug permeability in 16HBE14o- airway cell layers correlates with absorption from the isolated perfused rat lung*. Eur J Pharm Sci, 2005. 26(5): p. 414–20.
251. K. Berube, et al., *Human primary bronchial lung cell constructs: the new respiratory models*. Toxicology, 2010. 278(3): p. 311–8.
252. M. Hittinger, et al., *Autologous co-culture of primary human alveolar macrophages and epithelial cells for investigating aerosol medicines. Part I: model characterisation*. Altern Lab Anim, 2016. 44(4): p. 337–347.
253. C.A. Larregieu and L.Z. Benet, *Drug discovery and regulatory considerations for improving in silico and in vitro predictions that use Caco-2 as a surrogate for human intestinal permeability measurements*. AAPS J, 2013. 15(2): p. 483–97.
254. J. Arnemann, *DNA-/RNA-Konzentrationsbestimmung*, in *Lexikon der Medizinischen Laboratoriumsdiagnostik*, A.M. Gressner, Arndt, T. (eds), Editor. 2019, Springer Reference Medizin. Springer, Berlin, Heidelberg. p. 719.
255. T.D. Schmittgen and K.J. Livak, *Analyzing real-time PCR data by the comparative C(T) method*. Nat Protoc, 2008. 3(6): p. 1101–8.
256. A. Sormunen, et al., *Comparison of Automated and Traditional Western Blotting Methods*. Methods Protoc, 2023. 6(2).
257. K. Dilger, et al., *Identification of budesonide and prednisone as substrates of the intestinal drug efflux pump P-glycoprotein*. Inflamm Bowel Dis, 2004. 10(5): p. 578–83.
258. T. Mikkaichi, et al., *Edoxaban transport via P-glycoprotein is a key factor for the drug's disposition*. Drug Metab Dispos, 2014. 42(4): p. 520–8.
259. X. Chen, et al., *Tetrahydrocannabinol and Its Major Metabolites Are Not (or Are Poor) Substrates or Inhibitors of Human P-Glycoprotein [ATP-Binding Cassette (ABC) B1] and Breast Cancer Resistance Protein (ABCG2)*. Drug Metab Dispos, 2021. 49(10): p. 910–918.
260. H. Fischer, et al., *Calculation of an Apical Efflux Ratio from P-Glycoprotein (P-gp) In Vitro Transport Experiments Shows an Improved Correlation with In Vivo Cerebrospinal Fluid Measurements in Rats: Impact on P-gp Screening and Compound Optimization*. J Pharmacol Exp Ther, 2021. 376(3): p. 322–329.
261. G. Lian, et al., *In vitro Transport Ability of ABCC2 (G1249A) Polymorphic Variant Towards Anticancer Drugs*. Onco Targets Ther, 2020. 13: p. 1413–1419.

262. K.O. Hamilton, et al., *P-glycoprotein efflux pump expression and activity in Calu-3 cells*. J Pharm Sci, 2001. 90(5): p. 647–58.
263. D. Pamies, et al., *Guidance document on Good Cell and Tissue Culture Practice 2.0 (GCCP 2.0)*. ALTEX, 2022. 39: p. 30–70.
264. OECD, *Guidance Document on Good In Vitro Method Practices (GIVIMP)*. OECD Series on Testing and Assessment. Vol. No. 286. 2018: OECD Publishing, Paris.
265. T. Lehmann, et al., *Expression of MRP1 and related transporters in human lung cells in culture*. Toxicology, 2001. 167(1): p. 59–72.
266. S. Roy, et al., *MDR1/P-glycoprotein and MRP-1 mRNA and protein expression in non-small cell lung cancer*. Anticancer Res, 2007. 27(3A): p. 1325–30.
267. E. Courcot, et al., *Xenobiotic metabolism and disposition in human lung cell models: comparison with in vivo expression profiles*. Drug Metab Dispos, 2012. 40(10): p. 1953–65.
268. C.Q. Xia, et al., *Expression, localization, and functional characteristics of breast cancer resistance protein in Caco-2 cells*. Drug Metab Dispos, 2005. 33(5): p. 637–43.
269. K.A. Min, et al., *The extracellular microenvironment explains variations in passive drug transport across different airway epithelial cell types*. Pharm Res, 2013. 30(8): p. 2118–32.
270. R. Bednarek, *In Vitro Methods for Measuring the Permeability of Cell Monolayers*. Methods Protoc, 2022. 5(1).
271. M.A. Selo, et al., *Organic Cation Transporters in the Lung-Current and Emerging (Patho)Physiological and Pharmacological Concepts*. Int J Mol Sci, 2020. 21(23).
272. V. Shlyonsky, et al., *Differentiation of epithelial Na+ channel function. An in vitro model*. J Biol Chem, 2005. 280(25): p. 24181–7.
273. A. Stentebjerg-Andersen, et al., *Calu-3 cells grown under AIC and LCC conditions: implications for dipeptide uptake and transepithelial transport of substances*. Eur J Pharm Biopharm, 2011. 78(1): p. 19–26.
274. C. Ehrhardt, et al., *Drug absorption by the respiratory mucosa: cell culture models and particulate drug carriers*. J Aerosol Med, 2002. 15(2): p. 131–9.
275. J. Hukkanen, et al., *Induction and regulation of xenobiotic-metabolizing cytochrome P450s in the human A549 lung adenocarcinoma cell line*. Am J Respir Cell Mol Biol, 2000. 22(3): p. 360–6.
276. N. Banerjee, et al., *Differential role of organic anion-transporting polypeptides in estrone-3-sulphate uptake by breast epithelial cells and breast cancer cells*. J Pharmacol Exp Ther, 2012. 342(2): p. 510–9.
277. F. Ingoglia, et al., *Functional characterization of the organic cation transporters (OCTs) in human airway pulmonary epithelial cells*. Biochim Biophys Acta, 2015. 1848(7): p. 1563–72.
278. G. Bajraktari-Sylejmani, et al., *The "specific" P-glycoprotein inhibitor zosuquidar (LY335979) also weakly inhibits human organic cation transporters*. Naunyn Schmiedebergs Arch Pharmacol, 2024.
279. M. Belzer, et al., *Substrate-dependent ligand inhibition of the human organic cation transporter OCT2*. J Pharmacol Exp Ther, 2013. 346(2): p. 300–10.
280. Y.Q. Pan, et al., *The molecular mechanism underlying the induction of hepatic MRP3 expression and function by omeprazole*. Biopharm Drug Dispos, 2015. 36(4): p. 232–44.
281. C. Gedeon, et al., *Transport of glyburide by placental ABC transporters: implications in fetal drug exposure*. Placenta, 2006. 27(11-12): p. 1096–102.
282. H.M. Prime-Chapman, et al., *Differential multidrug resistance-associated protein 1 through 6 isoform expression and function in human intestinal epithelial Caco-2 cells*. J Pharmacol Exp Ther, 2004. 311(2): p. 476–84.
283. Y. Cui, et al., *Drug resistance and ATP-dependent conjugate transport mediated by the apical multidrug resistance protein, MRP2, permanently expressed in human and canine cells*. Mol Pharmacol, 1999. 55(5): p. 929–37.

284. M. Otter, et al., *Expression and Functional Contribution of Different Organic Cation Transporters to the Cellular Uptake of Doxorubicin into Human Breast Cancer and Cardiac Tissue*. Int J Mol Sci, 2021. 23(1).
285. A.K. Ghose and G.M. Crippen, *Atomic physicochemical parameters for three-dimensional-structure-directed quantitative structure-activity relationships. 2. Modeling dispersive and hydrophobic interactions*. J Chem Inf Comput Sci, 1987. 27(1): p. 21–35.
286. P. Pahal, et al., *Typical Bacterial Pneumonia*, in *StatPearls*. 2025: Treasure Island (FL) ineligible companies. Disclosure: Venkat Rajasurya declares no relevant financial relationships with ineligible companies. Disclosure: Sandeep Sharma declares no relevant financial relationships with ineligible companies.
287. G. Merino, et al., *Breast cancer resistance protein (BCRP/ABCG2) transports fluoroquinolone antibiotics and affects their oral availability, pharmacokinetics, and milk secretion*. Drug Metab Dispos, 2006. 34(4): p. 690–5.
288. K. Togami, et al., *Distribution characteristics of clarithromycin and azithromycin, macrolide antimicrobial agents used for treatment of respiratory infections, in lung epithelial lining fluid and alveolar macrophages*. Biopharm Drug Dispos, 2011. 32(7): p. 389–97.
289. K. Togami, et al., *Distribution characteristics of telithromycin, a novel ketolide antimicrobial agent applied for treatment of respiratory infection, in lung epithelial lining fluid and alveolar macrophages*. Drug Metab Pharmacokinet, 2009. 24(5): p. 411–7.
290. I.D. Angelis and L. Turco, *Caco-2 cells as a model for intestinal absorption*. Curr Protoc Toxicol, 2011. Chapter 20: p. Unit20 6.
291. J.D. Irvine, et al., *MDCK (Madin-Darby canine kidney) cells: A tool for membrane permeability screening*. J Pharm Sci, 1999. 88(1): p. 28–33.
292. K. Kuteykin-Teplyakov, et al., *Differences in the expression of endogenous efflux transporters in MDR1-transfected versus wildtype cell lines affect P-glycoprotein mediated drug transport*. Br J Pharmacol, 2010. 160(6): p. 1453–63.
293. P. Anderle, et al., *P-Glycoprotein (P-gp) mediated efflux in Caco-2 cell monolayers: the influence of culturing conditions and drug exposure on P-gp expression levels*. J Pharm Sci, 1998. 87(6): p. 757–62.
294. N.R. Mathia, et al., *Permeability characteristics of calu-3 human bronchial epithelial cells: in vitro-in vivo correlation to predict lung absorption in rats*. J Drug Target, 2002. 10(1): p. 31–40.
295. H.M. Braakhuis, et al., *An Air-liquid Interface Bronchial Epithelial Model for Realistic, Repeated Inhalation Exposure to Airborne Particles for Toxicity Testing*. J Vis Exp, 2020(159).
296. J.M. Byrne, et al., *FDA Public Workshop Summary: Advancing Animal Models for Antibacterial Drug Development*. Antimicrob Agents Chemother, 2020. 65(1).
297. A.V. Gontijo, et al., *Biopharmaceutical characterization of nebulized antimicrobial agents in rats: 1. Ciprofloxacin, moxifloxacin, and grepafloxacin*. Antimicrob Agents Chemother, 2014. 58(7): p. 3942–9.
298. F. Broccatelli, et al., *Application of Mechanistic Multiparameter Optimization and Large-Scale In Vitro to In Vivo Pharmacokinetics Correlations to Small-Molecule Therapeutic Projects*. Mol Pharm, 2024. 21(9): p. 4312–4323.
299. R. Fraczkiewicz, et al., *Best of both worlds: An expansion of the state of the art pK(a) model with data from three industrial partners*. Mol Inform, 2024. 43(10): p. e202400088.
300. K.A. Rodvold, et al., *Penetration of anti-infective agents into pulmonary epithelial lining fluid: focus on antifungal, antitubercular and miscellaneous anti-infective agents*. Clin Pharmacokinet, 2011. 50(11): p. 689–704.
301. G.T. do Vale, et al., *Three Generations of beta-blockers: History, Class Differences and Clinical Applicability*. Curr Hypertens Rev, 2019. 15(1): p. 22–31.

302. K. Wanat, *Biological barriers, and the influence of protein binding on the passage of drugs across them*. Mol Biol Rep, 2020. 47(4): p. 3221–3231.
303. C. Mauvezin and T.P. Neufeld, *Bafilomycin A1 disrupts autophagic flux by inhibiting both V-ATPase-dependent acidification and Ca-P60A/SERCA-dependent autophagosome-lysosome fusion*. Autophagy, 2015. 11(8): p. 1437–8.
304. S.S. Raesch, et al., *Proteomic and Lipidomic Analysis of Nanoparticle Corona upon Contact with Lung Surfactant Reveals Differences in Protein, but Not Lipid Composition*. ACS Nano, 2015. 9(12): p. 11872–85.
305. R. Schwameis, et al., *Effect of pulmonary surfactant on antimicrobial activity in vitro*. Antimicrob Agents Chemother, 2013. 57(10): p. 5151–4.
306. H. Fischer and J.H. Widdicombe, *Mechanisms of acid and base secretion by the airway epithelium*. J Membr Biol, 2006. 211(3): p. 139–50.
307. C. Jorgensen, et al., *Permeability Benchmarking: Guidelines for Comparing in Silico, in Vitro, and in Vivo Measurements*. J Chem Inf Model, 2025. 65(3): p. 1067–1084.
308. S. Ganger and K. Schindowski, *Tailoring Formulations for Intranasal Nose-to-Brain Delivery: A Review on Architecture, Physico-Chemical Characteristics and Mucociliary Clearance of the Nasal Olfactory Mucosa*. Pharmaceutics, 2018. 10(3).
309. Z. Enlo-Scott, et al., *Chapter 10 - Epithelial permeability and drug absorption in the lungs*, in *Inhaled Medicines*, S. Kassinos, et al., Editors. 2021, Academic Press. p. Pages 267–299.
310. D.A. Groneberg, et al., *Distribution and function of the peptide transporter PEPT2 in normal and cystic fibrosis human lung*. Thorax, 2002. 57(1): p. 55–60.
311. M. Takaai, et al., *Pharmacokinetic analysis of transcellular transport of levofloxacin across LLC-PK1 and Caco-2 cell monolayers*. Biol Pharm Bull, 2007. 30(11): p. 2167–72.
312. H.X. Ong, et al., *Ciprofloxacin is actively transported across bronchial lung epithelial cells using a Calu-3 air interface cell model*. Antimicrob Agents Chemother, 2013. 57(6): p. 2535–40.
313. M. Takano, et al., *Functional Expression of PEPT2 in the Human Distal Lung Epithelial Cell Line NCI-H441*. Pharm Res, 2015. 32(12): p. 3916–26.
314. P. Luckner and M. Brandsch, *Interaction of 31 beta-lactam antibiotics with the H+/peptide symporter PEPT2: analysis of affinity constants and comparison with PEPT1*. Eur J Pharm Biopharm, 2005. 59(1): p. 17–24.
315. M.E. Ganapathy, et al., *beta-lactam antibiotics as substrates for OCTN2, an organic cation/carnitine transporter*. J Biol Chem, 2000. 275(3): p. 1699–707.
316. A.C. MacIntyre and D.J. Cutler, *The potential role of lysosomes in tissue distribution of weak bases*. Biopharmaceutics & drug disposition, 1988. 9(6): p. 513–526.
317. E. Backstrom, et al., *Lung Retention by Lysosomal Trapping of Inhaled Drugs Can Be Predicted In Vitro With Lung Slices*. J Pharm Sci, 2016. 105(11): p. 3432–3439.
318. E. Backstrom, et al., *Development of a Novel Lung Slice Methodology for Profiling of Inhaled Compounds*. J Pharm Sci, 2016. 105(2): p. 838–845.
319. T. Rodgers, et al., *Physiologically based pharmacokinetic modeling 1: predicting the tissue distribution of moderate-to-strong bases*. J Pharm Sci, 2005. 94(6): p. 1259–76.
320. T. Rodgers and M. Rowland, *Physiologically based pharmacokinetic modelling 2: predicting the tissue distribution of acids, very weak bases, neutrals and zwitterions*. J Pharm Sci, 2006. 95(6): p. 1238–57.
321. M.J. Holtzman, et al., *Phospholipid fatty acid composition of pulmonary airway epithelial cells: potential substrates for oxygenation*. Biochim Biophys Acta, 1986. 877(3): p. 459–64.
322. T. Rodgers, et al., *Tissue distribution of basic drugs: accounting for enantiomeric, compound and regional differences amongst beta-blocking drugs in rat*. J Pharm Sci, 2005. 94(6): p. 1237–48.

323. J.N. van der Veen, et al., *The critical role of phosphatidylcholine and phosphatidylethanolamine metabolism in health and disease.* Biochim Biophys Acta Biomembr, 2017. 1859(9 Pt B): p. 1558–1572.
324. N. Yata, et al., *Phosphatidylserine as a determinant for the tissue distribution of weakly basic drugs in rats*. Pharm Res, 1990. 7(10): p. 1019–25.
325. G. Nardone, et al., *Phospholipid composition of human gastric mucosa: a study of endoscopic biopsy specimens.* Gut, 1993. 34(4): p. 456–60.
326. V. Nikolasev, *Phospholipid contents and their fatty acid compositions in human embryonic kidney, during development.* Int J Biochem, 1979. 10(5): p. 397–402.
327. R.C. Choudhary, et al., *The Role of Phospholipid Alterations in Mitochondrial and Brain Dysfunction after Cardiac Arrest.* Int J Mol Sci, 2024. 25(9).
328. H. Small, et al., *Measurement of binding of basic drugs to acidic phospholipids using surface plasmon resonance and incorporation of the data into mechanistic tissue composition equations to predict steady-state volume of distribution.* Drug Metab Dispos, 2011. 39(10): p. 1789–93.
329. A. Treyer, et al., *A Cell-Free Approach Based on Phospholipid Characterization for Determination of the Cell Specific Unbound Drug Fraction (f(u,cell)).* Pharm Res, 2019. 36(12): p. 178.
330. A. Kunze, et al., *In vitro-in vivo extrapolation method to predict human renal clearance of drugs.* J Pharm Sci, 2014. 103(3): p. 994–1001.
331. Y. Urakami, et al., *Transcellular transport of creatinine in renal tubular epithelial cell line LLC-PK1*. Drug Metab Pharmacokinet, 2005. 20(3): p. 200–5.
332. T.B. Emran, et al., *Multidrug Resistance in Cancer: Understanding Molecular Mechanisms, Immunoprevention and Therapeutic Approaches.* Front Oncol, 2022. 12: p. 891652.
333. J.M. Warawa, et al., *Validated Preclinical Mouse Model for Therapeutic Testing against Multidrug-Resistant Pseudomonas aeruginosa Strains.* Microbiol Spectr, 2022. 10(5): p. e0269322.
334. L. Campbell, et al., *Constitutive expression of p-glycoprotein in normal lung alveolar epithelium and functionality in primary alveolar epithelial cultures.* J Pharmacol Exp Ther, 2003. 304(1): p. 441–52.
335. A.H. Schinkel, et al., *Multidrug resistance and the role of P-glycoprotein knockout mice.* Eur J Cancer, 1995. 31A(7-8): p. 1295–8.
336. X. Chu, et al., *Species differences in drug transporters and implications for translating preclinical findings to humans.* Expert Opin Drug Metab Toxicol, 2013. 9(3): p. 237–52.
337. S. Jain, et al., *Interspecies comparison of putative ligand binding sites of human, rat and mouse P-glycoprotein*. Eur J Pharm Sci, 2018. 122: p. 134–143.
338. L.F.M. Verscheijden, et al., *Differences in P-glycoprotein activity in human and rodent blood-brain barrier assessed by mechanistic modelling*. Arch Toxicol, 2021. 95(9): p. 3015–3029.
339. N. Colclough, et al., *Species differences in drug plasma protein binding*. Med. Chem. Comm., 2014. 5: p. 963–967.
340. H. Ahmed, et al., *Interspecies differences in Plasma Protein Binding of Beta-Lactam Antibiotics.* Int J Antimicrob Agents, 2025: p. 107476.
341. I. Odenholt, et al., *Pharmacodynamics of telithromycin In vitro against respiratory tract pathogens*. Antimicrob Agents Chemother, 2001. 45(1): p. 23–9.
342. E. Frohlich, et al., *Measurements of Deposition, Lung Surface Area and Lung Fluid for Simulation of Inhaled Compounds.* Front Pharmacol, 2016. 7: p. 181.
343. P. Espie, et al., *Physiologically based pharmacokinetics (PBPK)*. Drug Metab Rev, 2009. 41(3): p. 391–407.
344. H. Wen, et al., *Translational Physiologically Based Pharmacokinetic Modeling to Predict Human Pulmonary Kinetics After Lung Delivery.* CPT Pharmacometrics Syst Pharmacol, 2025. 14(4): p. 796–806.

345. C.H.C. Litjens, et al., *Prediction of Moxifloxacin Concentrations in Tuberculosis Patient Populations by Physiologically Based Pharmacokinetic Modeling*. J Clin Pharmacol, 2022. 62(3): p. 385–396.
346. M.L. Vieira, et al., *Predicting drug interaction potential with a physiologically based pharmacokinetic model: a case study of telithromycin, a time-dependent CYP3A inhibitor*. Clin Pharmacol Ther, 2012. 91(4): p. 700–8.
347. J. Lettieri, et al., *Effect of food on the pharmacokinetics of a single oral dose of moxifloxacin 400mg in healthy male volunteers*. Clin Pharmacokinet, 2001. 40 Suppl 1: p. 19–25.
348. H.M. Siefert, et al., *Pharmacokinetics of the 8-methoxyquinolone, moxifloxacin: a comparison in humans and other mammalian species*. J Antimicrob Chemother, 1999. 43 Suppl B: p. 69–76.
349. V. Bhargava, et al., *Lack of effect of food on the bioavailability of a new ketolide antibacterial, telithromycin*. Scand J Infect Dis, 2002. 34(11): p. 823–6.
350. J.H. Lee and M.G. Lee, *Effects of acute renal failure on the pharmacokinetics of telithromycin in rats: negligible effects of increase in CYP3A1 on the metabolism of telithromycin*. Biopharm Drug Dispos, 2007. 28(4): p. 157–66.
351. A. Soman, et al., *Concentrations of moxifloxacin in serum and pulmonary compartments following a single 400 mg oral dose in patients undergoing fibre-optic bronchoscopy*. J Antimicrob Chemother, 1999. 44(6): p. 835–8.
352. B. Capitano, et al., *Steady-state intrapulmonary concentrations of moxifloxacin, levofloxacin, and azithromycin in older adults*. Chest, 2004. 125(3): p. 965–73.
353. O.A. Khair, et al., *Lung concentrations of telithromycin after oral dosing*. J Antimicrob Chemother, 2001. 47(6): p. 837–40.
354. C.T. Ong, et al., *Intrapulmonary concentrations of telithromycin: clinical implications for respiratory tract infections due to Streptococcus pneumoniae*. Chemotherapy, 2005. 51(6): p. 339–46.
355. SimulationsPlus, *GastroPlus™ User Manual Version 9.9*. Dec 2023: SimulationsPlus, Inc., Lancaster, CA, USA.
356. K. Togami, et al., *Involvement of intestinal permeability in the oral absorption of clarithromycin and telithromycin*. Biopharm Drug Dispos, 2014. 35(6): p. 321–9.
357. J.H. Lee, et al., *Effects of Escherichia coli lipopolysaccharide on telithromycin pharmacokinetics in rats: inhibition of metabolism via CYP3A*. Antimicrob Agents Chemother, 2008. 52(3): p. 1046–51.
358. P.A. Valitalo, et al., *Structure-Based Prediction of Anti-infective Drug Concentrations in the Human Lung Epithelial Lining Fluid*. Pharm Res, 2016. 33(4): p. 856–67.
359. S. Arnouts, et al., *There is no need for overnight fasting of rats in regulatory toxicology studies*. Toxicology, 2024. 509: p. 153937.
360. F. Pea, et al., *Pharmacokinetic and pharmacodynamic aspects of oral moxifloxacin 400 mg/day in elderly patients with acute exacerbation of chronic bronchitis*. Clin Pharmacokinet, 2006. 45(3): p. 287–95.
361. C. Perret, et al., *Pharmacokinetics and absolute oral bioavailability of an 800-mg oral dose of telithromycin in healthy young and elderly volunteers*. Chemotherapy, 2002. 48(5): p. 217–23.
362. H. Stass, et al., *Pharmacokinetics of moxifloxacin, a novel 8-methoxy-quinolone, in patients with renal dysfunction*. Br J Clin Pharmacol, 2002. 53(3): p. 232–7.
363. S. Ahmed, et al., *Involvement of Mrp2 (Abcc2) in biliary excretion of moxifloxacin and its metabolites in the isolated perfused rat liver*. J Pharm Pharmacol, 2008. 60(1): p. 55–62.
364. N.A. Charoo, et al., *Biowaiver Monograph for Immediate-Release Solid Oral Dosage Forms: Moxifloxacin Hydrochloride*. J Pharm Sci, 2020. 109(9): p. 2654–2675.
365. J. Shi, et al., *Clinical pharmacokinetics of telithromycin, the first ketolide antibacterial*. Clin Pharmacokinet, 2005. 44(9): p. 915–34.

366. S. Yamaguchi, et al., *Involvement of the drug transporters p glycoprotein and multidrug resistance-associated protein Mrp2 in telithromycin transport*. Antimicrob Agents Chemother, 2006. 50(1): p. 80–7.
367. J.H. Lee and M.G. Lee, *Telithromycin pharmacokinetics in rat model of diabetes mellitus induced by alloxan or streptozotocin*. Pharm Res, 2008. 25(8): p. 1915–24.
368. Z. Wang, et al., *Impact of Food Physical Properties on Oral Drug Absorption: A Comprehensive Review*. Drug Des Devel Ther, 2025. 19: p. 267–280.
369. N. Parrott, et al., *Predicting pharmacokinetics of drugs using physiologically based modeling--application to food effects*. AAPS J, 2009. 11(1): p. 45–53.
370. H.M. Jones, et al., *Predicting pharmacokinetic food effects using biorelevant solubility media and physiologically based modelling*. Clin Pharmacokinet, 2006. 45(12): p. 1213–26.
371. D. Dahlgren, et al., *Fasted and fed state human duodenal fluids: Characterization, drug solubility, and comparison to simulated fluids and with human bioavailability*. Eur J Pharm Biopharm, 2021. 163: p. 240–251.
372. P.H. Patel, et al., *Bronchoalveolar Lavage*, in *StatPearls*. 2025: Treasure Island (FL) ineligible companies. Disclosure: Marsha Antoine declares no relevant financial relationships with ineligible companies. Disclosure: Abdulghani Sankari declares no relevant financial relationships with ineligible companies. Disclosure: Saad Ullah declares no relevant financial relationships with ineligible companies.
373. C. Muller-Serieys, et al., *Bronchopulmonary disposition of the ketolide telithromycin (HMR 3647)*. Antimicrob Agents Chemother, 2001. 45(11): p. 3104–8.
374. D.R. Baldwin, et al., *Pulmonary disposition of antimicrobial agents: methodological considerations*. Antimicrob Agents Chemother, 1992. 36(6): p. 1171–5.
375. S.I. Rennard, et al., *Estimation of volume of epithelial lining fluid recovered by lavage using urea as marker of dilution*. J Appl Physiol (1985), 1986. 60(2): p. 532–8.
376. K. Yamazaki, et al., *Bronchoscopic microsampling method for measuring drug concentration in epithelial lining fluid*. Am J Respir Crit Care Med, 2003. 168(11): p. 1304–7.
377. L.B.S. Aulin, et al., *Validation of a Model Predicting Anti-infective Lung Penetration in the Epithelial Lining Fluid of Humans*. Pharm Res, 2018. 35(2): p. 26.
378. A. Talevi, Bellera, C.L., *Free Drug Theory*, in *The ADME Encyclopedia*, A. Talevi, Editor. 2022, Springer, Cham.
379. J.D. Crapo, et al., *Cell number and cell characteristics of the normal human lung*. Am Rev Respir Dis, 1982. 126(2): p. 332–7.
380. S. Sapich, et al., *Murine alveolar epithelial cells and their lentivirus-mediated immortalisation*. Altern Lab Anim, 2018. 46(2): p. 73–89.
381. K. Michalak, et al., *Treatment of the Fluoroquinolone-Associated Disability: The Pathobiochemical Implications*. Oxid Med Cell Longev, 2017. 2017: p. 8023935.
382. S. Kosol, et al., *Probing the interactions of macrolide antibiotics with membrane-mimetics by NMR spectroscopy*. J Med Chem, 2012. 55(11): p. 5632–6.
383. C.M. Roberts, et al., *Changes in epithelial lining fluid albumin associated with smoking and interstitial lung disease*. Eur Respir J, 1993. 6(1): p. 110–5.
384. G. Ahlin, et al., *Endogenous gene and protein expression of drug-transporting proteins in cell lines routinely used in drug discovery programs*. Drug Metab Dispos, 2009. 37(12): p. 2275–83.
385. C. Cordon-Cardo, et al., *Expression of the multidrug resistance gene product (P-glycoprotein) in human normal and tumor tissues*. J Histochem Cytochem, 1990. 38(9): p. 1277–87.
386. T. Berg, et al., *Expression of MATE1, P-gp, OCTN1 and OCTN2, in epithelial and immune cells in the lung of COPD and healthy individuals*. Respir Res, 2018. 19(1): p. 68.

387. D. Vivian and J.E. Polli, *Mechanistic interpretation of conventional Michaelis-Menten parameters in a transporter system*. Eur J Pharm Sci, 2014. 64: p. 44–52.
388. B. Feng, et al., *In vitro and in vivo approaches to characterize transporter-mediated disposition in drug discovery*. Expert Opin Drug Discov, 2014. 9(8): p. 873–90.
389. D. Roth, et al., *Structure and function relationships of mucociliary clearance in human and rat airways*. Nat Commun, 2025. 16(1): p. 2446.
390. E. Houtmeyers, et al., *Regulation of mucociliary clearance in health and disease*. Eur Respir J, 1999. 13(5): p. 1177–88.
391. S. Gizurarson, *The effect of cilia and the mucociliary clearance on successful drug delivery*. Biol Pharm Bull, 2015. 38(4): p. 497–506.
392. C. Gessner, et al., *Exhaled breath condensate acidification in acute lung injury*. Respir Med, 2003. 97(11): p. 1188–94.
393. D. Morales Castro, et al., *Pharmacokinetic Alterations Associated with Critical Illness*. Clin Pharmacokinet, 2023. 62(2): p. 209–220.
394. J.K. Metz, et al., *Modulating the Barrier Function of Human Alveolar Epithelial (hAELVi) Cell Monolayers as a Model of Inflammation*. Altern Lab Anim, 2020. 48(5-6): p. 252–267.
395. K. Horie, et al., *Isolation and characterization of Caco-2 subclones expressing high levels of multidrug resistance protein efflux transporter*. Pharm Res, 2003. 20(2): p. 161–8.
396. S. Simon, et al., *Mapping the ABC Transporter Landscape in the Human Lung: A Comprehensive Characterisation of P-gp, MRP1 and BCRP Expression and Functional Activity in Human Lung Epithelial Cells*. European Journal of Pharmaceutical Sciences, 2025. 215.
397. L.M. Koehn, *ABC Transporters: Individual-Specific Considerations*, in *The ADME Encyclopedia*, A. Talevi, Editor. 2022, Springer, Cham.
398. T. Murakami and R. Yumoto, *Role of phosphatidylserine binding in tissue distribution of amine-containing basic compounds*. Expert Opin Drug Metab Toxicol, 2011. 7(3): p. 353–64.
399. K. Huang, et al., *Protocol for detecting lysosome quantity and membrane permeability in acute myeloid leukemia cell lines*. STAR Protoc, 2024. 5(3): p. 103309.
400. W. Zhang, et al., *Differential Expression of ABC Transporter Genes in Brain Vessels vs. Peripheral Tissues and Vessels from Human, Mouse and Rat*. Pharmaceutics, 2023. 15(5).
401. D. Dimitrijevic, et al., *Rapid equilibrium dialysis, ultrafiltration or ultracentrifugation? Evaluation of methods to quantify the unbound fraction of substances in plasma*. Biochem Biophys Res Commun, 2023. 651: p. 114–120.
402. C.M. Perry and L.J. Scott, *Cefdinir: a review of its use in the management of mild-to-moderate bacterial infections*. Drugs, 2004. 64(13): p. 1433–64.
403. W.A. Alghamdi, et al., *Protein Binding of First-Line Antituberculosis Drugs*. Antimicrob Agents Chemother, 2018. 62(7).
404. D. Dahlgren, et al., *Direct In Vivo Human Intestinal Permeability (Peff) Determined with Different Clinical Perfusion and Intubation Methods*. J Pharm Sci, 2015. 104(9): p. 2702–26.
405. R.G. Greenberg, et al., *Population Pharmacokinetics of Moxifloxacin in Children*. Paediatr Drugs, 2022. 24(2): p. 163–173.
406. P.S. Caceres, et al., *Quantitative proteomics of MDCK cells identify unrecognized roles of clathrin adaptor AP-1 in polarized distribution of surface proteins*. Proc Natl Acad Sci U S A, 2019. 116(24): p. 11796–11805.

6. List of Figures

7. List of Tables

8. Publications

8.1 Publications in peer reviewed journals

Simon, S., Cantrill, C. and Lehr, C-M., The Role of ABC Transporters in the Human Lung Epithelium – Insights from and Limitations of Current *in vitro* Cell Models – Review article - Published - *In Vitro Models* (2025), DOI: 10.1007/s44164-025-00091-w

Simon, S., Shanmugalingam, T., Neu, T., Schneider-Daum, N., Cantrill, C. and Lehr, C-M., Mapping the ABC Transporter Landscape in the Human Lung: A Comprehensive Characterisation of MDR1, MRP1 and BCRP Expression and Functional Activity in Human Lung Epithelial Cells – Research article – Published – *European Journal of Pharmaceutical Sciences* (2025), DOI: 10.1016/j.ejps.2025.107333

Gill, E., Muenchau Schoepp, S., Simon, S., Harter, M., Nikolaev, M., Pereiro, I., Silva, I., Lopez-Sandoval, R., Berrera, M., Kam-Thong, T., Michalski, M., Aubert, J., Keemink, J., Stillhart, C., Hofmann, M., Fowler, S., Milani, N. and Gjorevski, N. (2025) - Application of a Bioengineered Intestinal Epithelium for Drug Permeability and Metabolism Studies – Research Article – Published - *Lab on a Chip* (2025), DOI: 10.1039/D5LC00626K

Simon, S., Westwood, M-A., Shanmugalingam, T., Cantrill, C. and Lehr, C-M., Transport of 20 Marketed Anti-Infectives Across the Human Lung Epithelium *In Vitro* – Research article – Published – *International Journal of Pharmaceutics* (2025), DOI: 10.1016/j.ijpharm.2026.126721

8.2 Poster and Oral Presentations

‘Elucidating the expression of drug transporters in the human lung epithelium and their role on pulmonary drug disposition of antibiotics – PhD project overview’, Academia meets Industry: Basel – Biozentrum/Roche Innovation Symposium, Virtual Meeting, December 2021, Virtual Poster presentation

‘The influence of culture condition on the expression of ABC transporters in different *in vitro* lung models’, LIVe conference, Nice, France, June 2022, Poster Presentation

‘Investigating the expression of ABC transporters in human lung epithelial cells’, Barrier- and Transporter-Days, Bad Herrenalb, Germany, May 2023, Poster Presentation

‘Assessing the role of ABC transporters in cell models of the human lung epithelium’, ISAM conference, Saarbrücken, Germany, August 2023, Poster presentation

‘Assessing the permeability of antibiotics (AbX) across the human lung epithelium’, LIVe conference, Nice, France, June 2024, Oral presentation

‘Elucidating the permeability and active efflux of antibiotics (AbX) across the human lung epithelium’, pRED PhD & Postdoc Science Days, Basel, Switzerland, February 2025, Poster presentation

‘Assessing the role of efflux transporters on the pulmonary drug disposition of antibiotics’, G7 Transporter Meeting 2025, Bayer AG, Wuppertal, Germany, July 2025, Oral presentation

‘Assessing the transport of antibiotics (AbX) across the human lung epithelium in vitro with a focus on permeability and active efflux’, CRSmBB26 Conference, Saarbrücken, Germany, March 2026, Oral presentation

9. Acknowledgements

I would like to take this opportunity to express my deepest gratitude to all the great people who supported me during this PhD project – I am grateful for the many things I learned and your contributions in any way, which turned my PhD journey into a truly enriching experience.

First, I would like to express my greatest thanks to my mentor and supervisor Dr. Carina Cantrill. You always believed in me and supported me from the very beginning to pursue a PhD in industry, for which I am deeply grateful. I am very thankful for your continuous support in every way needed, your time over the last years, your guidance and your huge knowledge, that you shared with me, from which I could learn a lot.

I would like to express my deepest thanks to Prof. Dr. Claus-Michael Lehr for accepting me as your external PhD student. I am deeply thankful for all the meetings we had, your scientific advice and guidance. I would like to further thank you for connecting me to your research group at HIPS and the resulting collaboration – it was a pleasure to work with you.

I would like to thank Prof. Dr. Marc Schneider for volunteering as my academic mentor and as the second reviewer. Further, I would like to thank Prof. Dr. Thorsten Lehr and Dr. Dominik Selzer for joining the thesis committee.

A big thank you go to all the many people within Roche and within the HIPS, who support me over the last years. I am profoundly grateful for all the support from my colleagues of the ADME chapter. Special thanks go to the Cellular Transport and PPB team, I am truly happy that I could continue working and learning in/from this fantastic team after my Master's internship. I am extremely thankful for the scientifically enriching and supportive discussions with Dr. Janneke Keemink and the fruitful and interesting conversations I had with Dr. Zachary Enlo-Scott regarding pulmonary pharmacokinetics. Further I am deeply thankful for the all the chats, both scientific and personal, I had with Tanvi Naik and Maja Gredelj – thank you so much that you always had an open ear for me, your positive spirit and helpful feedback regarding any scientific question. I am also very thankful for the many nice chats I had with Anne-Christine Cascais, Elisa di Lenarda and Marie-Elise Brun in the cell culture lab and beyond as well as for your support in any way. Further I would like to thank Victor Dudal for your positiveness, it was always a pleasure to share an office with Tanvi, Marie-Elise and you in our old building. I would also like to thank Dr. Alina Meyer for her support in creating the beautiful PhD hat. Many thanks also to Giulia Grancini Mitaini for the mutual cheering up while writing a thesis at the same time. It was also a great pleasure to collaborate with Dr. Stephanie Münchau-Schöpp on assessing the permeability and active efflux in the intestine-on-a-chip model. Moreover, big thanks go to Catherine Karrer, who was the first person introducing me to the culture of lung epithelial cells. My deepest thanks goes also to the bioanalytical team in ADME, especially to

Isabelle Walter for introducing my to the theoretical part of LC-MS/MS and your great support in any study of my PhD that involved LC-MS/MS, to Marie-Anne Westwood, who trained me on running the LC-MS/MS by myself – thanks so much for your patience and awesome way of teaching and further for your support in setting up all the AbX methods, and to Thanusa Shanmugalingam for your great support in the sample analysis and in setting up the AbX LC-MS/MS methods. Further I would like to thank Vincent Monin, Charles Alexandre Tournillac and Dr. Alex Schriewer, who always supported me, when there were any issues with the machines. I am also really thankful for my two people enablers Dr. Delia Bucher and Dr. Pietro Brunetti for all the discussion we had, sharing experiences from your own PhDs, which was truly valuable for me. I would also like to thank Björn Wagner for answering all my questions regarding Physchem. Moreover, I am very grateful to the enriching discussions around PBPK modelling with Dr. Kenichi Umehara and the valuable conversations I had with Neil John Parrot regarding the ELF modelling. Further I would like to thank Dr. Xiao Yu and Nicole Thuerkauf for your support and tips, when working with primary bronchial cells. I would also like to thank Isabelle Anderka and Aynur Ekiciler for positiveness inside and outside the lab, your support when facing issues with the qPCR machine, as well as the many lunches and coffee chats, we shared. Moreover, I would like to thank Dr. Simone Schadt and Dr. Christoph Funk for your support in implementing this PhD project.

It was a pleasure to meet many other PhD students within Roche and sharing our experiences of doing an industrial PhD. To mention a few: it was a nice surprise to meet Dr. Linda Steinacher again at Roche after already sharing lab experience during our Bachelor courses. Thanks for going through this PhD journey together, sharing conference experience at LIVe and the many great chats we had over lunch and coffee. Further, I would like to thank Dr. Apolline Lefèvre and Dr. Javier Sanchez-Fernandez for all our lunches and discussions with lots of laughter while enjoying tasty Schokocchinos. I would like to thank also my PhD colleague Alessandra Pugliano from the ADME chapter, for the nice conversations and lunches we had and especially for sharing your experience *on in silico* modelling. I also highly valued the many funny lunches with Evodie Lassalle – it was great to continue together at Roche after doing our Master's internship together.

I would like to express my deepest thanks to the colleagues from the research group 'Biologische Barrieren und Wirkstofftransport' at the HIPS for your support and contribution to my project, especially by isolating the primary alveolar cells and answering all my questions regarding this: special thanks go to Dr. Nicole Schneider-Daum, Dr. Lorenz Latta, Tobias Neu and Tabea Trampert. Moreover, I would like to thank Sarah Müller, who always supported me to find free meeting slots in the calendar of Claus-Michael. Further I would like to thank all the great students from the HIPS and the UdS who I met during the ISAM conference and the PhD

retreat. It was a pleasure connecting with you and learning from you and your projects - here I would like to thank especially Clémentine Richter, Daria Harig, Max Koumou-Okandze and Tobias Neu, who made me feel very welcome from the beginning.

I would like to express my deepest gratitude to my boyfriend Dominik. Thank you so much for your support during this whole PhD journey and that you always believed in me. Your unwavering understanding and patience, especially during the last months while writing this thesis, mean a lot to me and I am deeply thankful. I would like to take this opportunity to thank my family, especially my parents Beate and Alex and my brother Nicolas for your awesome support in any way and your commitment by trying to understand what I am doing in the lab. Ich möchte mich an dieser Stelle auch bei meinem Opa Manfred bedanken, der nie müde wurde zu fragen, ob ich meine Zellen schon gefüttert habe, um sicher zu sein, dass sie auf keinen Fall verhungern. Last but not least, I would like to extend my thanks to Mila, who was always there for me and cheered me up, when needed.

10. Appendix

A. Supplemental Material to Chapter 3.1

A1. Details on LC-MS/MS Analytics

Table A1: Setting of the mass spectrometer source parameters.

Parameter	Setting
Curtain gas [psi]	30
Collision gas [psi]	12
Ion spray voltage [V]	5500
Temperature [°C]	500
Ion source gas 1 [psi]	40
Ion source gas 2 [psi]	50

Table A2: Details of the mass spectrometer transition parameters with mass-to-charge ratio (m/z), declustering potential (DP) and collision energy (CE).

Compound	m/z for parent	m/z for fragment	DP [V]	CE [eV]
Edoxaban	548.1	366.2	171	26
Doxorubicin	544.2	397.1	126	17
Prazosin	384.2	95.1	141	77
Atenolol	267.2	190.2	66	25
Carbamazepine	237.1	194.1	90	20
Budesonide	431.1	147.2	50	40
Oxazepam (Internal Standard)	287.1	241.1	51	31

Table A3*:* Details of the liquid chromatography gradient.

Time [min]	Mobile phase B [%]
0.00	0
0.26	0
0.90	95
1.23	95
1.33	0
1.40	0

A2. Western Blot - Bands of MDR1, MRP1 and BCRP

Representative Western Blots showing the bands for MDR1, MRP1 and BCRP in lung epithelial cells and Caco-2. Transporter proteins bands were visualized via chemiluminescence and β-actin bands via near-infrared fluorescence. For cell lines, the Western Blot was performed three times with comparable results (Figure A1-A7). For primary cells (NHBE and hAEpC), each three donors were compared (Figure A8 & A9).

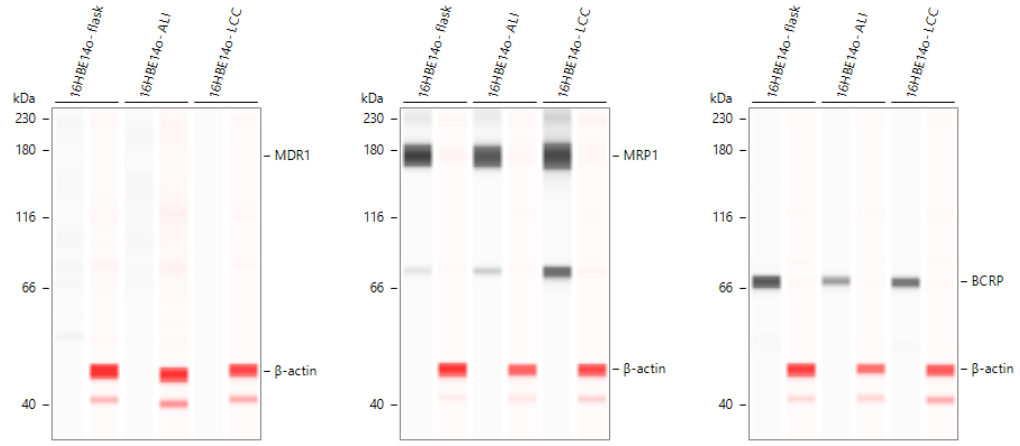

Figure A1: MDR1, MRP1, BCRP and β-actin expression in **16HBE14o-** cells, cultured either in flask, air-liquid interface (ALI) or liquid-covered condition (LCC) with n = 1.

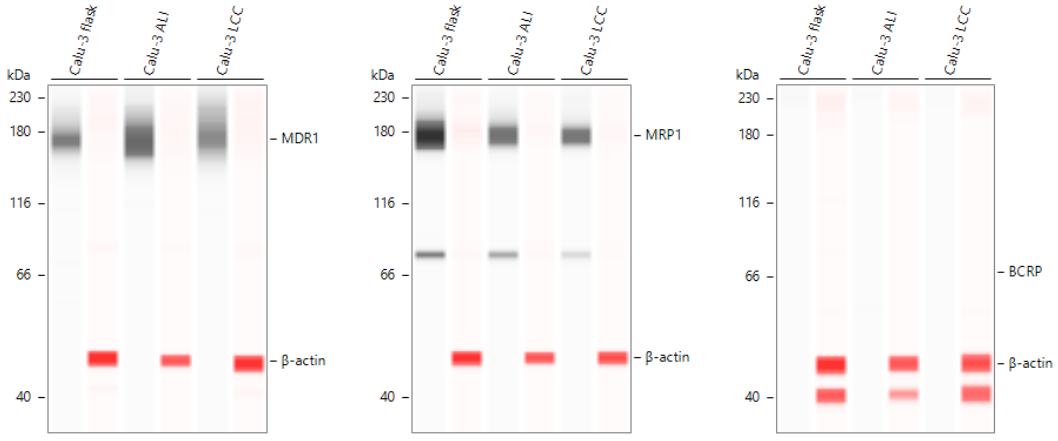

Figure A2: MDR1, MRP1, BCRP and β-actin expression in **Calu-3** cells, cultured either in flask, air liquid interface (ALI) or liquid-covered condition (LCC) with n = 1.

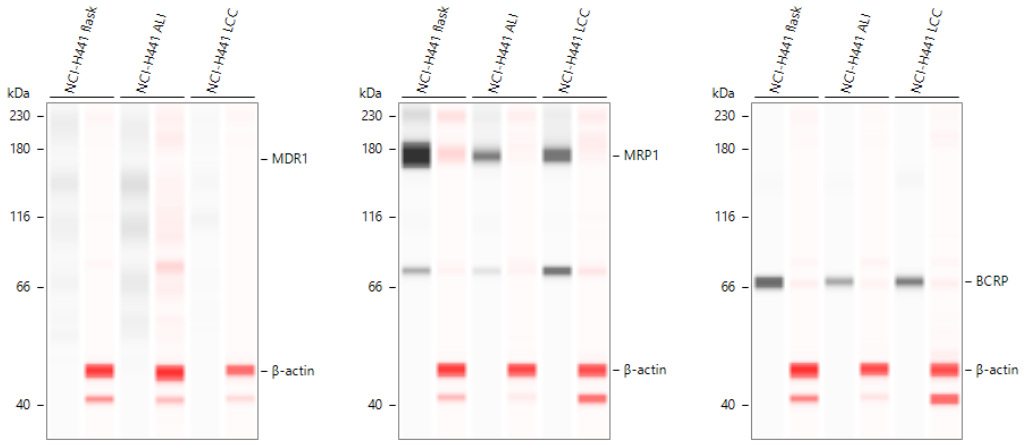

Figure A3: MDR1, MRP1, BCRP and β-actin expression in **NCI-H441** cells, cultured either in flask, air-liquid interface (ALI) or liquid-covered condition (LCC) with n = 1.

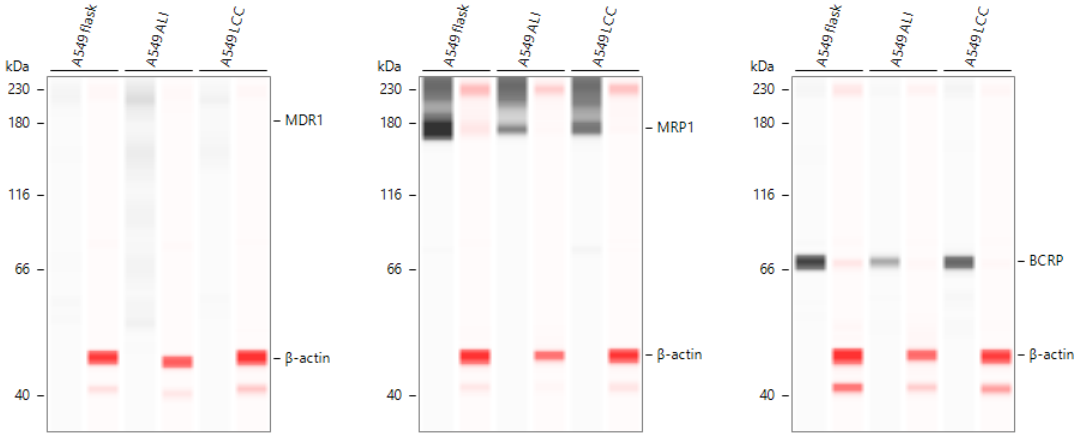

Figure A4: MDR1, MRP1, BCRP and β-actin expression in **A549** cells, cultured either in flask, air-liquid interface (ALI) or liquid-covered condition (LCC) with n = 1.

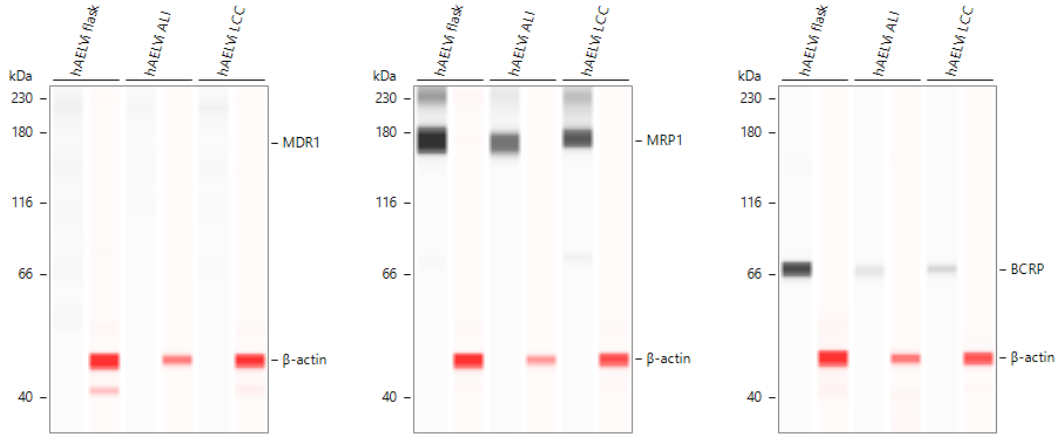

Figure A5: MDR1, MRP1, BCRP and β-actin expression in **hAELVi** cells, cultured either in flask, air-liquid interface (ALI) or liquid-covered condition (LCC) with n = 1.

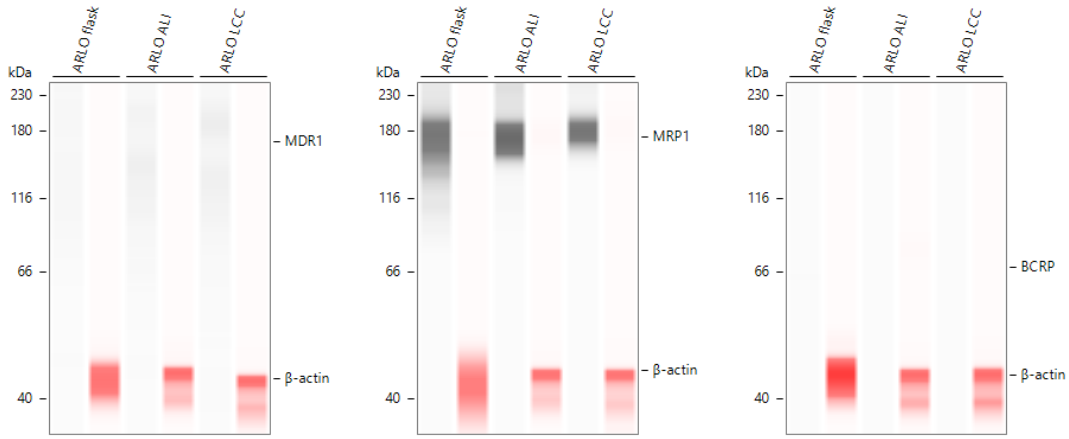

Figure A6: MDR1, MRP1, BCRP and β-actin expression in **Arlo** cells, cultured either in flask, air-liquid interface (ALI) or liquid-covered condition (LCC) with n = 1.

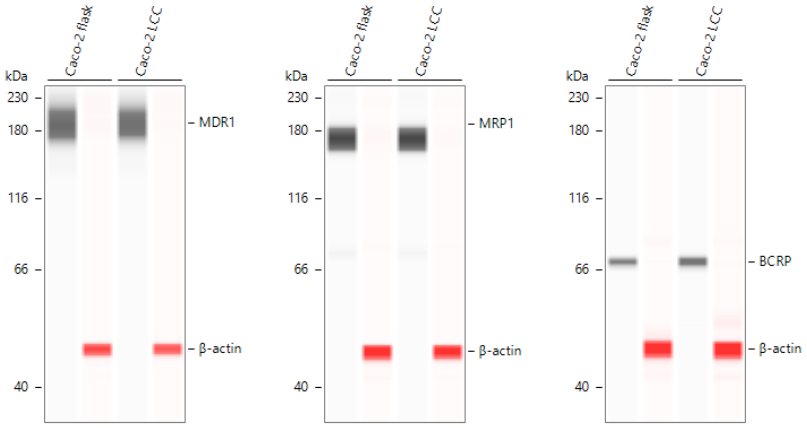

Figure A7: MDR1, MRP1, BCRP and β-actin expression in **Caco-2** cells, cultured either in flask or liquid-covered condition (LCC) with n = 1.

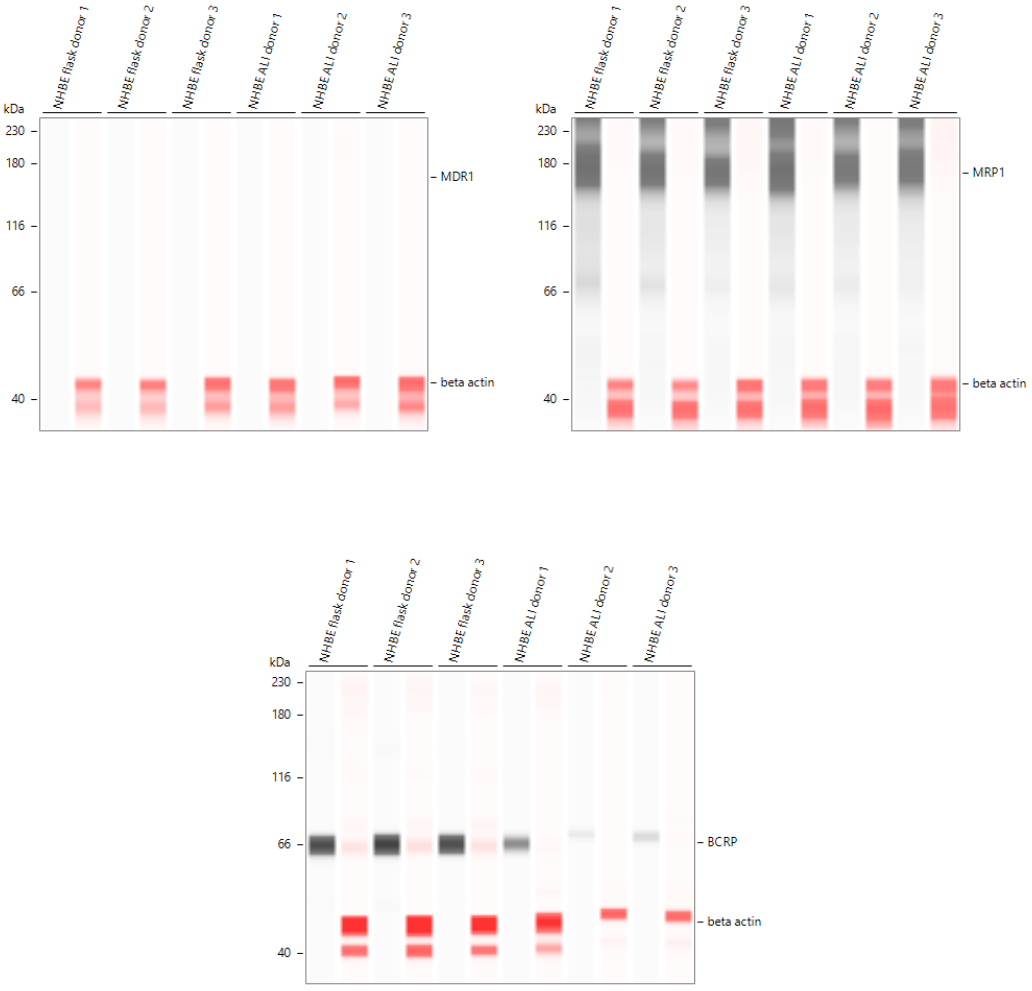

Figure A8: MDR1, MRP1, BCRP and β-actin expression in three donors of **NHBE** cells, cultured either in flask or air-liquid interface (ALI) with n = 1.

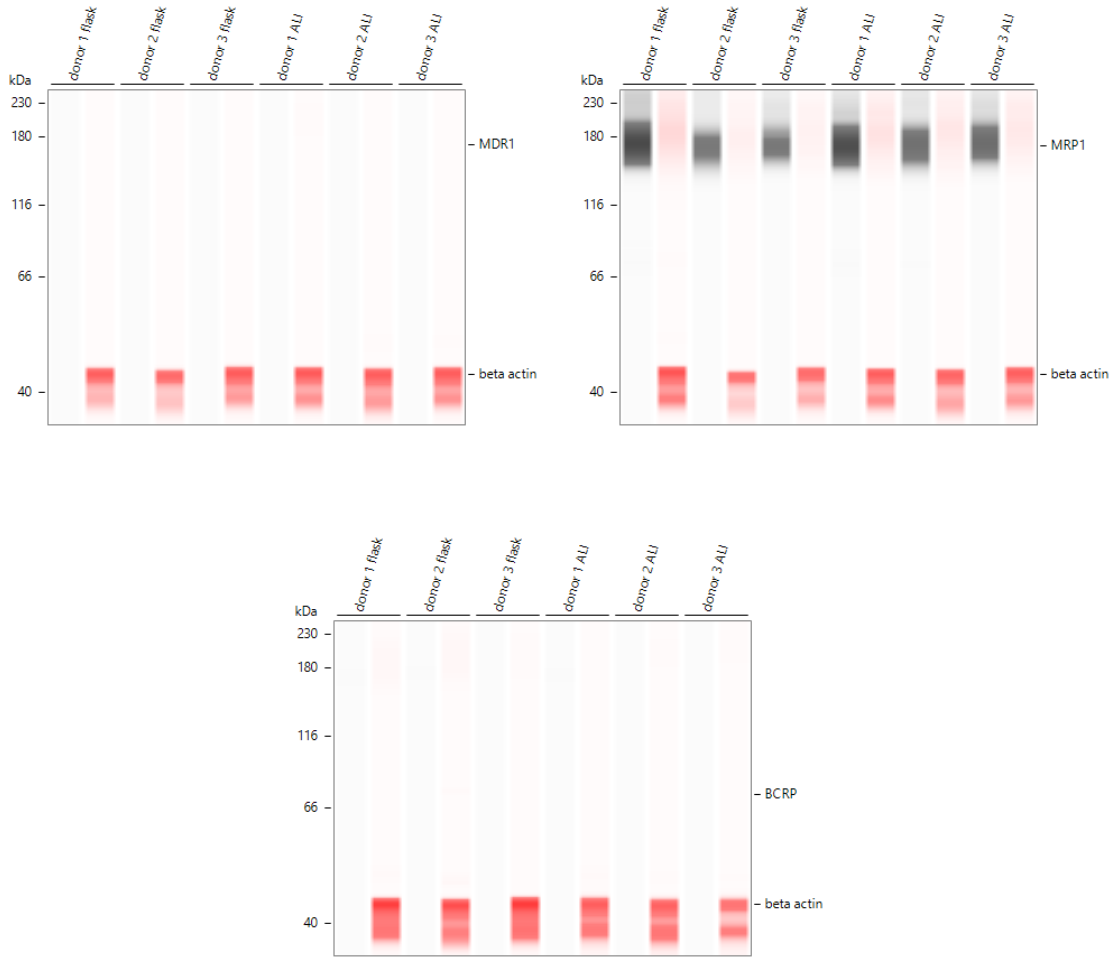

Figure A9: MDR1, MRP1, BCRP and β-actin expression in three donors of **hAEpC** cells, cultured either in flask or air-liquid interface (ALI) with n = 1.The flask condition refers to cells in suspension after the isolation and before the seeding (i.e. alveolar type II cells).

A3. Permeability of High Permeability Markers in Lung Epithelial cells

Figure A10 shows measured apparent permeability values for carbamazepine in lung epithelial cells and Caco-2. Values exceed the threshold of 100 nm/s (that classifies compounds as highly permeable [260]) and are comparable across all cell lines and between ALI and LCC cultured cells.

High permeability marker budesonide was measured in each three donors of NHBE and hAEpC. Measured values in NHBE did not exceed the threshold of 100 nm/s (that typically classifies compounds as high permeable). In comparison, budesonide shows a slightly higher permeability in hAEpC, as shown in Figure A11.

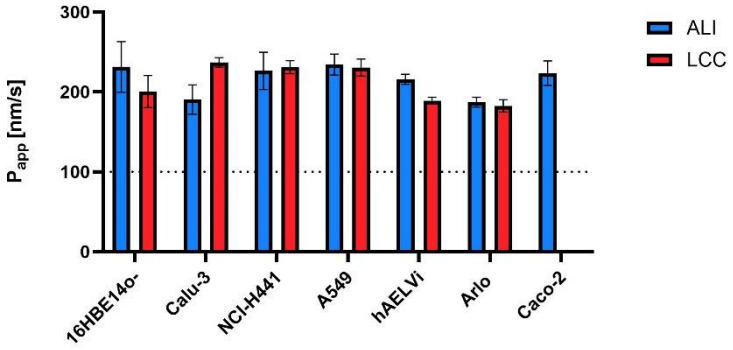

Figure A10: Average apparent permeability (P_{app}) of high permeability marker Carbamazepine in lung epithelial cells measured at air-liquid interface (ALI) and liquid-covered condition (LCC) and in Caco-2 at LCC. Dashed line at 100 nm/s represents threshold for high permeability. Values are shown as mean ± SD with n= 6. P_{app} values are shown as average of P_{app} AB and P_{app} BA.

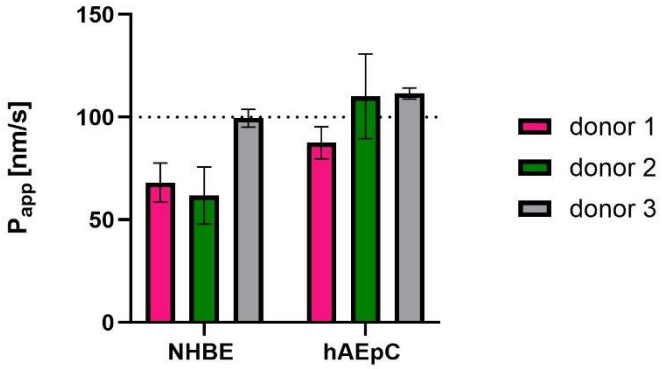

Figure A11: Average apparent permeability (P_{app}) of high permeability marker budesonide in each three donors of human bronchial (NHBE) and alveolar (hAEpC) primary lung epithelial cells at air-liquid interface (ALI). Dashed line at 100 nm/s represents threshold for high permeability. Values are shown as mean ± SD with n= 6. P_{app} values are shown as average of P_{app} AB and P_{app} BA.

A4. Calculation of the Uptake Ratio (UR) for Doxorubicin

As MRP1 was described to be expressed at the basolateral side of the cell membrane in the human lung epithelium, the inverse of the efflux ratio has been reported: the so-called uptake (UR) to assess active efflux at the basolateral side. UR is calculated as described in equation A1 [87].

$$UR = \frac{P_{app}\ AB}{P_{app}\ BA}$$

Equation A1: Formula to calculate the uptake ratio (UR). The permeability from apical to basolateral side (P_{app} AB) is divided by the permeability from basolateral to apical side (P_{app} BA).

If applying the threshold for active efflux based on the ER concept (see [18]), the UR would need to exceed the value of two (UR > 2) to confirm the presence of active efflux at the basolateral side. The UR was calculated for doxorubicin, which served as model substrate for MRP1 in this study. The UR was also calculated based on the permeability values measured in presence of MRP1 inhibitor MK-571 (UR,i). The results are depicted in Figure A12.

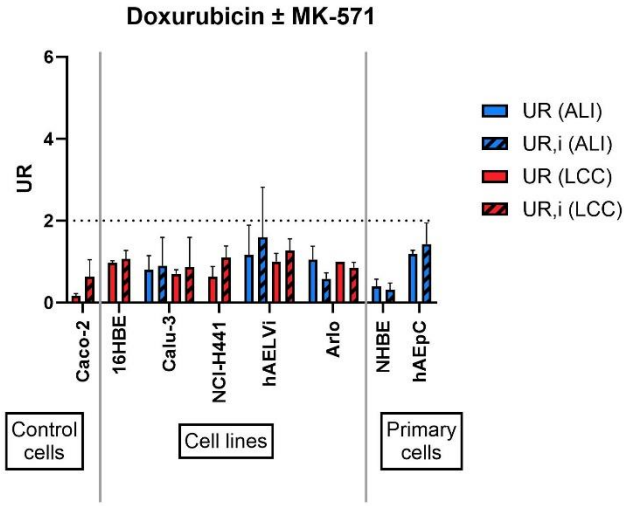

Figure A12: Calculated uptake ratios of ABC substrates in lung epithelial cells and Caco-2 in absence (UR) and presence (UR,i) of MRP1-specific inhibitor MK-571. Efflux in lung epithelial cell lines was compared at both air-liquid interface (ALI) and liquid-covered condition (LCC), but due to monolayer leakiness, no UR values are reported for 16HBE14o-/NCI-H441 at ALI and for A549 at ALI and LCC. In primary lung epithelial cells, UR was only assessed at ALI and Caco-2 at LCC. If UR > 2, this indicates active efflux present at the basolateral side of the cell membrane (indicated with dashed line). Data is presented as mean ± SD with n = 3 from three independent experiments.

Doxorubicin showed an average UR < 2 in all lung epithelial cells and in Caco-2, claiming the absence of functional active MRP1 at the basolateral side of the cell membrane.

A5. qPCR Analysis of MRPs Expression in Lung Epithelial Cells

A qPCR was conducted to measure the expression levels of MRPs in lung epithelial cells and compare it to MRP1 expression levels (as described in 3.2.2). This was conducted as no efflux of the MRP1 substrate doxorubicin was observed in the lung epithelial cells in bidirectional transport studies (see 3.3.5). This could be potentially explained by the presence of other MRPs in the lung epithelium. Further, doxorubicin was described in literature to be no specific substrate of MRP1 but appears to be transported as well by other MRPs like MRP2 [211, 283].

Sakamoto and colleagues had conducted a quantitative assessment of MRP1-9 protein expression in cell lines and primary cells derived from the human lung epithelium. They reported high expression levels of MRP1 compared to other MRPs. Interestingly, no MRP3, MRP5 and MRP6 was detected in Calu-3, NCI-H441 and A549, whereas it was detected in bronchial and alveolar primary cells [187, 194]. In contrast, at gene level, the expression of MRP1-9 was reported in the majority of human lung epithelial cell lines and primary cells [195].

In a recent review paper by Galetin and colleagues (2024), MRP2, MRP3 and MRP4 were described to transport a variety of different drugs, however there is only limited clinical evidence for their involvement in drug-drug interactions. Both MRP5 & MRP6 were found to transport rather endogenous substrates and only a small number of xenobiotics, however their potential contribution to clinically relevant drug-drug interactions is largely unknown [170].

Therefore, this study focussed on measuring the gene expression of MRP2, MRP3, MRP4, MRP5 and MRP6 in the lung epithelial cells and in Caco-2, comparing flask-cultured cells against cells grown on Transwell® inserts (ALI or LCC). Table A4 provides an overview of the TaqMan™ gene expression FAM assays used to determine the gene expression of MRPs.

Table A4: Overview of MRP2-6 primers used in qPCR.

Gene	Protein	TaqMan® Gene Expression Assay ID
ABCC2	MRP2	Hs00166123_m1
ABCC3	MRP3	Hs00978452_m1
ABCC4	MRP4	Hs00195260_m1
ABCC5	MRP5	Hs00981089_m1
ABCC6	MRP6	Hs01077866_m1

As shown in Figure A13 and Figure A14, there are differences in the gene expression levels of MRPs in the lung epithelial cells and the measured expression levels were partially comparable to those of MRP1. Moreover, several statically relevant differences in the expression of MRPs in flask vs ALI vs LCC cultured cells were found. Further research would be needed to investigate whether these expression levels are also comparable at protein level and to further elucidate the spatial expression of MRPs within the human lung epithelium [177].

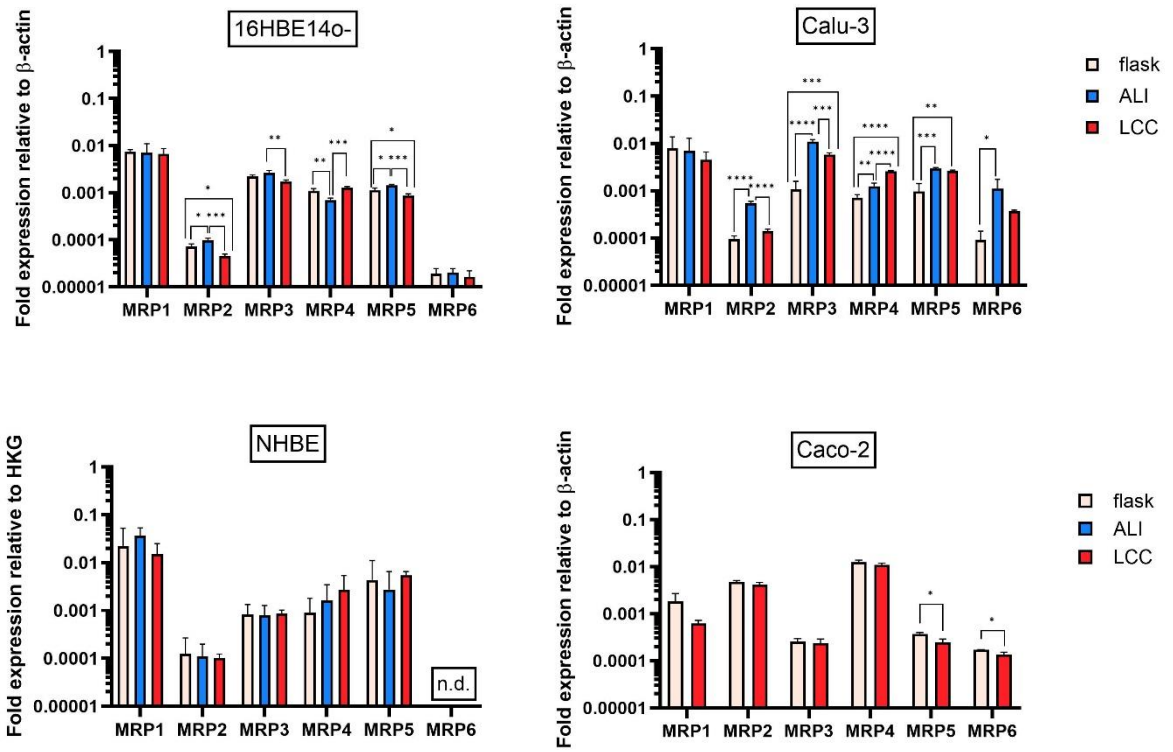

Figure A13. Gene expression of MRP1, MRP2, MRP3, MRP4, MRP5 and MRP6 in human lung epithelial cell lines and human primary epithelial cells derived from the **upper airways** and Caco-2 cells, analysed by qPCR and depicted as relative expression to housekeeping gene β-actin. Expression levels of ABC transporters in cells cultured in flasks or on Transwell® inserts at air liquid interface (ALI) or liquid covered condition (LCC) were compared. Whereas Caco-2, which serve as positive control, were cultured in flasks and at LCC on Transwell® inserts. Data are presented as mean ± SD with n = 3 and N = 3 for primary cells. MRP1 data are presented as reference and as a mean ± SD with n = 3 from three independent isolations (as depicted Figure 1). n.d. stands for non-detected. Differences in mean of three groups were analysed by One-way ANOVA followed by Tukey's multiple comparison test. Differences between two groups were analysed by un-paired two-sided t-test. *p ≤ 0.05, **p ≤ 0.01, ***p ≤ 0.001, ****p ≤ 0.0001.

Given the expression of MRP2, MRP3 and MRP4 in lung epithelial cells and their known involvement of transporting drugs across biological barriers [170], it is plausible to speculate that these efflux transporters might be involved in transporting compounds like doxorubicin across the lung epithelium. Therefore, the presence of functionally active MRPs on both sides of the pulmonary epithelium (i.e. apical and basolateral) could be a potential reason for the absence of active efflux of doxorubicin. Nevertheless, this hypothesis requires further investigation.

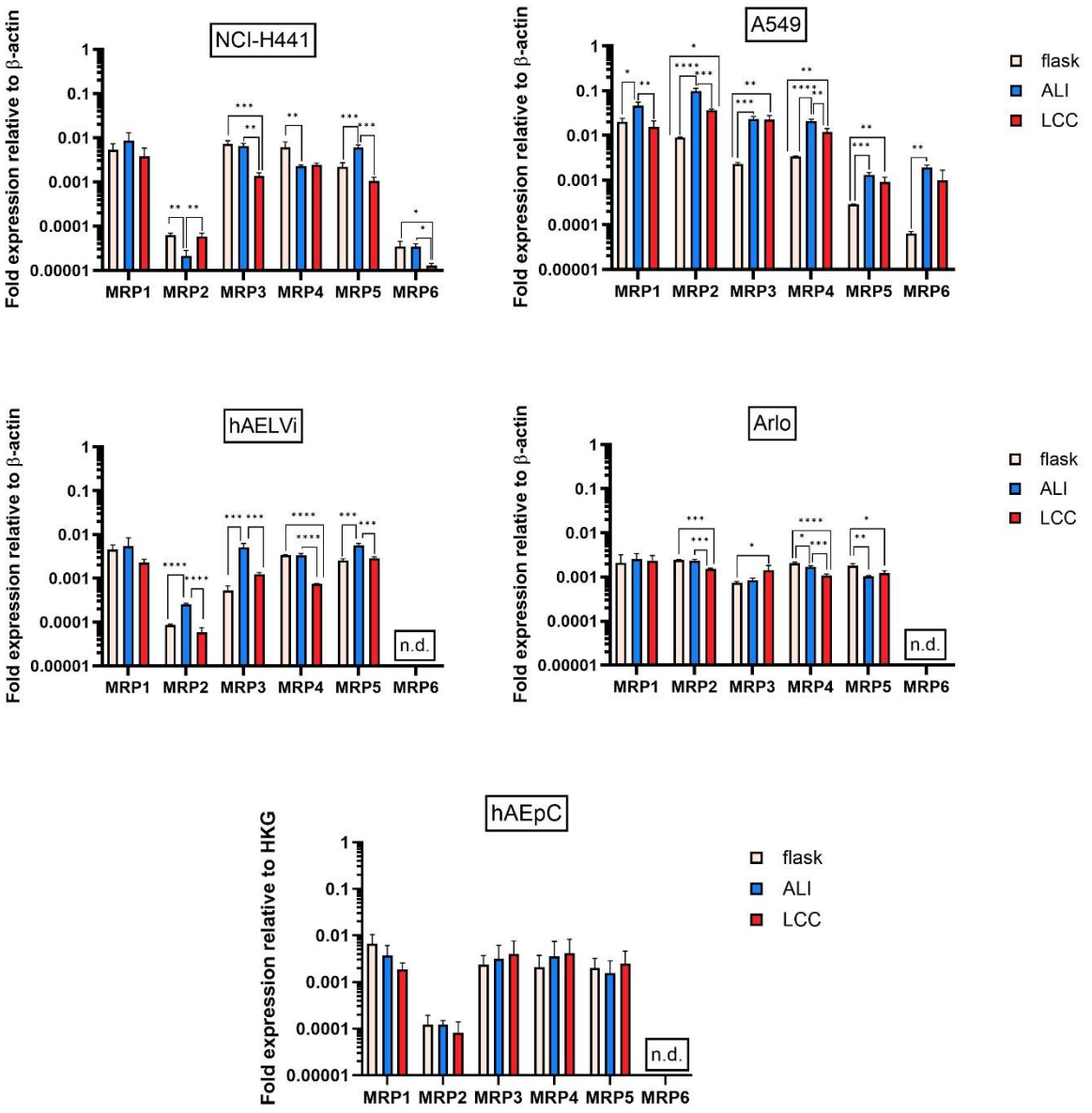

Figure A14. Gene expression of MRP1, MRP2, MRP3, MRP4, MRP5 and MRP6 in human lung epithelial cell lines and human primary epithelial cells derived from the **lower airways**, analysed by qPCR and depicted as relative expression to housekeeping gene β-actin. Expression levels of ABC transporters in cells cultured in flasks or on Transwell® inserts at air liquid interface (ALI) or liquid covered condition (LCC) were compared. For hAEpC, the flask condition refers to cells in suspension after the isolation and prior the seeding (i.e. alveolar type II cells). Data are presented as mean ± SD with n = 3 . Data are presented as mean ± SD with n = 3 and N = 3 for primary cells. MRP1 data are presented as reference ± SD with n = 3 from three independent isolations (as depicted in Figure 2). n.d. stands for non-detected. Differences in mean of three groups were analysed by One-way ANOVA followed by Tukey's multiple comparison test. *p ≤ 0.05, **p ≤ 0.01, ***p ≤ 0.001, ****p ≤ 0.0001.

B. Supplemental Material to Chapter 3.2

B1. Details on LC-MS/MS Analytics

Table B1: Details of Mass spectrometer transition parameters: mass-to-charge ratio (m/z), declustering potential (DP), collision energy (CE) and chromatographic conditions.

Compound	m/z for parent	m/z for fragment	DP [V]	CE [eV]	Injection volume µL	Mobile phase	Column
Amoxicillin	366.2	114.0	70	35	2	A1 / B1	2
Tazobactam	299.0	138.0	-30	-15	2	A1 / B1	1
Cefdinir	396.1	227.1	50	25	1	A1 / B1	2
Cefepime	481.0	125.0	50	75	1	A2 / B2	2
Imipenem	300.1	142.1	80	35	2	A1 / B1	2
Erythromycin	734.5	576.4	130	25	1	A1 / B1	2
Clarithromycin	748.5	158.2	130	35	1	A1 / B1	2
Azithromycin	749.5	591.5	90	45	1	A1 / B1	2
Telithromycin	812.4	655.4	100	45	1	A2 / B2	2
Ciprofloxacin	332.1	288.1	90	25	2	A1 / B1	1
Moxifloxacin	402.0	358.2	100	35	1	A1 / B1	2
Levofloxacin	362.1	318.1	90	25	1	A1 / B1	2
Lascufloxacin	440.3	317.2	100	45	1	A1 / B1	1
Gentamicin	478.2	322.0	80	20	2	A1 / B1	2
Vancomycin	725.3	144.1	116	23	1	A1 / B1	2
Linezolid	338.2	296.2	60	25	1	A1 / B1	2
Omadacycline	279.1	270.7	20	15	1	A2 / B2	2
Dapson	249.0	156.0	50	25	1	A2 / B2	2
Isoniazid	138.1	121.2	50	20	1	A1 / B1	2
Rifampicin	823.4	791.5	130	25	2	A1 / B1	2
Hydroxychloroquine	336.2	247.1	50	25	1	A1 / B1	2
Voriconazole	350.1	281.1	40	25	2	A1 / B1	2
Edoxaban	548.0	366.2	171	29	2	A1 / B1	2
Atenolol	267.2	190.2	66	25	2	A1 / B1	1
Propranolol	260.1	116.1	61	25	2	A1 / B1	2
Oxazepam (Internal standard for positive mode)	287.1	241.1	51	31	1 or 2	A1 / B1 A2 / B2	1 or 2
Roche internal compound (Internal standard for negative mode)	312.1	242.2	-80	-22	1 or 2	A1 / B1 A2 / B2	1 or 2

The details of the mass spectrometer and the liquid chromatography gradient were the same as described in Supplemental Tables A1 & A3. For compounds analysed in negative mode, the ion spray voltage was set to - 4500 V.

B2. Predicted pKa Values for Antibiotics

Table B2. Overview of predicted pKa values for antibiotics and permeability control markers. If several acidic (ApKa) and basic (BpKa) were predicted, all are reported.

Compound	ApKa 1	ApKa 2	ApKa 3	BpKa 1	BpKa 2	BpKa 3	Ionisation category at pH 7.4
Amoxicillin	3.10	10	-	6.95	-	-	Zwitter
Tazobactam	2.76	-	-	1.02	-2.59	-	Acidic
Cefdinir	2.62	7.20	10.9	3.66	-0.970	-2.35	Acidic
Cefepime	2.66	10.8	-	3.99	-1.12	-4.03	Zwitter
Erythromycin	-	-	-	8.23	-	-	Basic
Clarithromycin	-	-	-	8.21	-	-	Basic
Azithromycin	-	-	-	8.24	6.80	-	Basic
Telithromycin	7.43	-	-	8.47	5.28	2.84	Zwitter
Ciprofloxacin	5.88	-	-	8.89	0.160	-	Zwitter
Moxifloxacin	6.09	-	-	9.14	1.51	-	Zwitter
Levofloxacin	5.89	-	-	8.06	0.640	-	Zwitter
Lascufloxacin	6.01	-	-	8.15	2.43	-	Zwitter
Vancomycin	2.92	8.19	10.1	9.13	8.53	-	Zwitter
Linezolid	-	-	-	2.30	-	-	Neutral
Omadacycline	2.89	7.08	8.19	10.5	9.46	3.71	Zwitter
Dapsone	-	-	-	2.89	1.84	-	Neutral
Isoniazid	11.6	-	-	3.52	1.80	-	Neutral
Rifampicin	6.37	7.43	9.45	10.7	0.620	-3.46	Zwitter
Hydroxychloroquine	-	-	-	9.18	6.98	1.34	Basic
Voriconazole	-	-	-	2.42	0.820	-2.96	Neutral
Atenolol	-	-	-	9.60	-	-	Basic
Propranolol	-	-	-	9.47	-	-	Basic
Edoxaban	10.7	11.9	12.5	6.97	1.56	0.82	Basic

B3. The Impact of Physico-chemical Properties on Binding of Antibiotics to Human Plasma proteins and Components of a Human Simulated ELF

Bases were reported to show a stronger binding to components of the sELF than neutral or acidic compounds [156]. Although the compound set in this study consisted predominantly of zwitterionic compounds at 7.4, it was investigated what impact the ionisation category had an average unbound fraction in human plasma and sELF, as seen in Figure B1.

Data showed that the average unbound fraction for both sELF and plasma was lowest for basic compounds. Unbound values for zwitterions showed a broad range from 0.16 to 1.15 for human plasma and from 0.19 to 1.16 for sELF.

If taking further physico-chemical properties of the antibiotics into account, the unbound fraction in both plasma and sELF appeared to decrease with increasing AlogP and logD, see Figure B2.

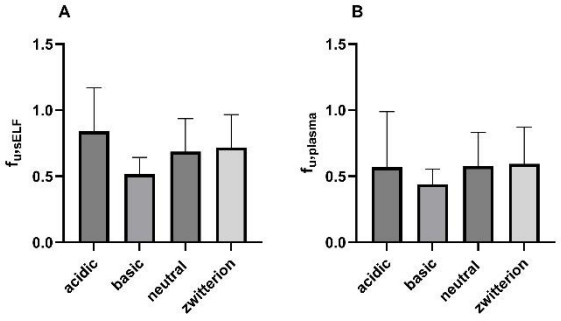

Figure B1. Average unbound fraction of antibiotics in human sELF ($f_{u,sELF}$) (A) or human plasma ($f_{u,plasma}$) (B) according to their ionisation category at pH 7.4. Data shown as mean ± SD with n = 2 for acidic, n = 4 for basic and neutral and n = 10 for zwitterions.

Figure B2 shows the increase in binding of antibiotics to human plasma proteins as well as to sELF with increasing lipophilicity (AlogP and ML_logD). This observation is aligned with previously published data [156, 401].

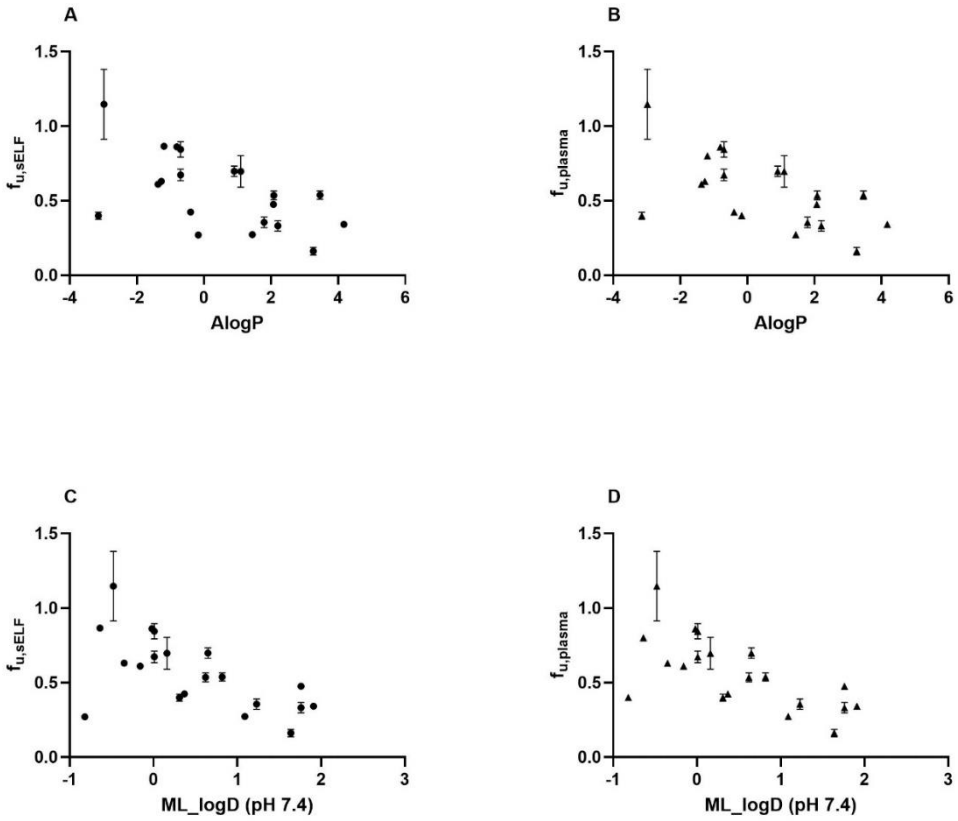

Figure B2. Comparison of unbound fraction of antibiotics in human sELF or plasma against AlogP (A & B) or ML_logD at pH 7.4 (C & D). Fraction unbound values are shown as mean ± SD with n =3 from three independent experiments, unless stated in Supporting Table B3.

B4. Binding of Fluoroquinolone, Ketolide and Macrolide Antibiotics to Rodent Plasma Proteins

In addition, a smaller compound test set, consisting of macrolide, ketolide and fluroquinolone antibiotics, was tested for their binding to rodent plasma proteins (mouse and rat), as shown in Figure B3. Measured values can be found in Table B3.

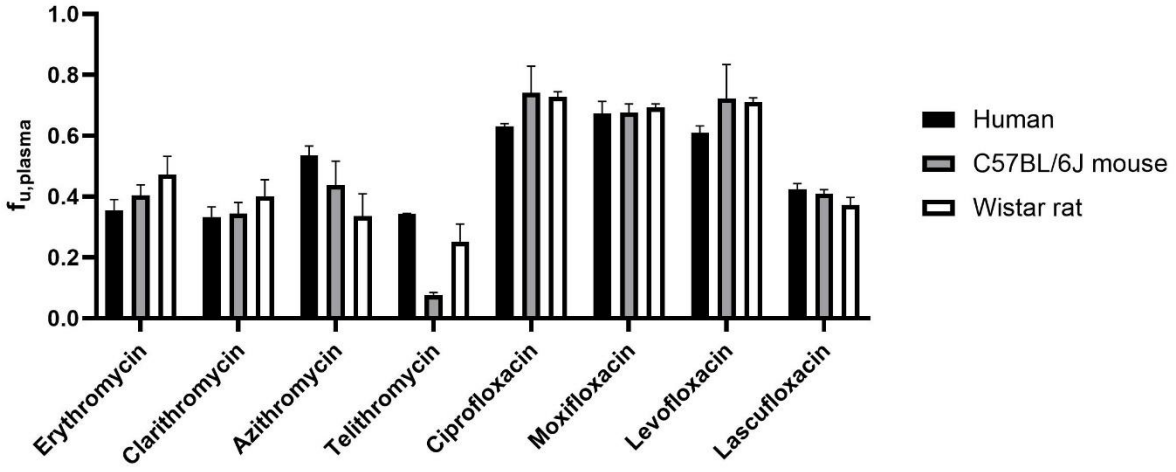

Figure B3. Comparison of unbound fraction of macrolide and fluoroquinolone antibiotics in human, mouse and rat plasma ($f_{u,plasma}$). Data is shown as mean ± SD with n =3 from three independent experiments.

For the majority of macrolide and fluoroquinolone antibiotics, a similar unbound fraction was observed across all three species (with rat $f_{u,plasma}$ being within 0.63 to 1.33-fold of respective human $f_{u,plasma}$ and mouse $f_{u,plasma}$ within 0.815 to 1.19-fold of respective human $f_{u,plasma}$).The only exception is telithromycin, which showed up to 4.5-fold stronger binding to mouse plasma proteins ($f_{u,plasma}$ of 0.076) than rat (0.251) or human (0.342).

B5. Measured Fraction Unbound of Antibiotics in Human & Rodent Plasma and in sELF

Table B3. Measured unbound fraction of antibiotics in human plasma ($f_{u,plasma}$) and human sELF ($f_{u,sELF}$). Data is shown as mean ± SD with n = 3 and N= 3. [a] Value taken from literature [156] [b] Value taken from literature, where a bound range of 0.60 to 0.73 was reported [402]. [c] For Cefepime, an unbound fraction > 1 was reported in sELF and plasma, likely arising from experimental variability. An unbound fraction of 1 indicates that whole compound is unbound. [d] Value taken from literature [403]. [e] Value taken from literature [156].

Compound	$f_{u,plasma}$	$f_{u,sELF}$
Amoxicillin	0.844 ± 0.05	0.893 ± 0.066
Tazobactam	0.865[a]	1.07 ± 0.06
Cefdinir	0.270[b]	0.607 ± 0.006
Cefepime	1.15 ± 0.23[c]	1.16 ± 0.12[c]
Erythromycin	0.355 ± 0.035	0.571 ± 0.070
Clarithromycin	0.332 ± 0.035	0.331 ± 0.083
Azithromycin	0.536 ± 0.030	0.553 ± 0.010
Telithromycin	0.342 ± 0.002	0.654 ± 0.019
Ciprofloxacin	0.630 ± 0.010	0.795 ± 0.042
Moxifloxacin	0.673 ± 0.039	0.782 ± 0.034
Levofloxacin	0.610 ± 0.022	0.724 ± 0.096
Lascufloxacin	0.424 ± 0.019	0.563 ± 0.026
Vancomycin	0.399 ± 0.024	0.627 ± 0.041
Linezolid	0.698 ± 0.035	0.677 ± 0.072
Omadacycline	0.697 ± 0.106	0.796 ± 0.027
Dapsone	0.274 ± 0.013	0.360 ± 0.039
Isoniazid	0.862[d]	0.964[e]
Rifampicin	0.161 ± 0.025	0.190 ± 0.022
Hydroxychloroquine	0.538 ± 0.027	0.612 ± 0.061
Voriconazole	0.475 ± 0.016	0.745 ± 0.024

Table B4. Measured unbound fraction of macrolide, ketolide and fluoroquinolone antibiotics in Wistar rat plasma ($f_{u,plasma}$ rat) and mouse C57BL/6J mouse plasma ($f_{u,plasma}$ mouse). Data is shown as mean ± SD with n = 3 and N= 3.

Compound	$f_{u,plasma}$ rat	$f_{u,plasma}$ mouse
Erythromycin	0.473 ± 0.059	0.404 ± 0.035
Clarithromycin	0.401 ± 0.55	0.344 ± 0.037
Azithromycin	0.336 ± 0.073	0.437 ± 0.079
Telithromycin	0.251 ± 0.059	0.076 ± 0.008
Ciprofloxacin	0.727 ± 0.017	0.741 ± 0.087
Moxifloxacin	0.692 ± 0.013	0.675 ± 0.029
Levofloxacin	0.711 ± 0.014	0.723 ± 0.111
Lascufloxacin	0.372 ± 0.026	0.409 ± 0.014

B6. Correlation of Antibiotics Permeability in Lung Epithelial Cells versus LLC-PK1 WT cells

Figure B4 shows the P_{app} BA and $P_{app,inh}$ BA of antibiotics in lung epithelial cells (Calu-3 and hAELVi) compared to LLC-PK1 WT. The majority of antibiotics showed a reduced permeability in the lung epithelial cells, especially those being classified as high permeable in LLC-PK1 WT (> 100 nm/s).

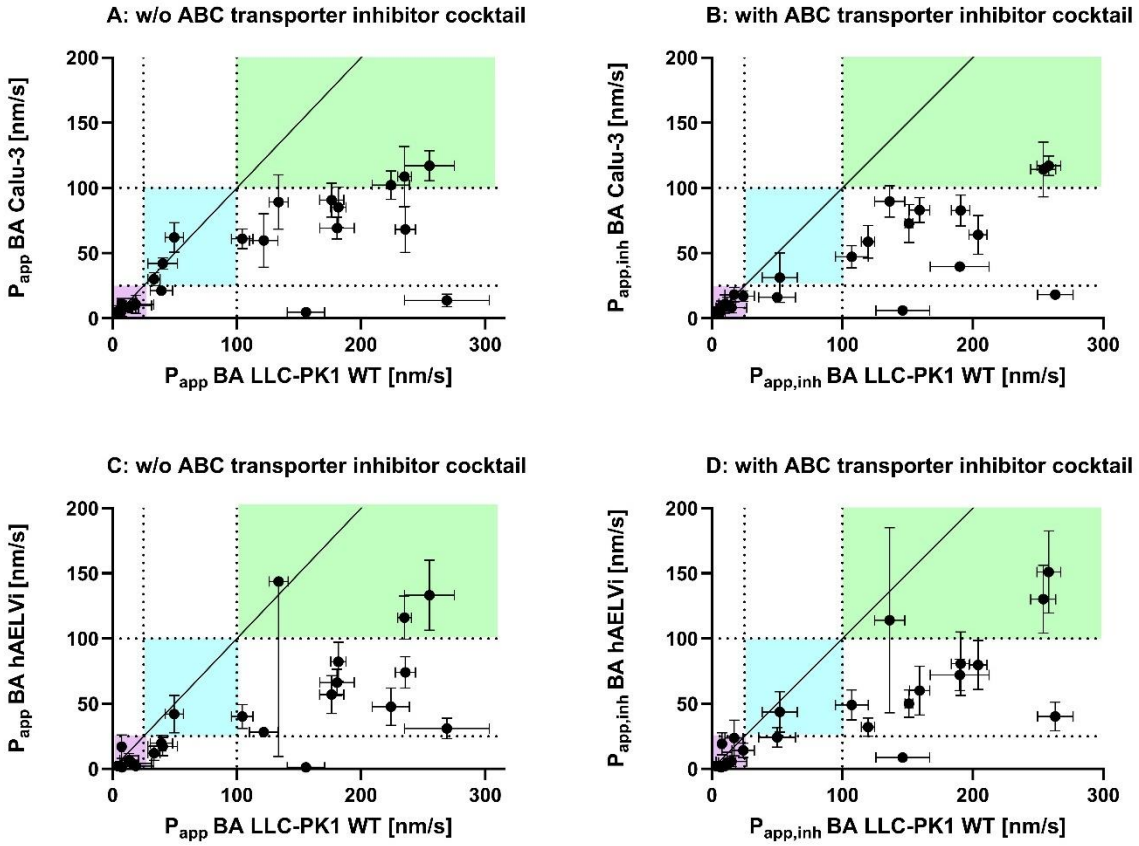

Figure B4. Comparison of basolateral to apical permeability of antibiotics and permeability markers in absence (P_{app} BA) or presence of ABC transporter inhibitor cocktail ($P_{app,inh}$ BA) in Calu-3 vs. LLC-Pk1 WT (A & B) or in hAELVi vs. LLC-Pk1 WT (C & D). Compounds were color-coded in violet if low permeable in both cell lines (< 25 nm/s), in blue if moderately permeable in both cell lines (25 -100 nm/s) or in green if high permeable in both cell lines (> 100 nm/s). The straight line represents the line of unity. Values are shown as mean ± SD with n =3 and N = 3. The R^2 values were calculated by a simple linear regression with R^2 = 0.483 (A) , R^2 = 0.546 (B), R^2 = 0.362 (C) and R^2 = 0.561 (D). w/o stands for without.

B7. Permeability of Paracellular markers

Figure B5 shows the apparent basolateral to apical permeability (P_{app} BA) and the apical to basolateral permeability (P_{app} AB) of the paracellular marker Lucifer Yellow in presence and absence of Bafilomycin A1 (1 µM), a disruptor of lysosomal acidification. For both Calu-3 and hAELVi cells, no statistically significant difference in permeability was observed across both conditions. Furthermore, the measured permeability values were below the threshold of 25 nm/s, which indicates the presence of a tight cell barrier under both conditions [78].

Figure B6 shows the average apparent basolateral to apical permeability (P_{app} BA) of atenolol in lung epithelial cell lines Calu-3 and hAELVi, as well as the reference cell lines Caco-2 and LLC-PK1 WT. No statically significant difference between the four cell lines were observed.

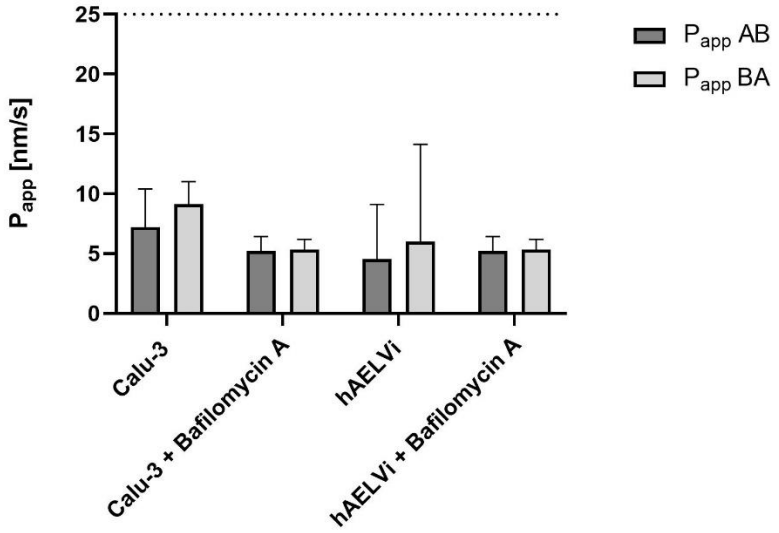

Figure B5. Apparent Permeability (P_{app}) of Lucifer Yellow in lung epithelial cells Calu-3 and hAELVi in the absence and presence of lysosomal trapping inhibitor Bafilomycin A1 (1 µM). Both permeability from apical to basolateral (P_{app} AB) and permeability from basolateral to apical side (P_{app} BA) are shown. Data is shown as mean ± SD with n = 3 and N = 3. The dotted line at 25 nm/s indicates the acceptance threshold for the paracellular markers Lucifer Yellow, that is typically confirmative of a tight monolayer [78].

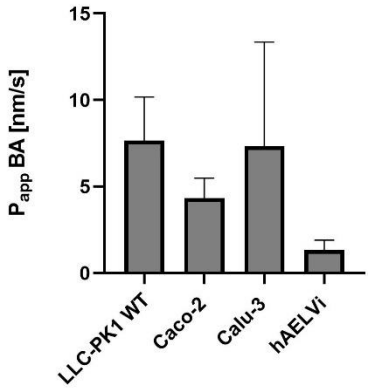

Figure B6. Comparison of average basolateral to apical permeability (P_{app} BA) of Atenolol in LLC-PK1 WT, Caco-2, Calu-3 and hAELVi. Data is shown as mean ± SD with n =3 and N = 3.

B8. Measured P_{app} of Antibiotics in LLC-PK1 WT, Caco-2, Calu-3 and hAELVi Cells

Table B5. Measured permeability values (P_{app}) and resulting efflux ratios (ER) of antibiotics and permeability control markers in absence and presence of ABC transporter inhibitor cocktail in **LLC-PK1 WT** cells. Values are shown as mean ± SD with n = 3 and N= 3.

Compound	P_{app} AB [nm/s]	P_{app} BA [nm/s]	$P_{app,inh}$ AB [nm/s]	$P_{app,inh}$ BA [nm/s]	ER	ER_i
Amoxicillin	5.00 ± 2.65	6.00 ± 3.61	3.67 ± 2.08	5.67 ± 4.62	1.27 ± 0.45	1.50 ± 0.36
Tazobactam	10.7 ± 9.9	13.3 ± 7.5	10.0 ± 11.3	15.0 ± 11.8	1.67 ± 0.64	1.80 ± 1.25
Cefdinir	8.67 ± 5.86	16.0 ± 15.4	17.0 ± 14.5	11.7 ± 6.7	1.60 ± 0.78	0.967 ± 0.451
Cefepime	9.33 ± 2.08	18.7 ± 14.5	13.3 ± 6.0	10.0 ± 4.6	1.90 ± 1.30	0.800 ± 0
Erythromycin	6.33 ± 1.15	40.3 ± 11.8	11.0 ± 1.0	17.0 ± 6.9	6.70 ± 3.04	1.50 ± 0.44
Clarithromycin	124 ± 5	181 ± 14	145 ± 16.9	190 ± 23	1.47 ± 0.12	1.30 ± 0.10
Azithromycin	10.0 ± 0	33.3 ± 4.9	9.67 ± 1.15	24.0 ± 8.7	3.43 ± 0.51	2.47 ± 0.55
Telithromycin	80.3 ± 23.5	104 ± 9	87.3 ± 11.0	107 ± 13	1.37 ± 0.31	1.23 ± 0.06
Ciprofloxacin	14.3 ± 0.6	39.3 ± 9.0	14.3 ± 3.2	50.0 ± 14.1	2.77 ± 0.61	3.53 ± 1.36
Moxifloxacin	187 ± 48	182 ± 6	165 ± 17	191 ± 7	1.00 ± 0.17	1.17 ± 0.12
Levofloxacin	45.0 ± 3.5	122 ± 12	58.0 ± 5.6	120 ± 5	2.73 ± 0.32	2.10 ± 0.10
Lascufloxacin	156 ± 6	236 ± 8	165 ± 4	204 ± 7	1.50 ± 0.10	1.20 ± 0
Vancomycin	2.67 ± 2.08	4.00 ± 3.46	3.00 ± 2.65	3.00 ± 1.73	1.30 ± 0.26	1.13 ± 0.38
Linezolid	127 ± 9	176 ± 10	154 ± 15	159 ± 8	1.40 ± 0.10	1.03 ± 0.15
Omadacycline	12.7 ± 6.0	7.33 ± 1.53	10.0 ± 4.6	7.67 ± 1.53	0.607 ± 0.21	0.867 ± 0.252
Dapsone	216 ± 4	235 ± 6	228 ± 6	254 ± 10	1.10 ± 0	1.10 ± 0
Isoniazid	128 ± 10	134 ± 8	132 ± 11	136 ± 12	1.07 ± 0.15	1.03 ± 0.06
Rifampicin	33.3 ± 3.5	49.7 ± 7.2	32.3 ± 3.1	52.0 ± 13.5	1.50 ± 0.30	1.83 ± 0.06
Hydroxychloroquine	120 ± 22	156 ± 15	116 ± 27	146 ± 21	1.33 ± 0.42	1.30 ± 0.17
Voriconazole	255 ± 12	255 ± 20	247 ± 11	258 ± 9	1.07 ± 0.06	1.03 ± 0.06
Atenolol	4.67 ± 2.08	7.67 ± 2.52	4.33 ± 2.31	7.33 ± 2.52	1.67 ± 0.72	1.87 ± 0.64
Propranolol	232 ± 32	269 ± 34	277 ± 83	263 ± 14	1.17 ± 0.25	1.00 ± 0.26
Edoxaban	122 ± 10	224 ± 15	155 ± 27	151 ± 3	1.87 ± 0.29	0.967 ± 0.208

Table B6. Measured permeability values (P_{app}) and resulting efflux ratios (ER) of antibiotics and permeability control markers in absence and presence of ABC transporter inhibitor cocktail in **Caco-2** cells. Values are shown as mean ± SD with n = 3 and N= 3.

Compound	P_{app} AB [nm/s]	P_{app} BA [nm/s]	$P_{app,inh}$ AB [nm/s]	$P_{app,inh}$ BA [nm/s]	ER	ER_i
Amoxicillin	3.00 ± 1.00	1.00 ± 0	2.67 ± 0.58	2.00 ± 0	0.367 ± 0.058	0.733 ± 0.058
Tazobactam	6.50 ± 0.71	3.33 ± 0.58	4.67 ± 2.08	3.67 ± 2.08	0.450 ± 0.071	0.600 ± 0.173
Cefdinir	4.07 ± 4.50	0.93 ± 0.12	1.10 ± 0.85	0.933 ± 0.112	1.27 ± 1.69	1.40 ± 0.70
Cefepime	0.533 ± 0.493	0.267 ± 0.153	0.500 ± 0.436	0.433 ± 0.322	1.01 ± 0.76	0.900 ± 0.265
Erythromycin	4.00 ± 1.00	85.7 ± 18.9	10.0 ± 1.0	18.3 ± 1.5	23.0 ± 8.6	1.83 ± 0.40
Clarithromycin	66.7 ± 7.0	245 ± 37	99.7 ± 9.2	129 ± 6	3.73 ± 0.81	1.33 ± 0.06
Azithromycin	5.77 ± 0.58	87.7 ± 16.6	11.0 ± 1.0	22.7 ± 0.6	15.4 ± 2.5	2.03 ± 0.12
Telithromycin	30.7 ± 1.2	196 ± 15	49.3 ± 7.0	132 ± 6	6.50 ± 0.70	2.73 ± 0.45
Ciprofloxacin	15.0 ± 3.6	66.0 ± 6.6	17.3 ± 5.9	34.7 ± 2.1	4.47 ± 1.08	2.12 ± 0.70
Moxifloxacin	119 ± 10	148 ± 11	133 ± 6	149 ± 6	1.27 ± 0.06	1.10 ± 0.10
Levofloxacin	49.3 ± 19.1	83.3 ± 4.0	65.7 ± 15.0	75.7 ± 11.9	1.93 ± 0.85	1.17 ± 0.12
Lascufloxacin	132 ± 14	191 ± 22	139 ± 17	170 ± 4	1.43 ± 0.06	1.17 ± 0.12
Vancomycin	0.967 ± 0.764	0.433 ± 0.288	0.767 ± 0.503	0.567 ± 0.377	0.567 ± 0.208	0.733 ± 0.115
Linezolid	128 ± 18	180 ± 9	142 ± 20	140 ± 5	1.43 ± 0.15	1.00 ± 0.17
Omadacycline	18.7 ± 4.7	24.0 ± 10.5	17.0 ± 6.2	18.0 ± 6.2	1.40 ± 0.79	1.13 ± 0.51
Dapsone	230 ± 21	224 ± 8.0	217 ± 13	240 ± 13	0.967 ± 0.058	1.10 ± 0
Isoniazid	203 ± 83	147 ± 10	208 ± 99	165 ± 1	0.833 ± 0.306	0.900 ± 0.346
Rifampicin	15.7 ± 5.5	109 ± 67	16.7 ± 3.8	111 ± 35	6.57 ± 2.49	6.53 ± 0.81
Hydroxychloroquine	34.3 ± 13.5	93.0 ± 9.8	60.7 ± 5.7	78.3 ± 10.5	2.97 ± 0.95	1.30 ± 0.10
Voriconazole	216 ± 10	239 ± 8	213 ± 31	247 ± 14	1.10 ± 0	1.17 ± 0.12
Atenolol	3.00 ± 2.00	4.33 ± 1.15	3.00 ± 2.00	2.67 ± 0.58	1.63 ± 0.75	1.23 ± 0.78
Propranolol	139 ± 27	179 ± 14	148 ± 22	169 ± 13	1.30 ± 0.17	1.17 ± 0.12
Edoxaban	58.7 ± 9.5	272 ± 37	106 ± 15	125 ± 12	4.60 ± 0.56	1.17 ± 0.12

Table B7. Measured permeability values (P_{app}) and resulting efflux ratios (ER) of antibiotics and permeability control markers in absence and presence of ABC transporter inhibitor cocktail in **Calu-3** cells. Values are shown as mean ± SD with n = 3 and N= 3.

Compound	P_{app} AB [nm/s]	P_{app} BA [nm/s]	$P_{app,inh}$ AB [nm/s]	$P_{app,inh}$ BA [nm/s]	ER	ER_i
Amoxicillin	3.67 ± 3.79	3.67 ± 2.08	3.00 ± 2.65	3.67 ± 2.08	1.70 ± 1.30	1.67 ± 1.11
Tazobactam	3.33 ± 1.53	8.00 ± 2.00	4.33 ± 3.21	8.33 ± 4.16	2.87 ± 1.03	2.10 ± 0.46
Cefdinir	2.67 ± 1.53	9.67 ± 5.51	3.67 ± 1.15	10.3 ± 6.1	3.53 ± 0.55	2.90 ± 1.15
Cefepime	3.33 ± 2.08	10.7 ± 7.1	5.00 ± 3.61	11.0 ± 7.0	3.10 ± 0.50	2.60 ± 0.80
Erythromycin	1.67 ± 0.58	42.0 ± 4.4	3.67 ± 0.58	18.3 ± 5.5	27.2 ± 3.8	5.53 ± 2.75
Clarithromycin	4.00 ± 1.00	69.3 ± 8.4	15.0 ± 4.4	39.7 ± 3.2	18.2 ± 6.8	2.90 ± 1.15
Azithromycin	2.67 ± 1.15	30.0 ± 5.0	4.33 ± 1.15	17.0 ± 4.0	13.1 ± 8.7	4.57 ± 2.07
Telithromycin	2.67 ± 0.58	61.0 ± 7.5	8.00 ± 2.00	47.3 ± 8.6	23.8 ± 4.8	6.17 ± 2.54
Ciprofloxacin	16.0 ± 1.7	21.3 ± 2.9	17.7 ± 2.1	16.3 ± 1.5	1.33 ± 0.15	0.93 ± 0.06
Moxifloxacin	57.3 ± 22.3	85.3 ± 15.5	72.3 ± 22.2	82.7 ± 11.9	1.57 ± 0.32	1.17 ± 0.15
Levofloxacin	50.0 ± 27.1	59.7 ± 20.6	53.7 ± 21.1	58.7 ± 12.5	1.30 ± 0.36	1.10 ± 0.17
Lascufloxacin	51.3 ± 11.0	68.3 ± 17.7	61.3 ± 18.3	64.0 ± 14.9	1.33 ± 0.42	1.07 ± 0.21
Vancomycin	1.00 ± 0	5.33 ± 3.06	1.00 ± 0	5.33 ± 3.79	5.63 ± 2.85	5.60 ± 3.3
Linezolid	70.3 ± 26.7	90.7 ± 13.0	81.0 ± 22.3	83.0 ± 9.5	1.33 ± 0.34	1.03 ± 0.15
Omadacycline	8.67 ± 5.51	11.3 ± 4.0	10.0 ± 4.0	9.67 ± 3.51	1.63 ± 0.76	0.933 ± 0.058
Dapsone	130 ± 38	109 ± 23	122 ± 35	114 ± 21	0.83 ± 0.06	0.967 ± 0.115
Isoniazid	89.7 ± 9.8	89.3 ± 21.0	101 ± 14	89.7 ± 12.0	1.00 ± 0.26	0.900 ± 0.200
Rifampicin	12.7 ± 2.1	62.0 ± 11.4	13.3 ± 8.5	31.3 ± 19.1	4.90 ± 0.70	2.30 ± 0.26
Hydroxychloroquine	2.33 ± 0.58	4.67 ± 0.58	6.67 ± 0.58	6.00 ± 1.00	2.13 ± 0.67	0.900 ± 0.173
Voriconazole	135 ± 15	117 ± 12	134 ± 18	117 ± 8	0.867 ± 0.058	0.867 ± 0.115
Atenolol	2.67 ± 1.53	7.33 ± 6.03	4.67 ± 3.51	6.67 ± 6.66	2.60 ± 1.95	1.37 ± 0.35
Propranolol	20.3 ± 7.6	13.7 ± 4.9	15.3 ± 9.9	18.3 ± 2.5	0.667 ± 0.115	2.00 ± 1.82
Edoxaban	14.3 ± 9.2	102 ± 11	41.3 ± 24.2	72.7 ± 14.5	8.60 ± 3.69	2.07 ± 0.86
Hydroxychloroquine + 1 µM Bafilomycin A1	74.3 ± 1.2	55.0 ± 3.6	78.0 ± 5.3	78.3 ± 1.5	0.733 ± 0.058	1.03 ± 0.06
Propranolol + 1 µM Bafilomycin A1	133 ± 3	108 ± 6	145 ± 6	142 ± 2	0.800 ± 0	0.967 ± 0.058

Table B8. Measured permeability values (P_{app}) and resulting efflux ratios (ER) of antibiotics and permeability control markers in absence and presence of ABC transporter inhibitor cocktail in **hAELVi** cells. Values are shown as mean ± SD with n = 3 and N= 3.

Compound	P_{app} AB [nm/s]	P_{app} BA [nm/s]	$P_{app,inh}$ AB [nm/s]	$P_{app,inh}$ BA [nm/s]	ER	ER_i
Amoxicillin	1.33 ± 0.58	2.32 ± 1.53	1.67 ± 1.16	1.73 ± 2.00	1.93 ± 0.06	1.07 ± 0.61
Tazobactam	4.00 ± 2.65	6.67 ± 5.03	6.33 ± 6.66	5.67 ± 4.04	1.70 ± 0.52	1.13 ± 0.59
Cefdinir	3.93 ± 6.12	4.33 ± 5.77	4.43 ± 6.56	5.07 ± 7.75	2.37 ± 1.40	1.07 ± 0.23
Cefepime	1.00 ± 0	2.33 ± 1.16	1.67 ± 0.58	2.32 ± 0.58	2.10 ± 0.61	2.10 ± 1.15
Erythromycin	15.7 ± 8.5	17.3 ± 7.0	19.7 ± 9.2	23.7 ± 13.8	1.17 ± 0.21	1.17 ± 0.25
Clarithromycin	47.7 ± 4.2	66.3 ± 10.3	57.3 ± 2.3	72.0 ± 12.1	1.40 ± 0.10	1.27 ± 0.12
Azithromycin	5.00 ± 5.29	12.0 ± 5.6	6.00 ± 4.36	14.3 ± 5.5	3.33 ± 1.51	2.87 ± 0.95
Telithromycin	31.0 ± 4.6	40.3 ± 9.3	33.3 ± 6.8	49.0 ± 11.5	1.30 ± 0.30	1.47 ± 0.15
Ciprofloxacin	17.7 ± 3.2	19.7 ± 6.0	19.7 ± 3.2	24.3 ± 7.5	1.10 ± 0.17	1.20 ± 0.27
Moxifloxacin	96.7 ± 17.2	82.3 ± 15.0	86.3 ± 26.3	80.7 ± 24.4	0.867 ± 0.058	0.933 ± 0.208
Levofloxacin	28.0 ± 2.0	28.2 ± 3.2	27.7 ± 2.5	32.0 ± 7.0	1.03 ± 0.06	1.20 ± 0.30
Lascufloxacin	83.3 ± 25.1	74.0 ± 12.2	77.7 ± 16.7	79.7 ± 18.9	0.933 ± 0.153	1.03 ± 0.25
Vancomycin	0.833 ± 1.012	2.33 ± 2.31	2.87 ± 4.45	2.33 ± 2.31	3.87 ± 2.50	3.80 ± 4.31
Linezolid	57.7 ± 16.2	57.0 ± 14.5	64.3 ± 12.7	60.0 ± 18.7	1.00 ± 0.10	0.900 ± 0.173
Omadacycline	17.3 ± 11.0	17.0 ± 9.2	19.0 ± 13.5	19.3 ± 8.5	1.03 ± 0.32	1.27 ± 0.72
Dapsone	98.3 ± 32.5	116 ± 17	98.3 ± 30.9	130 ± 26	1.33 ± 0.59	1.47 ± 0.67
Isoniazid	396.0 ± 289.1	148 ± 134	325 ± 154	114 ± 71	0.467 ± 0.404	0.400 ± 0.300
Rifampicin	25.0 ± 7.9	42.0 ± 14.4	29.3 ± 5.9	43.7 ± 15.5	1.67 ± 0.06	1.47 ± 0.42
Hydroxychloroquine	3.00 ± 2.65	1.33 ± 0.58	5.00 ± 2.00	8.67 ± 3.51	0.500 ± 0.173	2.10 ± 1.28
Voriconazole	152 ± 3	133 ± 27	155 ± 20	151 ± 32	0.867 ± 0.153	0.967 ± 0.115
Atenolol	0.567 ± 0.379	1.33 ± 0.58	0.600 ± 0.346	1.17 ± 0.76	2.80 ± 0.95	1.33 ± 0.12
Propranolol	39.3 ± 10.2	31.0 ± 7.9	45.7 ± 6.8	40.3 ± 11.0	0.867 ± 0.404	0.767 ± 0.153
Edoxaban	48.3 ± 12.4	47.7 ± 14.5	49.3 ± 16.3	50.0 ± 10.6	0.967 ± 0.058	1.07 ± 0.15
Hydroxychloroquine + 1 µM Bafilomycin A1	85.7 ± 12.2	64.7 ± 5.8	89.0 ± 11.1	94.0 ± 5.6	0.767 ± 0.058	1.03 ± 0.15
Propranolol + 1 µM Bafilomycin A1	132 ± 11	109 ± 6	144 ± 9	140 ± 3	0.833 ± 0.115	0.967 ± 0.058

C. Supplemental Material to Chapter 3.3

C1. Details on Clinical and *in vivo* Studies

The Tables C1 and C2 provide an overview of all clinical and *in vivo* studies that were used within the scope of this *in silico* study to compare the observed concentration-time profiles of moxifloxacin and telithromycin in plasma and epithelial lining fluid (ELF) of human and rat to the simulated profiles.

Table C1. Overview of clinical studies characteristics used as observed plasma & epithelial lining fluid (ELF) data in the scope of this *in silico* study. BAL stands for bronchoalveolar lavage.

Drug	Health state	Total Number of subjects	Percentage of male [%]	Age [year]	Dose [mg]	Frequency	Administration route	ELF collection method	Source
Moxifloxacin	Healthy	18	100	18 - 40	400	Single dose	oral	-	[347]
	Patients with diagnostic bronchoscopy	19	73.4	> 18	400	Single dose	oral	BAL	[351]
		16	81.3	67 ± 10	400	5 x 24 h	oral	BAL	[352]
Telithromycin	Healthy	18	100	18 -45	800	Single dose	oral	-	[349]
	Patients with diagnostic bronchoscopy	27	59.3	> 18	800	Single dose	oral	BAL	[353]
		17	52.9	65 ± 13	800	5 x 24 h	oral	BAL	[354]

Table C2. Overview of *in vivo* studies characteristics used as observed plasma & epithelial lining fluid (ELF) data in the scope of this *in silico* study. i.v. stands for intravenous and BAL for bronchoalveolar lavage.

Drug	Strain	Number of animals per time point	Gender	Dose	Frequency	Administration route	ELF collection method	Source
Moxifloxacin	Wistar	3	male	9.2 mg/kg	Single dose	i.v.	-	[348]
	Sprague-Dawley	6	male	5mg/kg	Single dose	i.v.	BAL	[297]
Telithromycin	Sprague-Dawley	8	male	50 mg/kg	Single dose	oral	-	[350]
	Sprague-Dawley	7	male	50 mg/kg	Single dose	oral	BAL	[289]

C2. Input Parameters for PBPK Models

The physicochemical and pharmacokinetic parameters not stated in Table C3 and C4 were used as predicted by GastroPlus™ based on the compound's chemical structure.

Table C3. Overview of input parameters for the Moxifloxacin PBPK model summarising *in vitro*, *in vivo* and clinical data.

Parameter	Value	Source
Physicochemical properties		
logD at pH 7.4	0.01	Inhouse prediction by machine learning model
Solubility [mg/mL] at pH 6.4	37.6	[364]
Absorption		
P_{eff} [10^{-4} cm/s]	2.8	Predicted by an inhouse developed conversion tool based on a correlation of *in vitro* P_{app} and P_{eff} by [404]
P_{app} Moxifloxacin in LLC-PK1 [nm/s]	148	Inhouse determination
P_{app} Propranolol in LLC-PK1 [nm/s]	232	Inhouse determination
Binding		
$f_{u,plasma}$ human	0.673	Inhouse determination
Adjusted $f_{u,plasma}$ human	0.670	Predicted by GastroPlus™ from $f_{u,plasma}$ taking plasma lipid binding into account
$f_{u,plasma}$ rat	0.699	Inhouse determination
Adjusted $f_{u,plasma}$ rat	0.698	Predicted by GastroPlus™ from $f_{u,plasma}$ taking plasma lipid binding into account
$f_{u,sELF}$	0.782	Inhouse determination
Distribution		
V_{ss} human [L/kg]	1.62[a]	Estimated by GastroPlus™
V_{ss} rat [L/kg]	2.21[a]	Estimated by GastroPlus™
$t_{1/2}$ human [h]	9.00[b]	Estimated by GastroPlus™
$t_{1/2}$ rat [h]	1.18[b]	Estimated by GastroPlus™
Transport		
K_m MDR1 [µM]	200[c]	[345]
V_{max} MDR1 [nmol/min/mg protein]	12[c]	[345]
CL_{diff} [µL/min/million hepatocytes]	32	[345]
Elimination		
$CL_{int,hep}$ human [µL/min/million hepatocytes]	1.00	Inhouse determination
$CL_{hepatic}$ human [L/h]	8	Scaled from *in vitro* hepatic intrinsic clearance by using the conversion module in GastroPlus™
CL_{renal} human [L/h]	2.6	[405]
CL_{sys} human [L/h]	10.6	Calculated by GastroPlus™
$CL_{int,hep}$ rat [µL/min/million hepatocytes]	4.22	Inhouse determination
$CL_{hepatic}$ rat [L/h]	0.172	Scaled from *in vitro* hepatic intrinsic clearance by using the conversion module in GastroPlus™
CL_{renal} mouse [L/h]	0.154[d]	[348]
CL_{sys} rat [L/h]	0.326	Calculated by GastroPlus™

[a] Literature reported a mean V_{ss} of 2.0 L/kg in human and a mean V_{ss} of 3.6 L/kg in rats [348].

[b] Literature reported a mean $t_{1/2}$ of 12.0 h in human and a mean $t_{1/2}$ of 1.2 h in rats [348].

[c] The values were estimated from available graphics within the publication. The V_{max} was converted to [nmol/min/mg protein] by assuming that 1.2 x 10^7 MDCK cells correspond to 1 mg of protein [406].

[d] Using the reported CL_{renal} rat (0.054 L/h) resulted in an overestimation of predicted plasma concentrations of Moxifloxacin in rats, therefore the reported CL_{renal} mouse was taken, as a better fit to observed data was seen.

Table C4. Overview of input parameters for Telithromycin PBPK model summarising *in vitro*, *in vivo* and clinical data.

Parameter	Value	Source
Physicochemical properties		
logP	3.00	Extracted from Certara Drug Interaction Data Base (DIDB)
Solubility [mg/mL] at pH 6.5	0.81	Inhouse determination
Absorption		
P_{eff} [10^{-4} cm/s]	1.99	Predicted by an inhouse developed conversion tool based on a correlation of in vitro P_{app} and P_{eff} by [404]
P_{app} Telithromycin in LLC-PK1 [nm/s]	80.3	Inhouse determination
P_{app} Propranolol in LLC-PK1 [nm/s]	232	Inhouse determination
Binding		
$f_{u,plasma}$ human	0.342	Inhouse determination
Adjusted $f_{u,plasma}$ human	0.120	Predicted by GastroPlus™ from $f_{u,plasma}$ taking plasma lipid binding into account
$f_{u,plasma}$ rat	0.285	Inhouse determination
Adjusted $f_{u,plasma}$ rat	0.178	Predicted by GastroPlus™ from $f_{u,plasma}$ taking plasma lipid binding into account
$f_{u,sELF}$	0.654	Inhouse determination
Distribution		
V_{ss} human [L/kg]	5.21	Estimated by GastroPlus™
V_{ss} rat [L/kg]	3.00	Estimated by GastroPlus™
$t_{1/2}$ human [h]	6.56	Estimated by GastroPlus™
$t_{1/2}$ rat [h]	2.13	Estimated by GastroPlus™
Transport		
K_m MDR1 [µM]	15	[16]
V_{max} MDR1 [nmol/min/mg protein]	20.8	[16]
CL_{diff} [µL/min/million hepatocytes]	100	[346]
Enzymes		
K_m Human CYP3A4 [µM]	58	[346]
V_{max} Human CYP3A4 [pmol/min/pmol of isoform]	7.3	[346]
K_m rat intestinal microsomes [µM]	7.10	[357]
V_{max} rat intestinal microsomes [nmol/min/mg protein]	0.0992	[357]
Elimination		
$CL_{int,hep}$ human [µL/min/million hepatocytes]	11.0	Inhouse determination
$CL_{hepatic}$ human [L/h]	26.0	Scaled from *in vitro* hepatic intrinsic clearance by using the conversion module in GastroPlus™.
$CL_{biliary}$ human [L/h]	7.0	[346]
CL_{renal} human [L/h]	14.0	[349]
CL_{sys} human [L/h]	47.0	Calculated by GastroPlus™
$CL_{int,hep}$ rat [µL/min/million hepatocytes]	10.4	Inhouse determination
$CL_{hepatic}$ rat [L/h]	0.149	Scaled from *in vitro* hepatic intrinsic clearance by using the conversion module in GastroPlus™.
CL_{renal} rat [L/h]	0.102	[350]
CL_{sys} rat [L/h]	0.251	Calculated by GastroPlus™

[a] Literature reported a mean V_{ss} of 2.9 L/kg in human and a mean V_{ss} of 3.5 L/kg in rats [350, 365].

[b] Literature reported a mean $t_{1/2}$ of 10.0 h in human and a mean $t_{1/2}$ of 2.2 h in rats [350, 365].

C3. Prediction of Human ELF Concentration-time Profiles for Moxifloxacin and Telithromycin and Comparison to Observed Values from a Further Clinical Study

The measured ELF concentration-time profiles of each one further clinical study of moxifloxacin and telithromycin were compared to simulated ELF concentration-time profiles, using the perfusion and permeability limited model, as described in 3.3.2.5. In summary, predicted ELF concentrations are underestimated compared to observed values for both moxifloxacin and telithromycin. The closest prediction was seen when using the perfusion-limited model based on $K_{ELF/p,u}$. This is well aligned with findings that were described in 3.3.3.3.

C3.1 Perfusion limited model – Simulation of the ELF concentration based on $K_{ELF/p,u}$

Figure C1 shows the estimated ELF concentration-time profiles of moxifloxacin and telithromycin in human, when using the perfusion limited model based on the ELF to unbound plasma partition coefficient ($K_{ELF/p,u}$).

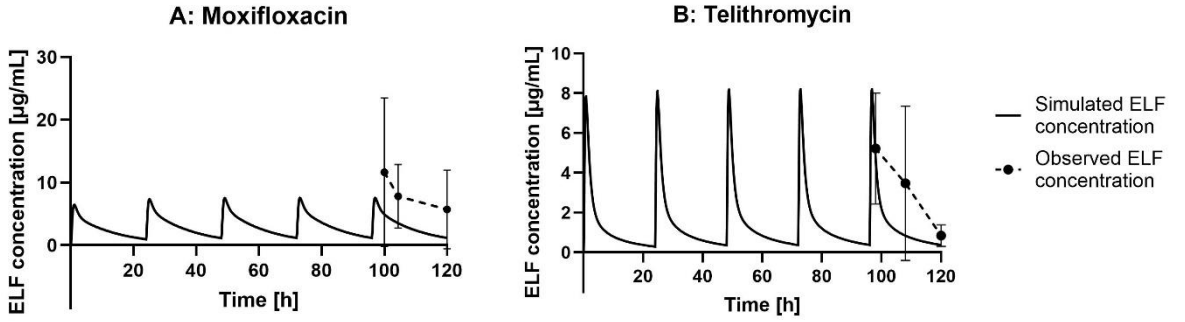

Figure C1. Simulated and observed ELF concentration-time profiles of **Moxifloxacin** (A) and **Telithromycin** (B) in human using the perfusion limited model based on the ELF to unbound plasma partition coefficient ($K_{ELF/p,u}$). Moxifloxacin was given as multiple oral dose of 400 mg (q24h x 5 doses) and Telithromycin as multiple dose of 800 mg (q24h x 5 doses) [352, 354]. The predicted ELF profiles are depicted as solid line (-) and observed profiles are shown as dotted line with measured means ± SD as dots (--·--).

The predicted ELF concentrations of moxifloxacin are within the standard deviation of observed values, however underpredicting the observed mean ELF concentrations by more than two-fold. For telithromycin, a good capture of clinical ELF data was seen for two sampling time points (96 and 120 h), whereas for the second time point (104 h), an underestimation of two-fold was seen compared to observed data, but within the reported standard deviation.

C3.2 Perfusion-limited Model – Simulation of the ELF concentration based on Ap PStc

Figure C2 shows the predictions of the ELF concentration-time profiles for moxifloxacin and telithromycin if using the perfusion-limited model and a slowed diffusion process on the apical side, defined by Ap PStc that was estimated from the hepatic passive diffusion clearance.

The simulated ELF concentration profiles were underestimating the observed concentrations for moxifloxacin (six-fold) and especially pronounced for telithromycin (more than 20-fold).

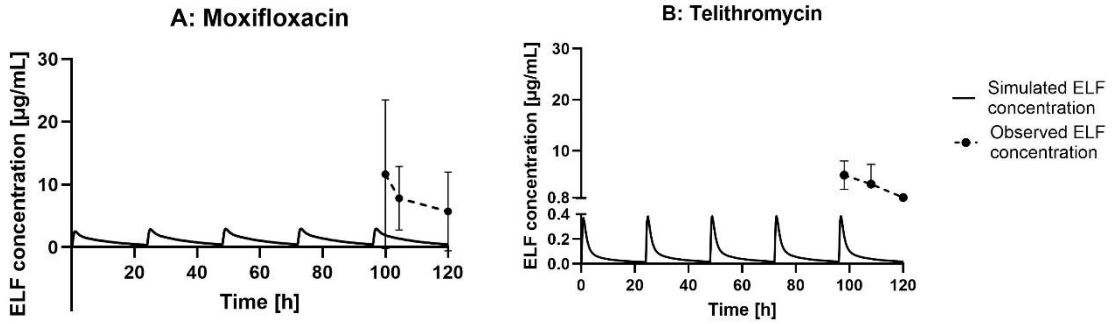

Figure C2. Simulated and observed ELF concentration-time profiles of **Moxifloxacin** (A) and **Telithromycin** (B) in human using the perfusion limited model with a scaled permeability surface area product on the apical side (Ap PStc). Moxifloxacin was given as multiple oral dose of 400 mg (q24h x 5 doses) and Telithromycin as multiple dose of 800 mg (q24h x 5 doses) [352, 354]. The predicted ELF profiles are depicted as solid line (-) and observed profiles are shown as dotted line with measured means ± SD as dots (--·--).

C3.3 Perfusion-limited Model – Effect of Pulmonary MDR1 Efflux on the Simulation of the ELF concentration

In addition to the Ap PStc, the active efflux transporter MDR1 was added to the perfusion-limited model within the lung tissue on the ELF-facing apical side.

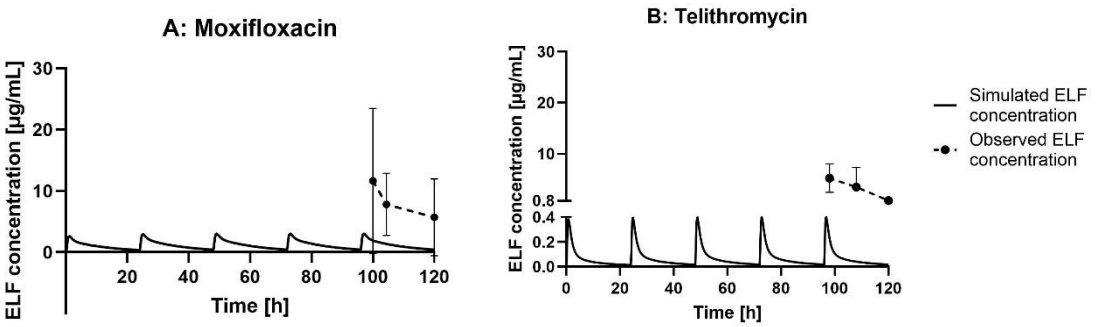

Figure C3. Simulated and observed ELF concentration-time profiles of **Moxifloxacin** (A) and **Telithromycin** (B) in human using the perfusion limited model with a scaled permeability surface area product on the apical side (Ap PStc) and active efflux by MDR1 on the apical side of the lung tissue. Moxifloxacin was given as multiple oral dose of 400 mg (q24h x 5 doses) and Telithromycin as multiple dose of 800 mg (q24h x 5 doses) [352, 354]. The predicted ELF profiles are depicted as solid line (-) and observed profiles are shown as dotted line with measured means ± SD as dots (--·--).

As shown in Figure C3, the predicted ELF concentration-time profiles did not change for both moxifloxacin and telithromycin, when incorporating MDR1 efflux into the PBPK model (see Figure C2 as comparison). The Predicted ELF concentrations for moxifloxacin are within or close to seen standard deviation of observed values, nevertheless the observed mean is more than six-fold underestimated.

C3.4 Permeability-limited Model – Simulation of the ELF concentration based on Ap & Ba PStc

In the permeability-limited model, the partition of a compound from the extracellular space via the lung tissue into the ELF is characterised by a passive diffusion. This value was estimated based on the passive hepatic clearance and upscaled by GastroPlus™ to the lung permeability surface area product (PStc). The same value was taken for the apical and basolateral PStc (Ap/Ba PStc).

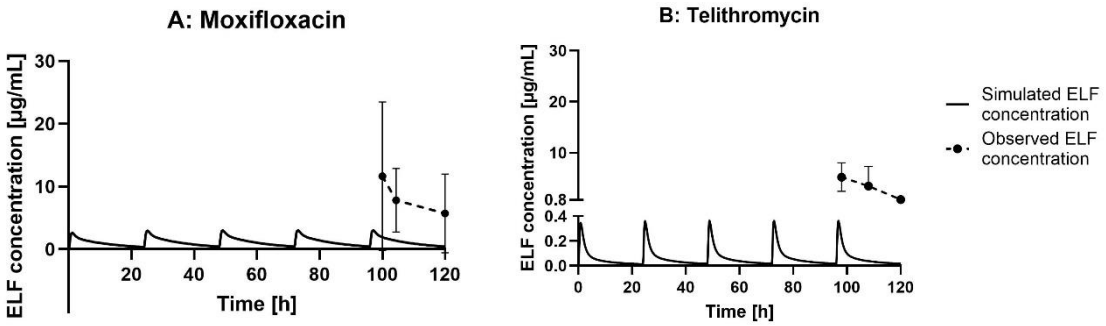

Figure C4. Simulated and observed ELF concentration-time profiles of **Moxifloxacin** (A) and **Telithromycin** (B) in human using the permeability limited model with a scaled permeability surface area product on the apical side (Ap PStc) and basolateral side (Ba PStc). Moxifloxacin was given as multiple oral dose of 400 mg (q24h x 5 doses) and Telithromycin as multiple dose of 800 mg (q24h x 5 doses) [352, 354]. The predicted ELF profiles are depicted as solid line (-) and observed profiles are shown as dotted line with measured means ± SD as dots (--·--).

Figure C4 shows the predicted ELF concentration-time profiles of moxifloxacin and telithromycin when using the permeability-limited model. Simulated values were similar to those received with the perfusion limited model, defined by PStc on the apical side only (see Figure C2). The simulated ELF concentrations underestimated the observed ones by around six-fold for moxifloxacin and 24-fold for telithromycin.

C3.5 Permeability-limited Model – Effect of Pulmonary MDR1 Efflux on the Simulation of the ELF concentration

In this simulation, the permeability-limited model was adapted to include MDR1 as efflux transporter on the apical side of the lung tissue. As shown in Figure C5, the predicted ELF concentration-time profiles were underestimated for both antibiotics and values were comparable to those predicted by the permeability-limited model without the incorporation of MDR1 (see Figure C3).

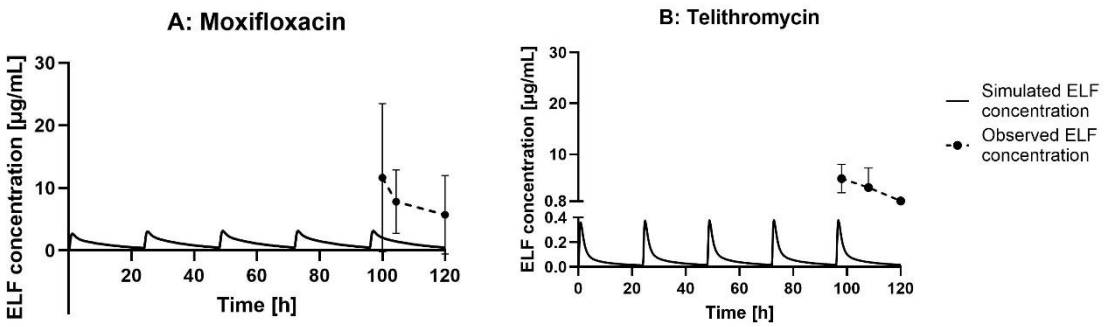

Figure C5. Simulated and observed ELF concentration-time profiles of **Moxifloxacin** (A) and **Telithromycin** (B) in human using the permeability limited model with a scaled permeability surface area product on the apical side (Ap PStc) and basolateral side (Ba PStc) and MDR1 efflux at the apical side of the lung tissue. Moxifloxacin was given as multiple oral dose of 400 mg (q24h x 5 doses) and Telithromycin as multiple dose of 800 mg (q24h x 5 doses) [352, 354]. The predicted ELF profiles are depicted as solid line (-) and observed profiles are shown as dotted line with measured means ± SD as dots (--·--).

C4. Parameter sensitivity analysis (PSA) of ELF Concentration-time Profiles of Moxifloxacin and Telithromycin when Using the Permeability-limited Model

As described in chapter 5.3.3, parameter sensitivity analyses (PSA) were performed to assess what impact a change in lung-specific Ap/Ba PStc, f,u_{ELF}, MDR1 pulmonary expression levels or antibiotics interaction kinetics with MDR1 (defined by K_m & V_{max}) have on simulated ELF concentration-time profiles when using the permeability-limited model of GastroPlus™. The observed findings were basically identical to those, when running the PSA of these parameters in the perfusion-limited model.

C4.1 Permeability-limited Model – Simulation of the ELF concentration based on Ap & Ba PStc & $f_{u,ELF}$

The PSA evaluating the impact of a change in Ap/Ba PStc and $f_{u,ELF}$ on ELF concentration-time profiles were performed using the permeability-limited model without the incorporation of MDR1 efflux into the lung tissue. The lung-specific PStc was scaled from GastroPlus™ based on the passive hepatic clearance. The results are summarised in Figure C6 – C9.

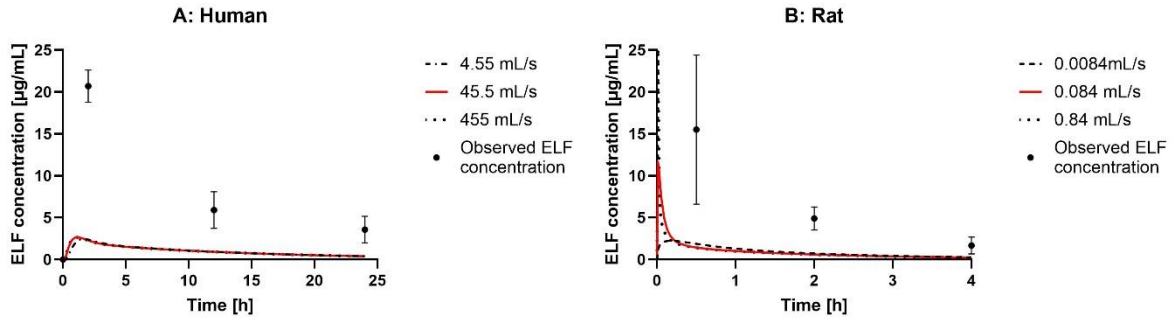

Figure C6. Parameter sensitivity analysis (PSA) of the predicted ELF concentration-time profiles of **Moxifloxacin** in human (A) and rat (B) if changing the apical/basolateral permeability surface area product (Ap/Ba PStc) and using the permeability-limited model. The simulated ELF concentration using the experimental Ap PStc is shown a solid red line, with a 10-fold lower Ap PStc as dashed line (---) and with a 10-fold higher Ap PStc as dotted line (⋯). Observed ELF concentrations are shown as measured means ± SD as dots (·) [297, 347].

As seen in Figure C6 and C7, a change in the Ap/Ba PStc (either 10-fold increase or decrease of initial scaled PStc) had no impact on predicted ELF concentrations of moxifloxacin and telithromycin in both human and rat.

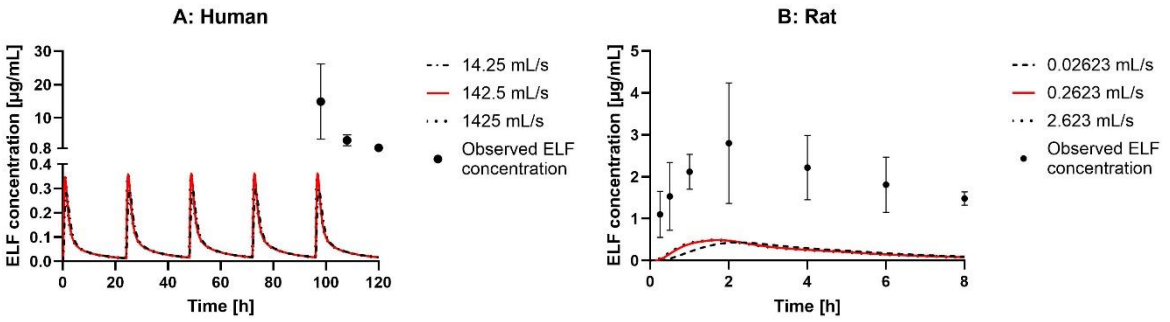

Figure C7. Parameter sensitivity analysis (PSA) of the predicted ELF concentration-time profiles of **Telithromycin** in human (A) and rat (B) if changing the apical/basolateral permeability surface area product (Ap/Ba PStc) and using the permeability-limited model. The simulated ELF concentration using the scaled Ap PStc is shown a solid red line, with a 10-fold lower Ap PStc as dashed line (---) and with a 10-fold higher Ap PStc as dotted line (⋯). Observed ELF concentrations are shown as measured means ± SD as dots (·) [289, 353].

The Figures C8 & C9 show the differences in predicted ELF concentration-time profiles of moxifloxacin and telithromycin when lowering the experimentally derived $f_{u,ELF}$ by 10-fold and when using the predicted value for $f_{u,ELF}$ by GastroPlus™.

Taking a 10-fold lower $f_{u,ELF}$ than the experimental value for moxifloxacin resulted in a great prediction of observed ELF concentration. For telithromycin, lowering the $f_{u,ELF}$ to the value predicted by GastroPlus™ resulted in a better capture of the observed ELF profile in human, whereas in rat an overestimation of observed values was seen.

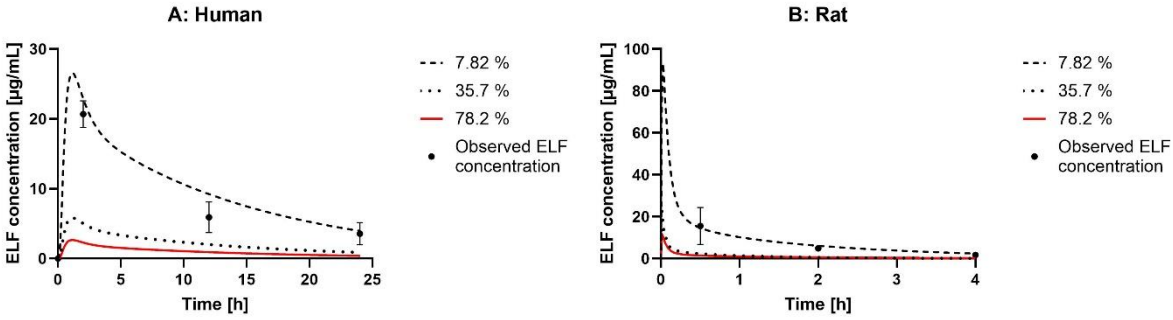

Figure C8. Parameter sensitivity analysis (PSA) of the predicted ELF concentration-times profiles of **Moxifloxacin** in human (A) and rat (B) if changing the unbound fraction in ELF ($f_{u,ELF}$) and using the permeability-limited model. The simulated ELF concentration using the experimental $f_{u,ELF}$ is shown a solid red line, with a 10-fold lower $f_{u,ELF}$ as dashed line (---) and with the predicted $f_{u,ELF}$ from GastroPlus™ as dotted line (⋯). Observed ELF concentrations are shown as measured means ± SD as dots (·) [297, 347].

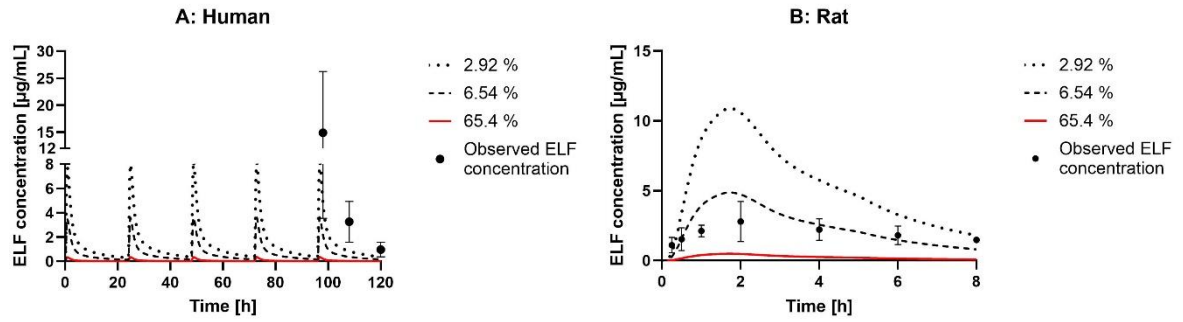

Figure C9. Parameter sensitivity analysis (PSA) of the predicted ELF concentration-time profiles of **Telithromycin** in human (A) and rat (B) if changing the unbound fraction in ELF ($f_{u,ELF}$) and using the permeability-limited model. The simulated ELF concentration using the experimental $f_{u,ELF}$ is shown a solid red, with a 10-fold lower $f_{u,ELF}$ as dashed line (---) and with the predicted $f_{u,ELF}$ from GastroPlus™ as dotted line (⋯). Observed ELF concentrations are shown as measured means ± SD as dots (·) [289, 353].

C4.2 Permeability-limited Model – Effect of Pulmonary MDR1 Efflux on the Simulation of the ELF concentration

In a last scenario, the PSA was performed to investigate how the predicted ELF concentrations change if MDR1 expression levels or antibiotics interaction kinetics with MDR1 (i.e. K_m and V_{max}) vary.

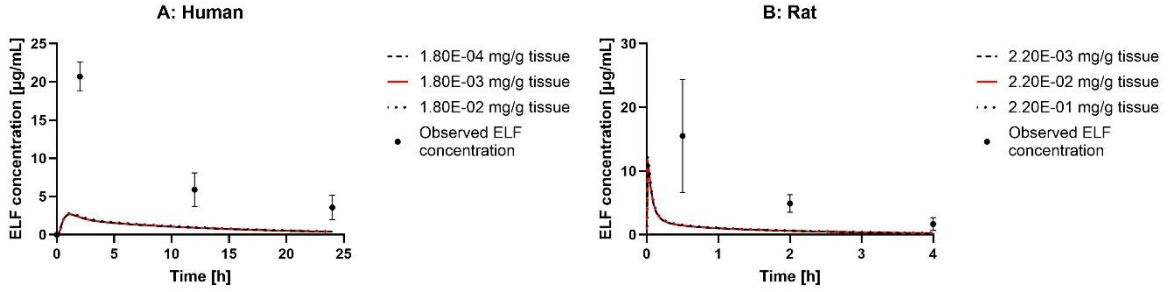

Figure C10. Parameter sensitivity analysis (PSA) of the predicted ELF concentration of **Moxifloxacin** in human (A) and rat (B) if changing the MDR1 expression level in the lung and using the permeability-limited model. The simulated ELF concentration using the estimated MDR1 expression is shown as solid red line, with a ten-fold lower MDR1 expression as dashed line (---) and with a ten-fold higher MDR1 expression as dotted line (⋯). Observed ELF concentrations are shown as individual measured means ± SD as dots (·) [297, 347].

As seen in Figure C10, a change in expression level of MDR1 had no impact on predicted ELF concentrations of moxifloxacin for both human and rat. The similar observation was made for telithromycin in human, however if increasing the pulmonary MDR1 expression level by 10-fold to the estimated level in rat, this resulted in a good capture of the observed profile (Figure C11).

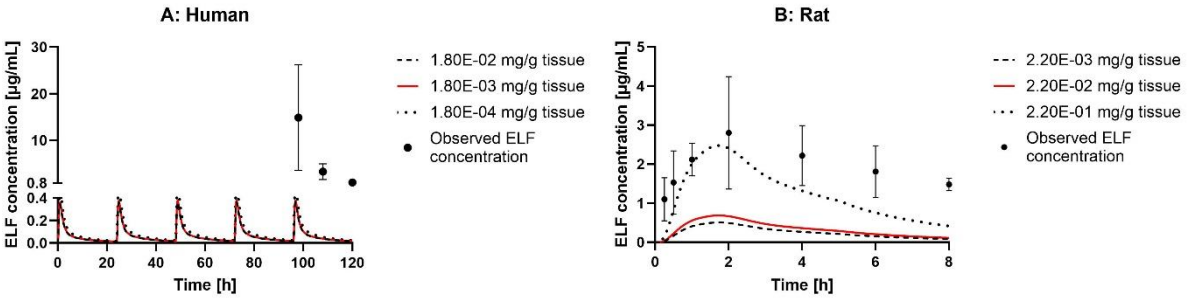

Figure C11. Parameter sensitivity analysis (PSA) of the predicted ELF concentration of **Telithromycin** in human (A) and rat (B) if changing the MDR1 expression level in the lung and using the permeability-limited model. The simulated ELF concentration using the estimated MDR1 expression is shown as solid red line, with a 10-fold lower MDR1 expression as dashed line (---) and with a 10-fold higher MDR1 expression as dotted line (⋯). Observed ELF concentrations are shown as individual measured means ± SD as dots (·) [289, 353].

Next, it was assessed where a change in K_m has an impact on simulated ELF concentrations. This was not observed for moxifloxacin in human, whereas decreasing the experimental K_m by 100-fold resulted in an increase of predicted ELF concentration in rat, being close or within standard deviation of observed data (as Figure C12).

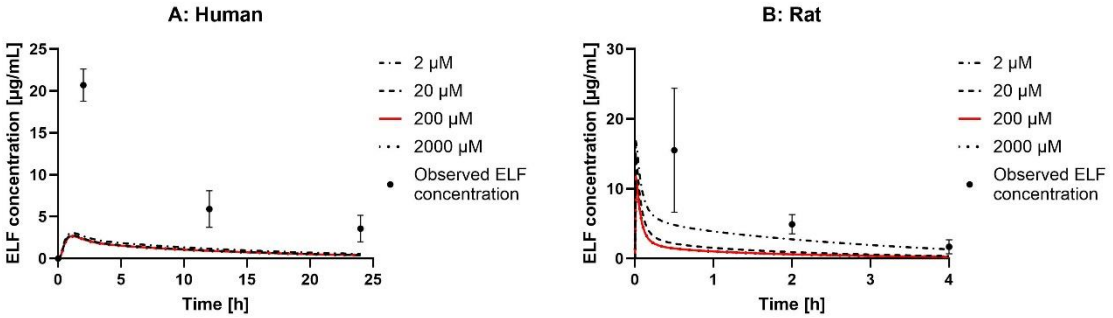

Figure C12. Parameter sensitivity analysis (PSA) of the predicted ELF concentration of **Moxifloxacin** in human (A) and rat (B) if changing the Michaelis-Menten constant (K_m) of MDR1 interaction and using the permeability-limited model. The simulated ELF concentration using the literature-retrieved K_m is shown as solid red line, with a 100-fold lower K_m as patterned line (-·-), with a 10-fold lower K_m as dashed line (---) and with a 10-fold higher K_m as dotted line (⋯). Observed ELF concentrations are shown as individual measured means ± SD as dots (·) [297, 347].

A slight increase in predicted ELF concentration of telithromycin was observed when decreasing the K_m by 100-fold in human, whereas a 10-fold reduction of the literature-retrieved K_m resulted in a good ELF prediction in rat (Figure C13).

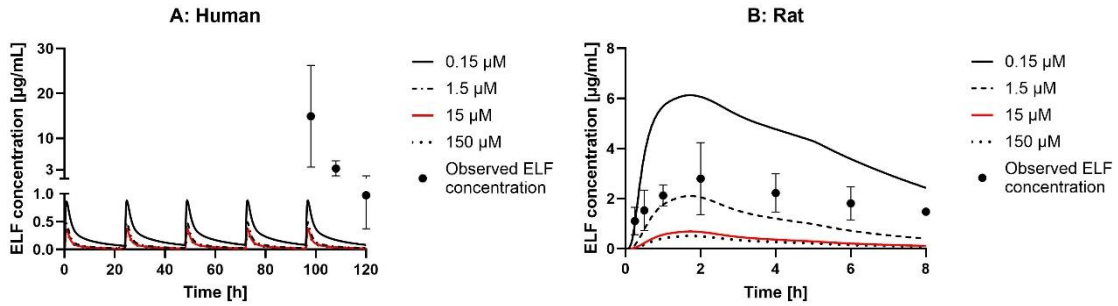

Figure C13. Parameter sensitivity analysis (PSA) of the predicted ELF concentration of **Telithromycin** in human (A) and rat (B) if changing the Michaelis-Menten constant (K_m) of MDR1 interaction and using the permeability-limited model. The simulated ELF concentration using the literature-retrieved K_m is shown as solid red line, with a 1000-fold lower K_m as black solid line, with a 100-fold lower K_m as patterned line (-·-), with a 10-fold lower K_m as dashed line (---) and with a 10-fold higher K_m as dotted line (⋯). Observed ELF concentrations are shown as individual measured means ± SD as dots (·) [289, 353].

As shown in Figure C14, a change in V_{max} did not impact the predicted ELF concentration profile for moxifloxacin in human and rat. The same was observed for the simulated ELF concentration of telithromycin in human, whereas a 10-fold increase of literature-retrieved V_{max} resulted in a more than three-fold higher predicted ELF concentration of telithromycin in rat, with values being close or within the standard deviation of observed numbers (Figure C15).

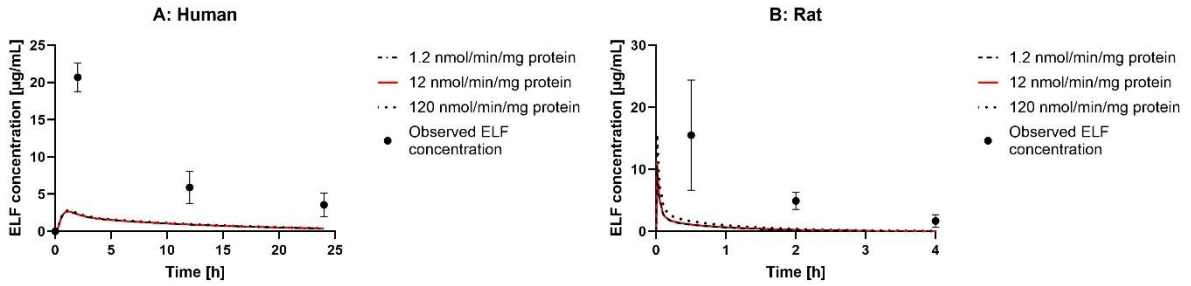

Figure C14. Parameter sensitivity analysis (PSA) of the predicted ELF concentration of **Moxifloxacin** in human (A) and rat (B if changing the maximal velocity (V_{max}) of MDR1 interaction and using the permeability-limited model. The simulated ELF concentration using the literature-retrieved V_{max} is shown as solid red line, with a 10-fold lower V_{max} as dashed line (---), with a 10-fold higher V_{max} as dotted line (⋯). Observed ELF concentrations are shown as individual measured means ± SD as dots (·) [297, 347].

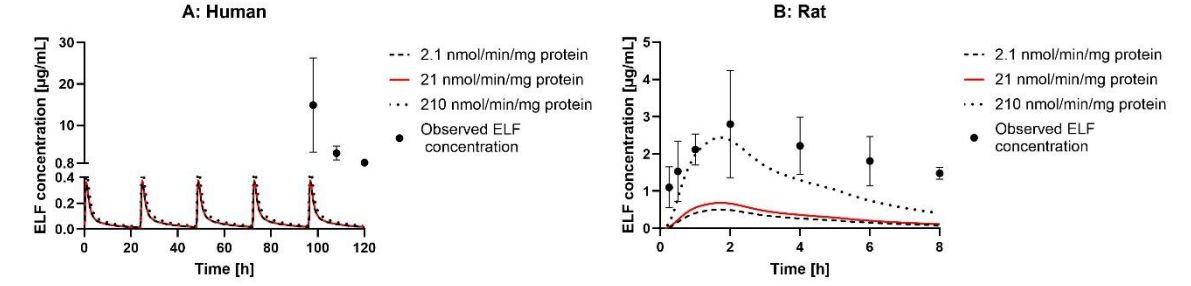

Figure C15. Parameter sensitivity analysis (PSA) of the predicted ELF concentration of **Telithromycin** in human (A) and rat (B) if changing the maximal velocity (V_{max}) of MDR1 interaction and using the permeability-limited model. The simulated ELF concentration using the literature-retrieved V_{max} is shown as solid red line, with a 10-fold lower V_{max} as dashed line (---), with a 10-fold higher V_{max} as dotted line (⋯). Observed ELF concentrations are shown as individual measured means ± SD as dots (·) [289, 353].

C5. Estimation of the Pulmonary Passive Diffusion Clearance

GastroPlus™ assumes that the passive permeability is the same across the different tissues. Therefore, the passive hepatic clearance (CL_{diff}) is typically used to scale the permeability surface area product (PStc) and if taking the tissue volume into account, to estimate tissue specific PStc values (GastroPlus™ user manual V 9.9, Dec 2023).

As a reduced P_{app} of antibiotics was observed *in vitro* (see Chapter 4), when using human lung epithelial cell lines (Calu-3 and hAELVi), compared to established LLC-PK1 WT (porcine kidney epithelial) and Caco-2 cells (human intestinal epithelial) cell lines, the question arose whether the scaled passive hepatic clearance adequately captures the passive pulmonary clearance of moxifloxacin and telithromycin. Therefore, an attempt to derive an estimate of the passive pulmonary clearance ($CL_{diff,pul}$).

The apparent permeability (P_{app}) values of Moxifloxacin and Telithromycin measured across the hAELVi cell line were taken. The hAELVi cells are an immortalised cell line, derived from human primary alveolar epithelial cells [105]. The P_{app} measured from basolateral to apical side in presence of ABC transporter inhibitor cocktail was taken (i.e. mimicking the passive diffusion from the blood vessel-facing side of the lung epithelium into ELF). A mean P_{app} BA of 80.7 and 49.0 nm/s was measured for Moxifloxacin and Telithromycin, respectively (see Supplemental Material B). The surface area of a single human alveolar pneumocytes type I that covers the pulmonary basement membrane was reported to be 5098 µm² in a study by Crapo and colleagues and taken as an estimate [379]. The calculations were made according to the following equation C1:

$$CL_{diff,pul}\left[\frac{mL}{min}\ per\ 10^{6}cells\right] = P_{app}\left[x\ 10^{-6}\frac{cm}{s}\right] * A_{pneumocyte\ type\ I}\ [\mu m^{2}] *\ 10^{6}\ cells * 60$$

Equation C1: Formula to calculate the passive pulmonary diffusion clearance ($CL_{diff,pul}$) based on the *in vitro* determined apparent permeability (P_{app}) and the surface area of an alveolar pneumocyte type I (A) corrected for a total of one million cells. The received number is then multiplied by 60 to convert from mL/s into mL/min.

Table C5 summarises the calculated $CL_{diff,pul}$ for moxifloxacin and telithromycin based on Equation C1. The received $CL_{diff,pul}$ was then incorporated into GastroPlus™ to estimate the human lung PStc considering the total lung cell volume of 700.4 mL (default value by GastroPlus™).

Table C5: Overview of measured in vitro apparent permeability from basolateral to apical side (P_{app} BA), estimated human pulmonary passive diffusion clearance ($CL_{diff,pul}$) and human lung permeability surface area product (PStc) for moxifloxacin and telithromycin.

Compound	P_{app} BA [nm/s]	$CL_{diff,pul}$ [mL/min per 10^6 cells]	Lung PStc Human [mL/s]
Moxifloxacin	80.7	0.024	28.7
Telithromycin	49.0	0.015	17.9